THE UNIVERSITY OF HULL

ULTRASONIC PROPAGATION IN CANCELLOUS BONE

being a Thesis submitted for the Degree of

PhD

at the University of Hull

by

Marion Lindsay McKelvie BSc.(Lond.)

August 1988.

ACKNOWLEDGEMENTS.

ABSTRACT.

The thesis covers two main areas of work. The first is detailed experimental work and the second is the evaluation of existing ultrasonic theories in attempt to apply them to the propagation in cancellous bone. The work is related to a new technique which uses ultrasonic attenuation to measure and predict osteoporosis, especially in the elderly population.

The ultrasonic attenuation, the longitudinal ultrasonic velocity, the scattering effect and the attenuation as a function of frequency were measured on a range of cancellous bone samples, from healthy to severely osteoporotic, and also a few cortical samples. The cancellous bone was human os calces and vertebrae. The relationships between the ultrasonic propagation and the structural parameters and density of the bone were investigated, and were considered both for whole bones and separate purely cancellous samples. Image analysis of photomicrographs taken under low magnification was carried out to find the architectural parameters of the bone structure. The ultrasonic measurements were also compared with quantitative computed tomography assessment and compressive strength testing.

Many theories which are currently used to evaluate ultrasonic propagation in a porous material are reviewed, and three particular ones are developed in detail and applied to models of cancellous bone. The self consistent theory (SCT), Biot's theory and the multiple scattering theory based on the work of Waterman and Truell were all assessed for their limits with repect to this particular application, and each had its own deficiencies. The Biot theory, however, proved the most successful at predicting the experimental attenuation results observed, but still only in a limited way.

CONTENTS.

INTRODUCTION.

Langton (1984) recently developed a new technique for diagnosing the bone disease called osteoporosis. The method involved finding the frequency dependence of ultrasonic attenuation over a range from 200 kHz to 1.0 MHz, and is referred to as Broadband Ultrasonic Attenuation (BUA, or sometimes UBA). Osteoporosis is a disease common in elderly people, especially postmenopausal women, which results in non-traumatic fractures, often of the wrist, hip and spine. Severe osteoporosis can cause great pain and discomfort, and the disease costs the National Health Service a great deal of money for hip replacements and orthopaedic beds.

Langton et al (1984) demonstrated that the frequency dependence of the ultrasonic attenuation of the heel bone or os calcis could differentiate between healthy individuals and those who had suffered a broken hip due to osteoporosis. This thesis describes work carried out on cancellous bone samples taken from the os calcis and vertebrae with the aim of relating the ultrasonic results to the physical parameters of the bone, such as the density, strength and the structural pattern.

Chapter 1 describes the composition of bone and the problems caused by osteoporosis. It is intended that this chapter gives the physicist sufficient background in the medical aspects of osteoporosis to appreciate the requirements of a new diagnostic technique.

The second chapter discusses in detail the techniques already available for diagnosing osteoporosis. All the methods currently in use involve radiation and are therefore not ideal, especially for follow-up work and repeated scans. The main aim of these descriptions is to compare the advantages and disadvantages of each system. The second part of chapter 2 describes the ultrasonic techniques that have been developed with the aim of diagnosing

osteoporosis. These methods are generally still considered to be experimental at present, and include the BUA technique.

Chapter 3 describes the experimental details of the ultrasonic measurements carried out in the current work and the preparation of the bone samples required to take consistent measurements. The reproducibility of the technique is assessed and compared to the other diagnostic methods, although the current work only considers *in vitro* measurements.

Chapter 4 describes the results obtained from all the ultrasonic measurements made on os calces and the cancellous samples obtained from them. This includes attenuation and velocity measurements as well as an attempt to assess the scattering from cylinders of cancellous bone. The ultrasonic attenuation and velocity was also measured in cortical samples for comparison with the results from the cancellous bone. Finally in this chapter, a comparison is made of quantitative computed tomography (QCT) and the ultrasonic attenuation measurements on the same os calces and cancellous samples. All the results are discussed and assessed in the last section of the chapter.

The strength of the cancellous bone is considered in chapter 5, which describes two sets of experiments aimed at relating the ultrasonic measurements to the compressive strength of the samples. Vertebral samples were used for this work.

If the ultrasonic measurements are to be related to the structural parameters of the bone, then the architectural details of the samples measured must be obtained. Chapter 6 describes the experimental technique used and the results obtained. Samples were studied under low magnification using a scanning electron microscope (SEM) and the images analysed by computer. The average structural parameters were calculated for each os calcis, and these can be used in the theories described in chapter 8.

Chapter 7 is a review of published work on ultrasonic propagation in composite materials and includes a discussion of the attenuation mechanisms that are involved. The main areas of work can be split into categories depending on the method used to explain the propagation.

Three theories are developed in detail in chapter 8: the self consistent theory of Berryman, Biot's theory and multiple scattering. The theory put forward by Langton (1984) is discussed in the light of the new results obtained in the current work. The three theories are applied in turn with parameters representing the range of cancellous bone samples used during the current work, with a varying degree of success. The effectiveness of the application is discussed for each of the theories.

The final section of this thesis is the conclusion and a discussion of possible further work. The appendices are the full listings of the computer programs written to evaluate the Biot and the multiple scattering theory.

Chapter One.

THE SKELETON AND OSTEOPOROSIS.

1.1 Introduction.

The skeleton is made up of over 300 separate bones, each helping to support the body and provide rigidity for the muscles. The bone itself is constantly changing, being resorbed and renewed with fresh material in the same way that old skin dies and is replaced by new layers of tissue.

The skeleton is usually split into two regions, figure 1.1. The peripheral or appendicular skeleton is mostly tubular or cortical bone, the strength of which depends directly on the thickness of the cortex. As the name implies, the peripheral skeleton comprises the limbs, the long, strong bones that act as levers. The second region is the axial skeleton, the spine which supports the torso. The vertebrae are composed of cancellous bone; its strength depends on its structure as well as the amount of material present. Cancellous bone is important in the appendicular skeleton too, acting as a shock absorber at joints at the ends of the long cortical bones.

1.2 The Composition of Bone.   (Bourne, 1956. Grech et al, 1985)

Bone structure and the vascular spaces depend on the external forces applied. As bone is living, vascular connections are vital for blood and fluid supplies, so all bone is porous, and can be categorised by this porosity. Cortical or compact bone does not appear porous and even under fairly high magnification can still appear solid, as the tiny pores are widely spaced. Cancellous or trabecular bone contains pores up to millimetres in diameter, and resembles a hard sponge, figure 1.2. This is what acts as a shock absorber,
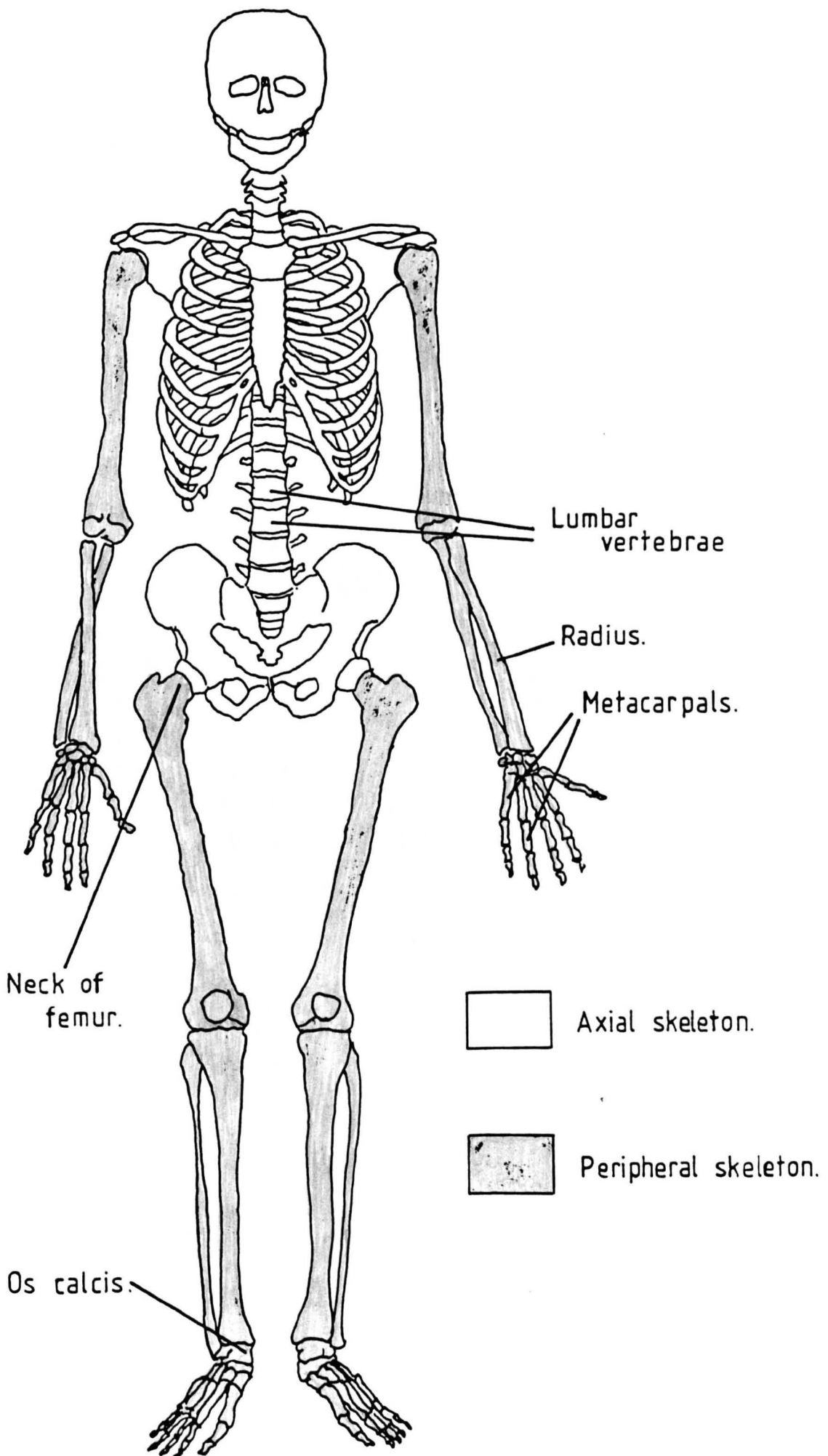
Figure 1.1 The human skeleton, showing the sites used by osteoporosis diagnosis techniques.

Figure 1.2 An example of the structure of cancellous
bone, with the marrow removed.

and the trabeculae, or bone filaments forming the sponge structure, are arranged to the greatest advantage to counteract the external forces acting on the bone. Fine cancellous bone is common only in the fetus and under certain pathological conditions, and has pores up to about 200 µm.

Cortical bone is often formed in a cylindrical pattern around a central hollow (Haversian Canal); this formation is said to consist of osteones of bone. On a large scale, the long bones such as the humerus and the tibia are formed in osteones around the central marrow which contains blood vessels and nerve fibres. Cancellous bone is similarly formed but with only the thicker trabeculae being complete osteones. Most are composed of osteon fragments. The surfaces are covered with both active and resting cells with the active cells responsible for the continuous production and resorption of the bone. Marrow bathed in body fluids is present in the pores of the cancellous bone, but the type of marrow depends upon the skeletal site. Most non-vertebral cancellous bone contains marrow that is almost completely made up of fat.

Bone itself is made up of an inorganic and an organic component. Bone mineral is the inorganic material responsible for the hardness of bone. There are a series of natural minerals called apatites, with calcium phosphate as the main constituent, and it is generally accepted that bone mineral is hydroxyapatite, $Ca_{10}(OH)_2(PO_4)_6$, tricalcium phosphate and calcium hydroxide mixed. The carbonate present in bone is from calcium carbonate which is adsorbed, with the other constituents, on the surfaces of the hydroxyapatite crystals. There is a faster turn over in younger bone, so it is thought that bone mineral is first laid down as calcium phosphate rather than an apatite. The hydroxyapatite is the component of bone that is usually detected by diagnostic systems.

The mineral is laid down on fibres by cells that are responsible for the manufacture and resorption of bone. The crystals are formed parallel to

the collagen fibres. Many factors influence the nucleation of the mineral salts and the complete mineralisation of the fibres, or osteoids, takes on average 23.5 days (Teitelbaum,1983). The fibres are made up of bundles of fine collagenous strings, similar to those in the skin and muscle tissue. Embryonic bone is said to be woven, as the fibre bundles run irregularly, while mature bone is lamellar, as the fibres run in a predominant direction in a particular layer. This gives bone an overall laminar appearance, although it is in fact completely continuous.

Of all the different types of bone in existence (eg. fish scales, eggshells, teeth and calcified tendons etc.) adult mammal skeleton is usually classified as stratified or lamellar finely bundled bone, as opposed to coarsely bundled and/or woven bone. After a fracture, woven bone is the first to form, but lamellar soon takes over. Both adult cancellous and compact bone is composed of finely bundled lamellar bone.

Cells called osteoblasts are responsible for the synthesis of the organic components and the hardening of the bone matrix. They may also have a part in controlling the bone resorption. As the production of collagen slows, the cells enter a resting form called osteocytes when they are completely surrounded by mineralised bone (Kimmel, 1981). Osteocyte numbers decrease with aging. Osteoclasts are responsible for resorption and are formed with a ruffled edge to increase surface area. Endosteal cells separate marrow tissue from the bone surface, such as on the inner cortical edges and the trabecular plates.

The initial formation or modelling of bone architecture stops by the age of 18 or 20, but remodelling continues throughout life involving all the bone surfaces. Rates of bone formation and resorption are closely linked and are usually equal but are affected by many hormones and drugs, some of which are discussed in the following section. As the individual grows older, there is a

slight increase in the resorption rate. This results in aging or senile osteoporosis. Other factors can lead to more severe forms of the disease. Remodelling results in older osteones being resorbed and new ones formed or trabeculae being strengthened and replaced.

1.3 Osteoporosis.

Osteoporosis is often defined simply as the straightforward loss of bone mass, with the constituents staying in the normal proportions. There are several categories of the disease: primary osteoporosis, dealt with here, can be either simple (senile) or accelerated (postmenopausal), but there is also disuse atrophy and disease secondary to other pathological states.

Osteoporosis was mainly undetected until the 1920s. There were no symptoms unless a patient fractured until the use of X-rays provided a means of visualising the bones. The longer life expectancy of recent times has meant that more people are affected more severely. Alwens described senile osteoporosis in 1926, with Albright et al describing the postmenopausal condition in 1941. It is the most common skeletal disorder in the world and is still often diagnosed by studying X-ray images for vertebral collapse and density changes in the bone.

The disease is characterised by the loss of bone mass and increased porosity. Cortical bone becomes thinner, as can be seen by measuring radiographs of the fingers, but the Haversian Canals increase in size, a condition that is much more difficult to detect. Trabecular bone is similarly affected but with different results. Whole trabeculae may disappear, substantially increasing porosity and decreasing the strength of the structure. Cortical and trabecular loss occurs at different rates because of the difference in bone turnover.

As the bone mass decreases in cancellous bone, the structure alters, so osteoporosis affects more than just the bone mass or bone mineral content. Other factors, such as the structural pattern or architecture must be taken into account. The term bone quality is often used to cover all these effects, rather than considering the bone quantity which is purely a measure of bone mass or bone mineral content (BMC). Volumetric and area bone density measurements (BMD) are also used, see section 2.1. BMC and BMD can be applied to both cortical and cancellous bone, but the structural information is specific to the latter.

The marrow present in the pores of the trabecular bone is also affected. The red haematopoietic marrow, which usually contains a large proportion of blood, becomes more fatty. Vertebral marrow is 75% red marrow in young adults, 50% in the elderly and as low as 25% in osteoporotics (Mazess, 1983b). The fat in the pores of non-vertebral cancellous bone is mainly unaffected (Webber, 1987).

As the bone mass decreases and the porosity increases, the overall strength of the bone is severely affected. The skeleton supports the weight of the body as well as the extra forces due to everyday activity. Eventually the stage will be reached where the bone can no longer stand the forces acting on it and a fracture results. This stage is often referred to as the fracture threshold (Wahner, 1982).

Vertebrae suffer wedge fractures from too much weight acting on them, and after severe trabecular loss will eventually crush, leading to Dowager's Hump and shrinkage of the spine, figure 1.3. These fractures show up clearly on radiographs and do not necessarily cause pain until many vertebrae have collapsed and the torso is pushed forward so that the lower ribs rest on the iliac crest. Breakages of the wrist, or Colles fractures, are often taken as an early indication of possible osteoporosis and are due to cortical loss. This loss is often small, about 10% (Nordin, 1983), but is sufficient to weaken the wrist so that a fracture occurs if, for example, a woman tries to protect herself from a fall using her arm. The broken hip or fractured neck of femur is probably the fracture that causes the most pain and suffering. It is often considered to be due to both trabecular and cortical loss and occurs with no extra force on the body, like the vertebrae collapsing. These are known as non-traumatic fractures. The person may be rising out of a chair when small stress fractures in the trabeculae give way under cyclic loading and cause the hip to break.

NORMAL

END-PLATE
DEFORMITY

WEDGE
DEFORMITY

COMPRESSION
DEFORMITY
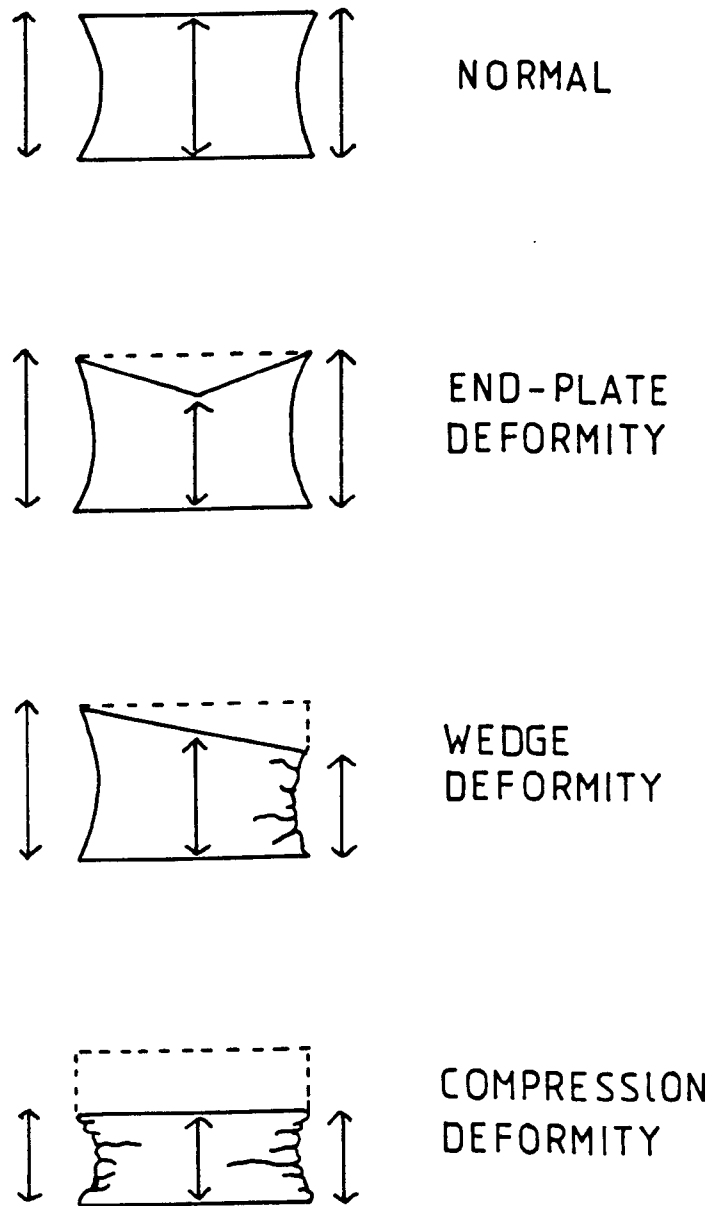
Figure 1.3 The three types of vertebral deformity with the site of
measurements arrowed, the relative values of which are used
to define the type of fracture suffered.

The likelihood of fracture depends not only on the state of the bone but also on the propensity to fall, which equally depends on the way of life. The importance of the type of fall causing a fracture has been highlighted by Cummings (1987), showing the younger mobile person will fall with forward momentum whereas a slower older person tends to collapse downward, which is more likely to cause a hip breakage. As a general illustration, the graph in figure 1.4 shows the sex and age specific incidence of all limb fractures among the residents of one United States city. The peak of teenage fractures for both males and females is outnumbered by the fracture rates of the elderly. The female rate begins a rapid rise around the age of early menopause whereas the male rate increases much later in life, when the slower bone loss begins to take effect. The distribution of type of fracture also shows an interesting trend. Colles fractures are common around the age of menopause but hip and vertebral fractures become much more frequent with age, figure 1.5.

The decrease in bone density is due to increased resorption of bone, but could also be due to decreased production in the more severe cases. Nordin et al (1981b) found an increased resorption surface area with age, and a greater increase with osteoporotic subjects, with a slight non-significant decrease in formation surfaces in females and a large decrease in males, as shown in figure 1.6.

Initial bone modelling is controlled by genetic factors but the constant remodelling is controlled by many external factors such as nutrition, exercise, hormones and drugs taken. The full details of 'normal' age related osteoporosis are unknown, but it is hormonal in origin in both men and women (Nordin, 1983). It is important to remember that bone loss occurs throughout adult life, but is most severe in females just after the menopause. It has been suggested that an operational definition of osteoporosis should be those with bone content values more than 2 standard deviations below young normal
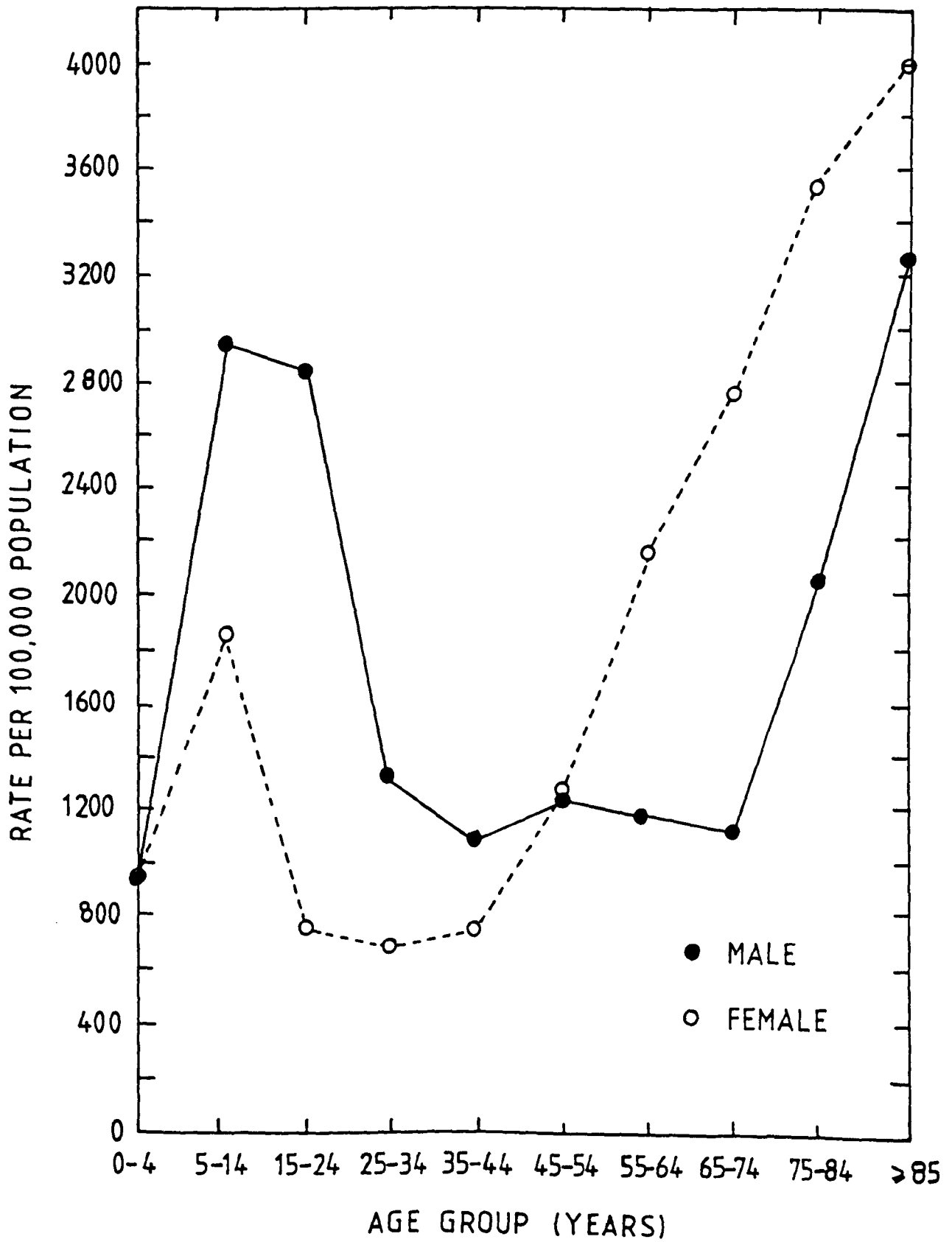
Figure 1.4 Age and sex specific incidence of all limb fractures among the
residents of Rochester, Minnesota 1969-1971.

(Melton and Riggs, 1983)
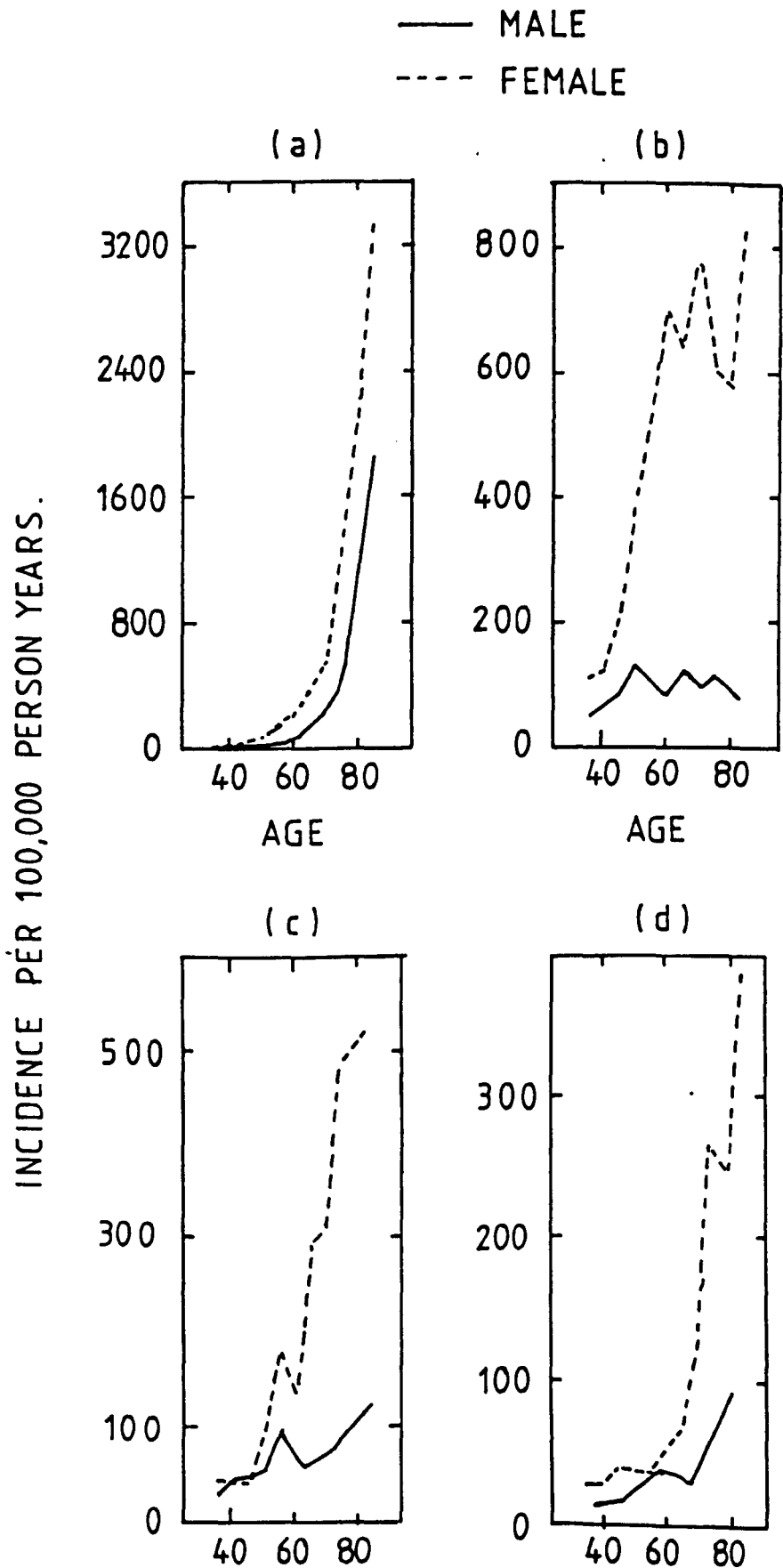
Figure 1.5 Distribution of the type of fracture suffered by males and females

a) proximal femur

b) Colles'

c) proximal humerus

d) pelvis.

(Melton and Riggs, 1983)
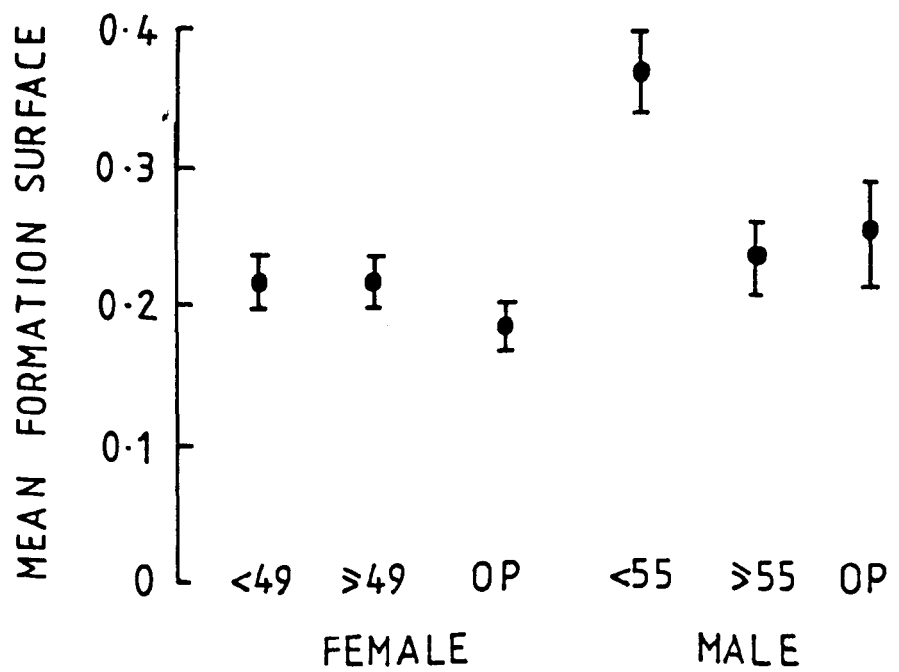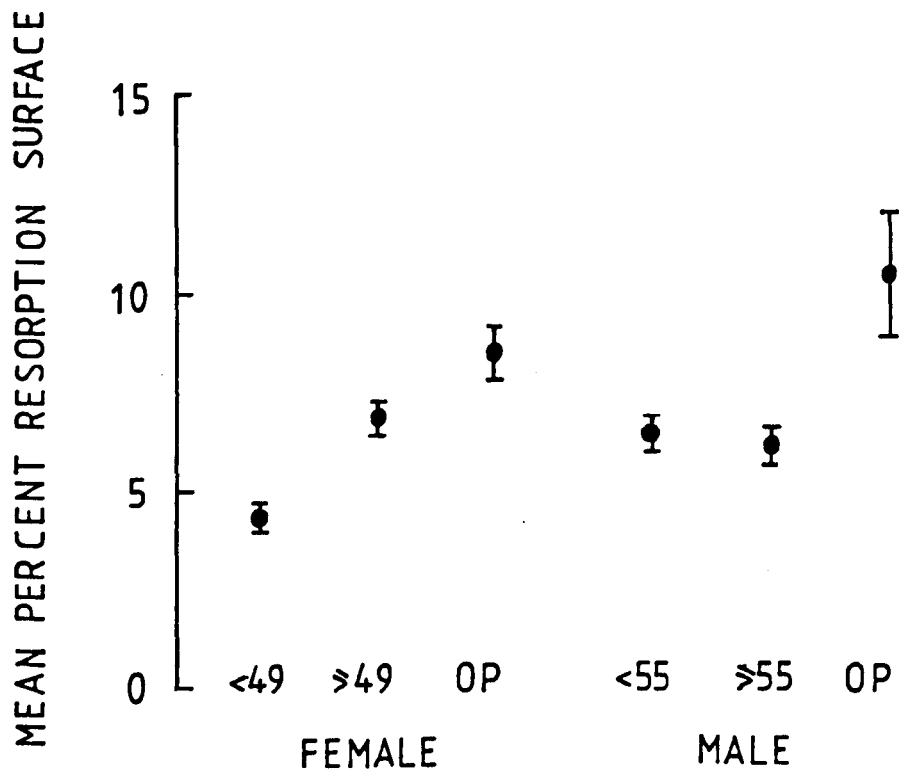
Figure 1.6 Mean resorption and formation surfaces in young, elderly and osteoporotic men and women.

(Nordin, 1981b)

subjects. This raises the problem of comparing different measuring techniques and different skeletal sites and Mazess (1987) shows that this method would not classify many patients with vertebral crush fractures if the wrist were the site measured.

Postmenopausal bone loss results from a decrease in blood plasma estrogen levels. Estrogen protects the bone from the resorptive action of the parathyroid hormone, so as estrogen levels decrease, an extra resorbing agent is working on the bone. Small increases in plasma and urinary calcium and phosphates are associated with the disease in females. Calcitonin is also thought to be involved at an intermediary stage (Nordin, 1983). Richelson et al (1984) used oophorectomy patients to compare an early menopausal population with an age matched perimenopausal group and natural postmenopausal females. Both postmenopausal groups had had low estrogen levels for a comparable time span. The oophorectomy group had almost an equally low bone mineral content as the postmenopausal population despite being significantly younger. Estrogen loss has a more dominant effect on bone loss than age, especially in the decade after menopause. There is no increase in plasma or urinary calcium or phosphates in men, indicating a slightly different mechanism, but it is thought the disease is a result of a decline of testicular and/or andrenal androgens (Nordin, 1983).

Unfortunately, the processes of bone formation and resorption are so complicated, involving many separate stages that results from studies trying to control one hormone or treatment may often be confused by effects from other stages in the remodelling (Raisz, 1984). Parathyroid hormone, vitamin D and related metabolites, prostaglandins, thyroxine, a lymphokine called osteoclast activating factor, calcitonin and androgenic hormones are some of the chemicals demonstrated to have an effect on bone metabolism along with calcium (Grech et al, 1985). This list does not include treatments for other
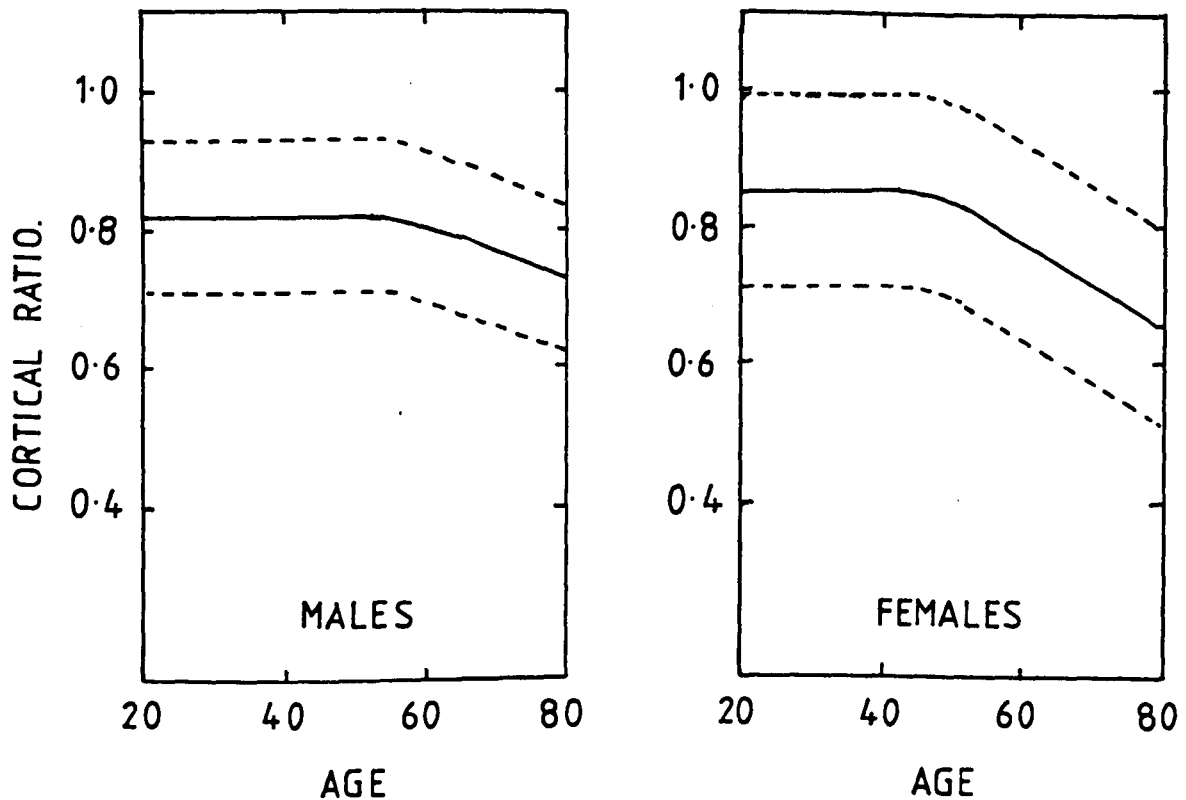
Figure 1.7 Cortical bone loss with age in normal men and women as measured by the metacarpal cortical area to total area ratio, showing mean and 2x standard deviation.

(Nordin, 1983)
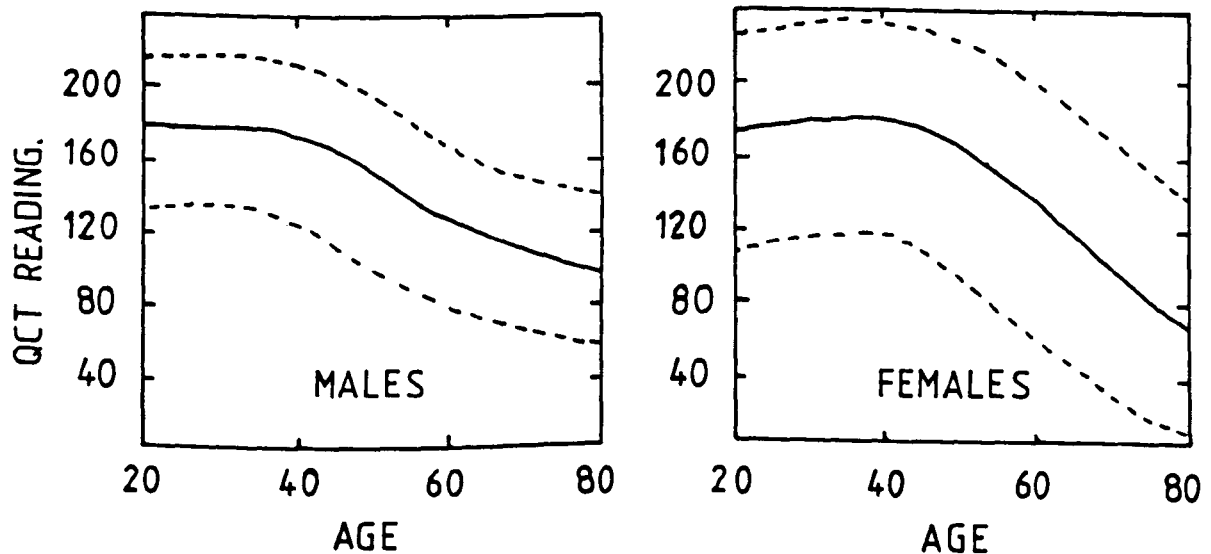
Figure 1.8 Cancellous bone loss with age in normal men and women as measured by quantitative computed tomography of the vertebrae, showing mean and 2x standard deviation.

(Genant et al, 1982)

diseases, such as corticosteroids that also influence bone turnover, and disease secondary to other pathological conditions such as rheumatoid arthritis, renal disorder and hyperparathyroidism.

There is much discussion about the rates of 'normal' bone loss and the age at which the effect starts, mainly because of differences between skeletal sites and measuring techniques. It is generally accepted that cortical bone is not lost in females until around the menopause when an average loss of 1% per annum starts and that cortical loss in men starts somewhat later in life and remains at a slower rate of 0.5% per annum (Bloom and Laws, 1970). Trabecular bone loss in females starts at around 30, with accelerated loss after the menopause which slows again some years later (Nordin, 1983) although some researchers suggest a continuous loss from the 20s (Recker, 1982). Most studies show a steady decrease in bone mass in populations, figures 1.7 and 1.8, but Ruegsegger et al (1984) reported sudden steps in bone loss in individuals. The estrogen loss is a far more important factor than age, so men only lose trabecular bone at a slow rate starting later in life than women. Initially it was thought that osteoporosis was a female problem, but now that there is a much longer life expectancy some males are losing sufficient bone to bring them below the fracture threshold.

The age-related factor is present in everyone, figure 1.9, but results in serious cases only when the initial bone mass is small or the rate of loss is particularly high. A heavily boned person could loose 1% a year without reaching the critical fracture level within his life expectancy, yet a frail , petite person losing at the same rate will quickly reach the fracture threshold, figure 1.10. Because the severity of the disease is determined by build, osteoporosis is race dependent (Garn, 1981). 25 to 30% of white women will develop the disease. 70% of fractures that occur in women aged 45 and over are due to osteoporosis, including hip, wrist and vertebral fractures.
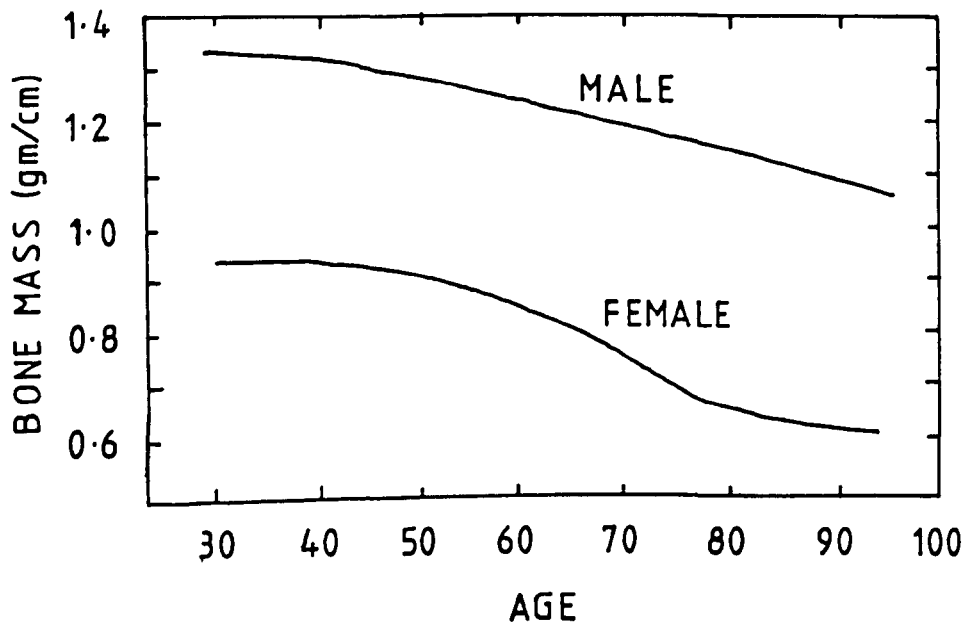
Figure 1.9 Model of age related bone loss in normal men and women.

(Johnston, 1983)
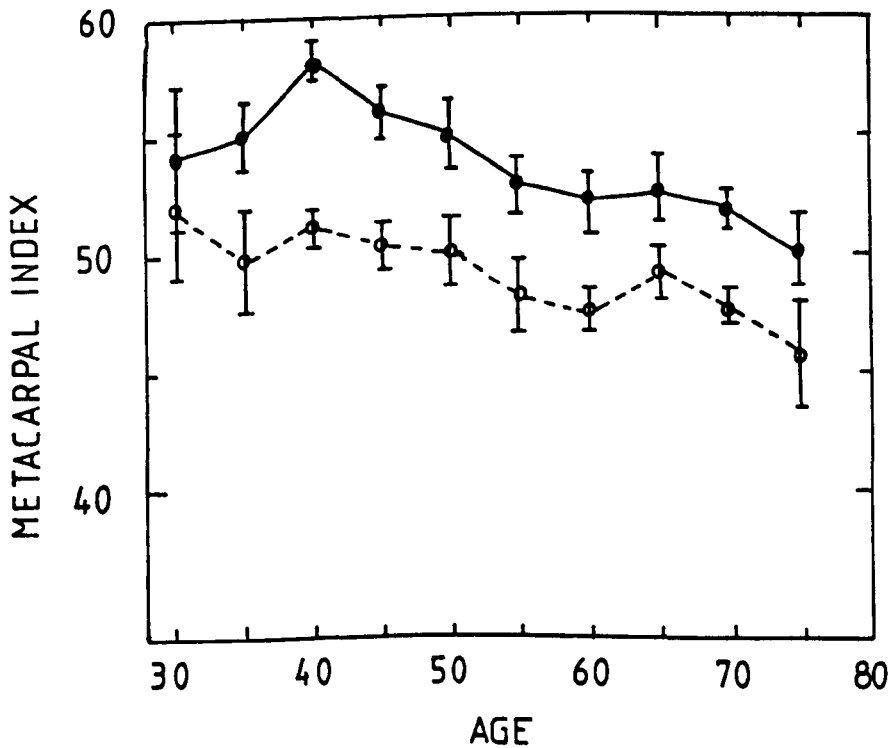
Figure 1.10 Loss of bone from metacarpals in two populations with different

peak adult bone mass.

(Heaney, 1983)

In America, hip fractures alone cost $1.4billion per annum (Davies and Saha, 1985). Many fractures are fatal, and most of those who survive are not able to look after themselves afterwards. Typically, there is a 12% reduction in survival rate after hip fracture (Melton and Riggs, 1983). In Britain, from 1959 to 1977 there was a 2.7 fold increase in hospital admissions for fractured neck of femur, and each annual increment costs £40million extra (Fenton-Lewis, 1981).

1.4 Trabecular Bone Loss.

All bone metabolism takes place on the surfaces of the bone, where the cells are situated, so because of its structure, cancellous bone has a turnover eight times higher than that of cortical, which results in cancellous bone being affected far more by osteoporosis (Genant and Cann, 1981). Schaadt and Bohr (1982) showed decreases of over 20% in the spine, around 19% in the neck of femur and only 6% in the femur shaft when they compared normal women aged around 35 to a normal postmenopausal group. A group of osteoporotics, defined by at least one crush fracture of the vertebrae, had lost over 30% of bone mass in the spine. The spine and the neck of femur, the sites with the greatest bone loss, are predominantly composed of trabecular bone. Leichter et al (1987) studied the distal radius and separated the trabecular and cortical components of the scan. They found that the density of the trabecular bone decreased more rapidly than the cortex, suggesting that trabecular bone gives a better indication of the severity of the osteoporosis.

The strength of cancellous bone depends more on its structure than the amount of bone present and often there is a large overlap in bone content and density in groups of age matched fracture and non-fracture individuals. Trabecular plates are laid down along lines of compressive and tensile stress, and are often considered to be sheets with cross bracing between them (Pugh et

al, 1973). The highest compressive strength will be in the direction of the greatest load (Galante et al, 1970). In the vertebrae, the horizontal struts are resorbed first, although this can initially cause the vertical plates to be strengthened by thickening (Mosekilde et al, 1985), although the overall structure will be weaker. Microfractures are most obvious in the horizontal plates. Eventually there is not enough support for the spine and the vertebra collapses. Similarly, in the neck of femur, groups of compressive trabeculae disappear first, weakening the entire structure (Singh et al, 1970).

There is still much discussion whether the mean trabecular width is narrowed, widened or unaffected, although the trabeculae definitely decrease in number. Parfitt et al (1983) found that normal loss with age predominantly removed entire trabeculae and only produced slight thinning of the remainder. Garrahan et al (1986) found no significant change in females but males had a decrease in plate width. Kleerekoper et al (1985) reported higher trabecular widths in the group of females they tested. Merz and Schenk (1970) suggest that initial microfracturing results in a build up of bone at that site, producing thicker trabeculae to strengthen the structure, and that the ability to do this is lost as more severe breakages occur and whole trabeculae are resorbed. However, the ability to repair these microfractures is retained by some individuals. A few elderly people can repair disuse osteoporosis as effectively as a youngster (Lanyon, 1981 and Heaney, 1983).

The trabecular plate diameter and separation can be studied by histomorphometry but no current non-invasive diagnosis technique has access to these details. Although bone mass may not be significantly different between age matched fracture and non-fracture groups, the trabecular plate density (spacing and number of plates) is very much lower for the latter group (Kleerekoper et al, 1985). Researchers are beginning to realise that a model to predict the risk of vertebral crush fractures must include structural

details in addition to the bone mass. Heaney (1987) suggested that low bone mass is a necessary condition for fracture, together with unrepaired fatigue damage, faulty trabecular architecture, increased brittleness and an accumulation of osteoid. All these effects, along with the propensity to fall should be taken in to account in the calculation of fracture risk for an individual.

1.5 Skeletal Site Factors.

There is still much discussion as to whether osteoporosis affects the whole skeleton equally or just particular sites. It seems to vary from study to study which makes it difficult to design an effective diagnostic technique. Wrist, spine and neck of femur are the obvious sites, but the latter two are difficult to access and scanners that appear to measure the former actually scan the cortical radius and ulna. The calcaneum (os calcis or heelbone) is also a candidate because it is a large volume of cancellous bone but it is susceptible to short term disuse and weight bearing although it can recover quickly (Overton et al, 1981). However, it should be noted that the main fracture sites are also weight bearing bones and there is only a correlation of 0.3 at best between bone mineral density of the os calcis and body weight (Rundgren et al, 1984). Both the neck of femur and the os calcis correlated with physical activity 0.18 and 0.25 respectively for males and females (Dalen and Jacobson, 1974). The correlations are poor, although the highest of all the sites tested, but they may indicate that the os calcis is a good indicator of the condition of the bone at the neck of femur, the fracture of which causes the most anguish for the sufferer. Wasnich et al (1987) measured the bone mineral content at the distal and proximal radius, os calcis and lumbar spine, and found that the os calcis was the best predictor of the fractures, both spinal and appendicular, suffered in the following years. Gotfredson et

al (1986) carried out measurements on regions of the skeleton (head, arms, chest, spine, pelvis and legs) using dual photon absorption (see section 2.2.7) and showed generalised loss throughout the skeleton in early menopause. This is not the same as using particular sites, and many studies show poor correlation between measurements made on different sites, usually because of the varying ratio of trabecular to cortical bone. Further complications arise when the rates of loss are compared. Riggs et al (1986) found reasonable correlations between the spine and the radius measured by different techniques, but there was no connection between the rate of loss at each site. The work of Schaadt and Bohr (1982), mentioned in the previous section, comparing trabecular to cortical bone sites, shows how different each measurement can be.

However, correlations between sites are vital for results to be generalised to the whole skeleton. Diagnostic equipment is often designed with one particular site in mind and that site will be the optimum for the precision of that technique. Some groups normalise bone mineral content or density to factors such as body mass, height, surface area and age. A general study including radius, ulna and calcaneum measurements produced a correlation of approximately 0.4 with body weight for all the sites (Yano et al, 1984), slightly higher than that of Rundgren et al (1984). In this case age and years since menopause were also considered, and produced very significant correlations for all sites, as would be expected.

Some studies compare sites by using different techniques while others carry out comparisons of sites using one technique by modifying the equipment. This is more useful but unfortunately inconclusive. No sites correlate consistently well with the vertebrae although the radius and ulna, humeral head, and femur shaft all correlated better ($r \simeq 0.6$) than other sites to values for the neck of femur using X-ray spectrophotometry (Dalen and

Jacobson, 1974). Spectrophotometry is a dual energy X-ray system that can be considered to be the precursor of dual photon absortiometry (Gustafsson et al, 1974). The calcaneum also correlated fairly well (r ≃ 0.5). Interestingly, among the groups of volunteers measured, normal males often produced significantly lower correlation coefficients between sites than females. Perhaps this is a demonstration of the effect of exercising parts of the skeleton regularly.

The degree of osteoporosis has never really been defined except when fractures actually occur. The axial skeleton is important if only vertebral fractures are to be investigated but hip fractures often cause more pain and suffering for the individual concerned, so perhaps measurements aimed at detecting risk of hip fracture are more relevant to the public than the actual bone mineral determinations.
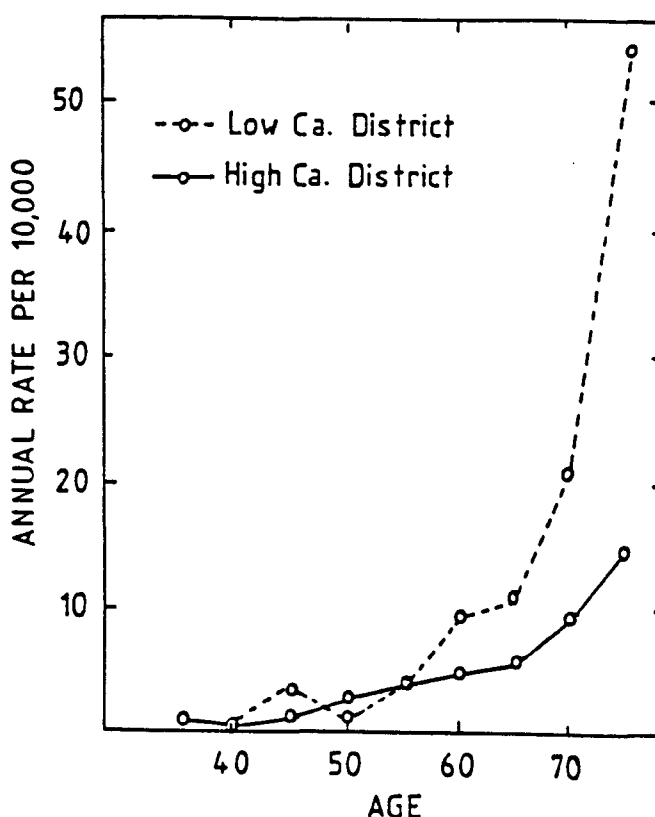
Figure 1.11 Annual proximal femur fracture rate in Yugoslavian women in high and low calcium districts.

(Avioli, 1983b)

1.6 Cures.

It is possible to affect the initial bone mass. Calcium is the primary mineral in bone and it is known that calcium deficiency is a major risk factor for fractures and fracture rates are lower in high calcium areas, figure 1.11. Throughout their life, the average woman ingests less calcium than is considered necessary (Avioli, 1983a). Calcium absorption decreases with age and the efficiency of absorption varies greatly between individuals. Nordin et al (1981a) found that a group of females with vertebral crush fractures absorbed calcium poorly compared to age matched non-fracture females, using radioisotope tracing. The use of calcium as a preventative measure for osteoporosis was generally accepted, but now some researchers argue whether it is actually beneficial (Heaney and Recker, 1981. Mazess et al, 1985). Some recent studies show little effect when only calcium is prescribed alone (Ettinger et al, 1987. Riis et al, 1987).

Trabeculae build up along the lines of stress, so exercising will build bones up in the same way it does for muscles. Bed rest, for instance, is known to induce bone loss, but this can be replaced even by the elderly (Lanyon, 1981). Some bone loss is reversible but most is not (Parfitt, 1984).

If bone mass is large before the age related loss starts, it is unlikely to reach the fracture threshold, so preventative measures such as calcium and exercise could be taken throughout life. Bone mass at menopause is a fairly good predictor of whether a female will suffer osteoporotic fractures later on in life (Heaney, 1984).

Research has so far produced ways of slowing down the rate of bone loss but has had little success in increasing the bone mass. The treatment must therefore be a preventative one, administered before the bone has decayed too much and well before the fracture level has been reached.

The obvious treatment for postmenopausal osteoporosis is hormone replacement therapy (HRT) which was even mentioned by Albright et al in the original work describing the disease (1941). This runs a high risk of side effects, including cancer, and not everyone can take hormone supplements (Jackson and Ullrich, 1984); yet some researchers say its beneficial effects clearly override any problems (Ross et al, 1984). However, if it cannot be used universally some other treatment is also needed. HRT is often given with extra calcium, and Cummings and Black (1986) discussed the effect of HRT compared with calcium and exercise alone, concluding that the estrogen is the most effective at reducing bone loss.

Flouride with calcium supplementation has been shown to reduce fracture rates (Avioli, 1983b) but some studies suggest that the increase in bone density is due to uncalcified material, even when extra calcium is supplied (Compston et al, 1980). Others suggest that the trabecular bone is built up at the expense of cortical, as no extra calcium is absorbed (Slovik et al, 1986). Flouride treatment also has its fair share of side effects, including nausea (Davies and Saha, 1985). Riggs et al (1982) conducted an interesting comparison between four different treatment regimes. Calcium, estrogen and flouride together produced the lowest fracture rate over a twelve year period.

Exercise is still recommended and has been shown to have a beneficial effect if treated as part of a cure with calcium supplementation. A review of exercise as a treatment is given by Yeater and Martin (1984).

One or two recent studies have demonstrated an increase in bone mass in males. Daily injections of parathyroid hormone and 1,25 dihydroxyvitamin D significantly increased vertebral bone mass in four osteoporotic patients measured out of the eight treated. Cortical bone density, measured at the forearm, increased for two patients, decreased for one and remained the same for the other (Slovik et al, 1986). Calcium retention had improved in the four

patients studied, suggesting that the vertebral build up was not at the expense of some other site. The work is currently being extended to women.

1.7 Summary.

Osteoporosis is an age related disease that weakens the bones of the skeleton, resulting in fractures for postmenopausal women and elderly men. The condition is present in everyone, but can be very severe in many cases. The rate of bone loss can be reduced, but ways of safely reversing the decrease in bone mass have not yet been found.

The effects of the disease need to be diagnosed at an early stage so that the patient may take preventative measures. The strength of bone depends on its structure as well as the quantity, so ideally both parameters are necessary to evaluate the quality of the bone. This thesis is an analysis of the propagation of ultrasound in cancellous bone, the bone responsible for support and the primary shock absorber of the body, in an attempt to obtain details about the quality of the bone.

Chapter Two.

DIAGNOSTIC TECHNIQUES.

2.1 Introduction.

The quality of bone mineral stays relatively constant so the amount of mineral was considered to give a good indication of the amount of bony material present. Nearly all current diagnostic techniques rely on finding the bone mineral content (BMC) or bone mineral density (BMD). The density measurements are often area rather than volumetric and can be compared to the total mineral content if the thickness of the bone is known at the site measured. This will vary from person to person. The thickness may be just as important as the density where fractures are concerned, so both parameters are usually considered to be of equal importance. However, the use of bone mineral content per unit area as a measure of density can lead to contradictions.

Ideally a technique which considers trabecular structure as well as the mineral content is needed, which can be used repeatedly in safety, as a large change in porosity may result in only a small change in bone mass (Mazess, 1983a). The best site to be measured is still uncertain, and must depend on whether risk of hip or spinal fracture is considered to be of the main importance. All the techniques described fall short in some way from the ideal but are still useful in the diagnosis of osteoporosis. Those techniques which measure the neck of femur or spine directly may appear to be preferable but they are far more expensive and time consuming than simple scans on other sites and may not be reproducible enough for serial measurements.

An easy and cheap method is required for scanning the entire perimenopausal population to decide who is at risk either because of low bone mass

initially or greater than average rate of loss. The risk of hip fracture is probably the most important to detect, as this causes the most anguish to the sufferer (Cummings and Black, 1986). Recent editorials have made much of the analysis of the necessity of a scanning programme for the perimenopausal population, and although generally it is a good idea, the authors conclude it is unnecessary at this time purely on the basis of the expense and limitations of the existing diagnosis techniques (Ott, 1986. Hall et al, 1987. Nordin, 1987).

One study carried out in Denmark suggested that a blood sample, a urine sample and height and weight measurements just after the menopause would predict, with some 80% certainty, whether the subject would be a fast or normal loser of bone, although of course such studies would have to continue for some decades to show fracture prediction (Christiansen, 1984). However, little differentiation was made in this study between initial bone masses or proximity to actual menopause of the volunteers. Testing of this kind requires massive resources for the analysis of the samples - the present chaos with cervical smear testing gives an indication of the possible problems. Other techniques include the monitoring of radioactive isotopes to assess the metabolic rates, but as the mechanisms of bone turnover are still not fully understood, these studies are open to misinterpretation (Mazess, 1983a). The increase in the use of nuclear magnetic resonance (NMR) has lead to experimental systems recording the phosphor ^{31}P spectrum, a direct indication of the amount of bone mineral present (Brown et al, 1987).

2.2 Hospital Diagnostic Techniques.

Early diagnosis techniques relied on tools already available in hospitals such as X-rays and, more recently, computed tomography (CT), but specialised equipment is also now in fairly common use. These descriptions are intended to

draw attention to the limitations and reproducibility of current methods, with the aim of screening all perimenopausal women for a prediction of fracture, with possible follow-up scans in later life.

The definitions of reproducibility or precision and accuracy are discussed in the experimental details of the current work (section 3.5) but generally the former is the ability to give the same result each time a measurement is made on the same sample, and the latter is the ability to correlate with an independent measurement, often the known quantity of bone mineral in specially made phantoms.

2.2.1 Radiogrammetical Measurements.

This is the simplest and most widely used method based on cortical thickness measured directly from an X-ray image of the limb on fine grain film using needle-tipped vernier calipers. Taking measurements of the internal and external diameters of the cortical bone in the second, third and fourth metacarpals is the most common way, but some experimenters have also used the femur and the humerus. The ratio of cortical area to total area is calculated, and values below 0.72 represent cortical osteoporosis (Nordin, 1983) and a typical value for a healthy young person is 0.85, figure 2.1.

subperiosteal area
$0.785 \, T^2$

medullary
cavity area
$0.785 \, M^2$

cortical area
$0.785 \, (T^2 - M^2)$
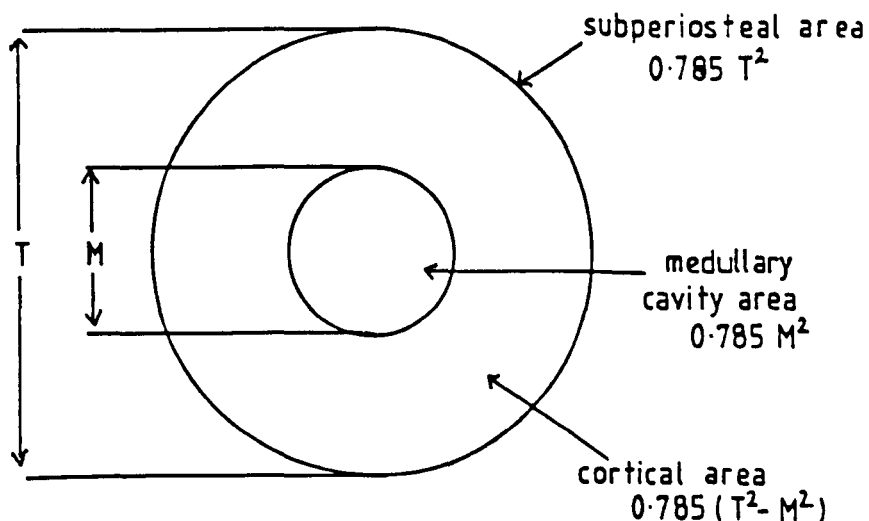
Figure 2.1 Calculation of the total and cortical areas for the evaluation of the metacarpal index.

The technique is insensitive to small changes and the coefficient of varia-
tion of repeated measurements is around 3%. Recker (1982) suggests that the
metacarpals are the best site for measurements but Bloom and Laws (1970) used
the humerus and reported they could detect changes of thickness of 5%.
Generally, the technique is considered imprecise, with more usual errors of 5
to 10%, and also inaccuracies of up to 25%. It can not account for any changes
in porosity and has no application to trabecular bone.

2.2.2 Singh Index.

The lines of trabeculae correspond to the lines of maximum pressure and
tension and are remarkably consistent from sample to sample, as seen by X-ray
imaging. This led to an index for the degree of osteoporosis based on the
trabecular pattern in the neck of femur (Singh et al, 1970). A grade of 1 to
6 was assigned to the trabecular pattern from severely osteoporotic to normal.
The tensile trabeculae are the first to decrease followed by the compressive
ones, figure 2.2.

Jhamaria et al (1983) suggested a similar grading system for the trabeculae
of the calcaneum. Grade 5 in this case is healthy. In the calcaneum, the
central compression trabeculae disappear first, but the borderline between
normal and osteoporotic is considered to be when the tensile trabeculae start
decaying, figure 2.3.

Both indices correlate well with age, but unfortunately the grading depends
on the orientation of the leg and the exposure and development of the film
(Mazess, 1983b). This technique grades the severity of the disease as it
exists and looks at the structure without the BMC. It would be of no use as a
predictive method.
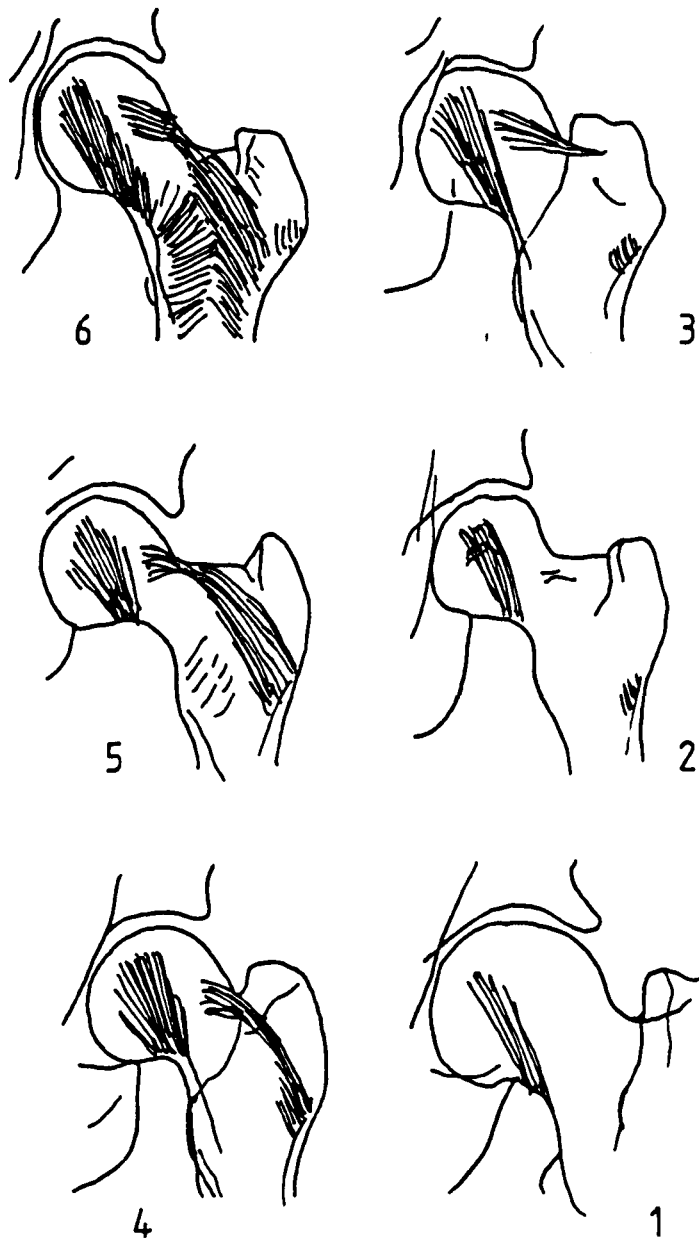
Figure 2.2 Diagrammatic representation of the Singh Index, showing the six grades from (6), normal, to (1), severely osteoporotic. (Nordin, 1983)
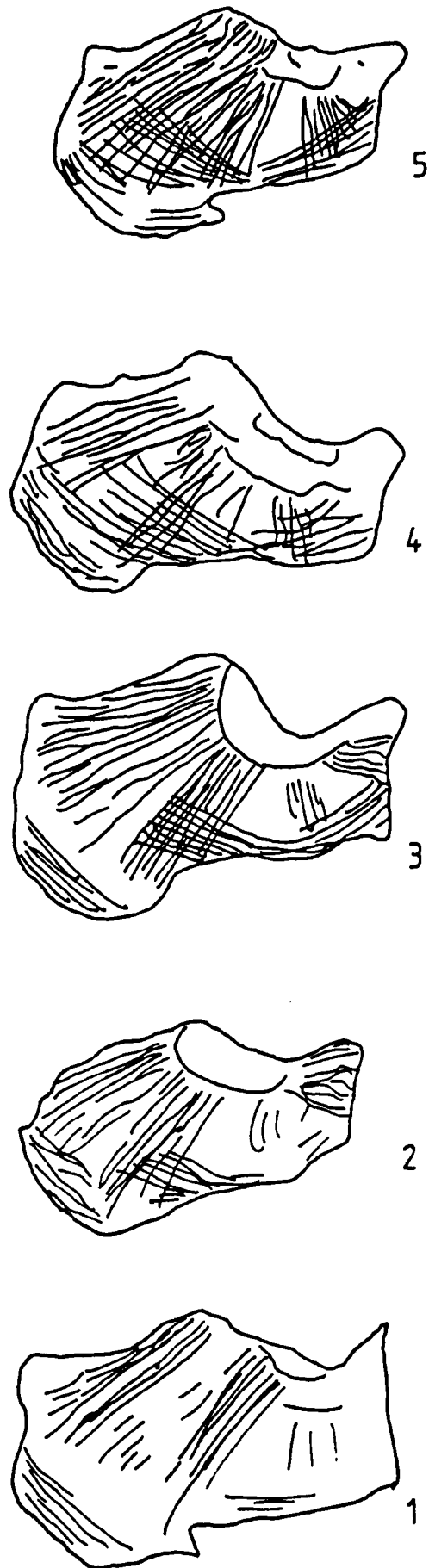
Figure 2.3 Diagrammatic representation of the index for the calcaneum,
showing the five grades from (5), normal, to (1), severely
osteoporotic.
(Jhamaria et al, 1983).

2.2.3 Neutron Activation Analysis (NAA).

Gamma rays, which are emitted by the patient after irradiation of low level exposure to fast neutrons, are counted and used to find the mass of calcium in the body, figure 2.4. The rare isotope of ^{48}Ca which is in constant proportion to the stable calcium, ^{40}Ca, is converted to ^{49}Ca which decays with an eight and a half minute half-life. The method was first demonstrated in 1964 (Anderson et al, 1964) and initial work suggested that the calcium content of the body, 98 to 99% of which is in the skeleton (Chesnut et al, 1981), could be measured to 8% accuracy and changes of 2% over a period of time could be detected (Palmer et al, 1968). It is often used as a standard for comparisons because of the versatility of measuring sites and the fact that elemental calcium is measured directly rather than via its attenuating effect. A series of calcium standards are used to account for source decay and drift.
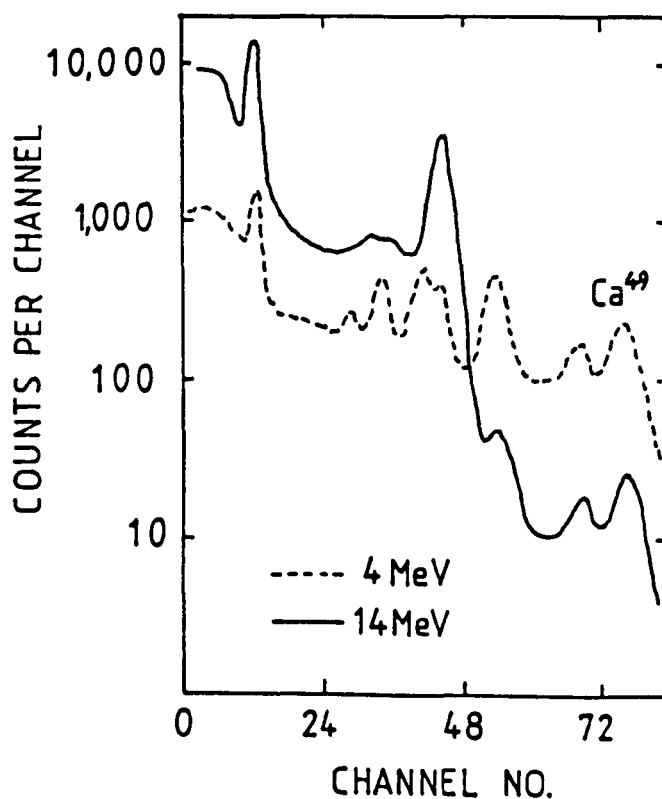
Figure 2.4 Gamma ray spectra from a phantom after irradiation with a neutron dose of 0.1 rad.

(Palmer et al, 1968)

The system has been refined to allow the analysis of parts of the body, the torso, or the whole body. The reproducibility for the torso is 5% with similar limits for a total body scan (Cohn, 1982). The equipment is rare because of the expense and although it measures calcium content directly at a variety of sites, it gives no differentiation between cortical and cancellous bone or any other calcified tissue, which becomes more common in the elderly. It can not be used on patients too often for serial measurements and is not an ideal method for general screening as radiation doses are very high, up to a few 1000 mrads (Mazess, 1983a), used so that only small errors occur in the counting statistics.

2.2.4 Quantitative Computed Tomography (QCT).

Computed tomography (CT) uses an X-ray source and receiver pair which scans around the patient and builds up a picture of a cross section through the body based on the absorption of the X-rays at different points. CT can produce a quantitative image and be used at a variety of sites to look at cancellous bone, cortical or both. The spine is imaged with X-rays from the side or the back and sections of 4 or 10 mm constructed through each vertebra, figure 2.5. The bone mineral density is found from the cross sectional area and the width of each section. Any part of the body can be imaged with computer enhanced diagrams showing the bone mineral concentration. The radiation dose can be up to 600 mrad for a full sectioned lumbar spine scan (Davies and Saha, 1985).

Bone contributes up to 30% of the average linear attenuation coefficient (CT no.) from which the resultant density is obtained, so variations in marrow composition and proportion have a large influence on the result (Genant and Cann, 1981). Marrow fat can vary up to 20% from patient to patient which can lead to uncertainties of up to 10% in the reading. Most scanners are calibrated to the Hounsfield Scale, where water is 0 and air is -1000. Thus
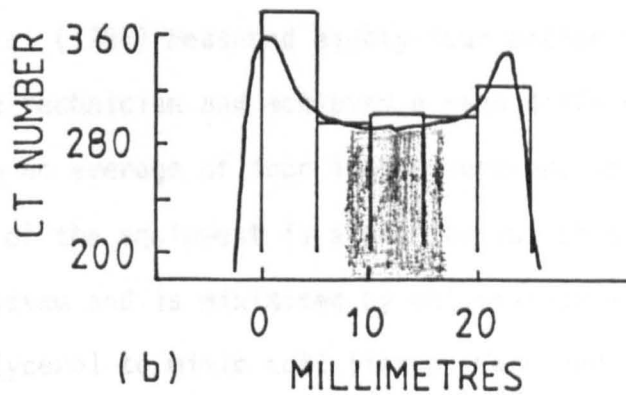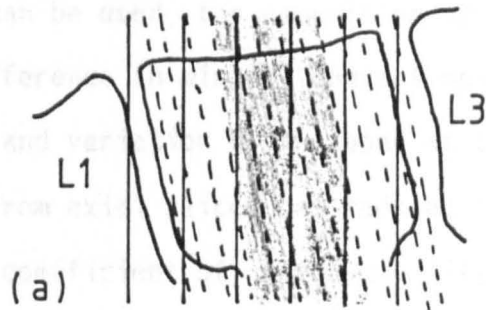
Figure 2.5 Diagram showing the reconstruction of images from computed
tomography scans.

a) Solid lines indicate original 5mm thick contiguous
transverse slices. Dashed lines show 1.35mm (one pixel)
thick reformatted true axial images.

b) CT number profile of a normal adult L2 vertebra.

(Cann and Genant, 1980)

1000 HU represents the change in linear attenuation coefficient corresponding to a density difference of 1 gm cm^{-3} in water. This is a direct indication of the volumetric density.

Because such small slices can be used, the repositioning is critical, with a 2 mm error causing a 10% difference in mineral content measured. This obviously depends on the site and variation of the bone at that site. A method of building up images from axial slices has reduced the overall errors. Genant et al (1982) suggest a coefficient of reproducibility of 1.6% but more generally only 3 to 4% is acheived. Ott et al (1986) managed 3.5% using a phantom. Rosenthal et al (1985) measured eighty-four patients twice on the same day with the same technician and achieved a mean difference of 5.5 CT units, around 5%, when an average of four lumbar vertebra measurements was used. Long term drift of the equipment is a problem but this is the case with any radiation based system and is minimised by calibration with a phantom of K_2HPO_4 in water and glycerol to mimic soft tissue. Cann and Genant (1980) suggested other calibration factors for machine drift and a detailed technique for repositioning producing a precision of 2.8% for excised samples. Many workers now use the Genant-Cann phantom and technique, but those that prefer other standards can produce very different results due to the variation in the calibration of the equipment (Steiger et al, 1987). Equipment is gradually being improved to reduce this repositioning error. One method used is to store the images so that the new scan can be compared directly with the previous image. The small sections that can be taken allow small volumes of only trabecular bone to be considered but this method gives no information about the structure of the filaments. New high resolution techniques are being tested, such as one system that has a resolution of 500 μm in vivo and an impressive 50 μm *in vitro* (Kleerekoper et al, 1987). This allows the full

detail of the trabecular structure of the vertebrae to be built up slice by slice in to a complete three dimensional pattern.

Accuracy depends mainly on the material used for calibration but there are errors introduced by scattering and the limits of pixel size, as a 4 mm slice is usually only around 3 pixels, figure 2.5. Dual energy CT helps reduce the problem of marrow variation and beam hardening (Pacifici et al, 1987) but is often considered unnecessary and the reproducibility is still fairly poor (Mazess, 1983b). It is assumed that single energy CT will give a result accurate to 8 to 10% in most cases, with this obviously being worse for severely decayed bone.

More specialised low energy iodine ^{125}I scanners have been manufactured. The precision of these instruments is remarkably good, quoted as 0.5% for several patients (Overton et al, 1981) and 0.3% for one patient measured eleven times over a period of fifteen weeks (Ruegsegger et al, 1981). However, most hospitals would prefer to buy a standard X-ray CT scanner as it would be more useful for general imaging and hence this equipment is becoming more widely available.

2.2.5 Single Photon Absorptiometry (SPA).

This specialist technique was introduced by Cameron and Sorenson in 1963. ^{125}I produces monochromatic (27.5 keV) gamma radiation which is detected by a collimated scintillation counter. The technique is based on the ability of different materials to absorb radiation at different rates. The use of a well collimated beam reduces scatter and a monochromatic beam avoids the problems of beam hardening, when lower energy photons are preferentially absorbed, distorting the beam energy distribution. Calibrated with water each day the equipment finds how much radiation is absorbed and therefore how much bone is present. It scans the peripheral bones, as the source and

detector must go either side of the site to be measured, so neither the spine nor the hip can be scanned. The usual site is the wrist which is subject to Colles fractures, often taken as an early indicator of osteoporosis.

Generally cortical bone is measured - the scanner moves along the lower arm until a gap of 8 mm is found between the radius and the ulna, figure 2.6. The two dimensional scan starts from that point in 4 mm steps so the cortex of both bones is included and the average of several scans is taken. Two sites are considered within the total scan. The proximal position is totally cortical bone, but the distal site, much nearer the wrist, is about 60% trabecular. Measurements on either side of the bones allow for a 'zero' for each patient to be calculated due to the soft tissue of the arm, although if there is any calcified tissue present this would result in a much lower value of BMC for the bone, figure 2.7. Fat produces a much lower zero line due to its lower density. The wrist is submerged in water during the measurement; this provides the equivalent of a constant layer of soft tissue. This technique measures the bone mineral content, although some versions allow for an area density measurement by normalising by the width of the bone scanned. This would only be equivalent to the actual photon path if the ulna and radius were circular.

Davies and Saha (1985) suggest the system lacks the sensitivity for individual diagnosis although Johnston (1982) thinks it is well suited to prospective studies. Most users find a 2 to 3% reproducibility (Ott et al, 1986). Again the problem is one of repositioning the patient so that the same site can be scanned each time. The arm is only positioned by the patient gripping an upright post and the arm being aligned to the side of the tank. Twist in any direction will result in the scanner finding a 8 mm gap at a different site and scanning from there.
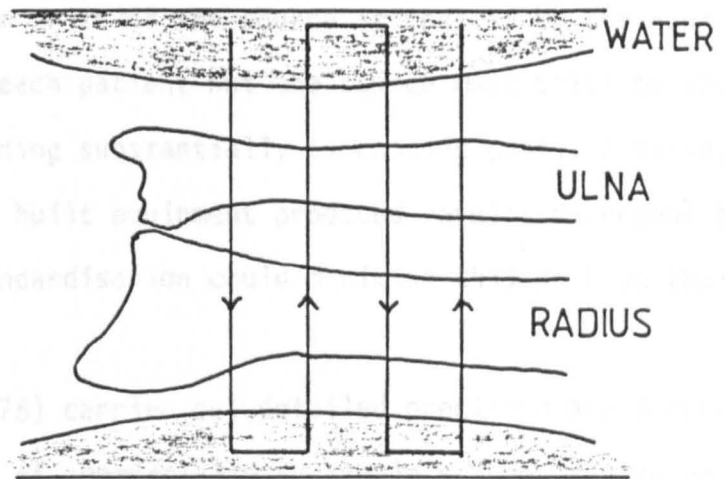
Figure 2.6 Scan pattern of a single photon absorptiometry technique across the distal radius and ulna.

Figure 2.7 Typical output of an SPA scan at the distal radius and ulna.
(Dalen and Jacobson, 1974)
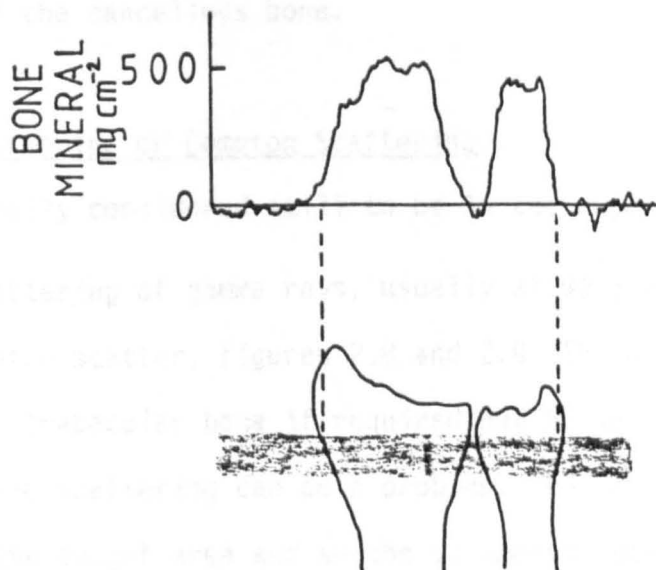
The effect of long term drift of the source is reduced by the equipment finding its own zero for each patient but the source must still be replaced more than once a year, adding substantially to running costs. A survey of commercial and laboratory built equipment produced results divergent by as much as 10%, although standardisation could minimise this problem (Mazess, 1983a).

Christiansen et al (1975) carried out detailed precision and accuracy measurements on one brand of commercially available scanner and found day to day reproducibility of 2% although for lower BMC values this was around 3 to 4% in a research situation. The radiation dose for scanning the wrist is only a few mrad.

Being cheaper than most of the alternatives, this technique is in fairly widespread use. It can not measure the spine or the neck of femur and is rarely used to measure trabecular bone although some experimenters have adapted the commercial equipment. This usually results in greater errors due to the marrow of the cancellous bone.

2.2.6 Photon Scattering or Compton Scattering.

This is generally considered still to be in the experimental stage. It is based on the scattering of gamma rays, usually at 90°, and uses the ratio of coherant to Compton scatter, figures 2.8 and 2.9. The beam can be aimed at small regions of trabecular bone if required but because of the structures involved, multiple scattering can be a problem. The technique only depends on the density of the target area and so the volumetric bone mineral density can be found. Initially attenuation corrections were made by using a second beam in the direction of the scattered radiation, but now a single source is used at 100 keV and accounts for this effect (Mazess, 1983a).

Figure 2.8 Block diagram of photon scattering equipment.

(Puumalainen et al, 1976)
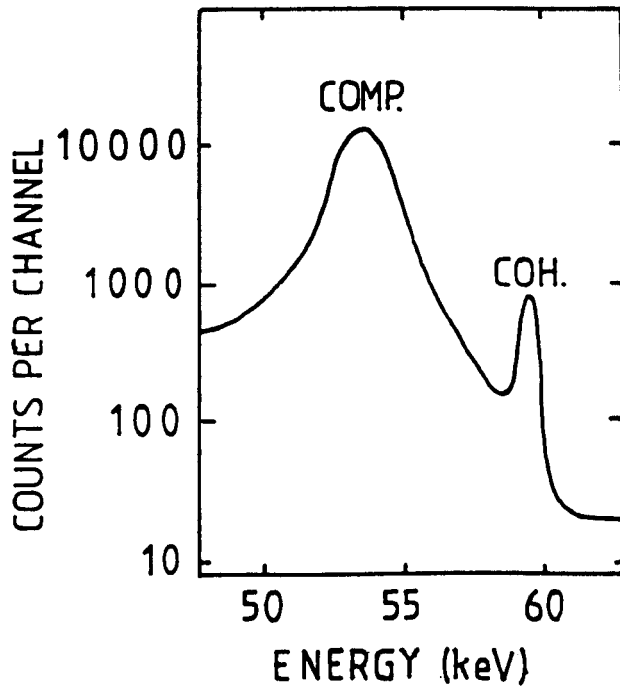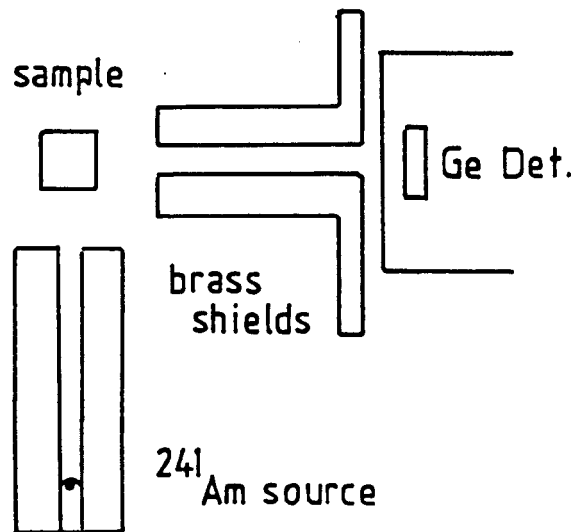
Figure 2.9 A typical scattering spectrum from a cancellous bone sample,
showing the coherant (coh) and Compton scattered (comp) peaks.
(Puumalainen et al, 1976)

Early work by Puumalainen et al appeared in 1976 and used calcium hydroxy-apatite in paraffin as test blocks with an accuracy of 2%. As a ratio of readings is used, the system is self calibrating. The os calcis proved a good site to measure for this method because of the large volume of trabecular bone. Roberts et al (1984) quote a reproducibility of 1.6% for a longitudinal study of postmenopausal women but Shukla et al (1985), measuring a phantom, gained a precision of 3% and an accuracy of 5%, somewhat worse than initial expectations. Ling et al (1982) mention that the total absorbed dose is around 700 mrad, more than a major CT scan.

2.2.7 Dual Photon Absorptiometry (DPA).

DPA uses two photon energies and is far more versatile than the single photon technique but depends on the same principle of different materials having different absorption properties. It is most frequently used to look at the spine and was first described by Krolner and Pors Nielsen (1980). ^{153}Gd is the most common source with beam energies of 44 and 100 keV, as in figure 2.10. The system requires calibration with a phantom. The technique has been used to show that patients with compression fractures of the spine are on average two standard deviations below the control populations, and this has been used to define the severity of the osteoporosis (Mazess, 1983a). The lumbar part of the spine is measured because of its accessibility but it is the thoracic region that fractures first. The lumbar spine is formed of generally larger and stronger vertebrae.

Although this technique can look directly at the spine, any results are a function of the total path and so involve cancellous and cortical bone. The total bone mineral content is found, but can be normalised by the area of the scan to give an area density measurement. Wahner (1982) has done measurements on the hip with comparable reproducibility to the spine and has suggested a

fracture threshold. A threshold would be required for scanning the general

population but unfortunately the cost of this system is prohibitive. Krolner

and Pors Nielsen (1982) report that although there is a good correlation in

normals between dual and single photon absorption (spine and wrist) there is

none for those classed as osteoporotics.

43 keV

———— UNATTENUATED

----- THROUGH PHANTOM

100 keV

ENERGY (keV)
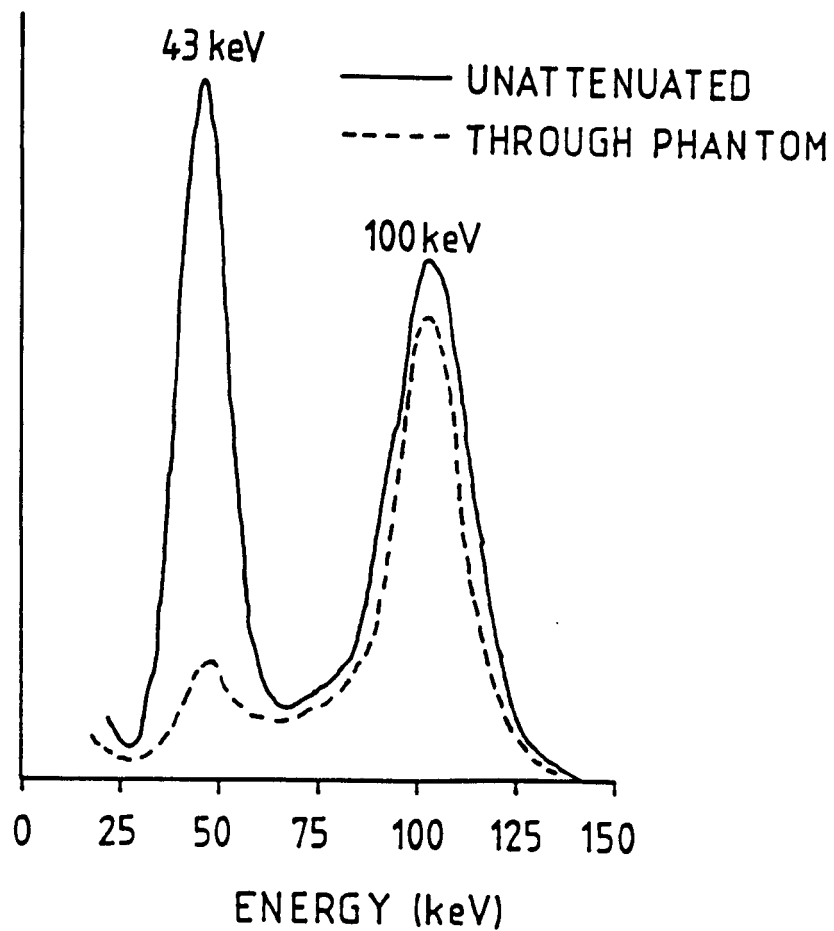
Figure 2.10 The ^{153}Gd spectra typical of dual photon absorptiometry.
(Mazess, 1983b)

Machine drift can be a problem, as with all radiation techniques. Ott et al (1986) found changes of 1 to 2% per annum with a 2 to 5% change on renewal of source. The coefficient of variation on measurements was 3% for this group, comparable to single photon absorption. Zero settings can be found along the whole spine, and the use of the ratio of two energies eliminates the problem of soft tissue and marrow variations. Wide variations of tissue thickness only produce changes of around 3% in the reading (Mazess, 1983a). This is an expensive system with an annual cost for source replacement. The radiation dose is in 10s of mrads (Davies and Saha, 1985).

The variety of possible measuring sites is a great advantage but the reproducibility is no better than many other systems due to source decay and repositioning of the patient. The cost is prohibitive for a general screening procedure.

A new technique using a range of energies from a continuous X-ray spectrum rather than two specific energies is being developed. The energy range allows more complete correction for the marrow and soft tissue (Jonson et al, 1986).

2.2.8 Quantitative Histomorphometry.

Although invasive, bone biopsies are often taken to diagnose some bone diseases, commonly from the iliac crest. A stainless steel cutting tool called a trochar which takes a core of 3 to 8 mm diameter is used. Many parameters can then be found from detailed microscopy of ultra fine sections from the sample. Trabecular surface area, density and bone and pore dimensions, osteoblast and osteoclast surfaces and degree of mineralisation are the usual parameters studied and may be used to find the degree of osteoporosis (Teitelbaum, 1983). Typically, the ratio of volume of tissue to volume of anatomic bone is used. If the value is within the range expected for the age

and sex, then simple osteoporosis is diagnosed, accelerated osteoporosis if it is below this range.

New and expensive equipment is available that digitises images and carries out the analysis under software control. Older methods include point counting on a variety of grids and the two methods of analysis produce a small variation in results (Meunier, 1983). Osteoporosis is easily identified since osteoid parameters are within normal levels but trabecular density is much reduced. New grid techniques use the branching of the trabeculae as an index of the bone state, to indicate the patterns of bone loss and the effect of treatments (Garrahan et al, 1986).

Studies have been carried out to find age dependent effects on the femur and all agree that volumetric and surface densities decrease with age. Some research suggests that whole trabeculae are removed with the remaining filaments substantially thinned, while other authors report thickened trabeculae (see section 1.4).

Histomorphometry is not a contender for a diagnosis technique that can be applied as a general scanning procedure. However, it is still used in experimental trials and provides useful parameters for the evaluation of bone turnover. One histomorphometry method is described in detail in chapter 6 and is used to obtain information about typical trabecular dimensions for the bone samples used in this work.

In conclusion, there is still much debate over which diagnostic system should be recommended for general use, and there is a long way to go for a system to screen the perimenopausal population cheaply and safely. Ultrasound offers the possibility of a method that may be used safely again and again on the same subjects. There have been many attempts to produce a satisfactory system using a variety of techniques.

2.3 Ultrasonic Diagnosis of Osteoporosis.

Many techniques have been used to study various parameters of bone in the laboratory, but this section reviews those methods that look towards *in vivo* diagnosis.

2.3.1 Velocity Based.

Velocity is the most common parameter measured to try and differentiate between bone qualities. Many groups have experimented using a variety of techniques, most commonly time of flight in both transmission and pulse-echo mode but also critical angle, sing-around, etc. As the porosity of bone changes with decay, so will the velocity of sound.

One research group that has worked on this for some time is based at UCLA. They used time of flight measurement for echoes from the cortical boundaries, figure 2.11. The outer and inner surfaces produce clear echoes spaced by a time which is dependent on the thickness of the bone and the velocity and hence bone quality. *In vivo* measurements were done by positioning a 5 MHz transducer at a site decided by X-ray imaging of the femur. Radiographic measurements are used to determine the thickness of the cortex (Andre et al, 1980).

Reproducibility is quoted at 2% for such measurements but total uncertainties are around 7%. This technique was compared to single photon absorption, both methods measuring the proximal radius (Greenfield et al, 1981). Again, radiogrammetic measurements were needed to find the path length of the ultrasound. No actual correlations were calculated in this study and volunteers were categorised by one vertebral fracture, with many patients classed as 'possible'. There was a wide scatter of results with many patients producing high BMC by photon absorption and low values by ultrasonic velocity and vice versa.
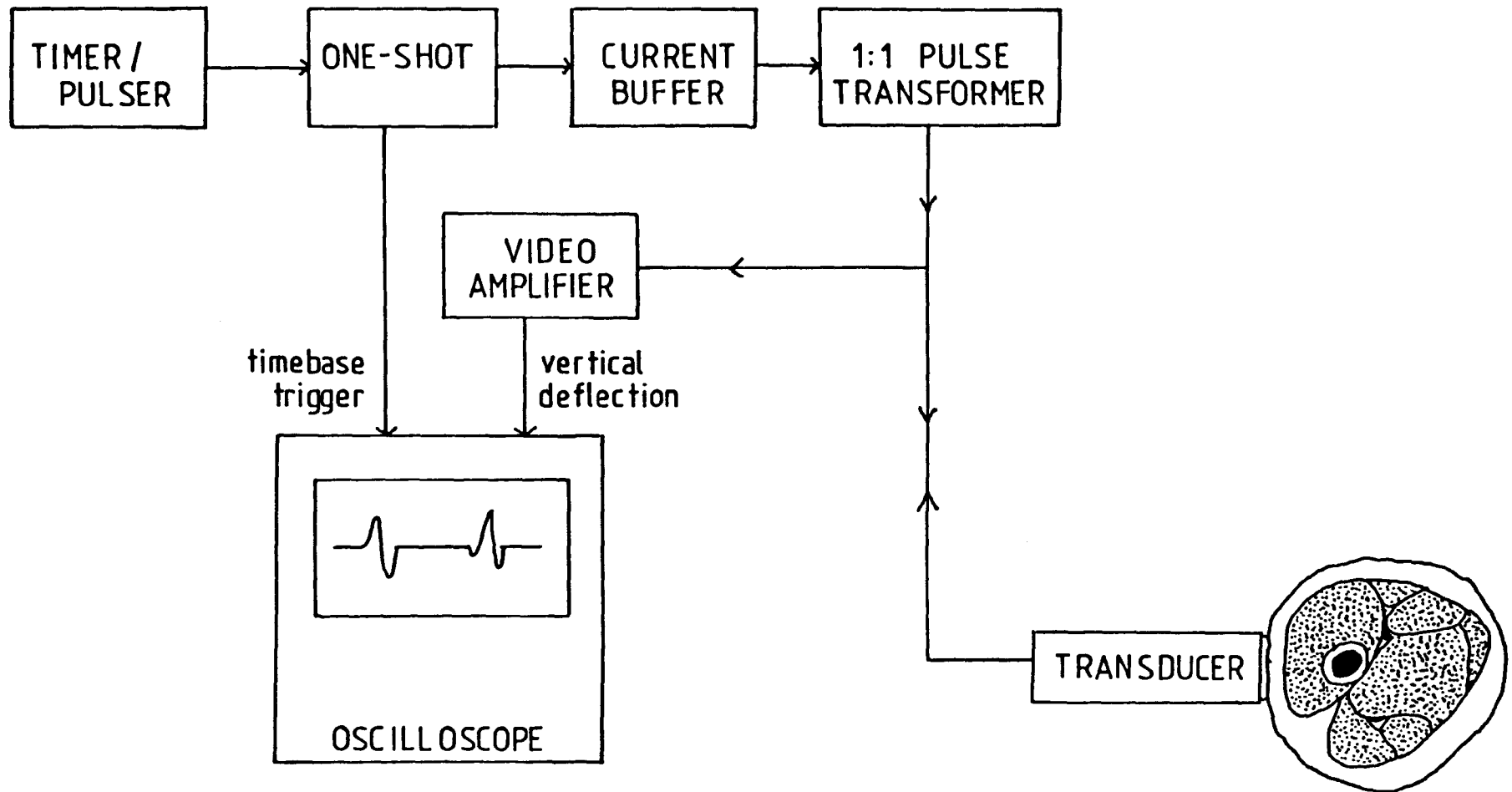
Figure 2.11 Schematic diagram showing the ultrasonic apparatus and the anatomical cross section of the femur, the site scanned. (Andre et al, 1980)

Yoon and Katz (1976) have carried out detailed analysis of the structure of cortical bone, reporting that it fits to a hexagonal crystalline structure. They have carried out velocity measurements in relation to the crystallographic axis of the bone samples. So far measurements have been *in vitro* but differences have been found between pathological samples. They report good correlations for longitudinal velocity, both parallel and orthogonal to the crystal axis, transverse velocities, and elastic constants to the physical density of the bone, with osteoporotics always distinct from the normal readings (Meunier et al, 1982). Several techniques were used to find the velocity of sound including pulse transmission time of flight, pulse echo overlap and the right angle reflector method. A few frequency dependent observations were done showing a linear dependence on 1 to 10 MHz frequency by both longitudinal and transverse waves (Katz and Yoon, 1984). Most of the measurements were done at 5 MHz.

A completely different approach has been used by Saha et al (1984). Assuming a constant ultrasonic velocity, they used time of flight measurements in pulse echo mode to deduce the thickness of the cortex in embalmed human femurs. Many readings were taken of only three bones and compared to the same number of repeated readings done by QCT. The ultrasound appeared to correlate far better to the actual cortical thickness than the QCT did. However, it must be assumed that the bones used were all normal, with little density variation between them so that it was acceptable to assume a constant ultrasonic velocity. This technique would become rapidly more inaccurate as the cortical bone becomes more porous, altering the velocity of the sound.

Biro et al (1983) have developed a transmission imaging system using the variations of velocity and phase throughout a two dimensional scan to produce a computer enhanced image. The system has been used to study *in vitro* specimens with optical and X-ray microscopy also taken for comparison. The

imager picked out lower velocity regions in osteoporotic femurs and has also been used to look at implants and teeth.

2.3.2 Resonance Based.

The resonant frequency of a long bone is dependent on the velocity of sound (hence bone density) and the length of the bone. Jurist (1970) has studied many aspects of various bones using resonance as well as velocity and phase measurements. In *vivo* measurements are carried out using a loudspeaker at the elbow and an accelerometer at the wrist, detecting waves travelling along the ulna. Typical response graphs were obtained to show the effect of the arm in the incorrect position. The parameter FL (resonance frequency multiplied by the length of the bone) is used as an index and found to a precision of at most 5%. The length of the ulna is measured using a metric rule from the elbow to the wrist. Muscle tension was found to affect the resonant frequency by as much as 15%. The technique has been used on groups of osteoporotic and normal volunteers, the former being defined on the basis of any non-traumatic fracture. Osteoporotic men and women did tend to form separate distributions but there was some overlap with age matched normals (Selle and Jurist, 1966). This is perhaps not surprising as a 'normal' could suffer a non-traumatic fracture the day after testing which is a problem with any population study. Doherty et al (1974) suggest the effect is due to the bone mass and the stiffness of the surrounding soft tissue rather than the bone deformation itself. Spiegl and Jurist (1975) produced mathematical models including one that fitted Doherty's hypothesis but did not fit the experimental results.

Other techniques use a ringing effect to find the resonant frequency of the bone with an impulse rather than a regular sinusoidal driving force (Saha and Lakes, 1977). Instrumented hammers are used to generate an impulse both *in vivo* and *in vitro* and accelerometers used to detect the stress waves. The

effect of the skin was modelled by layers of rubber over and around the bone *in vitro*. Different ways of coupling the accelerometer to the limb produced a variety of efficiencies at picking up the signal. Unfortunately loads which held the accelerometer in place became too heavy for the volunteers as obviously the heavier the load the better the coupling. Overlying tissue introduced errors of some 16% to the absolute accuracy of the response of the bone but presumably could be accounted for in comparative work.

2.3.3 Attenuation Based.

These studies fall into two groups - those done on cortical bone, as all the previous examples of ultrasonic diagnosis have, and those done on cancellous bone, the better indicator of osteoporosis.

Garcia et al (1978) used a transmission technique for both continuous wave (actually long pulse) and short pulse inputs, with Fourier analysis of the received signal carried out by computer to obtain the frequency dependent characteristics from 2 to 8 MHz using 5 MHz transducers. Interface losses were accounted for by the software. Reproducability of measurements was said to be 'good'. Polyethylene and lucite were measured as a test of the system and then bovine femurs were examined. It was noted that the scatter of the bone results was greater than that of the man-made samples. The experimenters then started decalcifying the bones. Small changes, up to 10%, could not be detected ultrasonically, but more substantial decalcification produced significantly lower ultrasonic attenuation. Shear waves were also investigated as they will be present *in vivo* by mode conversion, and found to be more greatly attenuated than the longitudinal waves.

Hyodynmaa et al (1986) used pulse echo mode on the femoral cortex using the same experimental apparatus as Andre et al (1980) for the velocity measurements, figure 2.11. Two sites were used where the inner and outer

cortical surfaces are most parallel, identified by radiography. The attenuation of the sites was calculated from the echoes displayed on an oscilloscope. A 2 MHz transducer was used and the cortical thickness measured from the radiographs. The velocity and attenuation were measured on 17 healthy volunteers, the former being fairly consistent. However, three attenuation values came out far smaller than the rest (one was even negative) and were put down to inaccuracies of measuring the cortical thickness at the sites scanned. This suggests there was no guarantee that the site scanned ultrasonically was the site measured on the radiograph. The group intend to expand the technique to frequency dependence.
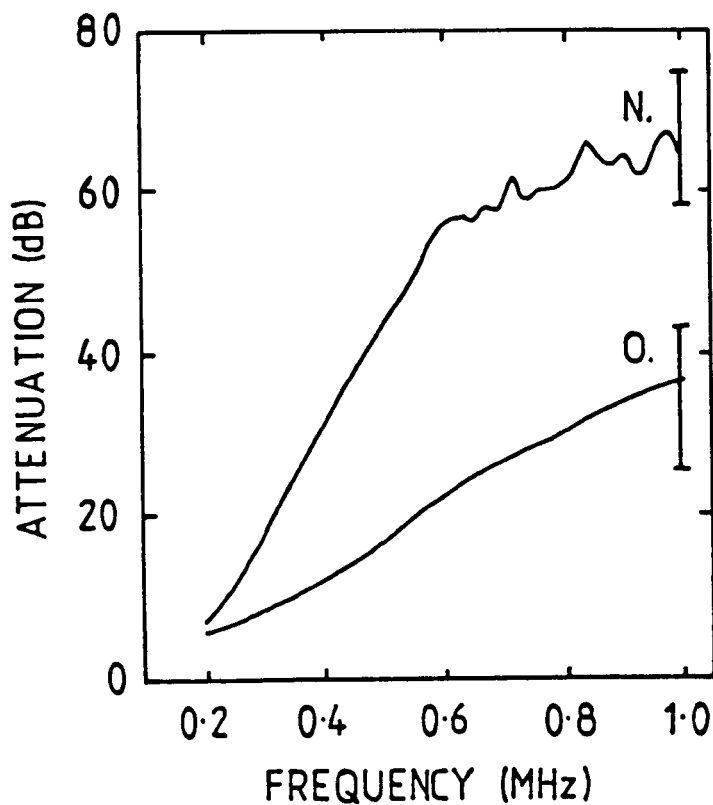
Figure 2.13 Comparative traces for a young normal female (N) and an elderly osteoporotic female (O). The error bars show the range of the populations tested.

(Langton et al, 1984)
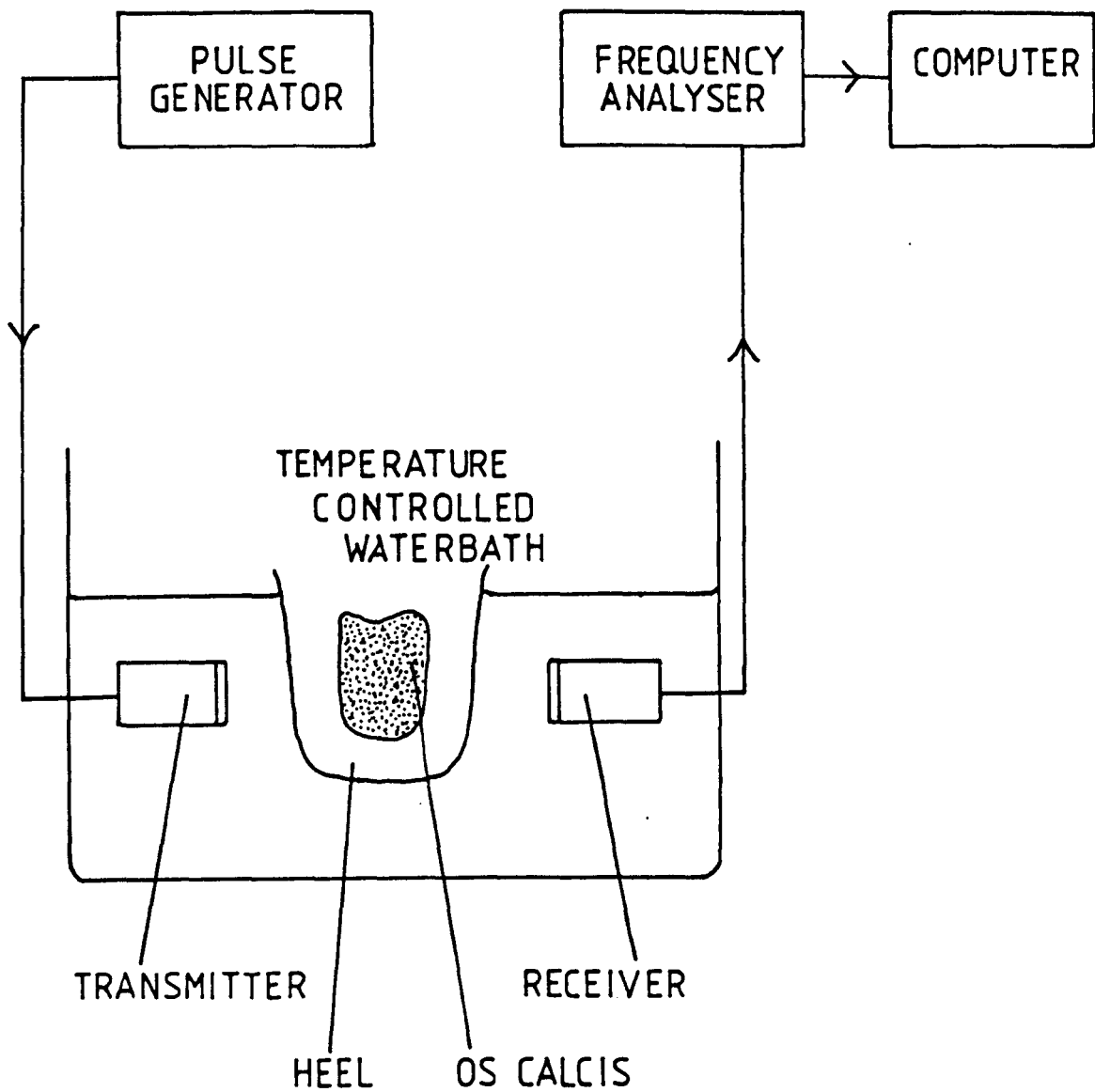
Figure 2.12 Schematic diagram of the system used by the broadband ultrasonic attenuation technique.

(Langton et al, 1984)

Langton et al (1984) have developed the only ultrasonic system that looks at cancellous bone, the broadband ultrasonic attenuation technique (BUA). Because of its structure, much lower frequencies than those used by the previous examples must be used by the pulse transmission method, 200 kHz to 1.0 MHz. This system finds the frequency dependence of the attenuation of the os calcis. Initially, radiographs were taken of the foot to ensure that the correct site in the heel bone was being scanned, but this positioning has been related back to anthropomorphic measurements of the foot for more general use (Langton, 1984).

A 1 MHz transducer is excited by an impulse and the received signal is analysed on a spectrum analyser, figure 2.12. It was found that normal cancellous bone^{attenuated} most of the higher frequencies in the range, producing a steep gradient on the graph of attenuation as a function of frequency, while osteoporotic bone transmitted all the frequencies, producing a much smaller gradient as illustrated in figure 2.13. This gradient from 200 to 600 kHz is used as the index of bone quality.

Studies were carried out on a female population and it was found that those who had fractured a neck of femur formed their own distinct group, although the bone loss in this case could be due to inactivity after the recent fracture (Langton, 1984). Many clinical studies are in progress at the moment, including one scanning a total of one thousand ladies aged 70 or over. The subjects are then traced to identify those who suffer a non-traumatic hip fracture, to see if the ultrasonic method can be used as a predictive index. The early results look encouraging and show a true predictive rate of 73.3% after only one year for all fractures suffered (Miller and Porter, 1987). One group has compared a wide range of rheumatoid patients using the ultrasonic system and single photon absorption (Poll et al, 1986). Overall there was a good correlation of 0.8 but there were one or two volunteers who produced very

different readings for the two sites. Hosie et al (1987) obtained a correlation of 0.66 between BUA and their own low dose gamma-ray computed tomography of the distal radius, with a better correlation of 0.81 for the proximal site, composed mainly of cortical bone. Petley et al (1987) compared BUA readings to SPA of both the wrist and the os calcis, using an adapted SPA tank. The correlation was 0.72 for the SPA of the wrist and BUA of the os calcis and 0.75 for both measurements on the heel bone. The fact that the same site was measured in the latter case did not improve the correlation between the measurements.

A recent review of the work involving the BUA technique was given by Langton (1987) and discusses the work already done as well as further investigations that must be carried out. Little detail is known of the propagation of the ultrasound through the cancellous bone and how it relates to the bone density and the trabecular structure. The ultrasonic slope and the attenuation at 200 kHz are used to uniquely characterise each os calcis. A different bone may have the same slope but a different attenuation at 200 kHz, even when normalised for bone width. It may be that one parameter gives an insight in to the bone mineral content while another parameter gives more information about the trabecular pattern.

The aim of this thesis is to attempt to explain the ultrasonic propagation in terms of the bone density and structure. The following two chapters describe the ultrasonic experiments carried out to obtain the parameters representing the range of cancellous bone from normal to osteoporotic. There is also a comparison of the BUA technique with another diagnostic method, and chapter 5 describes the comparison of BUA with the compressive strength of the cancellous bone. Chapter 6 discusses a histomorphometry technique used to

different readings for the two sites. Hosie et al (1987) obtained a correlation of 0.66 between BUA and their own low dose gamma-ray computed tomography of the distal radius, with a better correlation of 0.81 for the proximal site, composed mainly of cortical bone. Petley et al (1987) compared BUA readings to SPA of both the wrist and the os calcis, using an adapted SPA tank. The correlation was 0.72 for the SPA of the wrist and BUA of the os calcis and 0.75 for both measurements on the heel bone. The fact that the same site was measured in the latter case did not improve the correlation between the measurements.

A recent review of the work involving the BUA technique was given by Langton (1987) and discusses the work already done as well as further investigations that must be carried out. Little detail is known of the propagation of the ultrasound through the cancellous bone and how it relates to the bone density and the trabecular structure. The ultrasonic slope and the attenuation at 200 kHz are used to uniquely characterise each os calcis. A different bone may have the same slope but a different attenuation at 200 kHz, even when normalised for bone width. It may be that one parameter gives an insight in to the bone mineral content while another parameter gives more information about the trabecular pattern.

The aim of this thesis is to attempt to explain the ultrasonic propagation in terms of the bone density and structure. The following two chapters describe the ultrasonic experiments carried out to obtain the parameters representing the range of cancellous bone from normal to osteoporotic. There is also a comparison of the BUA technique with another diagnostic method, and chapter 5 describes the comparison of BUA with the compressive strength of the cancellous bone. Chapter 6 discusses a histomorphometry technique used to

obtain structural parameters for the range of cancellous bone. These details are needed, together with the ultrasonic information, for the application of any theory.

The theoretical aspect of the ultrasonic propagation is considered in chapters 7 and 8. The former is a review of the theories which evaluate ultrasonic propagation in composite materials, and includes a discussion of all the possible attenuation mechanisms. The final chapter contains the detailed application of three theories to cancellous bone.

Chapter Three.

EXPERIMENTAL TECHNIQUE.

3.1 Introduction.

The experimental work was intended to mimic the broadband ultrasonic atten-
uation (BUA) system to be used in hospitals, designed by Langton (1984) and
currently manufactured by Walker Sonix Inc. Only *in vitro* samples were to be
measured in the laboratory. The tank allowed general positioning of both the
transducers and the sample.

This chapter discusses the technique and problems associated with measuring
the ultrasonic velocity, the frequency dependent attenuation and the
preparation of the bone samples. In the final section the errors and
limitations of the system are analysed and the precision of the technique
calculated and discussed.

3.2 Apparatus.

The technique is based on a broadband pulse transmission method and the
measurements are carried out in a water bath using the water as the couplant
between the transducers and the sample. A voltage spike is applied to the
transmitter and the received signal fed to a frequency analyser. The equipment
is controlled by a computer which also handles the data and calculates the
attenuation of the ultrasound. The parameter used to categorise the bone is
the frequency dependence of the attenuation over the range from 200 to 600
kHz, and is referred to as the ultrasonic or attenuation slope.

3.2.1 Experimental System.

Two 1.0 MHz broadband transducers (Panametrics V302), with a face diameter of 30 mm, were mounted in a specially constructed scanning tank, figure 3.1. One transducer was mounted on an arm connected to an anti-backlash stepping motor that was geared to give a minimum step of 0.5°. The motor was controlled via an IEEE network and a Bede Scientific Instruments 4-phase unipolar stepping motor driver by a BBC microcomputer. Both transducers could move in and out along the main axis of the rig so that the central position was always the centre of rotation. Each transducer was in a mount that could be adjusted for tip, swivel and to a small extent height and lateral position. The central beam axis was at a known position above the central sample table, which rotated independently of the transducers and could be raised by inserting machined spacers between it and the main stand.

The tank (0.5 m by 0.5 m by 0.3 m deep) was filled every day with cold water and Diagnostic Sonar Echowet added at a concentration of about 0.7%.

The transmitter was excited by a 1 kV spike of 3 µs duration at a repeat rate of 600 kHz, which allowed distinct pulses to be received and analysed. The receiving transducer was mounted on the rotating arm, although the system was found to be completely reversible. The received pulse was fed either to an oscilloscope or to a 3585A Hewlett Packard spectrum analyser, with the option of a gating pulse being applied by a Brookdeal boxcar pair (gate type 415 with scan delay generator 425A), figure 3.2.

The spectrum analyser was connected via an IEEE network to the BBC micro, which then controlled the data acquisition. Readings could be taken at a specific frequency or over a range. Limits of 0 to 2 MHz were usually displayed on the analyser so readings could be taken every 2 kHz. The time sweep ensured that each pulse was completely analysed.
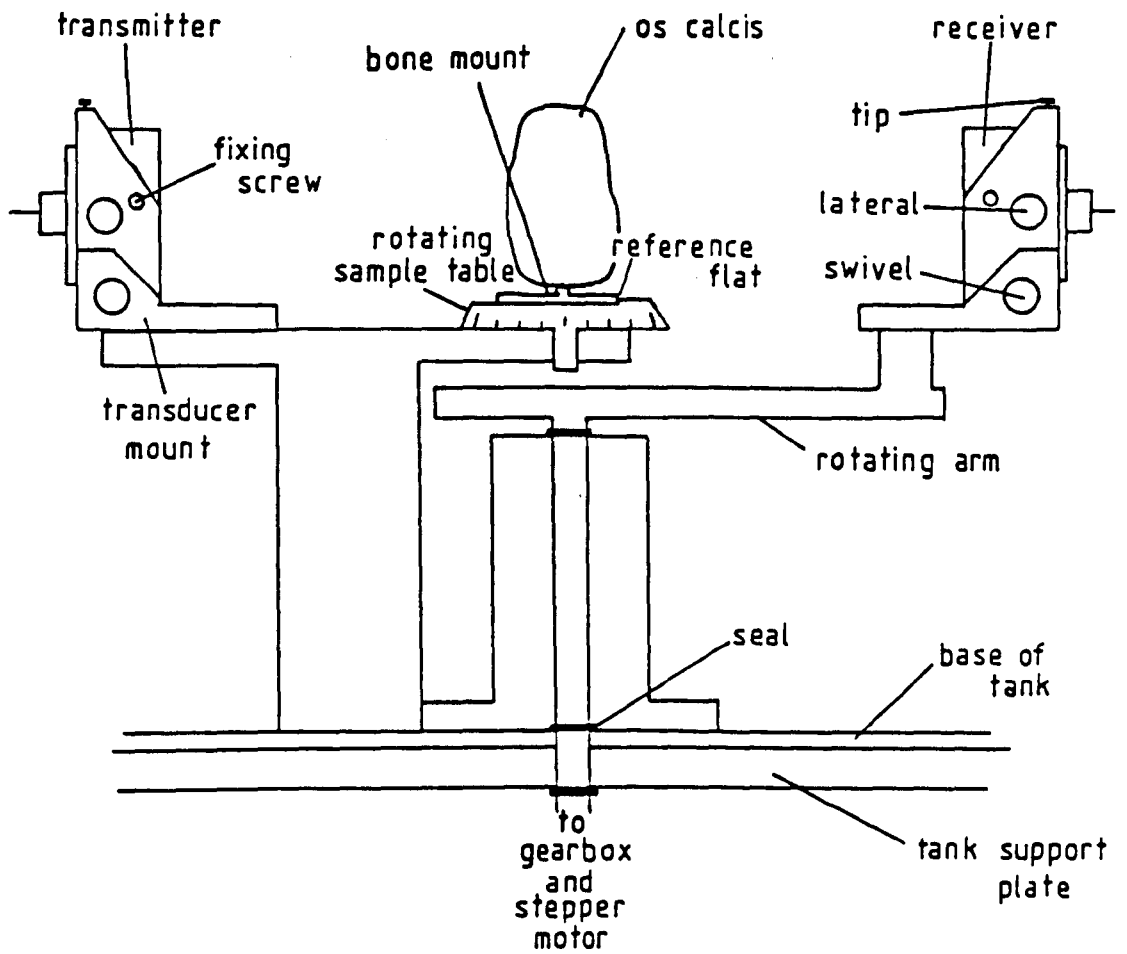
Figure 3.1 Diagram showing the detail of the transducer holders and sample mount in the ultrasonic tank.
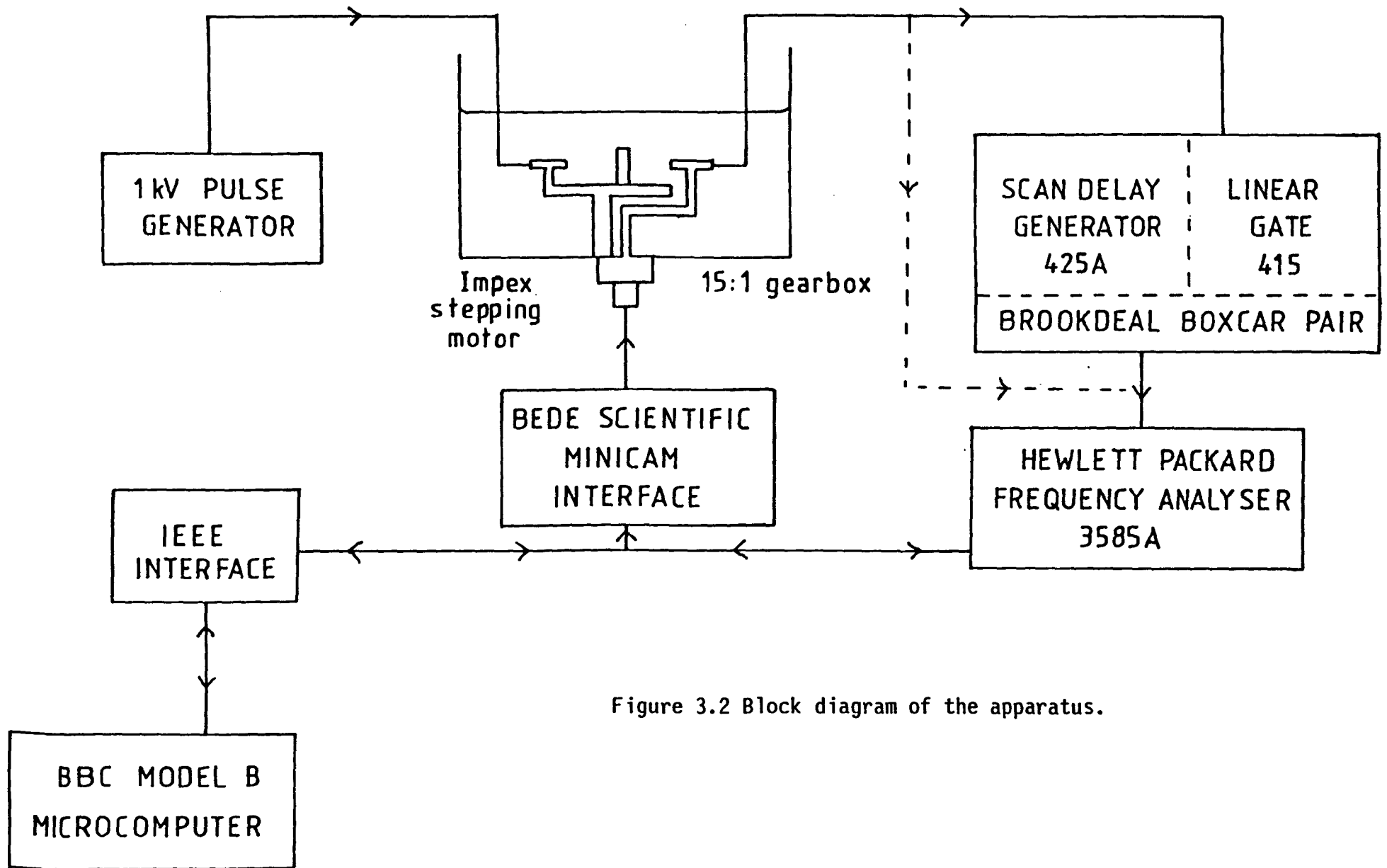
Figure 3.2 Block diagram of the apparatus.

The index used by Langton (1984) is the gradient of the attenuation of ultrasound as a function of frequency over the range from 200 to 600 kHz (often referred to as the attenuation slope or ultrasonic slope). Over this range, Langton suggested that the attenuation can be approximated by a linear dependence on frequency so the best fit straight line is calculated. The linear fit is less accurate at the low frequency end of the range. The computer first reads and stores the water trace, which acts as a calibration. A typical water trace was stored on disc for comparison. The spectrum analysis of the signal transmitted through the sample under test was then read by the computer from 100 kHz to 1.2 MHz and subtracted from the stored water trace to find the attenuation, as all the readings were taken in dBm.* A least squares regression was applied to the attenuation values from 200 to 600 kHz (the index used) and also from 200 kHz to 1.0 MHz, and the slope values calculated were printed together with the errors associated with the fitting procedure.

A typical output from the system appears in figure 3.3, where the amplitudes at certain frequencies are listed. The spectrum of the pulse transmitted through the water, the amplitudes of the signal transmitted through the sample and the spectrum analysis of the attenuation from 100 kHz to 1.2 MHz are also presented. Finally the attenuation at certain frequencies is calculated and given, followed by the two slopes produced by the least squares fitting.

The computer was also programmed to take readings at specific frequencies if required and controlled the stepping motor for the scatter experiments.

3.2.2 Evacuating.

Ultrasound is highly attenuated by air and the presence of the wetting agent is insufficient to allow measurements to be taken immediately. The

---

* decibels magnitude
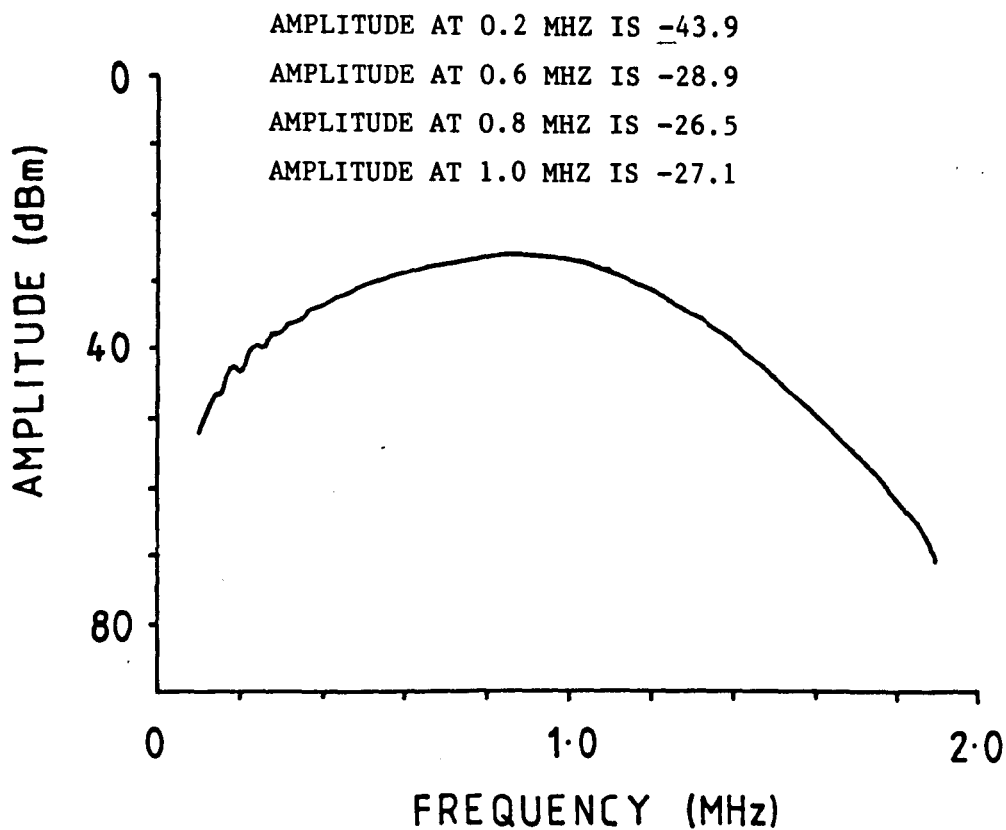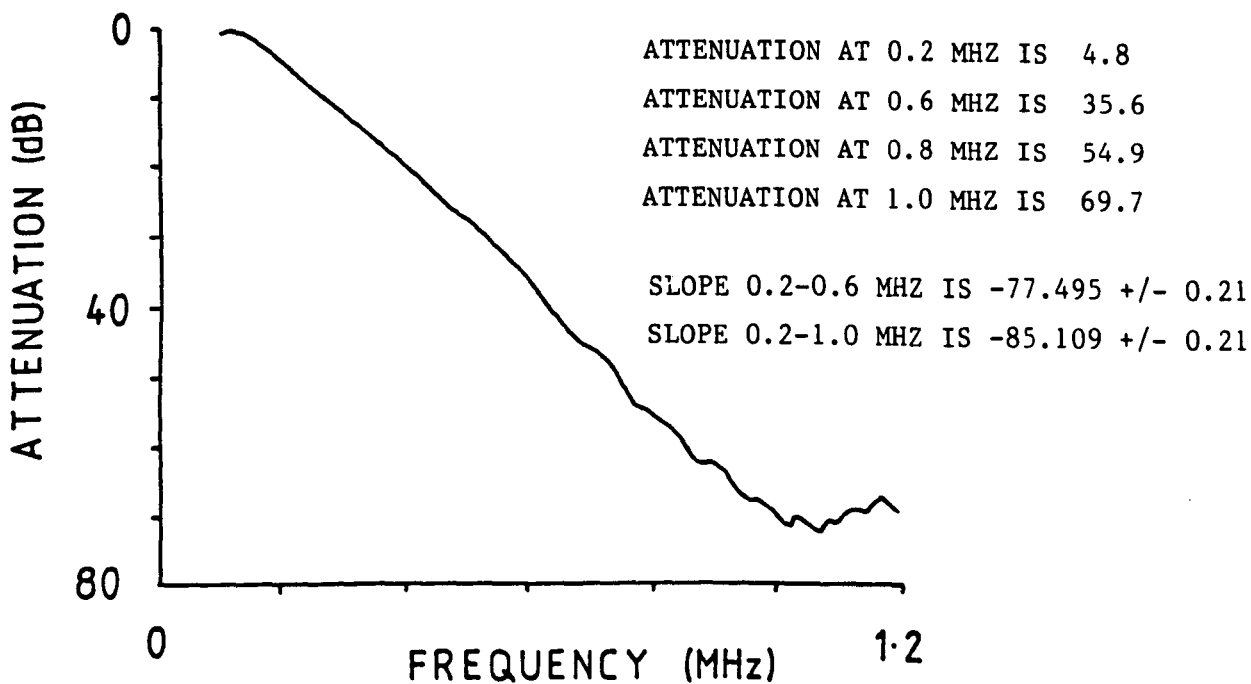
Figure 3.3 Typical output from the apparatus, showing the water trace,
amplitude values, attenuation trace, attenuation values and the
calculated slope with errors associated with the calculation.

system was left for over an hour after setting up to allow the water to settle, air bubbles to disperse and the electronics to warm up. Samples were also allowed a settling time of around 10 minutes in the water, although there was usually little change in the reading after 5 minutes. The main aim of this stabilising period is to allow air bubbles introduced by placing the sample to escape. With samples such as whole os calces it would take much longer for complete temperature equalisation; however as the bones have been stored in water overnight beforehand and extra cold water added (see below) such differences would be insignificant.   Langton (1984) found that the bone samples have an attenuation at 200 kHz of under 8 dB *in vivo*. In practise, any slight introduction of air would increase the attenuation substantially, and of course, no air would be present *in vivo*. To ensure that no air pockets are left inside the samples, the bones were evacuated using a water powered vacuum pump connected to a dessicator containing the samples immersed in water. Soaking the bones proved insufficient so the samples were left evacuating overnight at a pressure of 30 inches of mercury on a Bowden guage prior to any measurements being made. In the morning, the water was topped up with fresh cold Echowetted water to equilibriate the bones to the conditions under which they would be measured. The bones had to be re-evacuated every night prior to measurements as the water in the tank still contained a fair amount of dissolved air despite the presence of Echowet.

3.2.3 Transducers and Diffraction.

The transducer frequency profile was taken as the ideal water trace, centred around 0.9 MHz and extending from 100 kHz to 1.8 MHz. The divergence of the beam is frequency dependent so it may be considered that the total broad bandwidth beam is composed of many monochromatic beams. The lower frequency ones will have a nearfield/farfield boundary close to the transducer
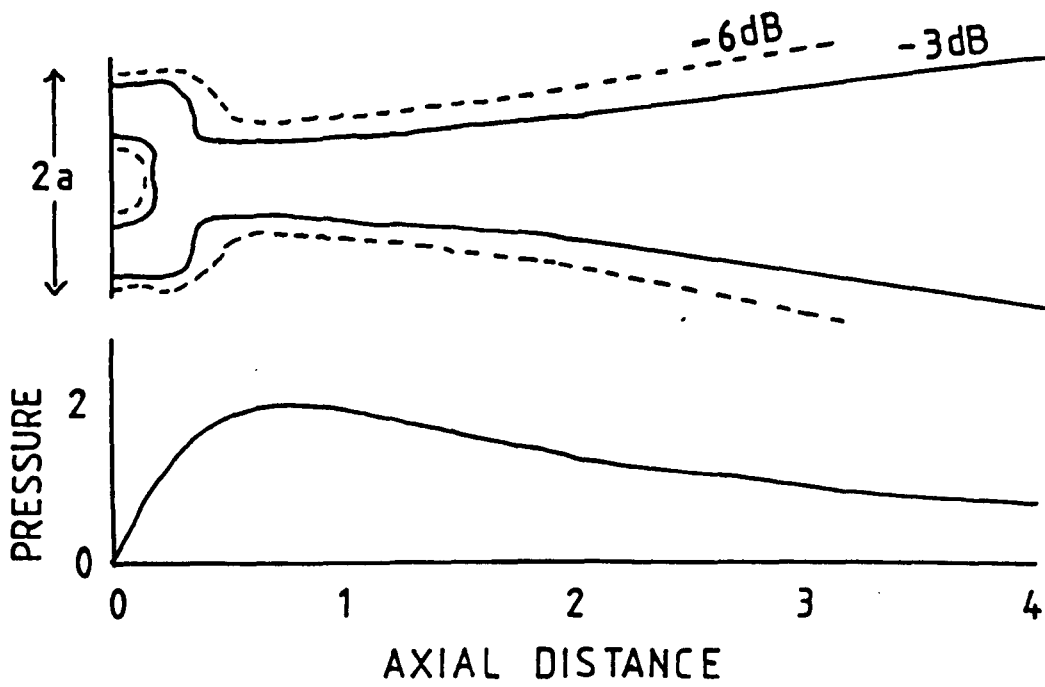
Figure 3.4 Sound pressure contour plots and pressure magnitude along the axis for a transducer of radius a with wavelength λ such that

a) a/λ = 1.0
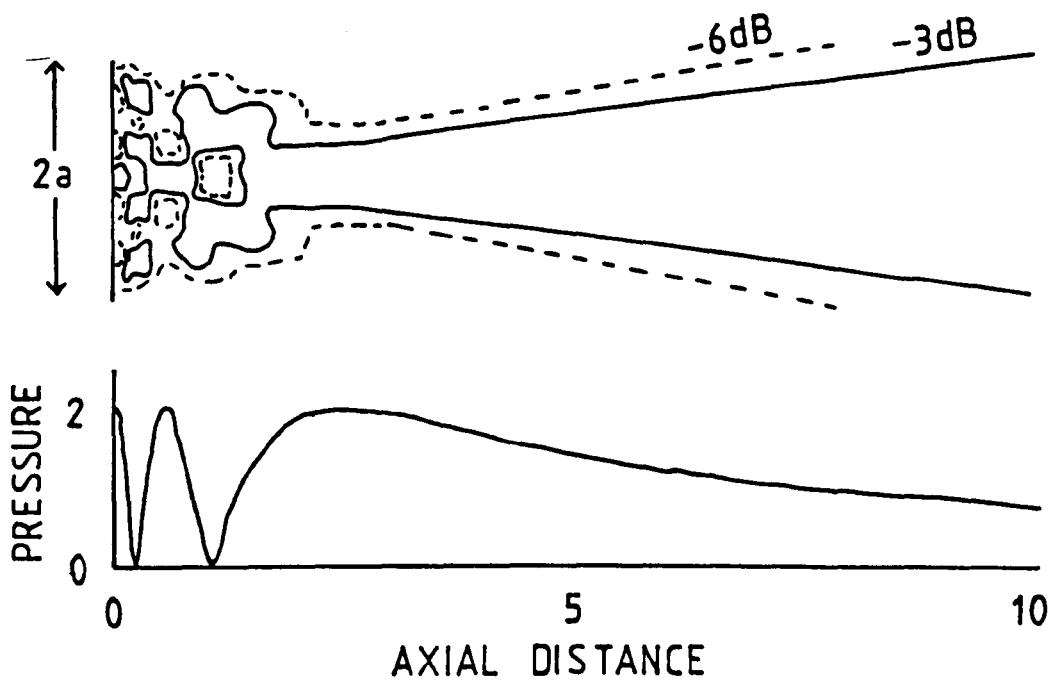
b) a/λ = 2.5, ie. increased frequency.

(Zemanek, 1971)

face, with the beam diverging after this distance. As the frequency increases the field boundary moves further from the face of the transmitter, figure 3.4. The intensity of the beam in the farfield is evenly distributed, and it is preferable because of this to carry out measurements in the farfield of both the transmitter and receiver.

As the transducer moves further from the sample, the ultrasonic beam propagating through the sample becomes much wider. With a large test block this effect will be negligible, as the beam will not reach the edges of the sample. The heel bone is only slightly larger than the transducer diameter, so a small divergence will result in the edges of the bone affecting the beam, figure 3.5.
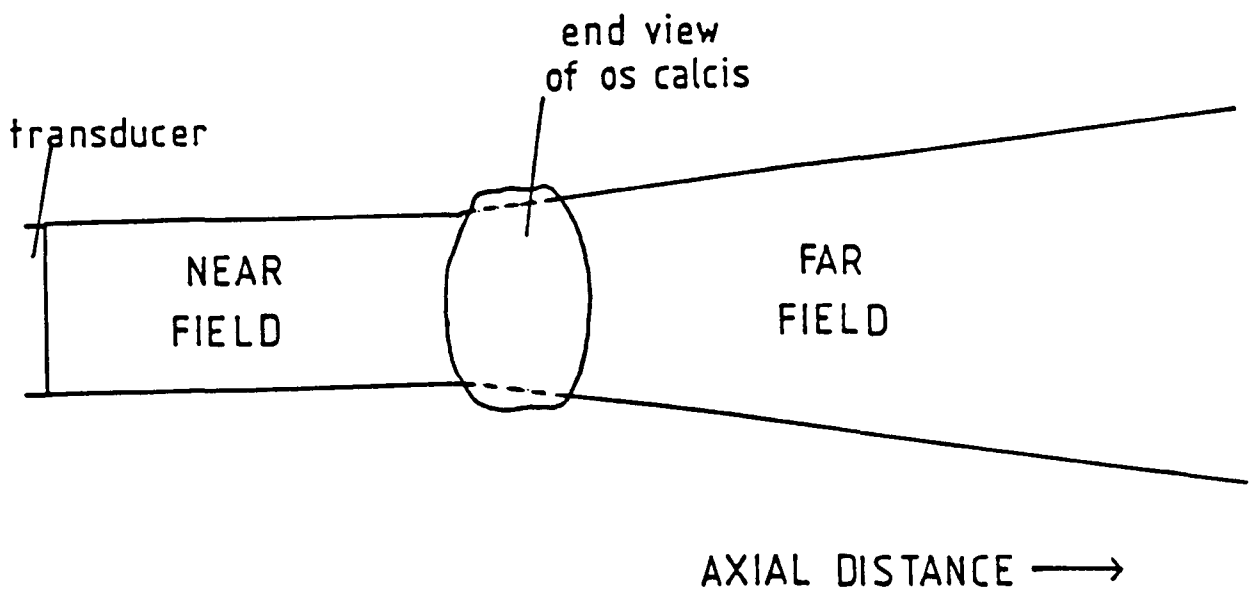
Figure 3.5 Simplified diagram showing the beam contour with respect to a typical os calcis.

The diffraction effect means that the results obtained are dependent on the transducer separation with respect to the sample. The clinical BUA system has the transducers fixed at 15 cm apart, with the heel placed centrally between them. This separation was based on the largest foot available. A series of measurements were carried out varying the transducer separation with the bone remaining in the central position. The water trace was taken for each separation and used to calculate the attenuation. Reflections from the sample table would be present in both the water trace and the signal transmitted through the bone, so their effect will be nullified by the subtraction of one trace from the other.

The attenuation at the low frequency end (up to 300 kHz) decreased as the transducers were moved symmetrically away from the sample, resulting in an increasing slope value, figure 3.6. This is probably because the diverging beam is reflected towards the receiver particularly by the rounded end of the heel bone. The lower frequencies are more divergent and so are affected more, although as the transducers become more widely spaced higher frequencies will also be involved. This hypothesis is backed by similar measurements carried out on a cylindrical core, figure 3.7. As there are no surfaces outside the core region the attenuation slope did not increase once the beam covered the whole cross section of the core. There would however be more reflections within the sample in this case. The results shown are typical of several samples tested.

Ideally, measurements should be carried out in the farfield of the transducers, but with small samples the beam must also be well collimated. Thus measurements were carried out with a transducer separation of 17 cm. This meant that from 200 to 600 kHz, the range in which the slope is taken, the sample is in the farfield of the transmitter and the receiver. However, comparisons were done with the samples measured adjacent to the transmitter
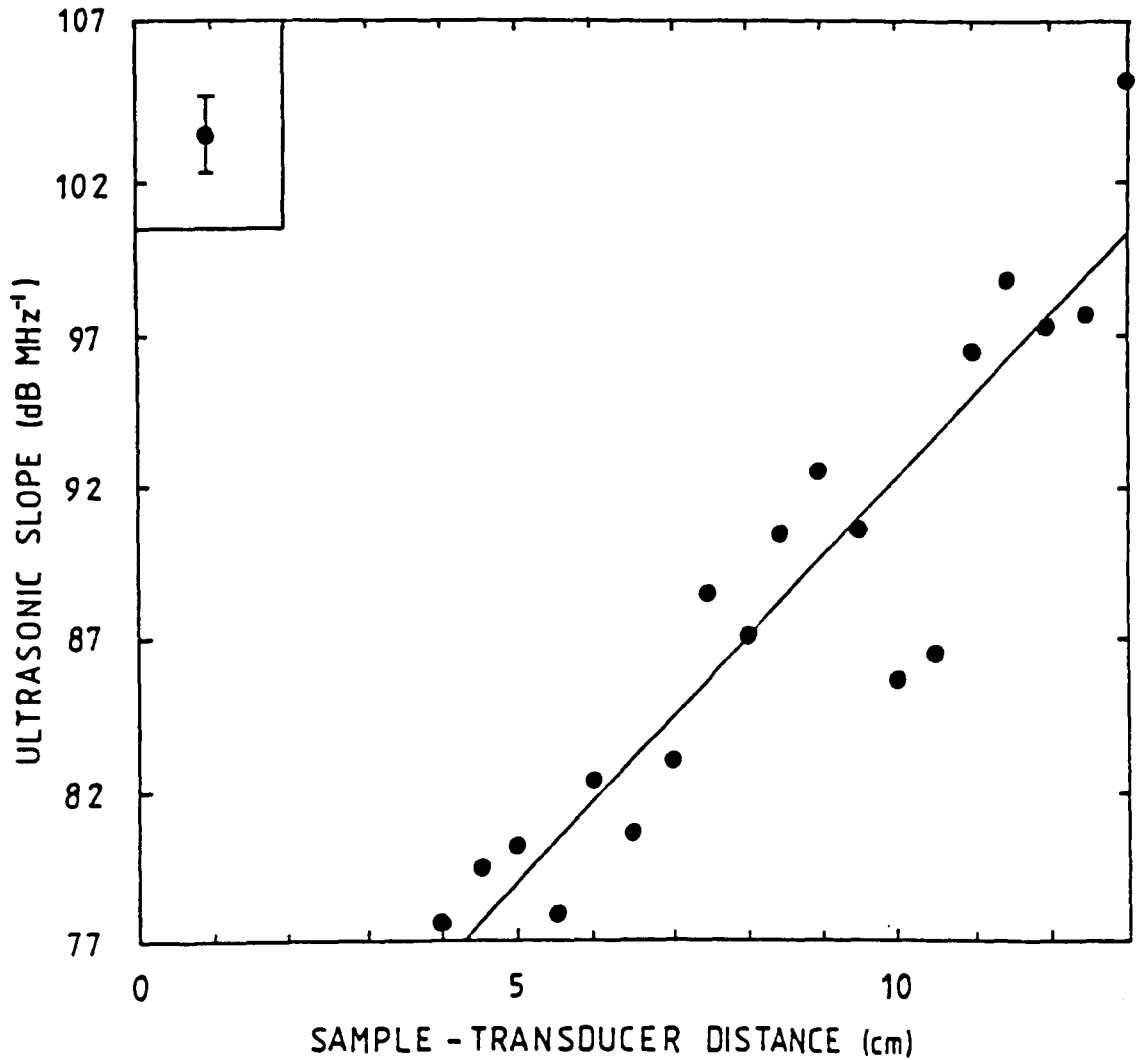
Figure 3.6 Diffraction results for a typical os calcis. A graph of the ultrasonic slope plotted against the sample - transducer separation.

Error bars on this and all subsequent graphs represent the standard error of measurement (section 3.5).
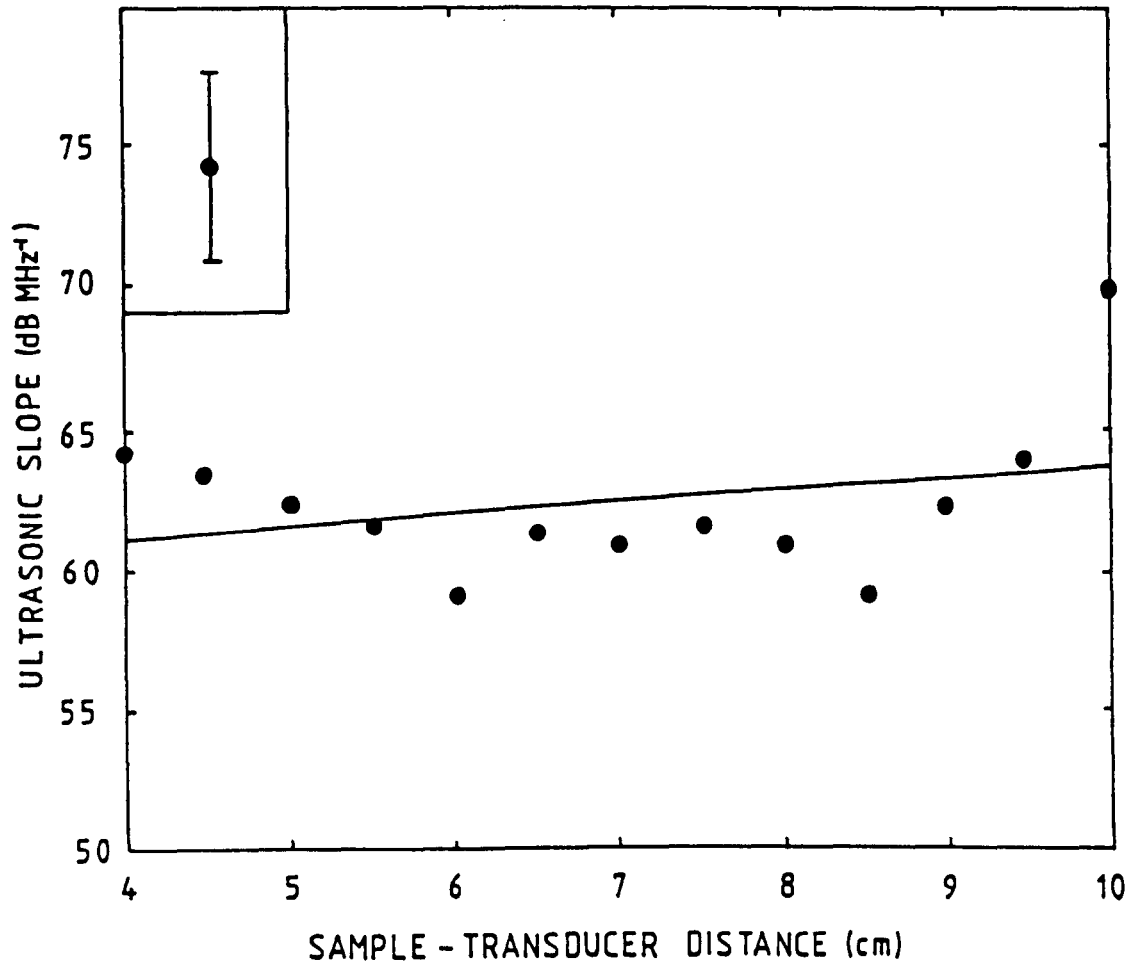
Figure 3.7 Diffraction results for a typical bone core. A graph of the
         ultrasonic slope plotted against the sample - transducer
         separation.

face with the receiver 13.5 cm away from the sample centre. This meant the beam entering the sample was well collimated as for all but the lowest frequency the sample was in the nearfield, with the receiver being in the farfield for the whole frequency range. Although this probably produced some difference in the actual propagation of the beam, there was an insignificant difference in the gradient of the attenuation as shown by the graph of readings for both the os calces and the cancellous samples in the near and far field positions, figure 3.8 and 3.9.

For the results in the two positions to be identical, the graphs would show a regression line of gradient 1.0, passing through the origin, and all the points within an experimental error of the line. For the whole os calces, figure 3.8, the gradient is 1.05 +/- 0.05 and the intercept is -3 +/- 4. The results are evenly distributed with the exception of the bone with the highest slope value, which produced a much larger reading at the near field position. The cancellous samples showed a similar trend, figure 3.9, with the higher slope values the furthest from the regression line. The unpaired 2-tailed Student's t-test showed no significant difference between the group of results for either pair of measurements.

It can be concluded that as long as all bones are measured in an identical known fashion, comparisons can be made between the readings.

3.2.4 The Attenuation Measurements.

The ultrasonic attenuation of the bone as a function of frequency from 200 to 600 kHz is the parameter used in the present technique.

The attenuation can be due either to scattering, absorption, reflection from surfaces or a combination of these mechanisms, figure 3.10. The main aim of this thesis is to relate the attenuation to the physical parameters of the cancellous bone, such as the density and trabecular structure. However, the
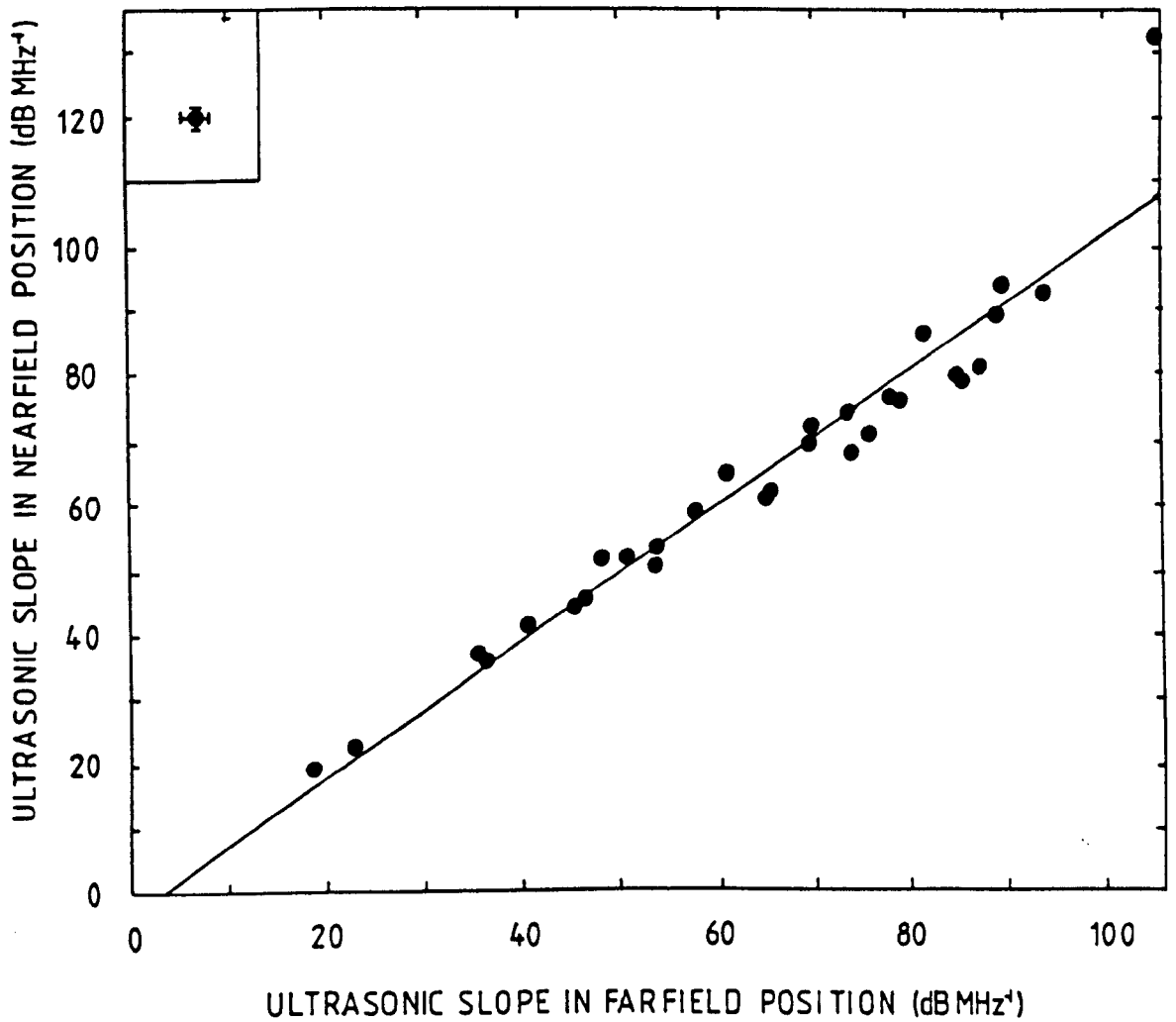
Figure 3.8 Nearfield - farfield comparison of ultrasonic slope for 30
os calces.

$$\text{gradient} = 1.05 +/- 0.05$$

$$\text{intercept} = -3.2 +/- 3.6$$

$$\text{correlation coefficient} = 0.97$$
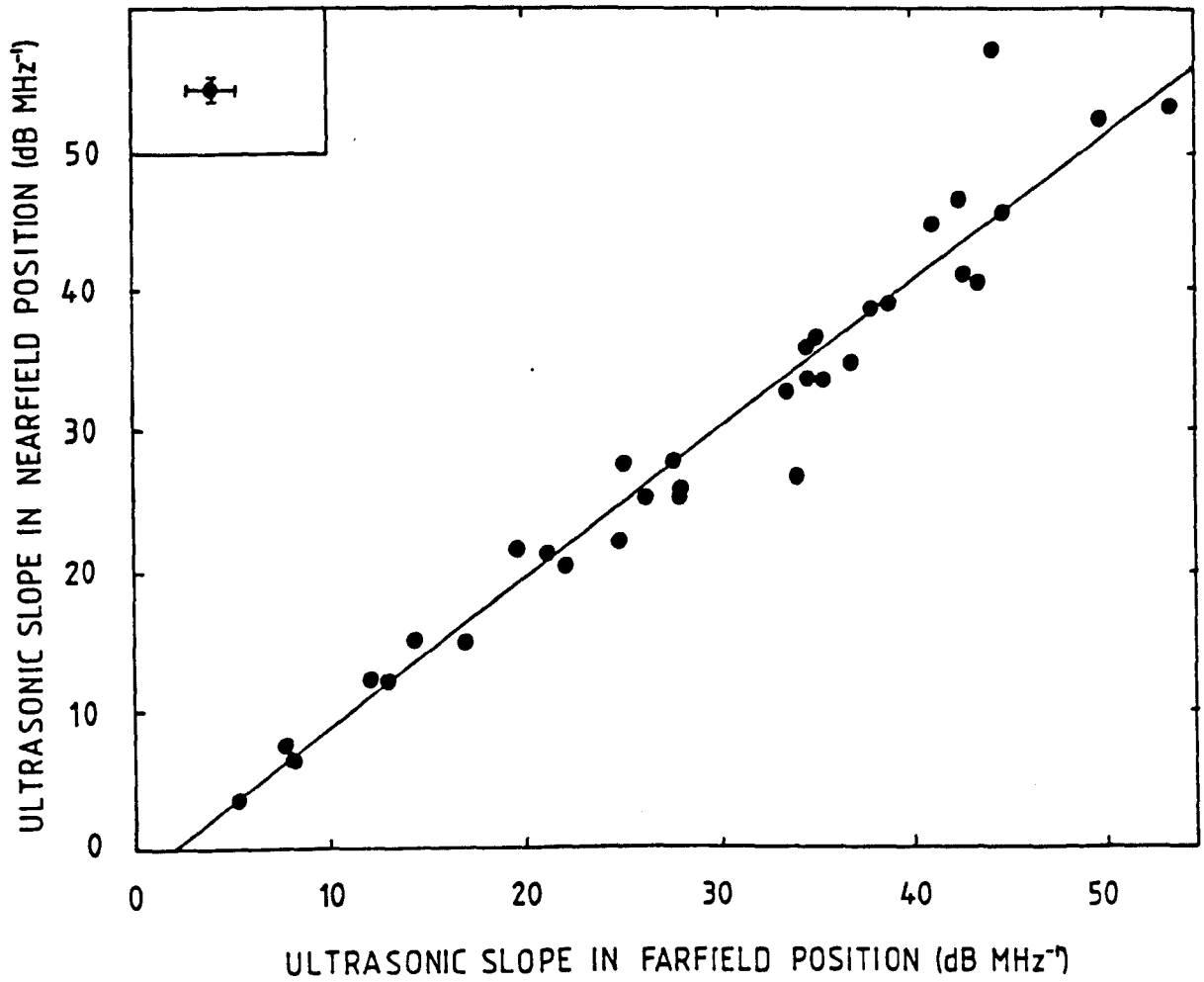
Figure 3.9 Nearfield - farfield comparison of ultrasonic slope for 33
cancellous cores.

$$gradient = 1.06 +/- 0.04$$

$$intercept = -2.0 +/- 1.4$$

$$correlation \ coefficient = 0.97$$
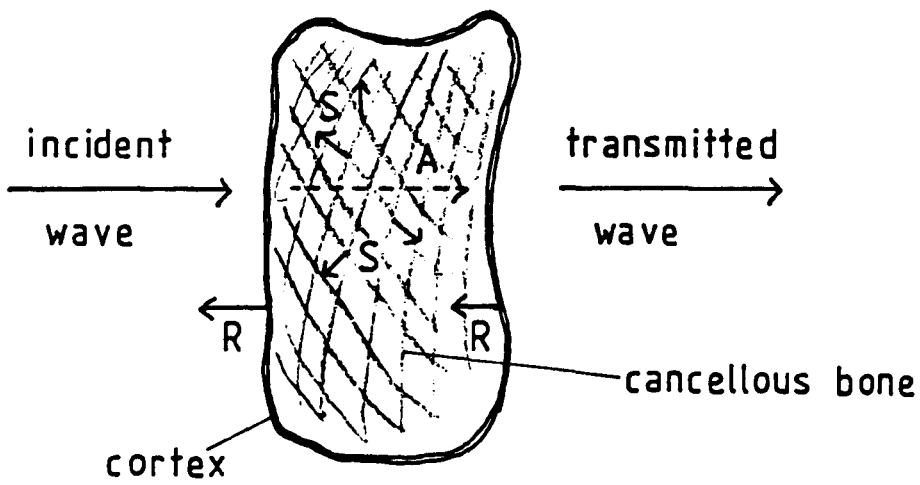
Figure 3.10 Idealised diagram of possible attenuation mechanisms in an os

calcis: R   reflection

                                S   scatter

                                A   absorption.

reflection losses from the surfaces of the bone will have some effect on the attenuation values obtained. Irregularity of shape may also affect the frequency dependence of the reflection losses, especially as the broadband beam will be more divergent for the lower frequencies.

The density and velocity of sound in the regularly shaped cancellous cores were used to calculate the impedance. Reflection losses for the purely cancellous bone were only very small (see section 4.4). However, for actual bones these losses will increase because of the irregularity of the surface and the layer of cortical bone on the outside. Although the cortex layer is generally less than the wavelength of the ultrasound, it may have some effect. An example of this can be demonstrated by the whole core measurements and those of the cancellous cores. The slope per unit length changed irregularly, depending on the core. If the ends were particularly uneven the slope per cm reduced much more for the cancellous core than if the ends were fairly smooth. In some cases there was a negligible difference, indicating the thinness of the cortical layer. This effect is discussed in more detail in section 4.4.2.

Losses due to the irregularity of the bone surface would be extremely difficult to account for *in vivo* and are difficult to describe numerically *in vitro.* All the attenuation measurements discussed in the current work include these reflection losses.

3.2.5 Gating.

The Brookdeal Boxcar Pair allowed variable gating of the time dependent signal, to exclude echoes from the sample and the mountings in the tank.

Figure 3.11a shows the time dependence of the receiver output for propagation in water. The initial large peak is associated with the main ultrasonic pulse and is followed by low level noise and subsequently with two small peaks of low frequency which are reflections from the central sample

Figure 3.11 Time dependence of ultrasonic signal amplitude for

a) water trace

b) typical os calcis.
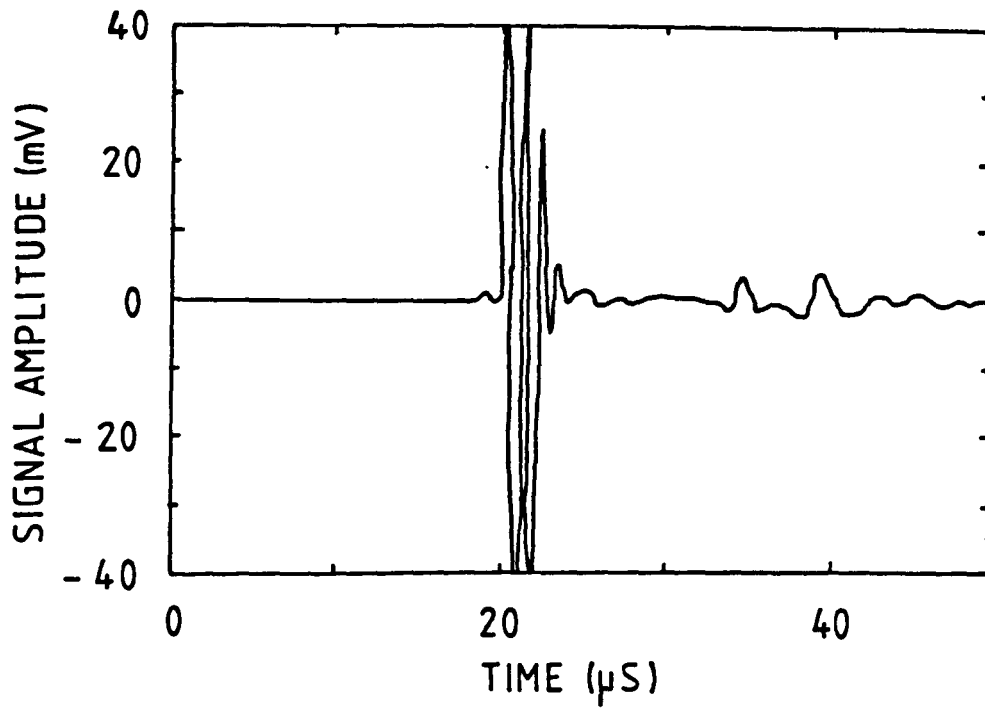
(a)
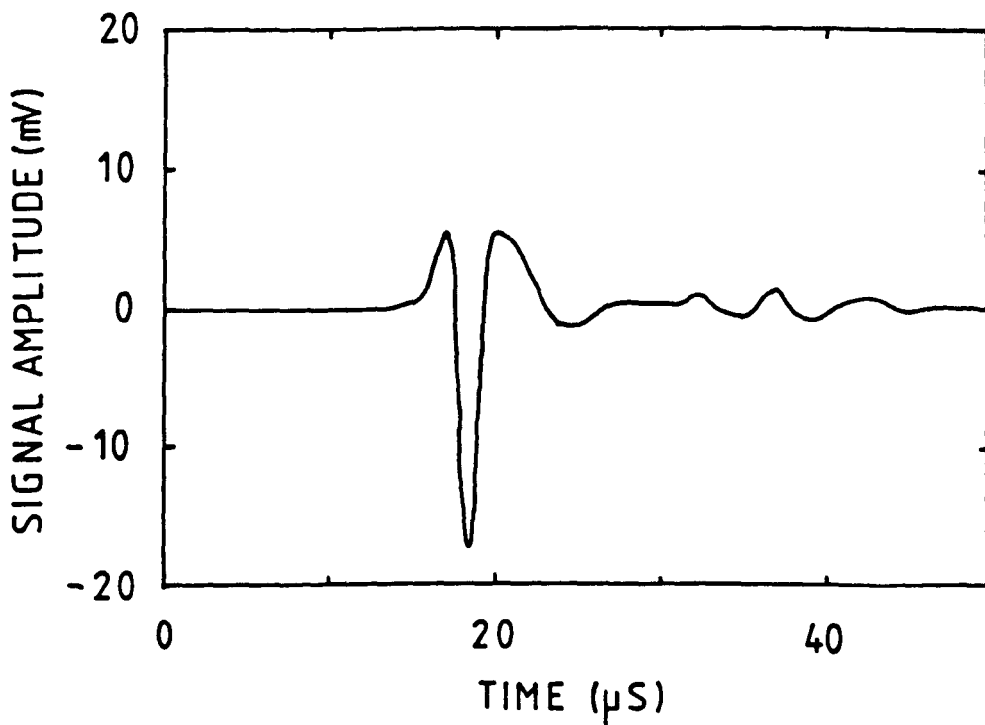
(b)

table. Similarly, a bone produced an initial peak followed by a low level low frequency noise train, figure 3.11b. A gate of approximately 10 μs could easily be applied to cut out most of this noise train including the two echoes from the mount. This resulted in little difference in the attenuation slopes of, for example, the cancellous cores, figure 3.12. The gradient of the regression line is 0.99 +/- 0.03, suggesting that the gated and ungated readings are completely comparable, but the regression line has an intercept of 1.3 +/- 0.9, in agreement with the mean difference between the pairs of readings of 1.02 dB MHz^{-1}. However, differences in results are entirely consistent, shown by the regression line gradient, so the overall measurements are unaffected for comparisons between results. There appeared to be no effect from multiple reflections in the cancellous samples as the attenuation was generally too great. The situation often described by scatter and absorption experiments (Nicholas and Hill, 1975) where a wavetrain consists of two peaks representing the surface effects from the sample edges spaced by a signal considered to be from the bulk of the material could not be applied here. This is due to the high attenuation and fairly small ultrasonic path length.

10 μs is still large with respect to the initial received pulse, but as a shorter gate was applied reproducibility rapidly decreased because it became difficult to define the beginning and the end of the main pulse. With different sized samples and a variation in velocity the gate could not be left in a fixed position.

The effect of the 10 μs gate on the attenuation gradient was negligible, so in general gating was not included; the subtracting of the water trace can be considered to cancel many of the effects gating would normally remove, such as the reflections from the central mount.

With solid samples, such as cortical bone, multiple reflections did become a problem. Unfortunately these samples were usually less than 5 mm thick, and
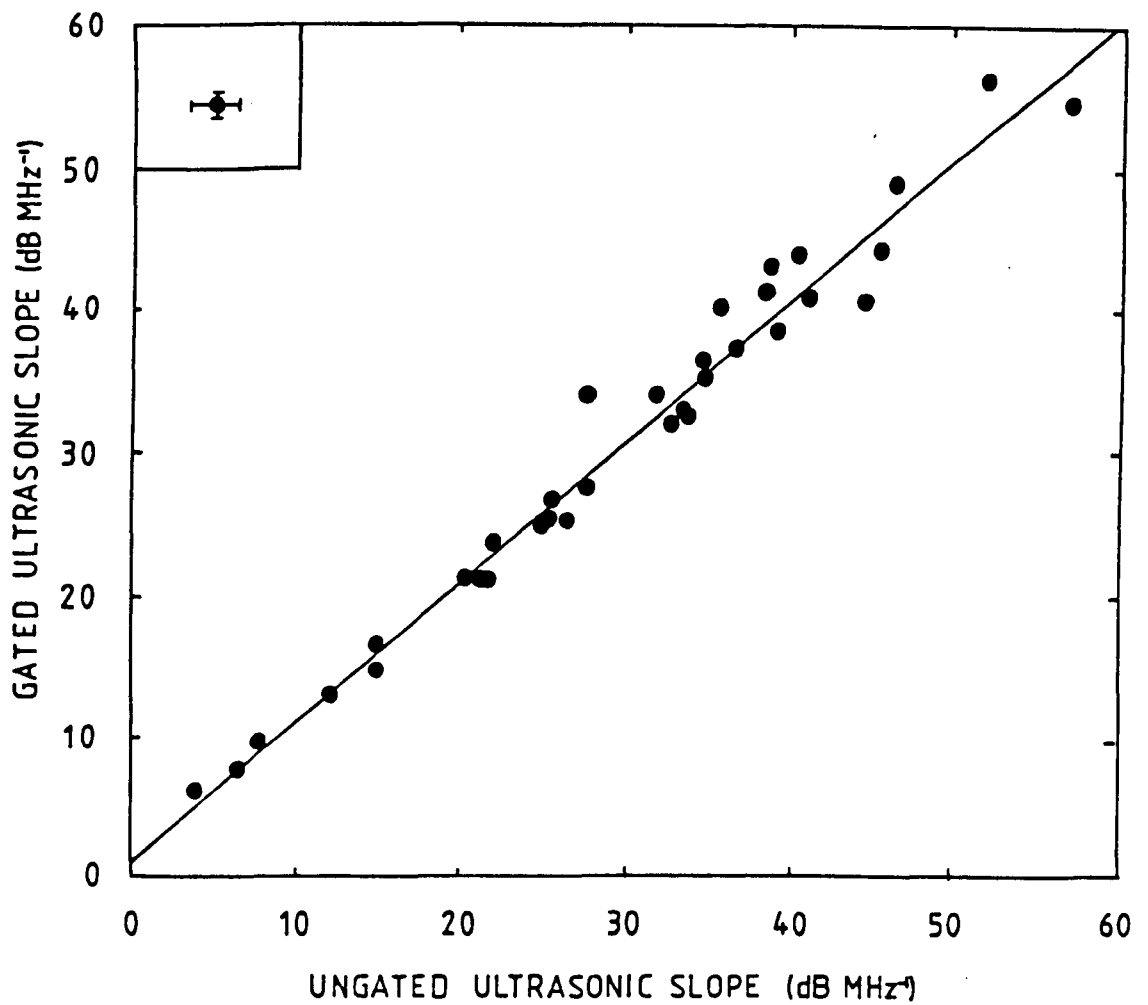
Figure 3.12 Gated and ungated signal comparison of ultrasonic slope for 35 cancellous cores

gradient = 0.99 +/- 0.03

intercept = 1.3 +/- 0.9

correlation coefficient = 0.99

it proved difficult to resolve the echoes on a time base so that a complete pulse could be analysed, figure 3.13. The complete initial ultrasonic pulse itself was about 5 μs and the echoes were produced every 3 μs for a 5 mm sample. However, one group of echoes was used for analysis and the least squares fit for the whole range produced a mean slope for the attenuation as a function of frequency. This means that absolute values for the attenuation are not correct as the transmission effect is not accounted for, but the average slope will still be meaningful.

Only longitudinal waves were considered in this work, as water is used as the couplant. Some mode conversion may occur at the sample boundary, but the lack of any consistent peak arriving after the main pulse implies that the effect is insignificant. Phase information was also not considered, as the HP frequency analyser reacted only to the magnitude of the received signal. The velocity measurements discussed in section 4.3 were carried out with nominal 500 kHz transducers, and dispersion was not assessed.
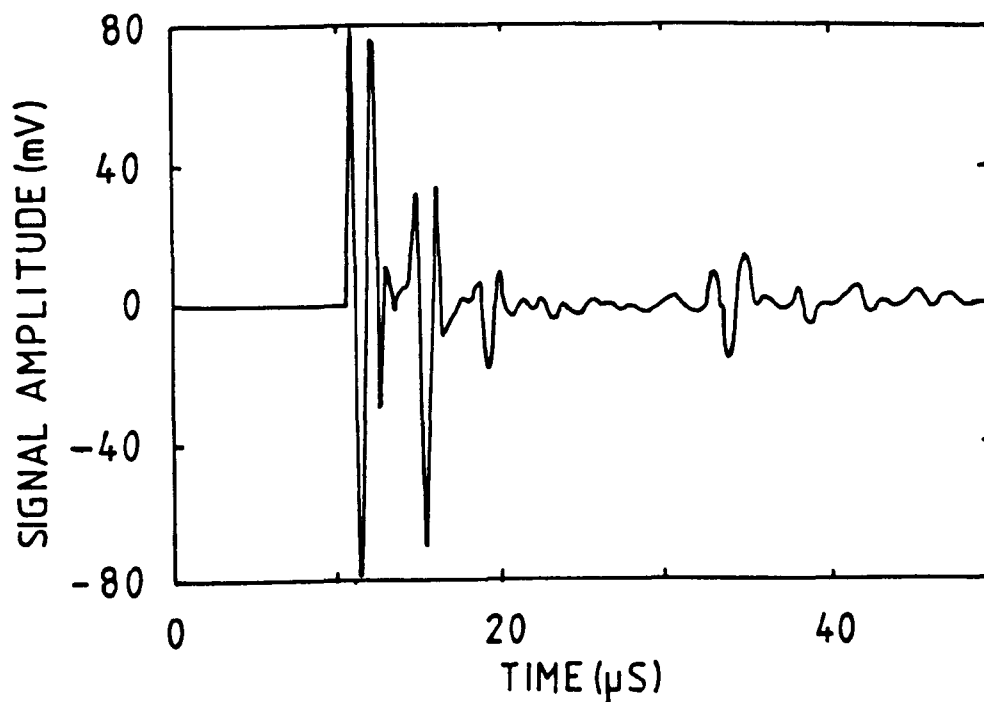
Figure 3.13 Time dependence of ultrasonic signal amplitude for a typical cortical sample.

3.3 The Bone Samples.

The bones were obtained in two main batches from Middlesbrough and Sheffield, with the samples for strength testing from Aarhus, Denmark and Leeds. All the bones were treated in an identical fashion except for the Danish samples which remained frozen rather than fixed, as described below. The Middlesbrough set will be referred to as batch one, and those from Sheffield as batch two. A detailed list of the two batches is given in tables 3.1 and 3.2, and an overall comparison in table 3.3, showing that the two batches were not significantly different. The samples were obtained from post mortems and are mainly from the elderly, over 60 years old. This means that general comparisons with age could not be undertaken, but a good range of samples was available when the physical density, and therefore the bone mineral content, was considered. It was noticable throughout, however, that the bones from the youngest cadaver, 20 years old, produced results consistent with a much higher bone density than many of the remaining samples.

3.3.1 Preparation and Mounting.

Bones were removed during post mortem and immediately put in buffered formal saline solution for fixing (Smeathers, 1986). Although tissues can be affected by this fixing process bone itself appears to remain unchanged ultrasonically (see section 3.5.4). The bones had to remain fresh and safe throughout the preparation, measurement and coring and then stay in the same condition for subsequent analysis such as strength testing and computed tomography. It was therefore decided that fixing was vital. An attempt was made to measure a batch of frozen, unfixed os calces. These had been irradiated from frozen by Isotron Ltd., to the standard required for sterilizing tissues (Ley, 1973), and then refrozen until mounting and measuring. They were stored under water during measuring and then dried in air

Table 3.1 Details of the individual os calces from Middlesbrough (Batch 1).

No.	Age	M/F	Width (mm)	Weight (gm)	Length (mm)
1	66	F	27.6	62.0	72.8
2	50	F	28.0	72.6	77.5
3	79	F	30.8	91.3	88.6
4	50	F	27.6	69.8	75.8
5	79	F	30.9	96.5	90.5
6	78	F	30.1	76.5	78.6
7	66	F	27.8	60.9	70.2
8	49	M	33.2	96.3	83.1
9	49	M	33.8	96.1	84.5
10	65	F	24.3	60.9	69.0
11	50	M	30.6	111.6	85.6
12	50	M	31.3	112.8	88.1
13	63	M	29.2	84.8	82.6
14	63	M	27.4	85.1	79.9
15	78	F	27.8	75.5	78.3
16	64	F	27.9	72.7	77.2
17	84	F	26.6	56.7	71.1
18	65	M	28.3	71.5	68.3
19	65	M	28.9	*	*
20	65	F	24.4	62.1	71.4
21	84	F	26.8	58.6	71.6
22	70	F	29.5	61.4	72.0
23	70	F	29.0	58.7	72.6
24	65	M	34.4	126.6	92.6
25	80	M	30.3	90.0	79.6
26	80	M	30.2	*	77.7
27	74	M	27.8	83.5	80.4
28	64	F	28.6	72.8	77.7
29	65	M	34.9	127.8	95.5
30	70	M	29.4	92.8	85.0
31	20	M	29.7	101.3	80.4
32	20	M	34.2	101.8	80.5
33	84	F	25.4	45.8	66.0
34	84	F	23.7	44.9	66.3
35	53	F	25.5	71.0	71.0
36	80	F	25.0	57.2	71.8
37	77	M	31.6	96.5	88.0
38	63	F	29.3	83.1	84.3
39	75	M	31.0	94.6	81.8

* indicates that a measurement is not valid because the bone had been cut

Table 3.2 Details of the individual os calces from Sheffield (Batch 2).

No.	Age	M/F	Width (mm)	Weight (gm)	Length (mm)
1	68	M	29.8	82.2	75.9
2	75	M	30.5	105.9	90.1
3	74	F	24.6	57.1	74.1
4	79	M	26.3	73.0	77.6
5	67	F	27.5	78.5	77.8
6	67	M	27.0	96.9	86.0
7	67	F	22.8	56.1	77.6
8	47	F	28.5	85.9	78.5
9	82	F	24.6	63.5	75.8
10	79	M	32.8	104.4	84.4
11	86	F	26.2	62.1	75.9
12	59	M	29.1	101.0	88.6
13	59	F	23.0	62.0	83.9
14	48	M	25.6	94.6	84.3
15	69	F	25.4	63.6	75.5
16	78	F	27.4	76.5	81.4
17	68	M	31.1	101.4	89.6
18	81	F	24.4	*	*
19	66	M	31.5	105.1	91.9
20	62	F	25.8	80.2	84.0
21	51	F	31.4	94.0	88.0
22	53	M	30.6	90.1	83.9
23	88	M	34.4	126.7	86.4
24	70	M	27.5	74.0	75.9
25	62	M	32.2	108.7	83.6
26	81	F	27.2	72.8	82.2
27	44	F	26.1	**	74.6
28	64	F	23.9	**	77.8
29	66	M	24.3	**	79.6
30	**	F	25.5	**	77.5

* indicates that a measurement is not valid because the bone had been cut
** indicates the data not available

Table 3.3 Comparison between Middlesbrough and Sheffield os calces.

Batch number Source	1 Middlesbrough	2 Sheffield	Diff
Number of samples	39	30	
Mean age (yr)	66	68	NS
Standard Deviation age (yr)	15	12	
Percentage female	53	59	
Mean width (mm) standard deviation	29.0 2.8	27.6 3.1	NS
Mean weight (gm) standard deviation	80.6 20.9	84.7 18.9	NS
Mean length (mm) standard deviation	78.6 7.5	81.5 5.3	NS

before refreezing. This turned out to be unsatisfactory, probably because of the time scale involved for mounting and measuring. On thawing for later coring, there was definite marrow and bone deterioration to the extent that later ultrasonic readings were lower than before and the bones felt noticably softer during coring, a phenomenon that did not occur for the fixed samples.

The bones were scraped as clean as possible, numbered and the maximum height and length measured, figure 3.14. The wet weight of each bone was also recorded.

The os calcis has a small flat surface on the base and could be mounted upright because of this. Many identical small brass mounts, as illustrated in figure 3.15, were made with a flat for alignment on the sample table in the tank and a 3 mm stub for mounting the bone. Cyanoacrylate glue worked excellently. The centre of the mount, perpendicular to the alignment flat, was marked and used as the reference point for a particular sample, allowing positioning from this known point for each individual sample.

3.3.2 Positioning

To position the foot for the early measurements, Langton (1984) took radiographs of a selection of feet and found the site required by measuring offsets from the back of the heel and the sole of the foot and related his results to anthropomorphic measurements of the foot itself. There was a correlation of over 0.8 for approximately twenty people for each offset (up/down and front/back). This did not help for the excised os calces so X-ray images had to be taken of each mounted bone and the offset required found from the reference point on the mount.

X-ray images were taken at the Princess Royal Hospital in Hull on Cronex Detail Screens at 52 kV and 100 cm source to film distance with the bone lying on the film container, producing an image of zero magnification, figure 3.16.
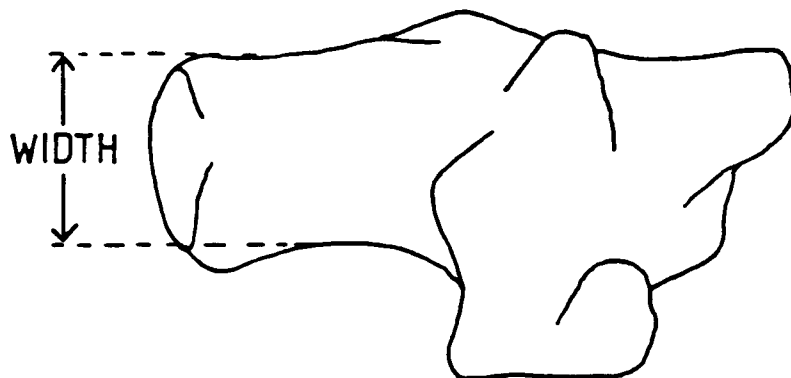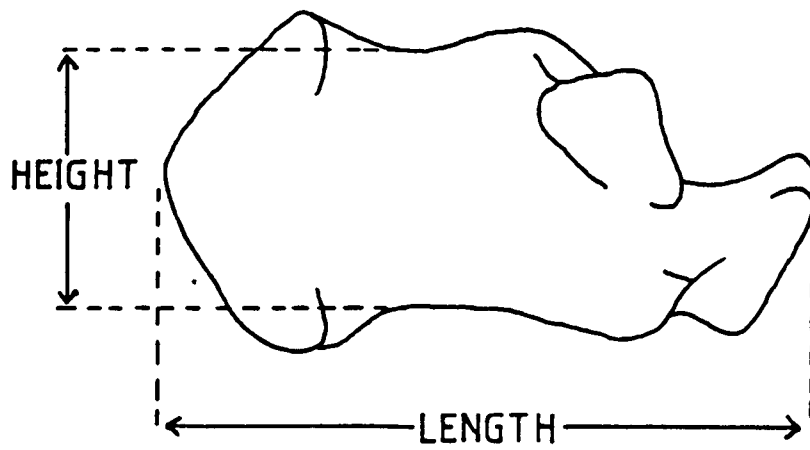
Figure 3.14 Dimensions of an os calcis.

reference
point

machined
flat
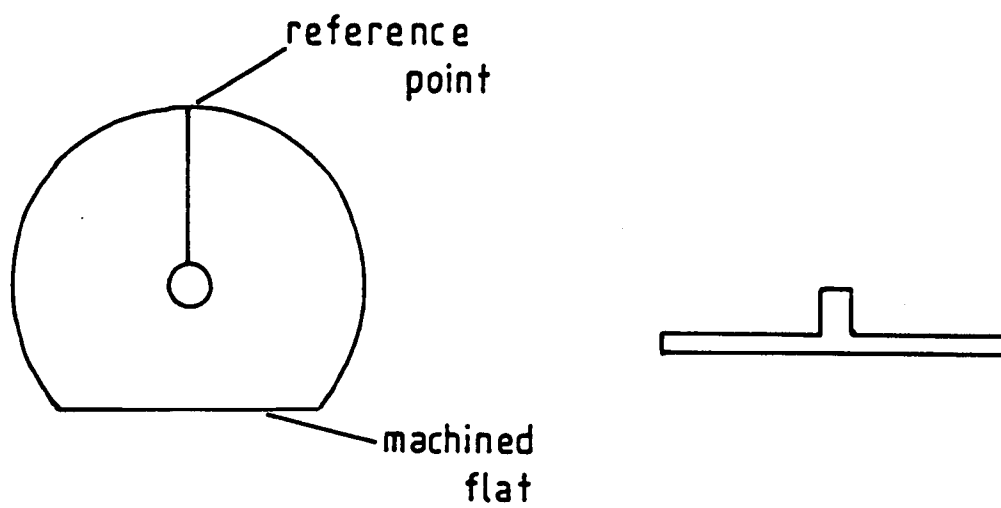
(a)
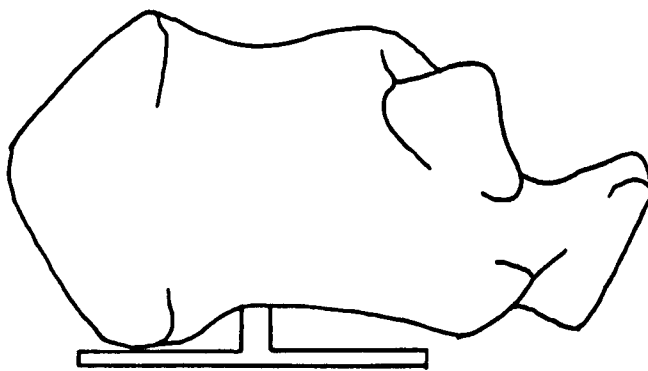
(b)

Figure 3.15 a) Diagram of a bone mount.

b) Diagram showing a mounted bone.

Figure 3.16 X-ray images of mounted os calces, used for
calculating the offsets for positioning each
bone.
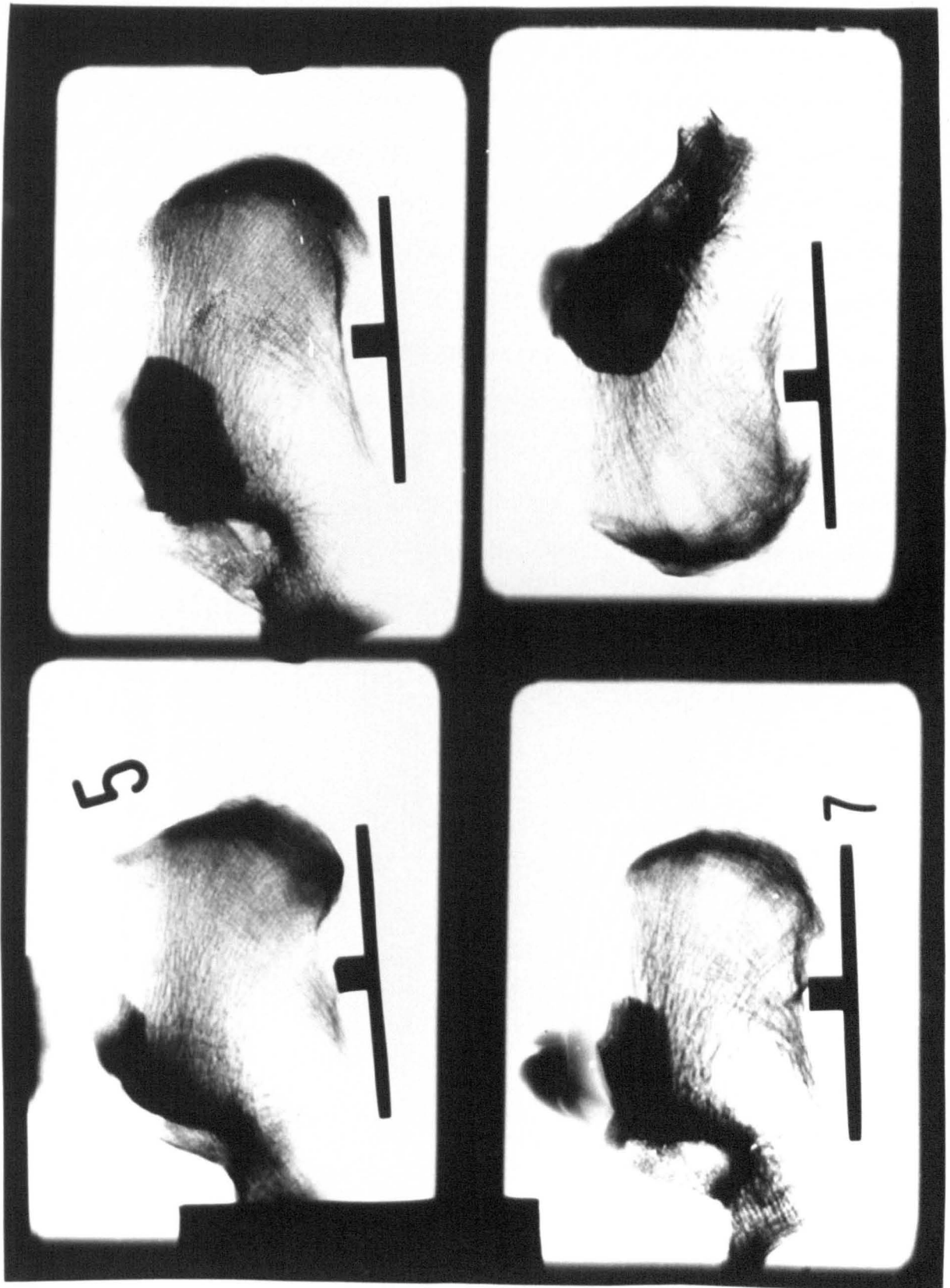
Measurements on the image related directly to the bone itself. The flat on the mount was used to ensure that the bone was perpendicular to the X-ray path as it would be for the ultrasound. The site for the ultrasonic measurement is marked in figure 3.17 and was defined by taking an equal distance from the base of the bone and the inner edge of the back plate, shown as clear white on the X-ray image. An equal distance from the flat top of the bone to the outer rounded back surface was also used as a guide, although the first alignment is more important. The centre of the site was measured from the centre of the brass mount, so that the offset required to position the bone correctly in the path of the beam in the tank was known. If the centre of the site was 7 mm to the right of the reference point on the mount and 25 mm above the base of the mount, then the bone had to be set 7 mm to the left of the transducer axis and spacers of 8 mm, (ie. the distance between the centre of the beam and the top of the sample table minus the height of the site to be measured on the bone) placed under the brass mount to raise the bone to the correct level as in figure 3.17.

This meant samples could be placed repeatedly in the tank and if one was knocked off its mount, it could be remounted and re-X-rayed so that the same site could be measured again.

Attempts to relate the position of the site to the parameters of the heel bone were unsuccessful, probably due to the irregular nature of the shape of the os calcis.

The effect of positioning the bone incorrectly has been investigated by Miller (1987) *in vivo* as well as the work done here *in vitro*. The correct site produces a smooth spectrum with decreasing amplitude as the frequency increases. If there is any upward trend in the amplitude trace over the full 1.8 MHz range visible on the analyser screen, the trace is considered unacceptable. These generally occur around 900 kHz hence the whole frequency
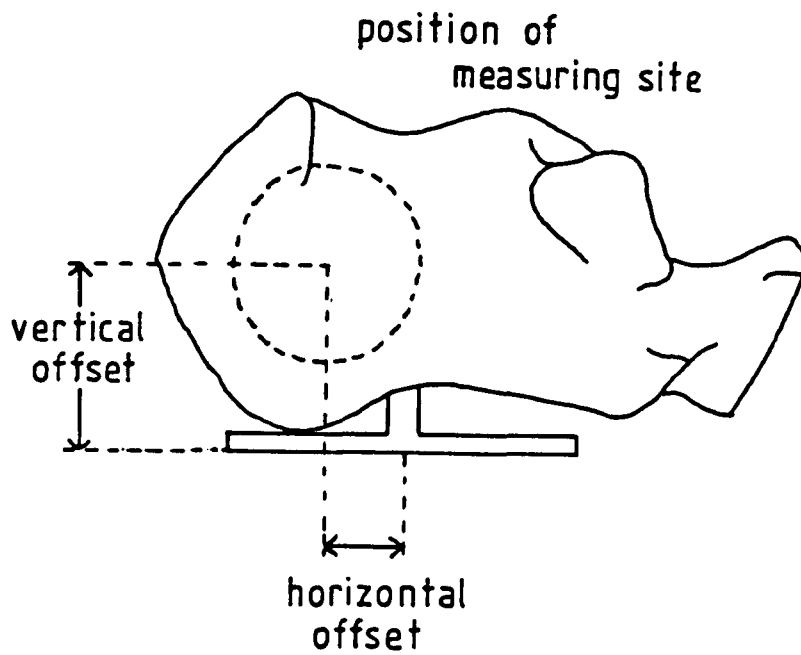
Figure 3.17 Diagram showing the site of measurement and the offsets required for positioning each os calcis.

range of the transducer is displayed to check there are no such anomalies rather than just the range over which the attenuation gradient is calculated. At positions further from the correct site, the traces become more irregular and the slope can change substantially, obviously depending on the size and the cancellous structure of the bone. These typical traces could be used to define the correct position by a reverse process of analysing the pattern of the trace, to avoid X-ray pictures each time a bone is to be measured, although at present this represents a very subjective technique.

Bones were always aligned with the flatter side parallel to the flat of the mount, so left and right os calces faced opposite ways in the tank. The ultrasonic path was completely reversible and results were identical whichever transducer was used as transmitter. Similarly, the bone could be rotated through 180° with no effect.

3.4 Bone Cores.

To gain greater knowledge of the internal structure of the bone and ultrasonic values for regular cancellous samples, the os calces had to be cored at the site measured, producing a cylinder of cancellous bone with irregular ends of the cortical surface layer of the bone.

3.4.1 Coring.

The bones, still mounted, were placed in a rectangular plastic box with the base of the mount against the side and the flat of the mount against the bottom. A peg held the bottom of the mount to the side of the box. Four bones could generally be mounted this way in each box. Molten paraffin wax was poured over until the bones were covered but with the top edge of the mount showing where the reference point is marked. When the wax had set, the clips were removed and the position of the measured site drawn on the flat wax

surface, taken from the reference point on the mount and measured using the horizontal and vertical offsets. A 30 mm circle was drawn to mark the site for coring where the ultrasonic beam had propagated through the os calcis. The box could be held firmly under an 1.25 inch coring drill and the wax acted as a guide ensuring that there was no snatching as the drill entered the bone, and a clean cut cylinder could be taken from the site required, figure 3.18.

It was found that measurements of the core agreed well with the results from the original whole os calces. A comparison of nearfield and core measurements of the same bones are given in figure 3.19. The regression line has a gradient of 0.90 +/- 0.05, and an intercept of 1 +/- 4, showing that the results are consistent although with some variations occuring, with the gradient suggesting that the cores produce slightly lower results than the whole os calces. There is a larger scatter around the regression line for the higher slope values. Some difference would be expected due to the divergence of the beam at low frequencies since with the whole bone, there is continuous material around the 'ideal' cylinder that represents the collimated ultrasonic beam. With the core, there is a distinct boundary at the cylinder edge, and although the impedance mismatch is not great, this will still produce reflections, especially at the more divergent low frequencies. As a further check, the os calcis, still mounted after coring, was remeasured in the tank. With an ideally cylindrical beam, the ultrasound would remain unaffected by the cored bone and pass through the hole. In practise, received signals at frequencies up to 300 kHz were slightly higher (1 to 3 dB) than the water trace, indicating that these more divergent frequencies were being reflected from the surface on the inside of the cored heel bone.

Both batches of os calces were cored in this way and were measured using the mount described for the trabecular samples in section 3.4.3. One core was discarded due to an error made on positioning the bone under the drill.

OS CALCIS

OS CALCIS

BONE CORE

CANCELLOUS
CORE
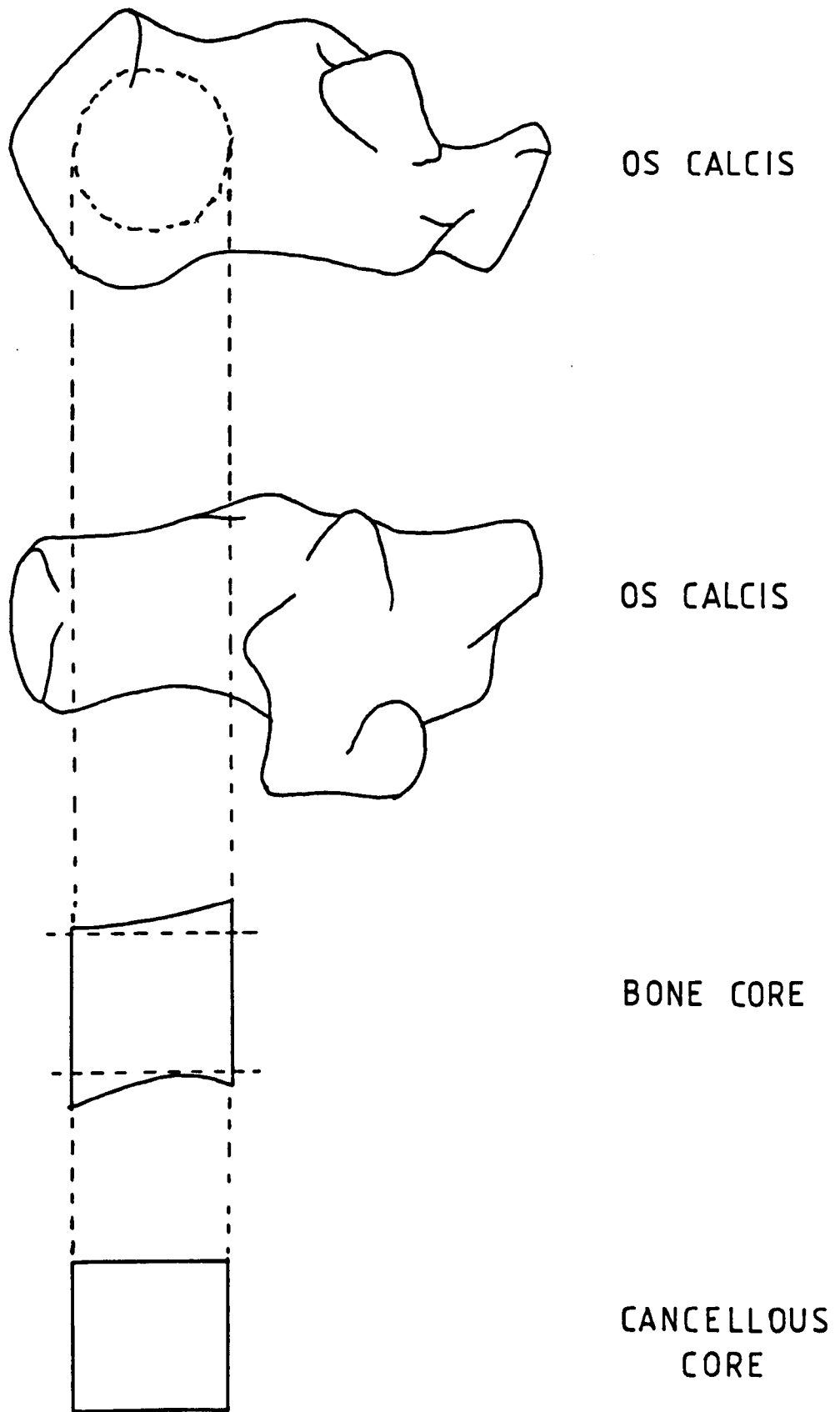
Figure 3.18 Diagram showing the position of measurement and coring for a
typical os calcis.
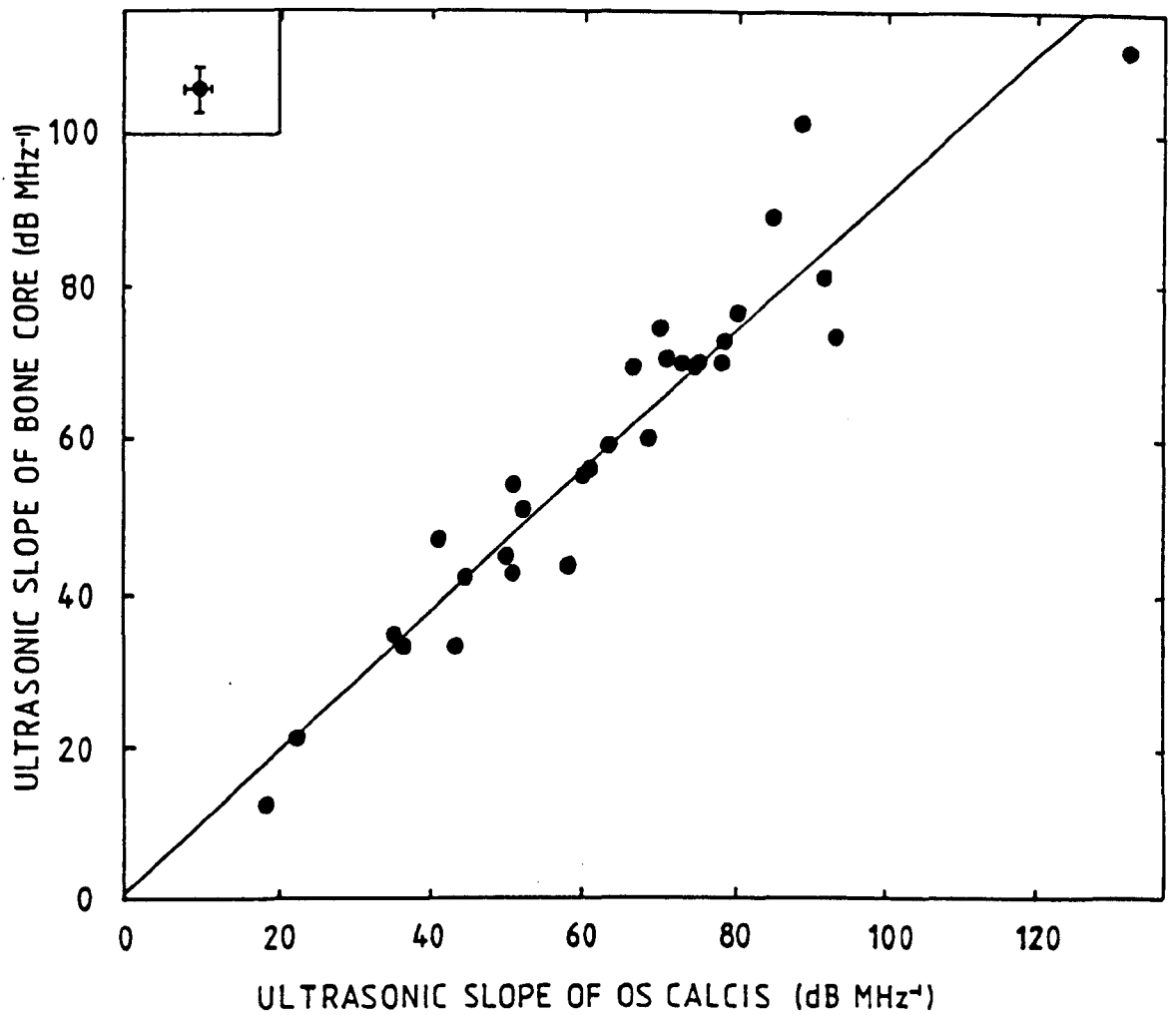
Figure 3.19 Graph of the ultrasonic slope of 30 bone cores plotted against
the ultrasonic slope of the corresponding os calces, both
measured in the nearfield position.

gradient = 0.90 +/- 0.05

intercept = 1.0 +/- 3.7

correlation coefficient = 0.95

3.4.2. Density Measurements.

The cores were composed of cancellous bone and irregular end surfaces with a cortical bone layer.

The overall physical density of each sample was found by a simple immersion technique. The wet bone was suspended in a beaker of water on a digital balance to give the volume and then dropped to the bottom of the beaker to find the mass. The typical error for each reading is 0.05 gm, representing an average error of 0.5% in the density calculated.

Problems can arise when defining the density of a porous substance such as trabecular bone. The fatty marrow of the pores would contain fluid *in vivo*, so the wet mass and volume were used rather than dry measurements or with the bones fully saturated with water. Thus the 0.5% error is the error of measurement for this technique rather than a limit on the possible density values. The values obtained were the mean physical density of the complete core and are intended for comparison between samples rather than an absolute value, including the bulk trabecular bone and surface cortex. The fatty marrow is not affected by age and so the overall physical density is a function of the bone to marrow ratio and the density of the bone itself.

All the samples were treated in the same way throughout the current work, so the densities are comparable from sample to sample. The density of the core was taken as the representative density of the os calcis at the site measured ultrasonically.

3.4.3 Cancellous Samples.

To obtain a regularly shaped purely cancellous sample, the ends of the cores were sliced off using the bone cutter made by Mr. Boyer for Langton (1984). Only batch one was prepared in this way, giving a total of 37 purely

trabecular samples. These are important for finding the ultrasonic properties of cancellous bone from regular specimens.

The density of these samples was found by measuring the wet mass and calculating the volume from the dimensions of the cylinder. All the samples were of the same radius, as they had been produced with the same coring drill, but of varying lengths, depending on the width of the original os calces. The values represented the mean physical density of the sample, and are comparable to the apparent density of Carter and Hayes (1976) as the pore spaces are taken into account. The apparent density is calculated from the mass of the bone material alone and the total sample volume and could not be established for the current samples as the marrow was required *in situ* for the ultrasonic readings and the other diagnosis techniques.

The cylindrical cancellous samples were measured by seating them in a cut away mount so that they were centralised in the ultrasonic beam. The water trace was taken with the empty mount in place, although it produced no significant effect. Initially, measurements were done with the bone sitting in the shaped cradle but this was not reproducable, especially with the lighter samples, so an elastic band was used to hold the cores in place, apparently with no effect to the actual attenuation slope values obtained.

Rotation of the cylinders around their central axis in this mount produced little difference in the ultrasonic slope. This is perhaps not surprising as the reading will represent the integral of the ultrasound over the whole area of the sample as received by the transducer. This will not be affected by a rotation as the total volume and its contents will remain the same.

The trabeculae in the sample follow the lines of stress within the bone and are not in a random pattern, so the ultrasonic attenuation will depend upon the direction through which the beam propagates. This was difficult to investigate with the sample available due to their cylindrical shape, although

four cubic samples were produced from cylinders of cancellous bone and measured in each of the three axes, section 4.6. The experiments were designed to mimic the clinical BUA system which always measures through the heel bone in the same direction, so the samples were cut to simulate this method.

3.5 Technique Evaluation.

Reproducibility is the ability of a technique to produce the identical result for the same sample on separate occasions, and is often referred to as the precision.

The numerical representation of reproducibility can be made in several ways. If many samples are measured twice, the mean difference between pairs of readings can be used. Equally, the standard deviation from this mean (sd), or the standard error of measurement (SE_m), given by the 95% confidence level from the standard deviation, may also be quoted. This is given by

$$SE_m = \frac{1.96 \times sd}{1.414}$$ (3.1)

and in fact often produces the largest error.

Reproducibility over a long period of time is often given by a typical sample measured many times. The standard deviation as a percentage of the mean reading is used in this case.

It is generally accepted medically that precision in a research situation is better than that of the daily hospital environment (Cummings and Black, 1986). However, scans to check effects such as the long term drift of equipment are often taken using an ideal phantom rather than a typical sample. Reproducibility tests for the current work were carried out either using a sample

representing the median of the range of possible readings or many samples covering the whole range obtained.

Errors of clinical methods are usually quoted as percentages which can sometimes be misleading. Although the actual error of a technique is often constant, the samples being measured represent a large range, resulting in a variation in the percentage error for each measurement. For the measurement of bone mineral, the osteoporotic readings are very low, so the percentage error is consequently higher. Errors quoted as percentages in the present work are calculated from the median of the range of readings obtained for those samples.

Accuracy is the term given to the ability of a technique to measure a known quantity correctly, but can also be used to describe the correlation of one measuring system with an independent measurement. This type of comparison is discussed in chapter 4.

Further parameters for the evaluation of a system are the sensitivity and the specificity of the technique. These describe the number of false results. For a clinical system this covers the ability of a technique to diagnose a complaint correctly or not, which is of vital importance in the hospital environment. Often this can be the only difference between techniques that otherwise correlate extremely well as there will always be one or two individuals that produce a low reading by one method and a high value on another. These parameters are not relevant for the present *in vitro* system and so will not be considered further but have been investigated by Murray et al (1987).

3.5.1 Short term reproducibility.

Each bone was measured twice, on different days, and the standard error of measurement calculated from the thirty bones of the second batch. The results are given in table 3.4. The mean difference in readings was 0.9 dB MHz^{-1}, with a standard deviation of 1.0 dB MHz^{-1}. The range of readings was from 18 to 107 dB MHz^{-1}, but the first batch increased this range slightly to 110 dB MHz^{-1}. Figure 3.20 shows the even distribution of the two sets of readings.

The main source of error is the repositioning of the bone and the transducers. The transducers were removable from their mounts as well as the mounts movable along the arm and table in the tank. The bones were positioned using spacers and a fixed millimetre scale on the table for lateral movement.

Another source of error from day to day is the evacuating. Although left overnight prior to measurement and at the same pressure, it is possible that some differences occur each time.

The reproducibility for cores and cancellous samples was found in the same way, tables 3.5 and 3.6. The actual repositioning of the cores was probably less accurate than that of the mounted bones as they were just held within a cut away cradle between the transducers, and this accounts for the larger mean difference in readings of 2.3 dB MHz^{-1} for the core measurements. No significant differences were introduced by rotating the core around its central axis. The cancellous samples were also held in the cut away mount, but did not have the irregular surfaces of the bone cores. Thus a small difference in position did not produce such a large variation in the ultrasonic slope, resulting in a smaller mean difference in readings, 1.12 dB MHz^{-1}. The percentage error of these cancellous samples, however, is comparable to that of the cores because of the much lower median value.

Table 3.4 Short term reproducibility for 30 os calces.

No.	First Reading		Second Reading	
	attenuation at 200 kHz	slope	attenuation at 200 kHz	slope
	(dB)	(dB MHz^{-1})	(dB)	(dB MHz^{-1})
1	10.6	106.8	10.4	105.0
2	5.6	88.5	5.5	87.2
3	2.3	35.3	2.5	35.4
4	5.3	64.5	6.4	61.3
5	5.0	72.1	4.6	70.0
6	3.5	48.8	3.3	48.4
7	2.3	36.3	2.2	36.3
8	3.2	65.1	3.2	65.0
9	3.8	40.4	3.2	40.8
10	5.2	74.2	5.2	73.9
11	2.0	22.9	1.9	22.8
12	3.9	74.3	4.0	73.8
13	4.9	51.2	5.0	50.9
14	4.1	77.0	3.8	78.2
15	3.0	53.6	2.9	53.4
16	4.4	54.3	4.4	53.8
17	6.0	81.4	5.8	81.5
18	1.6	18.0	1.6	18.7
19	5.6	65.3	5.9	65.5
20	4.5	59.1	4.1	57.9
21	3.1	47.0	3.0	46.7
22	5.3	85.5	5.2	85.7
23	5.7	89.5	5.8	88.6
24	5.2	93.1	5.1	93.7
25	5.9	81.4	6.1	84.9
26	3.3	45.9	3.4	45.4
27	7.1	76.7	7.0	75.9
28	5.8	91.9	6.4	89.5
29	4.2	79.2	3.6	79.2
30	4.5	66.3	4.3	69.5

mean difference in slope = 0.907 dB MHz^{-1}

standard deviation of difference in slope = 1.02 dB MHz^{-1}

standard error of measurement = 2.2%
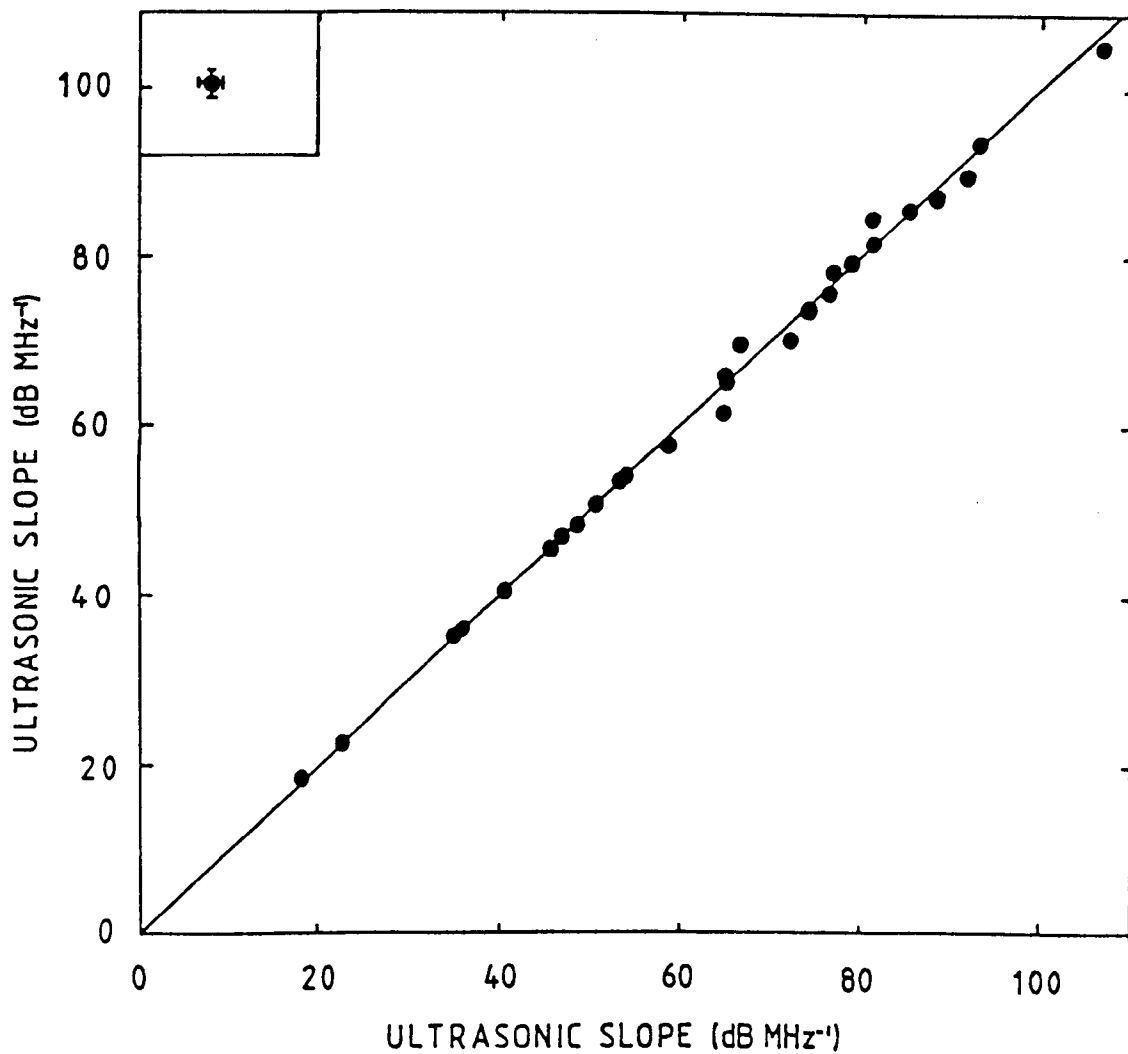
Figure 3.20 The short term reproducibility represented by two readings of the
ultrasonic slope taken on separate occasions for 30 os calces.

gradient = 0.99 +/- 0.1

intercept = 0.4 +/- 0.9

correlation coefficient = 0.99

Table 3.5 Short term reproducibility for 30 bone cores.

No.	First Reading		Second Reading	
	attenuation at 200 kHz	slope	attenuation at 200 kHz	slope
	(dB)	(dB MHz^{-1})	(dB)	(dB MHz^{-1})
1	14.4	115.5	16.6	110.5
2	7.1	76.9	7.7	75.9
3	4.2	33.6	4.0	32.9
4	7.5	61.1	7.9	58.3
5	6.6	71.1	7.9	70.2
6	5.3	42.5	5.6	42.0
7	3.5	34.5	4.1	34.1
8	7.3	56.1	7.8	54.5
9	5.8	47.4	7.3	46.6
10	8.3	69.6	9.4	69.8
11	3.8	22.2	3.1	20.8
12	7.5	74.7	7.6	69.2
13	5.6	53.4	6.3	53.8
14	7.8	69.6	6.9	69.5
15	5.4	45.2	4.9	44.4
16	6.0	50.4	6.0	50.2
17	8.1	91.6	6.3	88.8
18	3.6	14.8	5.0	12.2
19	7.5	57.4	8.8	55.0
20	8.3	44.0	13.0	43.3
21	5.4	40.8	4.3	41.5
22	11.8	65.6	9.9	69.3
23	12.5	89.4	12.0	100.8
24	9.1	83.2	8.9	81.1
25	10.1	75.1	8.0	72.4
26	8.3	38.1	10.9	32.9
27	10.7	81.5	8.8	74.2
28	7.6	70.5	6.9	72.9
29	8.4	67.5	8.8	69.1
30	8.4	61.7	9.0	59.7

mean difference in slope = 2.3 dB MHz^{-1}

standard deviation of difference in slope = 2.5 dB MHz^{-1}
standard error of measurement = 4.8%

Table 3.6 Short term reproducibility for 37 cancellous cores.

No.	First Reading		Second Reading	
	attenuation at 200 kHz	slope	attenuation at 200 kHz	slope
	(dB)	(dB MHz^{-1})	(dB)	(dB MHz^{-1})
1	1.5	4.6	1.7	3.8
2	4.0	24.9	4.9	22.4
3	2.6	20.9	2.8	20.3
4	3.6	27.5	3.3	26.7
5	2.7	21.9	2.3	22.9
6	3.3	25.1	2.9	26.7
7	1.4	5.7	1.6	4.9
8	3.9	35.0	3.6	35.6
9	4.5	34.8	4.1	36.9
10	4.1	40.2	3.9	38.8
11	2.8	14.4	2.9	14.8
12	3.6	21.2	3.2	21.5
13	4.5	31.9	3.9	32.6
14	5.5	38.4	4.0	41.1
15	2.5	21.2	2.7	20.9
16	3.4	25.4	3.6	25.5
17	2.0	11.9	1.7	12.1
18	4.5	39.3	4.3	38.7
19	3.5	27.7	3.5	31.8
20	3.2	32.6	3.1	33.6
21	1.2	7.7	0.6	9.4
22	2.4	14.0	2.0	15.1
23	4.7	42.2	4.7	44.5
24	6.6	46.8	5.8	43.7
25	4.7	33.4	3.9	33.4
26	5.3	53.0	5.4	51.9
27	3.4	26.4	3.2	25.8
28	5.7	52.8	5.4	51.9
29	4.4	38.4	4.3	38.8
30	4.9	57.0	5.6	57.3
31	5.0	43.9	4.9	45.3
32	1.3	6.5	0.9	7.8
33	2.2	12.2	2.2	11.9
34	4.4	36.5	3.1	38.8
35	4.7	37.3	4.3	34.6
36	4.4	38.8	3.9	38.9
37	4.3	30.8	3.8	31.8

mean difference in slope = 1.15 dB MHz^{-1}

standard deviation of difference in slope = 0.97 dB MHz^{-1}

standard error of measurement = 4.4%

3.5.2 Long term reproducibility

The long term reproducibility was investigated over a period of 11 months using one bone that represented an average attenuation value for the os calces of around 70 dB MHz^{-1}. This bone was measured 26 times at irregular intervals before being cored. The results are given in table 3.7.

The standard deviation from the mean is an indicator of the precision. The mean result was 76.9 dB MHz^{-1}, with a standard deviation of 1.7 dB MHz^{-1}, or 2.2%. The numbers listed show that there was no particular drift in the equipment or the state of the os calcis at any time during the year of testing. The mean attenuation at 200 kHz was 4.5 dB with a standard deviation of 0.5 dB. This variation of 11% is large because the actual attenuation is very small.

Long term reproducibility is due to much the same factors as the short term, but here perhaps repeated remounting of the transducers becomes more important. The fact that there was no long term drift shows that the bones were fixed in the formal saline satisfactorily and no deterioration took place.

3.5.3 Precision Comparisons with Existing Methods.

The reproducibility percentages obviously increase for a bone of lower slope. As with most diagnostic techniques, the actual error remains constant and does not depend on the sample being measured.

Taking percentages for the heel bone tested in the long term (ie. an average reading), the reproducibility is 2.2%. The slope of the os calces varied from around 20 to 110 dB MHz^{-1}, so a slope of 70 represents a median value, although the vertebrae and cancellous samples produced lower results. For the whole os calces, the short term reproducibility is also 2.2% of the

Table 3.7 Long term reproducibility of one os calcis.

Reading no.	attenuation at 200 kHz (dB)	slope (dB MHz^{-1})
1	4.8	75.6
2	4.8	74.9
3	4.8	78.1
4	4.3	77.6
5	4.5	74.6
6	4.9	76.6
7	4.6	76.3
8	5.1	79.8
9	4.6	80.2
10	3.9	76.5
11	5.3	75.9
12	4.6	74.6
13	4.5	73.7
14	4.8	78.9
15	4.7	78.9
16	4.4	76.1
17	4.7	75.6
18	4.5	74.5
19	5.0	77.1
20	5.3	78.2
21	4.8	77.5
22	3.8	77.9
23	3.5	77.7
24	3.9	76.9
25	3.8	77.0
26	4.3	77.7

mean slope = 76.9 dB MHz^{-1}

standard deviation slope = 1.7 dB MHz^{-1}

standard error of measurement = 2.2%

median value, although this percentage error would increase substantially for an osteoporotic, low slope bone.

This compares very favourably with the accepted diagnostic techniques. Obviously, it is not comparable to an *in vivo* precision, as a whole new design of tank would be required and repositioning would have to involve a completely different process, as with the present clininal system. The transducers would remain fixed in an *in vivo* situation and no evacuating would be necessary. Many diagnostic systems use phantoms containing known quantities of bone mineral which can be accurately positioned for *in vitro* measurements. The tests described here used an actual os calcis, which represents a far more realistic sample.

Single photon, dual photon and CT are considered to be reproducible to 2 to 3% for phantoms, which can be assumed to represent the error on the median of the range of values that can be measured. The problems involved in reproducibility for the individual techniques are discussed in Chapter 2. Such equipment measures the actual bone mineral content or density so its accuracy can also be investigated with phantoms containing known quantities of bone mineral. This is more difficult for the ultrasonic system, as it would be expected that the ultrasound will be affected by the dimensions of the trabecular structure as well as the quantity of material. However, this structural information is just as important as the mineral content, and the work of Chapters 6, 7 and 8 aims to quantify it, while section 4.8 compares the broadband ultrasonic attenuation technique to quantitative computed tomography.

3.5.4 *In vivo* to *in vitro*

The whole purpose of doing *in vitro* studies for medical use relies on the fact that the technique is equally valid *in vivo*, but no studies have yet been published relating the two for the current ultrasonic work or indeed for any other technique of bone mineral evaluation.

Murray (1986) measured a prospective amputee using the BUA equipment for *in vivo* measurements. The measurement was repeated with the amputated leg and then as the skin and flesh was removed around the measuring site. No significant difference was noted. The bone, fully stripped of flesh, and evacuated was also remeasured with no apparent change. It was then fixed in buffered formal saline solution and remeasured. Again, no significant difference was found. This confirmed earlier, less rigorous studies by Miller (1987) that the results *in vitro* apply directly to *in vivo* measurements.

Chapter Four.

EXPERIMENTAL RESULTS.

4.1 Introduction.

This chapter describes the ultrasonic results from all the os calces obtained and the measurements carried out on the samples cored from the heel bones. The implications of the acoustic characteristic impedance and reflection losses are considered. Ultrasonic measurements were also obtained from cortical samples for comparison with the trabecular bone. All the samples were categorised by their physical density.   Two batches of os calces, obtained from different laboratories as detailed in section 3.3, were used for the work and initial ultrasonic measurements were carried out on all the bones. Later experiments involved fewer samples, as only one batch of heel bones was used to produce the purely trabecular cores, section 3.4.3. A comparison between quantitative computed tomography and the ultrasonic measurements has also been carried out.

Significance tests were based on the correlation coefficient for the number of samples used (Goldstone, 1983), with the 1% level (p < 0.01) being regarded as significant, and the 0.1% level (p < 0.001) as highly significant. The units of the gradient of a least squares regression are not considered as the value itself will not be of further use except in comparisons between graphs.

4.2 Attenuation Measurements.

Ultrasonic attenuation as a function of frequency is the parameter used by the BUA technique to classify the bone mineral content of the os calcis. This must be related to a physical parameter of the bone to begin an explanation of the variation in results from bone to bone. In this work, the physical density

of the bone is used as an indication of the bone mineral content. The fatty marrow of the os calcis stays constant in composition with age, (Webber, 1987), so changes in the physical density are due to variations in the bone and the ratio of bone to marrow. The physical density therefore gives a direct measurement of the bone mineral present. The bones have deliberately not been classified as osteoporotic or healthy, as such a diagnosis in the clinical situation would depend on bone mineral measurements made at several skeletal sites and include any fractures suffered by the patient. It would also depend on whether the clinician uses vertebral or hip fractures to diagnose a patient as osteoporotic.

The ultrasonic slope can be considered to be a measurement of the total bone mineral content of the site studied. Some clinical methods provide a value for the total content whereas others give estimates of the bone mineral density. If the ultrasonic slope is normalised to attenuation per unit frequency per unit length, a value representing the bone mineral density can be obtained. This value is more useful in the laboratory, as attenuation coefficients are normalised to unit length.

The attenuation measurements have been carried out on the whole os calces, on the bone cores and on the trabecular samples obtained from the cores.

4.2.1 The os calces.

The attenuation slope per unit length is plotted as a function of density in figure 4.1 for all the 69 os calces measured in batches one and two. The gradient of the least squares regression line is 0.14 +/- 0.01. The correlation of 0.85 is highly significant, showing that the ultrasonic attenuation is dependent on the density of the bone. The scatter around the regression line is not fully accounted for by the errors in the measurements

Figure 4.1 The ultrasonic slope per unit length plotted against the physical

density for 69 os calces.

gradient = 0.14 +/- 0.01

correlation coefficient = 0.85

so other factors such as the trabecular structure and the shape of the bones themselves must also affect the ultrasonic propagation.

The clinical BUA system produces an ultrasonic slope value that has not been normalised for unit length. Figure 4.2 shows the correlation between the unnormalised slope and the physical density. The correlation of 0.88 is also highly significant, proving that the clinical system gives an excellent indication of the density of the *in vivo* heel bone. The correlation is comparable to that for the slope per unit length, so the size of the heel is not an important factor in establishing the physical density. However, for bone mineral content and volumetric bone mineral density measurements to be obtained, the bone width must be known.

The ultrasonic slope per unit length is plotted against age in figure 4.3. The two regression lines represent the effect of age for the males (solid line) and the females (dashed line). There is a significant difference between the gradient of the lines, with the gradient for the female group -0.34 +/- 0.09 and that of the males -0.02 +/- 0.06. The female population have a generally lower ultrasonic value as the age increases. Very few samples below the age of 50 were available, but the trend with age can still be seen. The regression line for the female population is steeper than would be expected over all ages, but represents the typical rate of loss after the menopause. The male population shows a much slower loss. 54% of the samples were female, so there is a fairly even split in the population. This loss of bone in females after the menopause agrees with other studies carried out both *in vivo* and *in vitro* (section 1.3). Far too few samples were available from the under 50 age group for a comparison to the premenopausal population to be carried out.
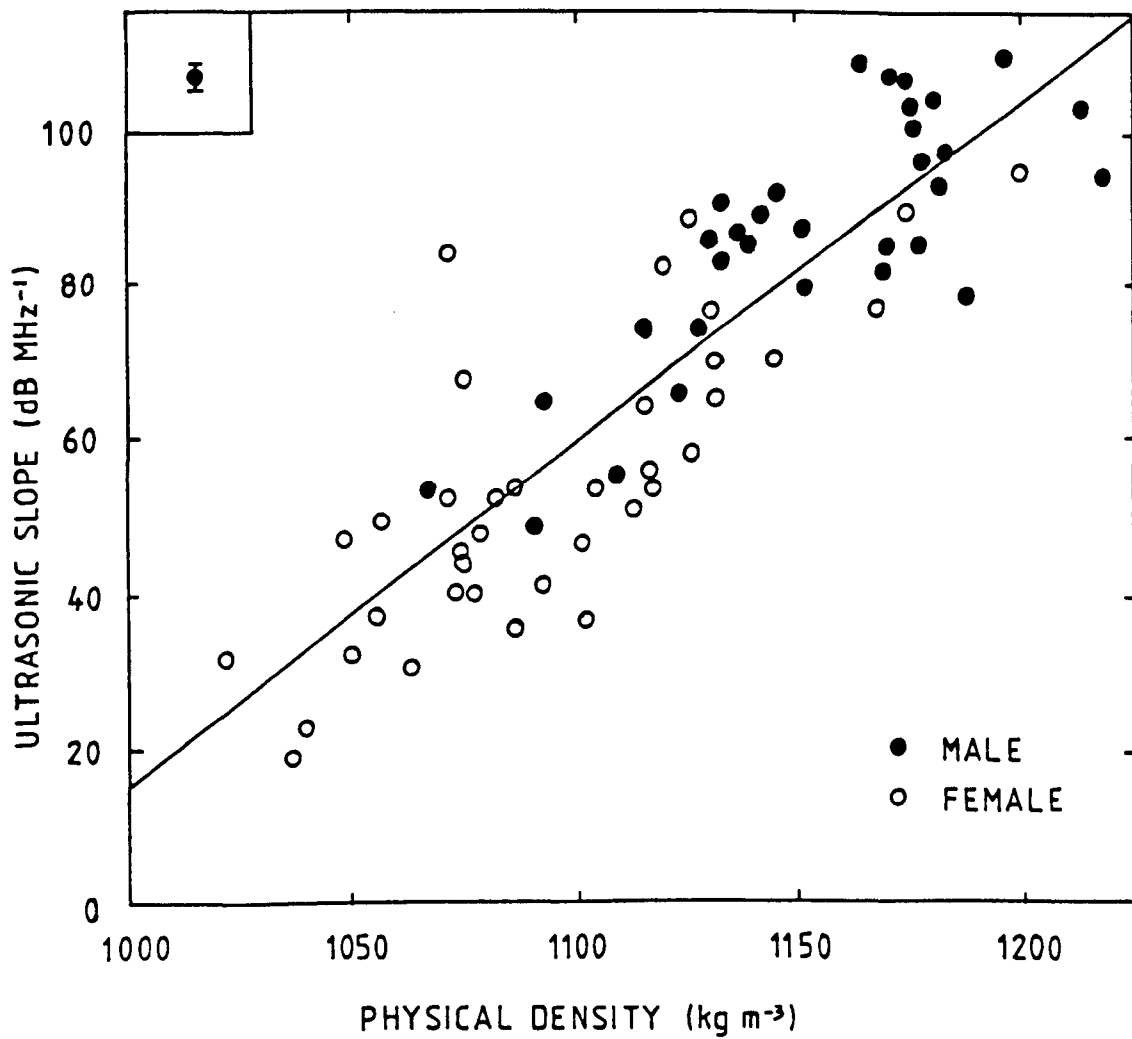
Figure 4.2 The ultrasonic slope plotted against the physical density for 69 os calces.

$$gradient = 0.44 +/- 0.03$$

$$correlation\ coefficient = 0.88$$
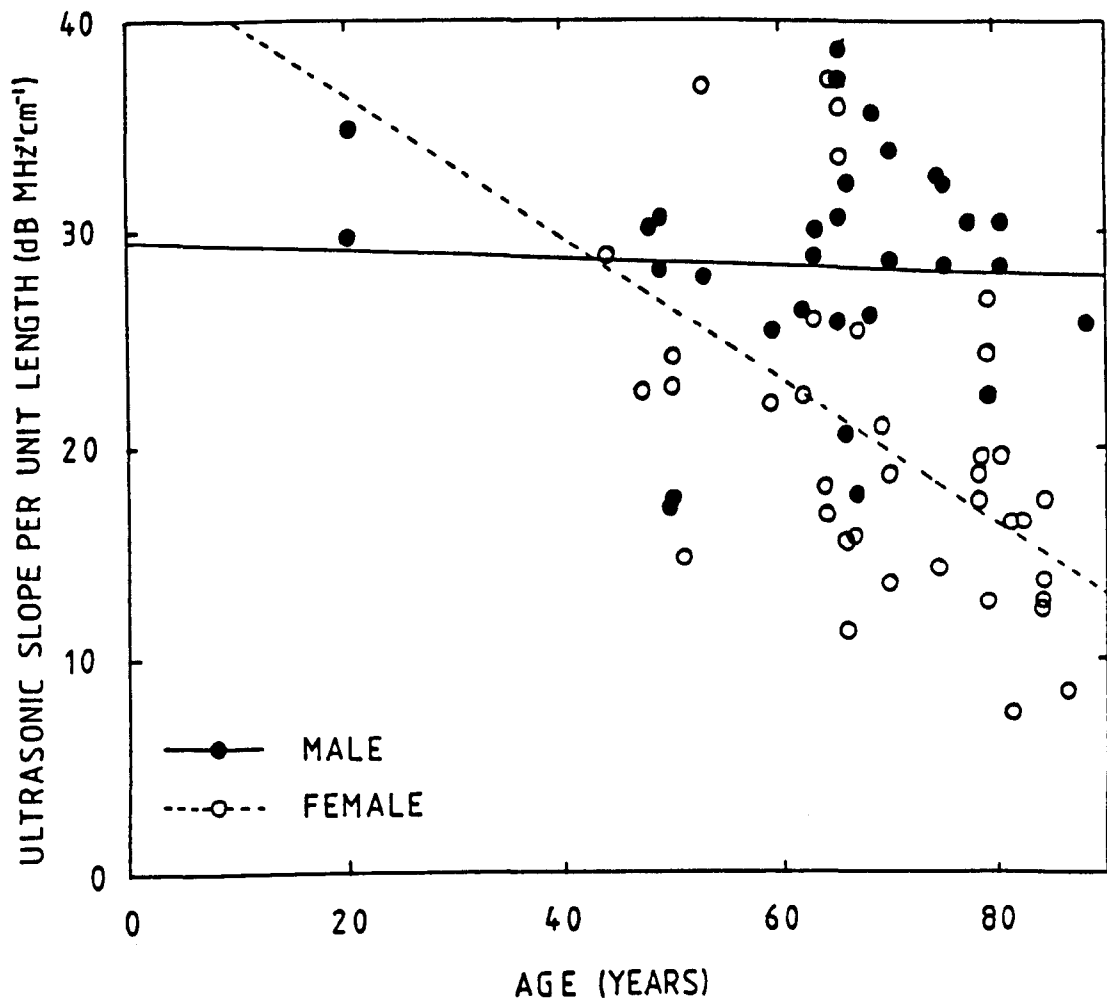
Figure 4.3 The ultrasonic slope per unit length plotted against age, showing the male and female regression lines.

female: n = 36

               gradient = -0.34 +/- 0.09

male: n = 32

               gradient = -0.02 +/- 0.06

4.2.2 Bone cores.

The main reason for measuring the attenuation dependence on frequency for the bone cores was for comparison between these measurements and either those for the whole os calces or those for the trabecular samples obtained from the bulk central part of the cores.

The results of the correlation between the slope per unit length and the density of the cores for all the 68 os calces cored is shown in figure 4.4. It is obviously similar to the equivalent graph for the whole os calces (figure 4.1), with a comparable highly significant correlation of 0.86 and the regression line of gradient 0.15 +/- 0.01. The core measurements are entirely consistent with those of the whole os calcis.

The slope per unit length for the whole os calces and that of the corresponding core is plotted in figure 4.5. Ideally, the gradient of the regression line should be 1.0, the line should pass through the origin and all the points should be within the experimental error of the regression line, that is, the ultrasonic results for each core should be the same as that for the corresponding whole os calcis. In practise there will be some differences in propagation, as discussed in section 3.4.1 where the slope values, unnormalised for unit length, are compared. On average, however, the regression line of gradient 0.94 +/- 0.06 and intercept -0.3 +/- 1.5 shows that such differences produce only a small variation in the resultant ultrasonic slope per unit length, as would be expected from the results discussed in section 3.4.1.

Much more noticeable is the distribution of results around the regression line. The low density samples produce very similar results for the whole heel bone and the core, seen by the proximity of the points to the regression line, but the higher density samples produce a much greater scatter around the best fit line. This could be due to at least two reasons. The coring procedure may
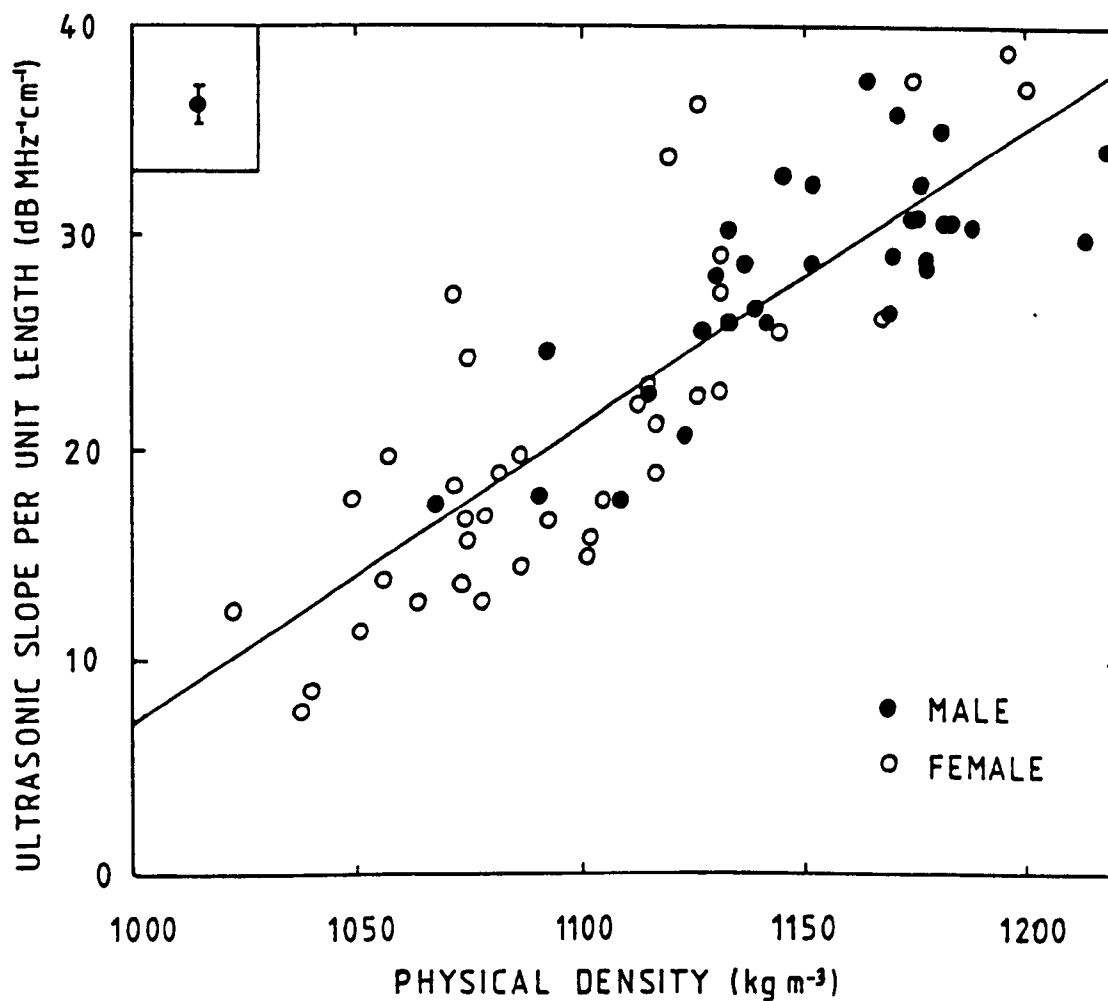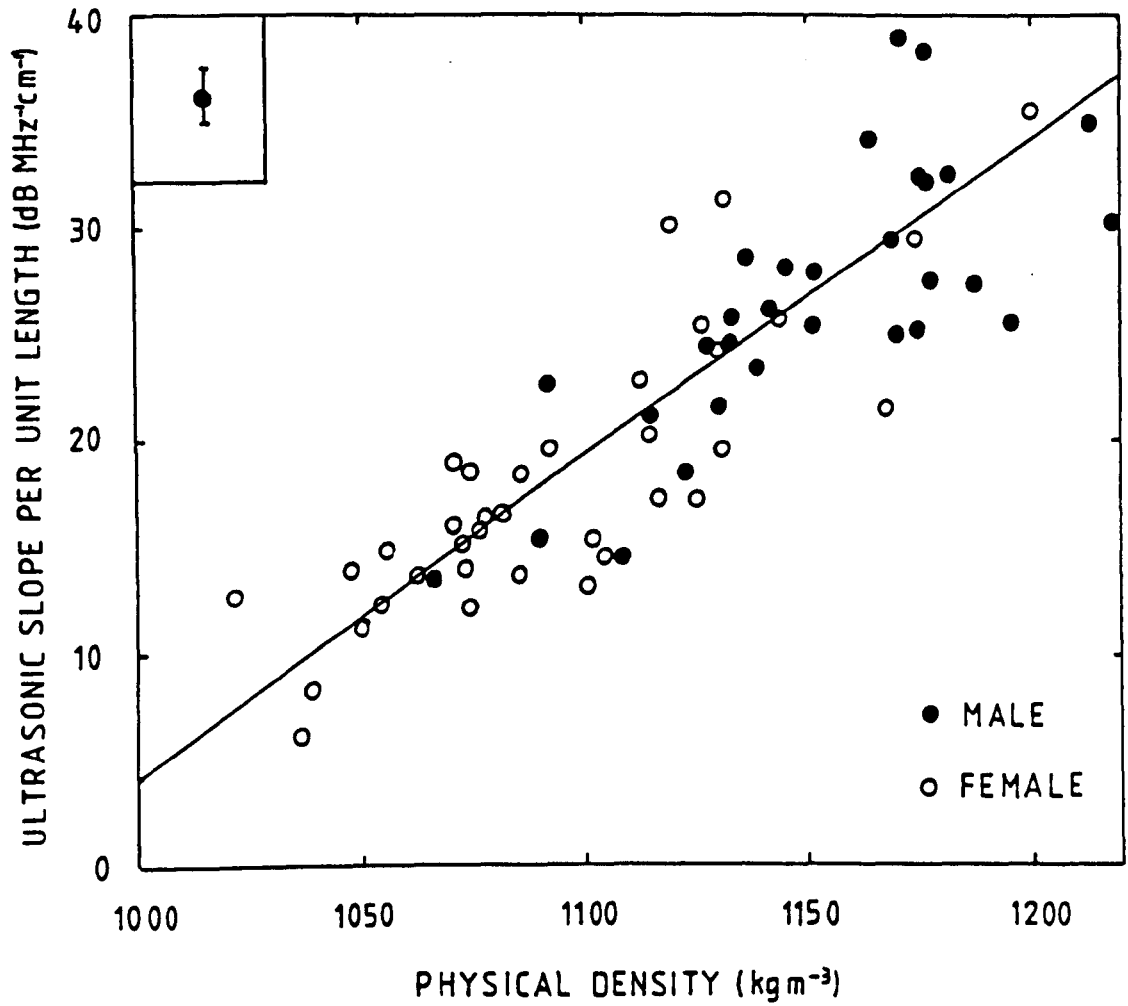
Figure 4.4 The ultrasonic slope per unit length plotted against the physical density for 68 cores.

gradient = 0.15 +/- 0.01

correlation coefficient = 0.86
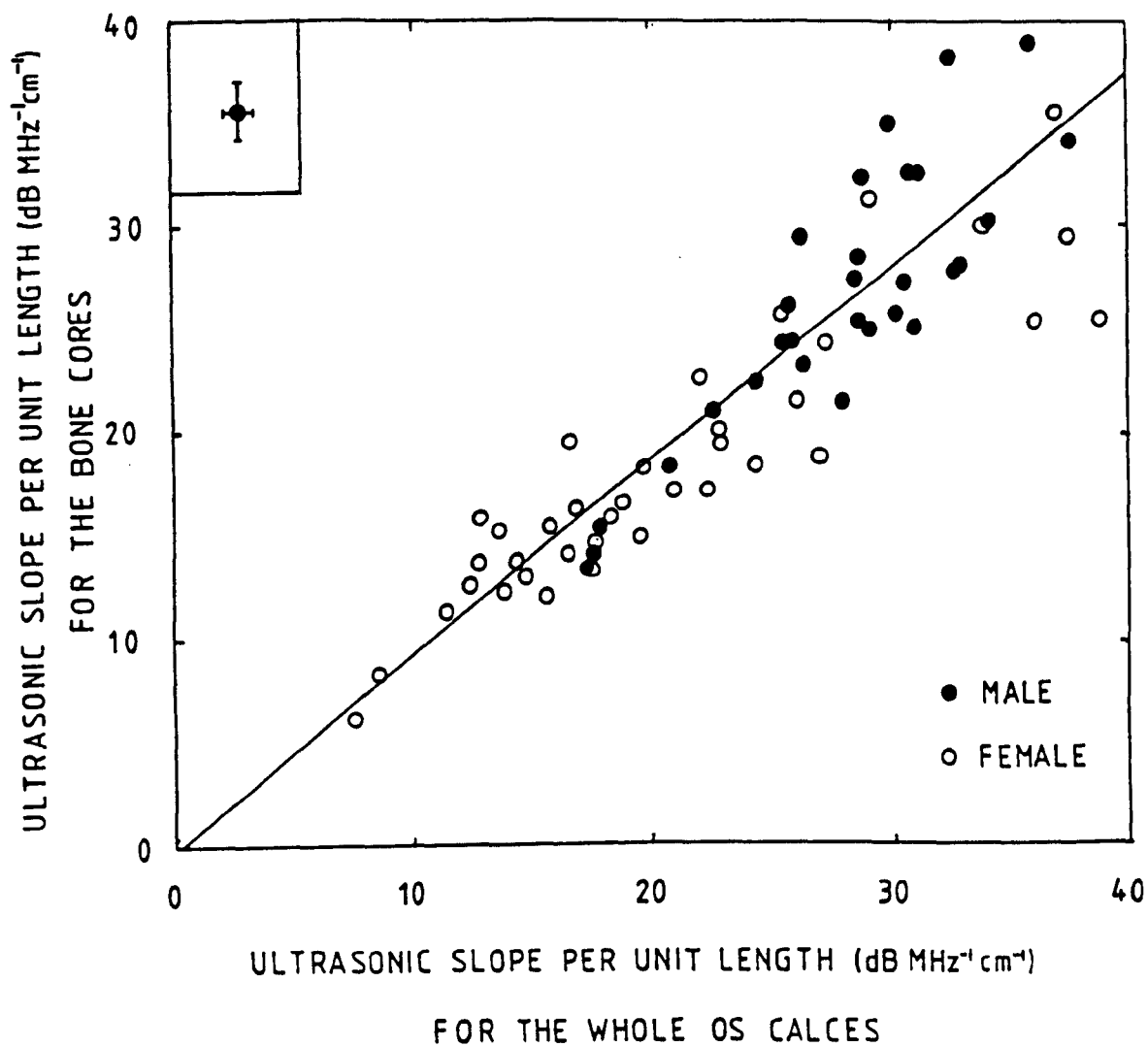
Figure 4.5 The ultrasonic slope per unit length for 68 cores plotted against that for the corresponding os calces.

$$\text{gradient} = 0.94 \ +/- \ 0.06$$

$$\text{intercept} = -0.3 \ +/- \ 1.6$$

$$\text{correlation coefficient} = 0.88$$

actually produce a core at a slightly different position to that measured in the whole os calcis. In a dense bone the trabecular pattern varies enormously within the bulk of the os calcis, so a measurement at a millimetre or so from the position measured previously will produce a large variation in the result. In a less dense bone, the trabecular pattern does not change much except at the very edge of the os calcis, so a small variation in the measuring site will produce little effect on the ultrasonic attenuation. A second possible reason is that the greater density of the bone sample introduces a difference in the ultrasonic propagation in the core. The impedance difference between the bone and the surrounding water is larger for the more dense samples, resulting in a greater reflected signal when the wave meets the discontinuity. The more divergent frequencies will be reflected back in to the cylinder with greater efficiency, changing the frequency profile of the propagating wave. However, it can be seen by the regression line that on average the core and whole os calcis results are comparable.

4.2.3 Trabecular samples.

The ultrasonic attenuation measured in the wholly trabecular samples is probably more useful than the results described above. The trabecular samples are regular with smooth surfaces and contain only cancellous bone. They were obtained from the cores by slicing off the ends so that the cortical bone was removed and the irregular surfaces flattened, section 3.4.3.

The attenuation slope per unit length is plotted against the physical density of the trabecular samples in figure 4.6. Only the cores from batch one were used to produce the 37 trabecular samples. The correlation is again highly significant, 0.81, and the regression line has a gradient of 0.12 +/- 0.01, slightly lower than that for the complete os calces. The densities of
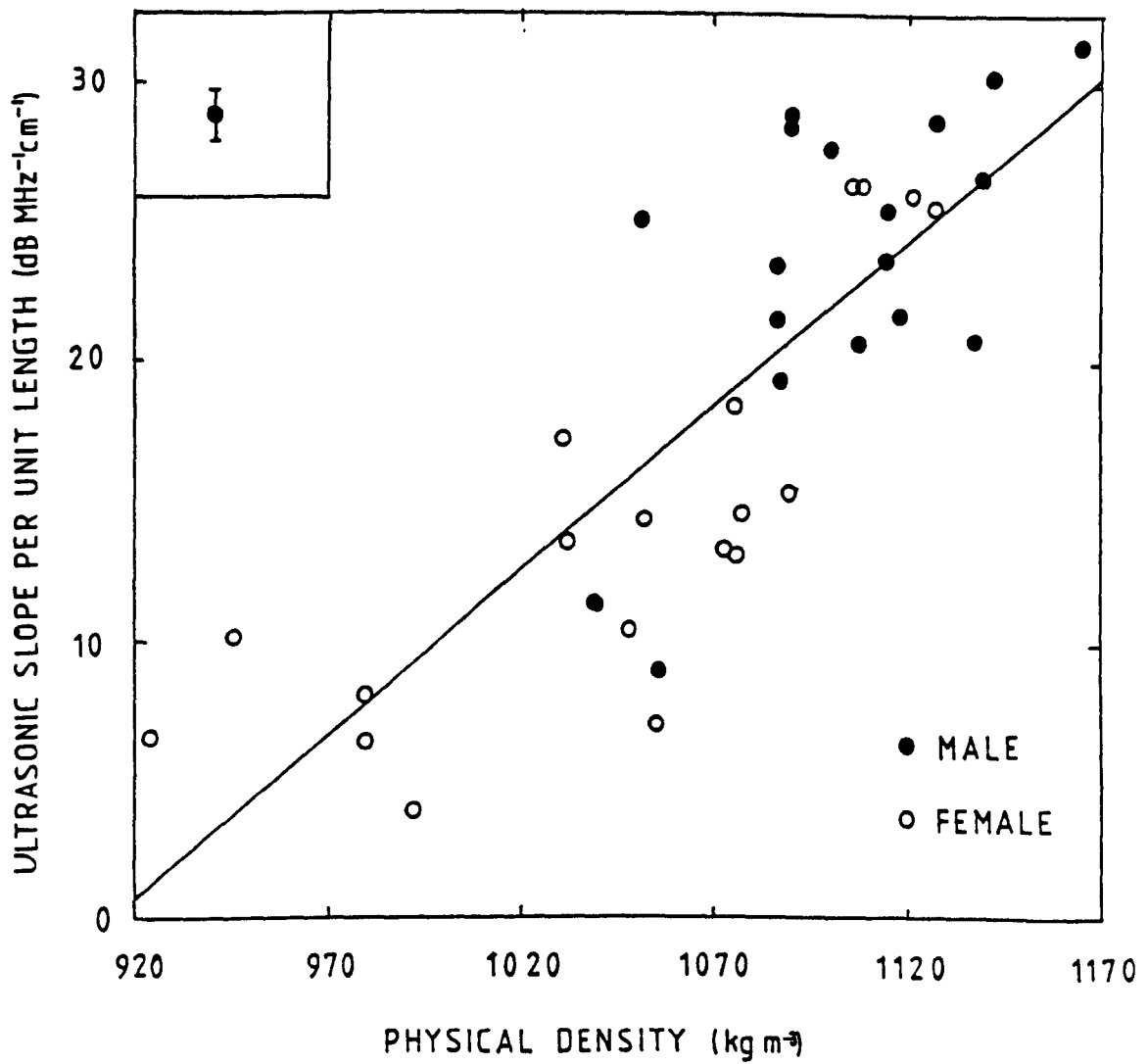
Figure 4.6 The ultrasonic slope per unit length plotted against the physical

density for 37 trabecular samples.

gradient = 0.12 +/- 0.01

correlation coefficient = 0.81

these samples are smaller than the corresponding cores because the cortical layer effectively increases the average density of each core.

These samples represent the range of trabecular bone in the human os calcis. Other skeletal sites require a different structural pattern and this will result in different densities and therefore different ultrasonic properties (section 1.5).

4.3 Velocity Measurements.

The longitudinal ultrasonic velocity was measured in the cancellous samples by a time delay method using Harrisonic 500 kHz focussed transducers. Figure 4.7 shows the frequency distribution of the transducers peaking at 430 kHz with a 3 dB bandwidth of 178 kHz, together with the time base trace. The broadband transducers were not used because of any dispersion that would be introduced by the inhomogeniety of the samples. A Gould 1425 digital storage oscilloscope first captured and stored the pulse transmitted through the water. The core was then placed in position in the cut away mount between the transducers and the transmitted pulse captured. The temporal difference between the arrival of the pulse via the water and that via the bone sample was noted. The measurements were repeated five times and the mean result used to calculate the velocity, producing an error of +/- 8%.

Figure 4.8 shows the ultrasonic velocity found for 33 of the trabecular samples as a function of density. A regression line is shown, but the errors are fairly large and the correlation is only 0.67, although still significant at p < 0.01. There is a wide scatter of results around this line, partly due to the larger errors involved in the measurements.
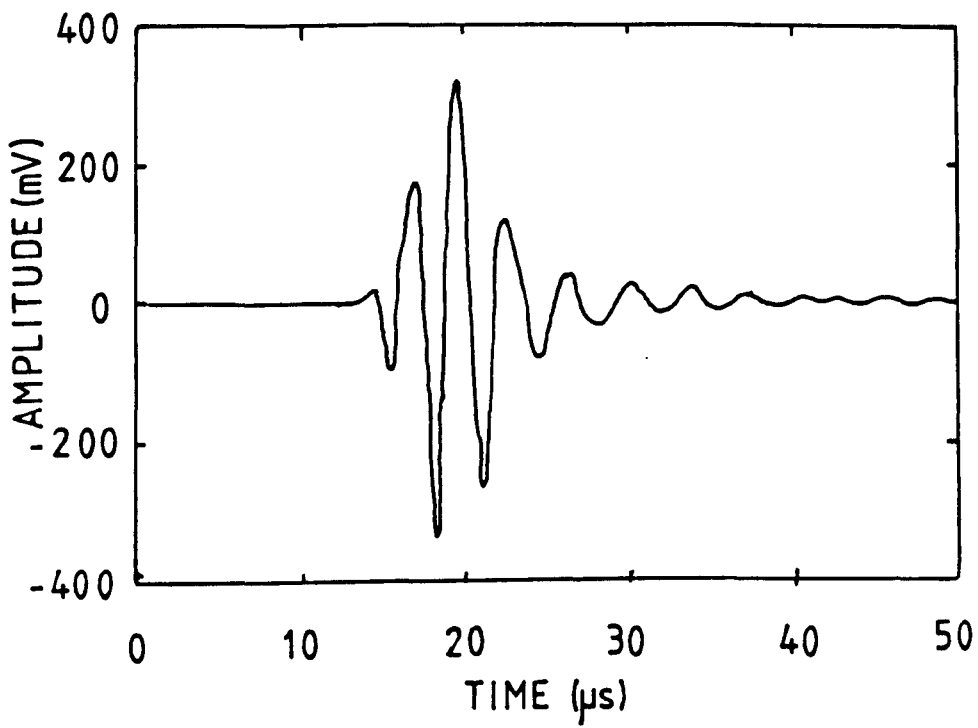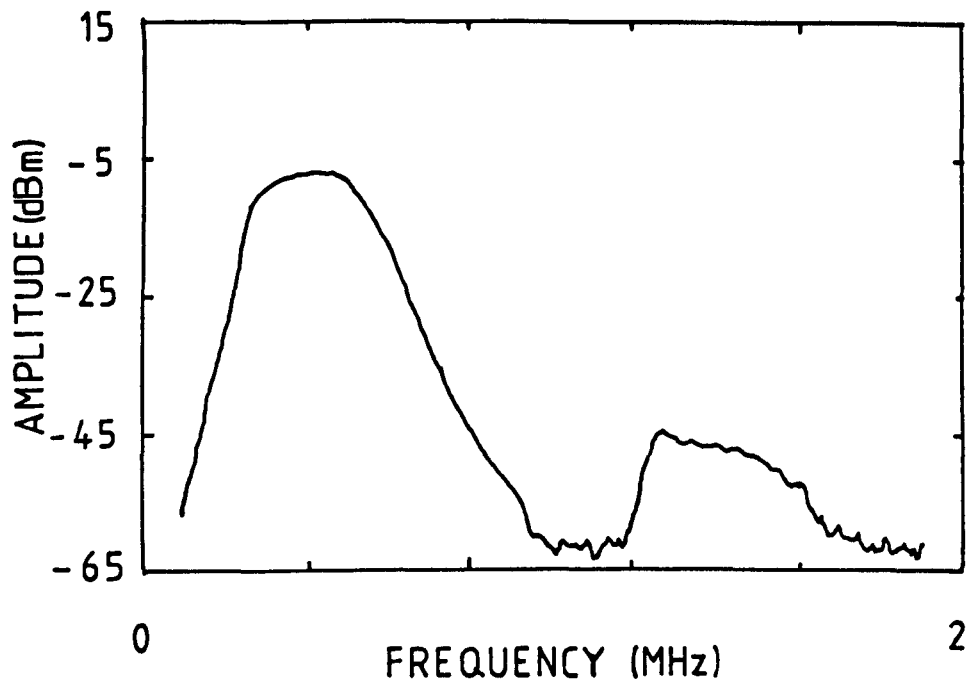
Figure 4.7 Frequency and time base characteristics for the 500 kHz Harrisonic
transducers.
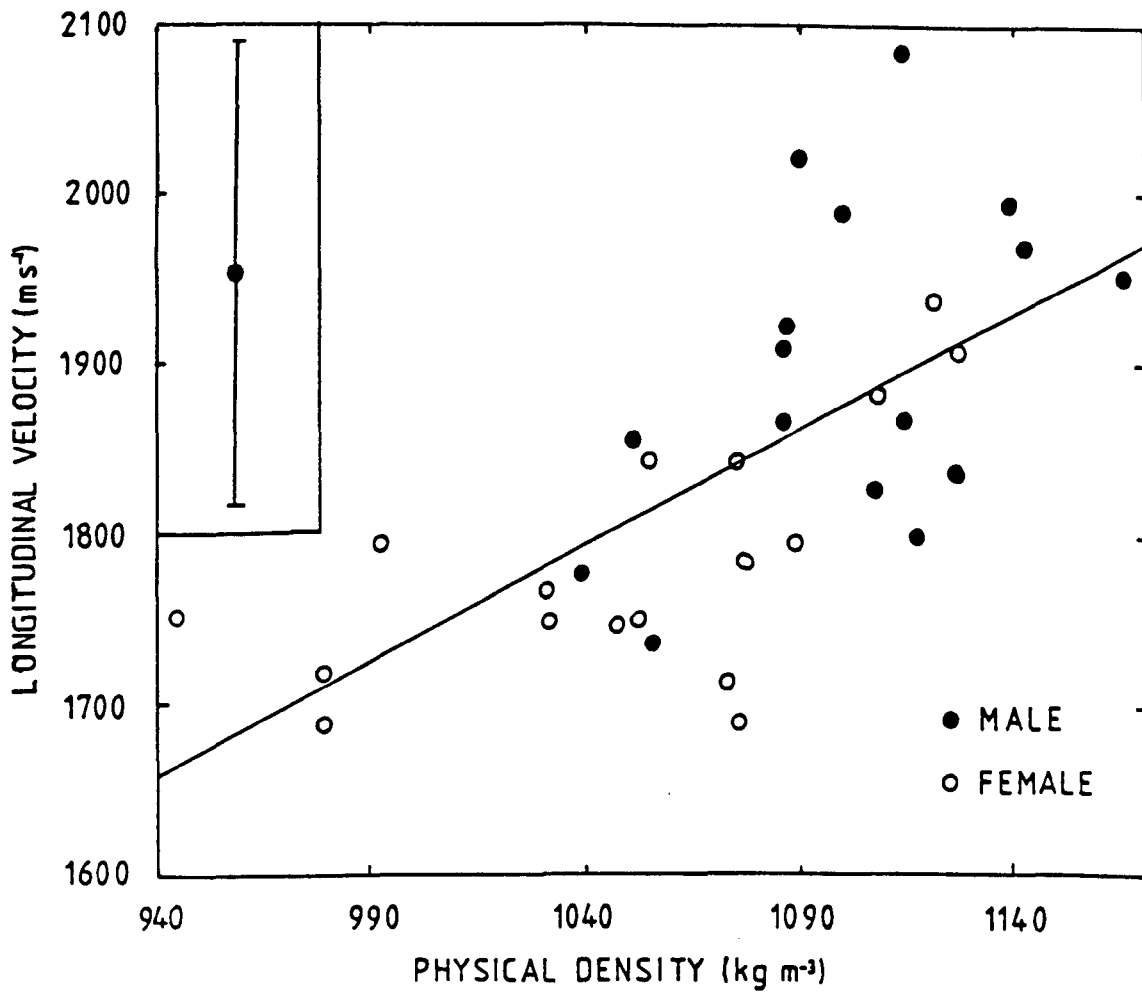
Figure 4.8 Ultrasonic longitudinal velocity plotted against the physical

density for 33 trabecular samples.

gradient = 1.3 +/- 0.3

correlation coefficient = 0.67

4.4 Impedance Measurements.

The ultrasonic velocity and the density of the samples can be used to find the characteristic acoustic impedance and hence the acoustic losses due to the interfaces between the sample and the water. The velocity has been measured using nominal 500 kHz transducers, so the results are limited to that frequency. Velocity dispersion was not assessed. However, it will be found that the losses are so small that they are almost negligible, and therefore can be considered negligible over the frequency range of 200 to 600 kHz.

4.4.1 Reflection Losses.

The reflection losses are calculated from the different characteristic impedances of the bone and water (Kinsler et al, 1982). The bone sample is a layer of density ρ_b and impedance Z_b separating two regions of water of impedance Z_w. The surface is smooth so the incoming wave is at normal incidence. The wave will be split into a transmitted and reflected signal at each boundary between the bone and the water, figure 4.9.
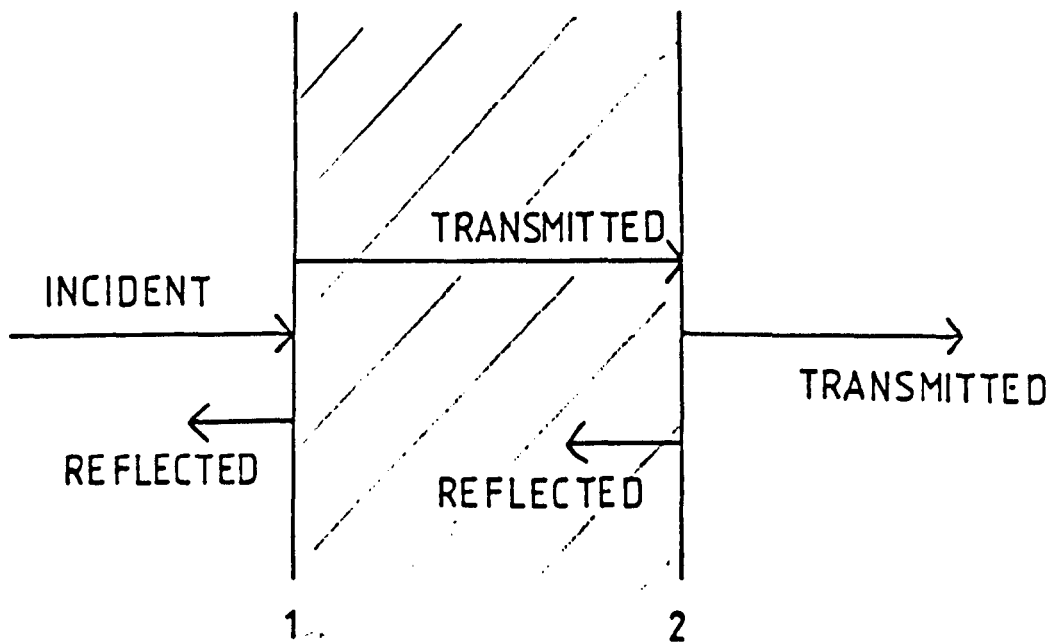
Figure 4.9 Transmitted and reflected waves at a boundary at normal incidence.

The duration of the incident signal, 3 μs, is small compared to the time the signal takes to travel through the bone samples, typically 9 μs, but because the attenuation of the cancellous bone is large, separate reflected signals can not be seen. It is assumed for this analysis that the surface is smooth and the sample is represented by a homogeneous material that has the impedance value of the cancellous bone, see section 7.2.1.

The transmission coefficient for each surface, T, is given by

$$T = \frac{4 \, Z_b \, Z_w}{(Z_b + Z_w)^2} \qquad (4.1)$$

and the total transmission coefficient is therefore T^2.

The signal lost can then be written as $10 \, \log_{10} (T^2)$ dB. The results for the cancellous samples are shown in table 4.1 which lists the density, velocity, impedance and reflection loss for each sample. The losses are all very small, under 0.5 dB. Figure 4.10 shows the attenuation per unit length at 200 kHz as a function of density and figure 4.11 shows the same results once the reflection losses have been taken into account. There is little difference between the two graphs, with the gradient of the regression line comparable within the error from the least squares fitting procedure.

As the velocity will not vary significantly within the frequency range considered, the impedance and therefore the reflection losses will be constant over the frequencies from which the ultrasonic slope is calculated, especially as they are so small compared to the losses due to the other attenuation mechanisms. Thus they will not affect the slope value found for each sample. As the overall reflection losses are so small for the cancellous bone they are

Table 4.1 Density, velocity, impedance and reflection losses for 33 cancellous samples.

No.	Density (kg/m^3)	Longitudinal Velocity (m s^{-1})	Characteristic Impedance (kg m^{-1} s^{-1})	Reflection Losses (dB)
1	992	1793	1.78	0.06
2	1089	1794	1.95	0.15
3	1076	1688	1.82	0.08
4	1075	1844	1.98	0.17
5	1031	1766	1.82	0.08
6	1073	1713	1.84	0.09
8	1142	1968	2.25	0.35
9	1087	1921	2.09	0.24
10	1108	1882	2.09	0.24
11	1056	1737	1.83	0.09
12	1039	1776	1.85	0.10
13	1086	1908	2.07	0.22
14	1086	1867	2.03	0.20
15	1052	1747	1.84	0.09
16	1077	1783	1.92	0.13
17	979	1719	1.68	0.03
18	1107	1827	2.02	0.19
19	1139	1993	2.27	0.37
20	1121	1935	2.17	0.29
21	979	1689	1.65	0.02
23	1048	1746	1.83	0.09
24	1051	1855	1.95	0.15
25	1090	2021	2.20	0.32
26	1114	2084	2.32	0.41
27	1127	1836	2.07	0.22
28	1032	1748	1.80	0.07
29	1118	1799	2.01	0.19
30	1100	1988	2.19	0.31
31	1165	1950	2.27	0.37
32	1115	1866	2.08	0.23
33	1055	1843	1.94	0.14
34	945	1752	1.66	0.02
35	1127	1906	2.15	0.28
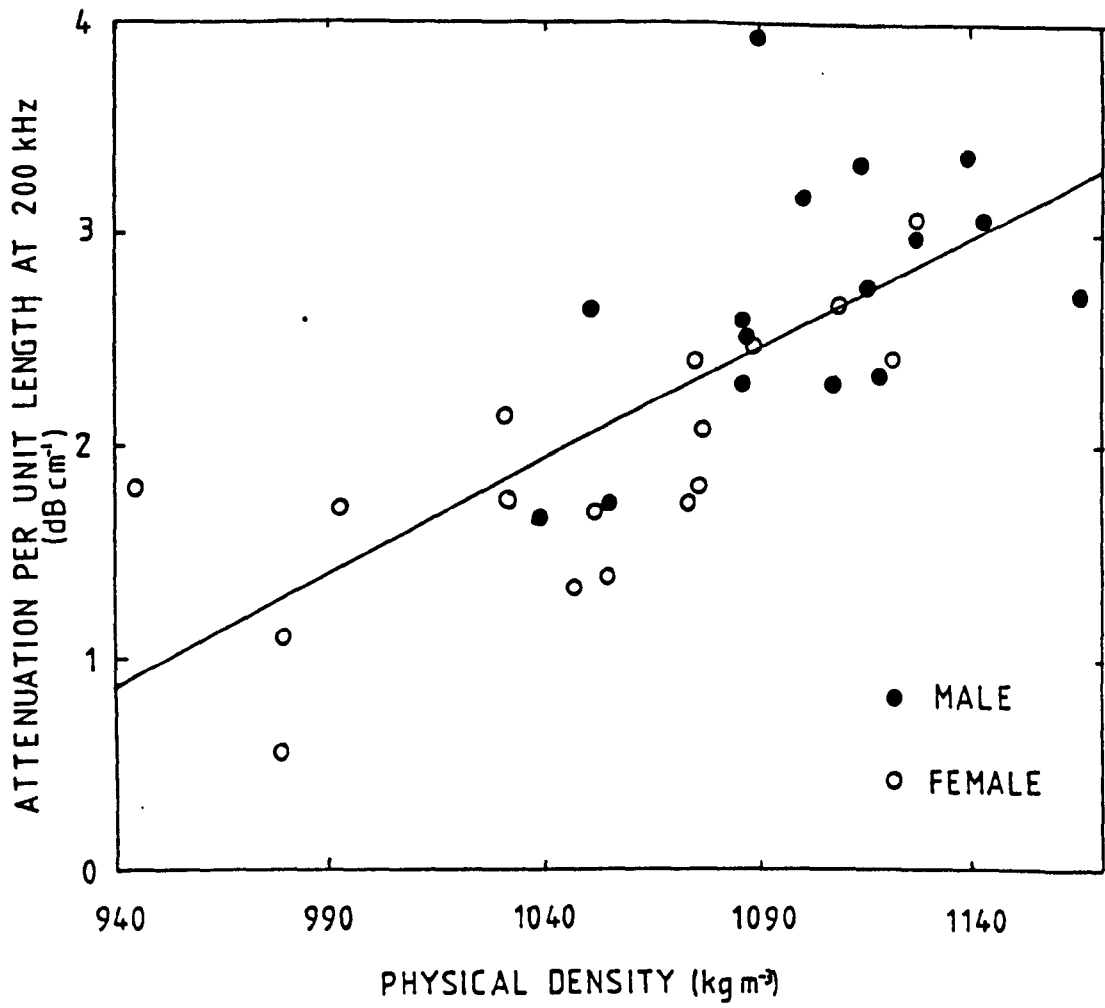
Figure 4.10 Attenuation at 200 kHz per unit length against the physical
        density for 33 trabecular samples.

                   gradient = 0.011 +/- 0.002

      correlation coefficient = 0.74
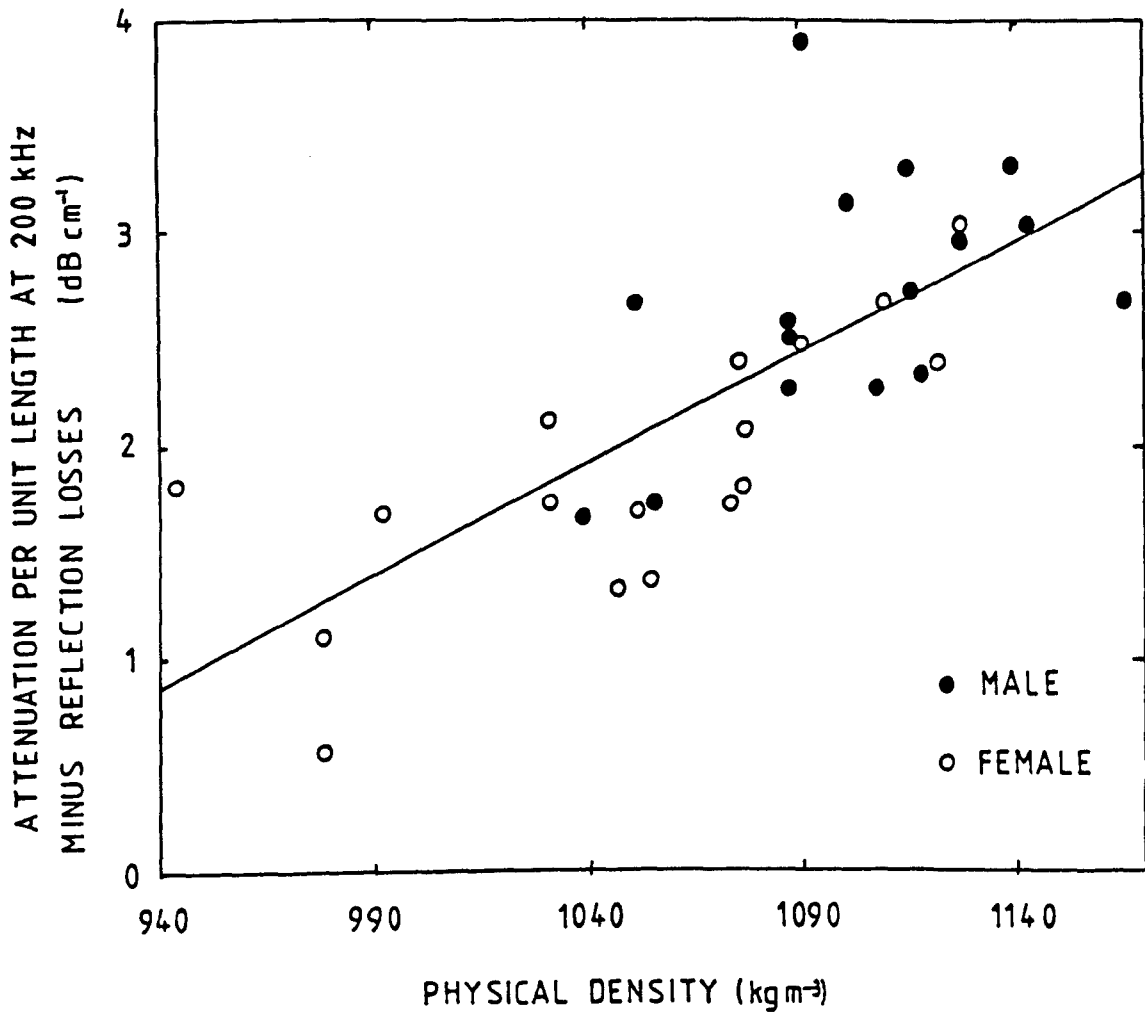
Figure 4.11 Attenuation at 200 kHz per unit length minus reflection losses

plotted against the physical density for 33 trabecular samples.

gradient = 0.010 +/- 0.002

correlation coefficient = 0.74

not specifically accounted for in the attenuation results in the other sections of the current work.

4.4.2 Comparison Between Os Calces and Trabecular Samples.

The graph in figure 4.12 shows the attenuation slope per unit length plotted for the bone cores against the values for the corresponding trabecular samples. It is clear that the ultrasonic attenuation as a function of frequency varies just as much with density for the cancellous samples as the whole bone cores with the correlation of 0.87 highly significant, as would be expected. The gradient, 1.0 +/- 0.1, shows that the variation in ultrasonic slope for the os calces is entirely due to the differences in the cancellous bone. There is however a definite offset showing that, on average, the whole os calcis produces an ultrasonic slope 4.6 dB MHz^{-1} cm^{-1} higher than the cancellous bone alone. The offset represents the attenuation due to the cortical surface layer and the irregular shape of the os calcis. The average value will be representative of the attenuation due to these factors, but it will vary from bone to bone because the curvature of the os calcis at the site measured can differ greatly from person to person. Taking an average os calcis thickness of 2.9 cm yields a typical value of 2.7 dB for the attenuation due to the cortex and shape of the bone at 200 kHz, which is well within the range of the attenuation results obtained at this frequency.

4.5 Scattering Measurements.

The cylindrical cancellous samples were all the same diameter because they had been cut by the same drill bit, but were of different lengths depending on the width of the os calcis from which they were cored. Experiments to invest-igate any scattering from the bone could be carried out in either of two dimensions. The core could be placed so that its longitudinal axis runs along
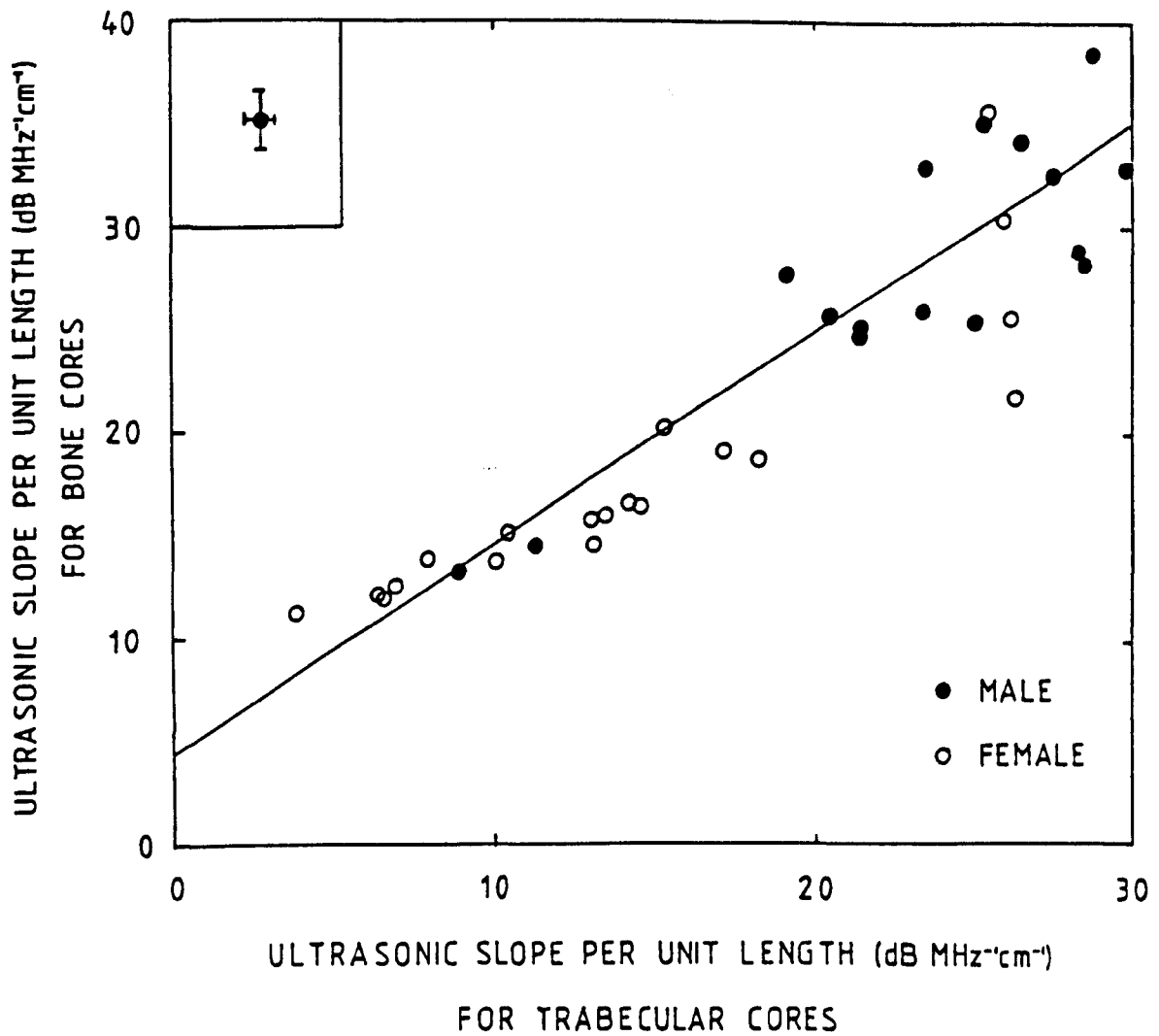
Figure 4.12 The ultrasonic slope per unit length for 37 whole bone cores
against the slope per unit length for the corresponding
trabecular samples.

gradient = 1.00 +/- 0.1

intercept = 4.6   +/- 2

correlation coefficient = 0.87

the axis of the transmitting transducer. This does not represent a particularly symmetrical arrangement, although it does mean that the scattering experiment is carried out in the same orientation as the attenuation measurements. A better method is to scan around the circular side of the cylinder so the core must be placed with its longitudinal axis normal to the axis of the transducer system, figure 4.13. Both orientations were tried, and gave similar results. The scans for the second method are presented here.
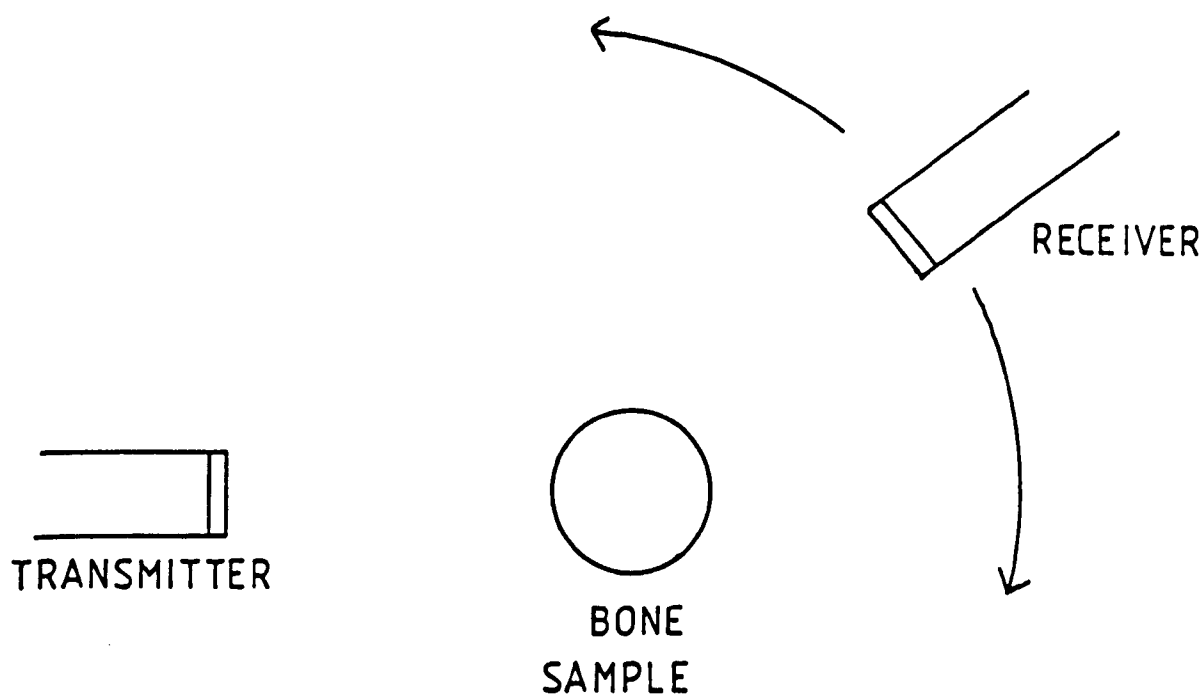
Figure 4.13 Simplified diagram showing the position of a bone core with respect to the ultrasonic transducers during the scattering measurements.

The polar plot of the water trace is shown in figure 4.14 for four frequencies, 0.2, 0.4, 0.6 and 1.0 MHz. The main transmitted beam is clearly visible. The side lobes are not as clear as might be expected because the receiver is scanning around a central position between itself and the transmitter, rather than scanning from the transmitter face. Hence the beam profile of the transducer is not so clear. The scan was taken to 120° on each side of the zero position, and those illustrated are typical of several scans taken. The magnitude of the signal was read directly from the spectrum analyser at the frequencies required by the computer before the receiver was stepped another 1°. A pause allowed for any water movement to settle before the next reading was taken.

The polar plots of the ultrasonic signal with a bone sample in place are shown in figure 4.15. The transmitted beam is attenuated as expected, and some of the ultrasound is scattered around the wider angles. The reflections from the bone have been considered in section 4.4.1 and are all very small, so the bulk of the signal is not being reflected back to the transmitter. When the patterns for the ultrasound in water are compared to those with the bone in place, it is obvious that there is a wider distribution around the angles scanned. This may be due to the shape of the bone sample rather than its internal structure.

The way in which ultrasound is scattered by a cylindrical sample depends upon the wavelength of the incident signal with respect to the radius of the cyllinder. It can be calculated for an ideal cylinder assuming that the material forming the cylinder is non-absorbing in its own right. If the material is absorbent, then the main transmission peak would be attenuated accordingly.

Morse and Ingard (1968) develop the theory for the whole range of ka values, where ka is the product of the incident wave number, k, and the radius
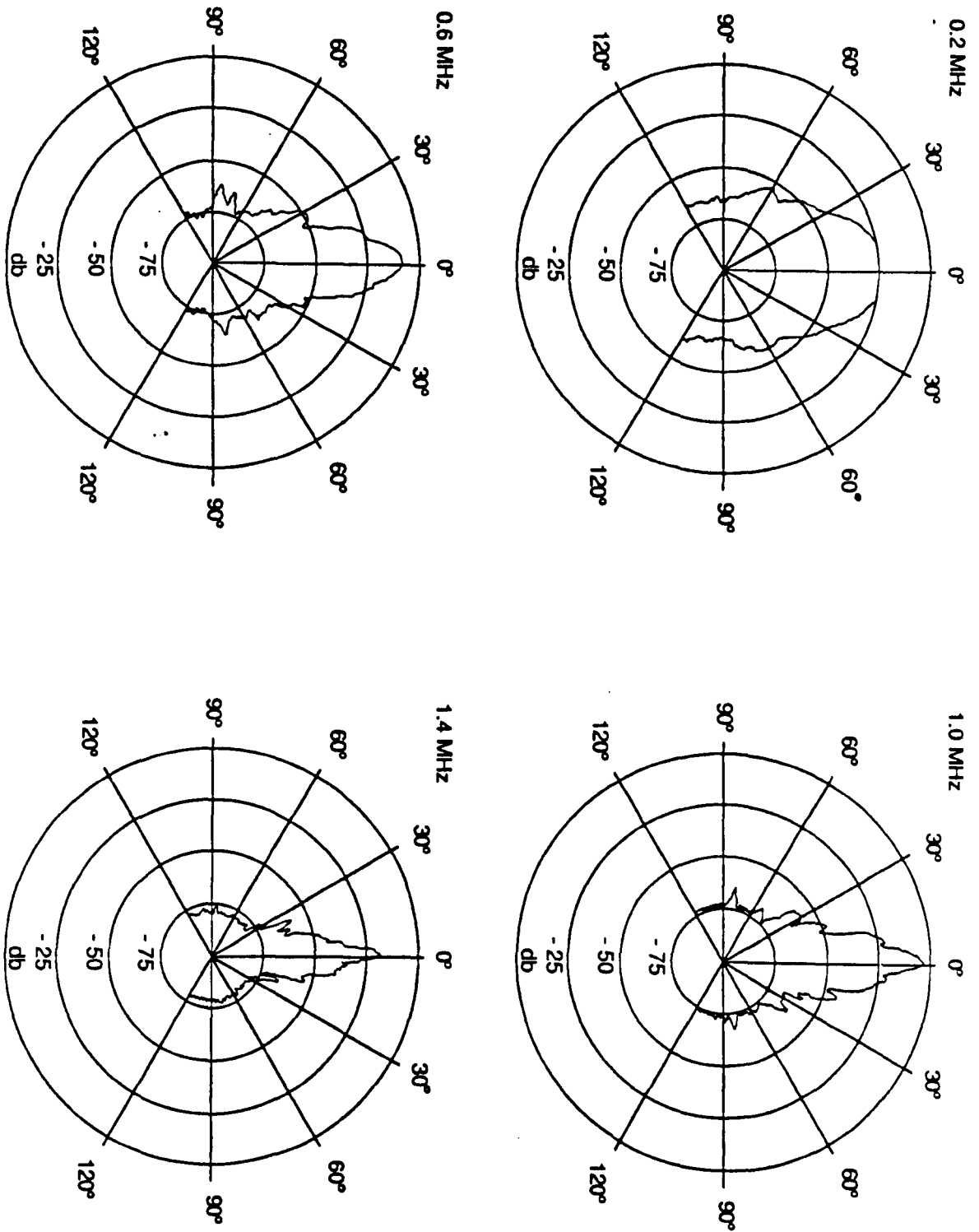
Figure 4.14 Polar plots of the ultrasonic signal amplitude propagating through water, at 0.2, 0.6, 1.0 and 1.4 MHz.
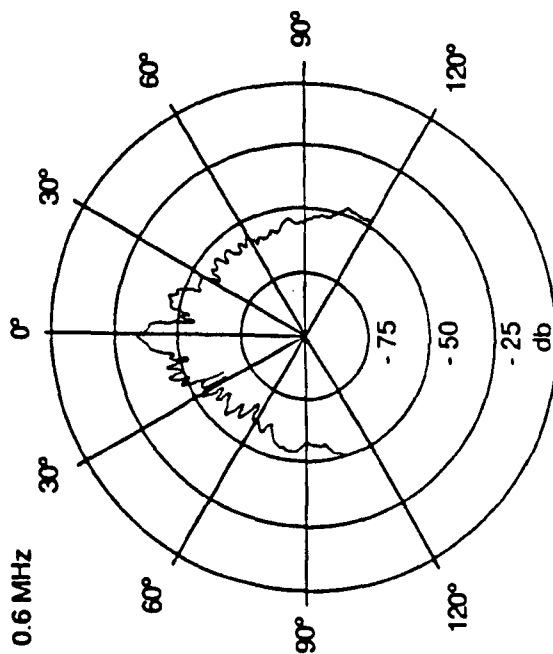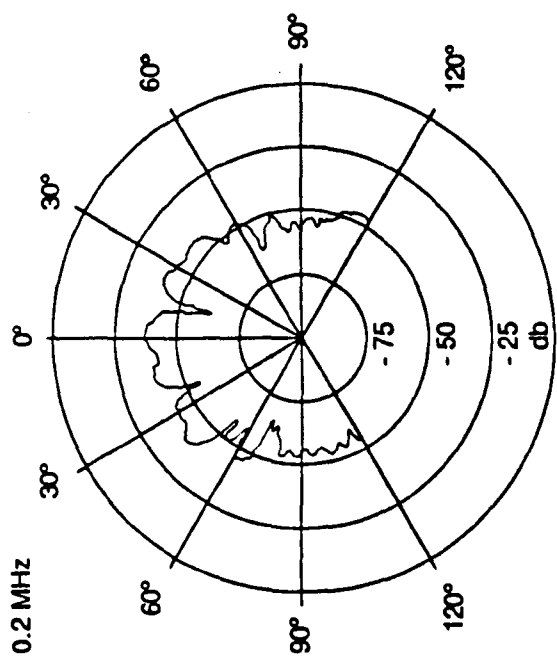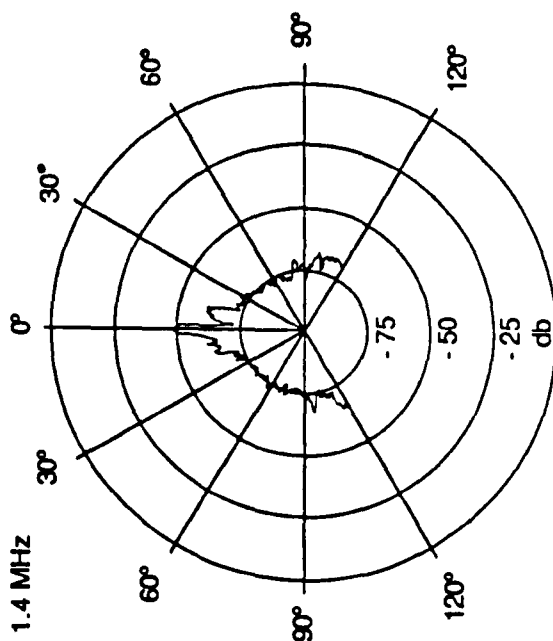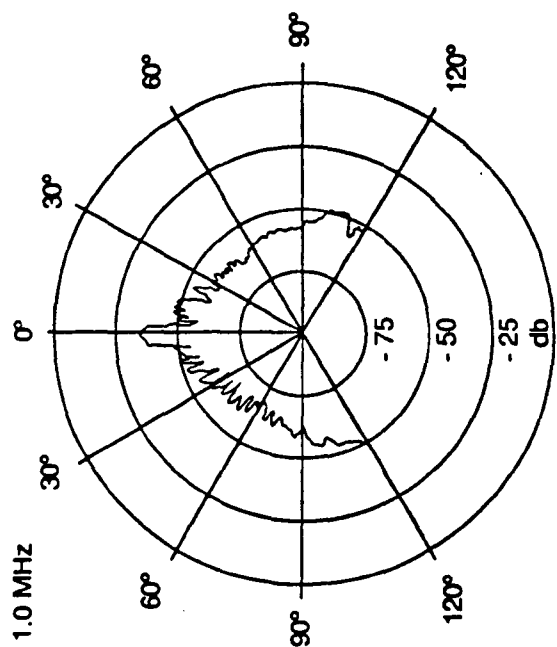
Figure 4.15 Polar plots of the ultrasonic signal amplitude propagating through
water and a bone core, at 0.2, 0.6, 1.0 and 1.4 MHz.

of the cylinder, a. For the bone samples, of radius 15 mm, the 200 kHz limit
represents a ka value of 12.7, increasing to 89.2 at 1.4 MHz. Thus in all
cases ka >> 1, allowing a simplification of the formula for the ratio of
scattered intensity I_s to the incident intensity I:

$$\frac{I_s}{I} = \frac{a}{r} \sin (\phi / 2) + \frac{1}{kr} \cot^2 (\phi/2) \sin^2 (ka \sin \phi) \quad (4.2)$$

where r is distance from the centre of the cylinder

and ϕ is the angle of scatter.

The results of this calculation are shown in figure 4.16 for the same
frequencies shown in the experimental results. As the frequency increases, the
main peak becomes much narrower with little or no side lobes present. The same
pattern can be seen for the bone sample, with a fairly even distribution
around the other angles, although the transmission peak is much smaller. It
would seem that the bone core is scattering the ultrasound as a cylinder with
perhaps some extra scattering from the internal structure of the sample. The
areas under the plots can not be compared accurately because all the possible
angles have not been considered. It was impossible to measure the signal
reflected from the sample with the equipment used because of its small size
compared to the initial spike of the transmitted pulse.

4.6 Direction of Propagation Through Cancellous Bone.

Six cores were drilled from os calces and the cortical surfaces sliced off
as described in section 3.4. Four samples were then used to produce cubes with
sides of approximately 15 mm. This size represents the largest cube that could
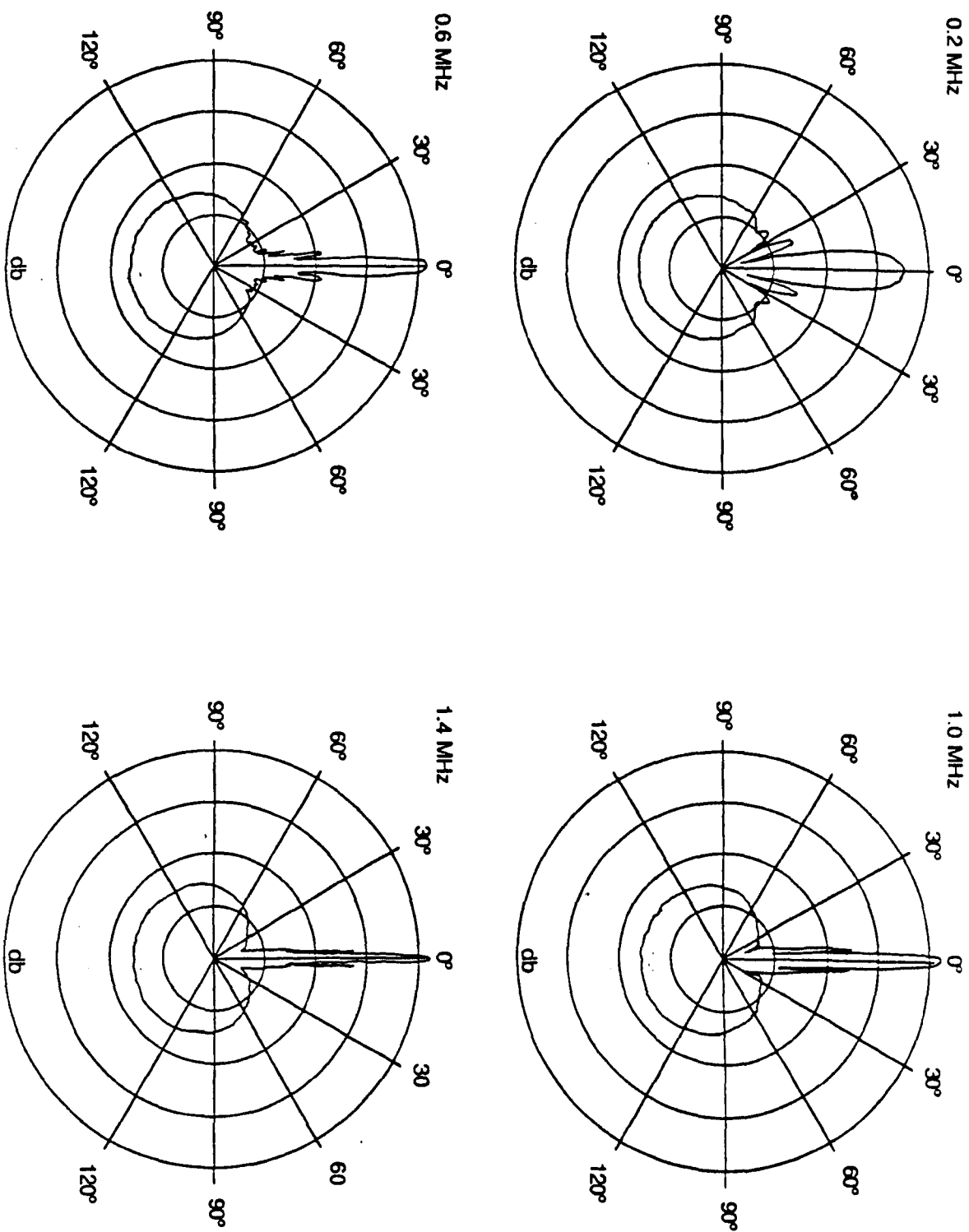
Figure 4.16 Theoretical polar plots for the signal scattered from an ideal
cylinder.

be cut from the os calces at the site scanned by the BUA technique because of the widths of the heel bones used. It could therefore be cut directly from the cores. Two cores were too small. A block for positioning the cores during cutting was made and the four cubes cut in an identical fashion, using the sides and guide cuts in the block to keep the sample as square as possible.

The cubes were too small to be measured with the 1 MHz broadband transducers. Severe diffraction would have occurred around the sample due to the large beam width. The spherically focussed 500 kHz transducers were used instead, focussed at the centre of the cube, allowing attenuation values to be found from 250 to 600 kHz, from which the slope per unit length was calculated. The cubes were positioned on the central mount which did not affect the focussed beam.

The three axes of each cube were marked, and attenuation values recorded for each orientation in 50 kHz steps. The tests were repeated to check the consistency of the results. A linear least squares fit was applied to the attenuation as a function of frequency, and the slope normalised for unit length.

The results are listed in table 4.2, showing the values obtained from both sets of tests. The attenuation slope per unit length depends upon the direction of propagation through the cancellous bone. The axes were numbered arbitrarily for the measurements. Unfortunately, when the cubes were cut, it was not recorded which axis corresponded to the direction of propagation of the ultrasound during the ordinary BUA measurement.

The aim of this section was to compare the ultrasonic slope per unit length for cancellous samples of the same density but different trabecular pattern. However, because of the small size of the cubes, focussed transducers had to be used. This means that the actual volume of bone the ultrasound propagates through is different for each orientation, figure 4.17, so the density may

Table 4.2 Ultrasonic slope as a function of the orientation of the sample with respect to the transducers.

	ultrasonic slope per unit length $(dB\ MHz^{-1}\ cm^{-1})$		
axis cube no.	1	2	3
1 (i)	3.5	14.2	6.5
(ii)	0.7	11.8	6.4
2 (i)	19.9	4.1	8.2
(ii)	20.2	4.9	8.9
3 (i)	8.6	13.0	3.1
(ii)	7.6	12.9	3.6
4 (i)	9.3	4.3	9.6
(ii)	9.1	4.1	9.5
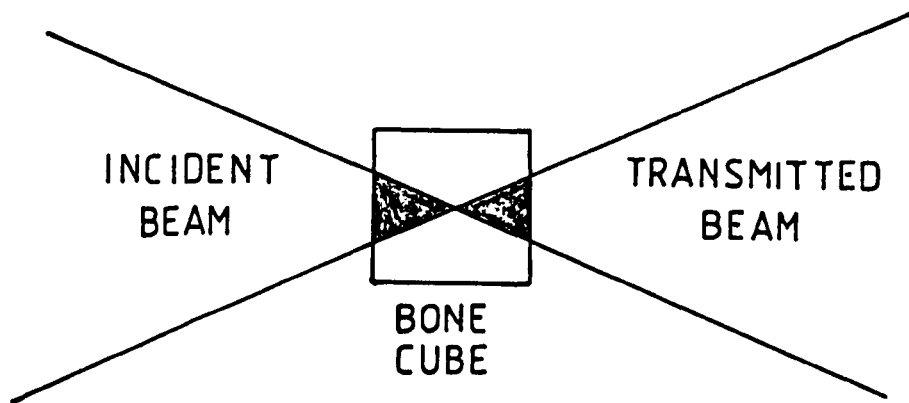
Figure 4.17 Diagram showing the orientations of the bone cube with respect to the ultrasonic beam.

also vary. The variation in ultrasonic reading for each cube is fairly substantial, with the results for two of the cubes changing by up to a factor of 5. Using the graph of slope per unit length against density for the cancellous samples, figure 4.1, this change in ultrasonic result represents a variation in density of about 70 kg m^{-3}. It seems unlikely that there would be such a large variation in density within the small cubes, although a significant change in the trabecular pattern would be expected because of the way that the trabeculae are oriented along the lines of stress.

4.7 Cortical Bone Results.

The ultrasonic attenuation and velocity measurements were repeated on ten cortical samples. The samples were cores from fresh bovine femur which were stored in formal saline. The surfaces were ground flat on coarse glass paper to produce a cylinder of the same diameter as the cancellous samples. All the cortical samples were much shorter than the cancellous samples, with an average length of 5 mm. The density was found using the submersion method described in section 3.4.2.

The velocity was found as described in section 4.3. Multiple reflections were produced in these samples due to their smaller size, lower attenuation and faster ultrasonic velocity. A typical trace is shown in figure 4.18. The velocity could still be established from the first arrival of the signal.

The cortical samples were measured using the broadband transducers in the same way as the cancellous samples. The frequency dependent traces included the effects of multiple reflections, with constructive interference producing peaks at the frequencies given by

Figure 4.18 Time dependence of the ultrasonic signal propagating through a
cortical sample.
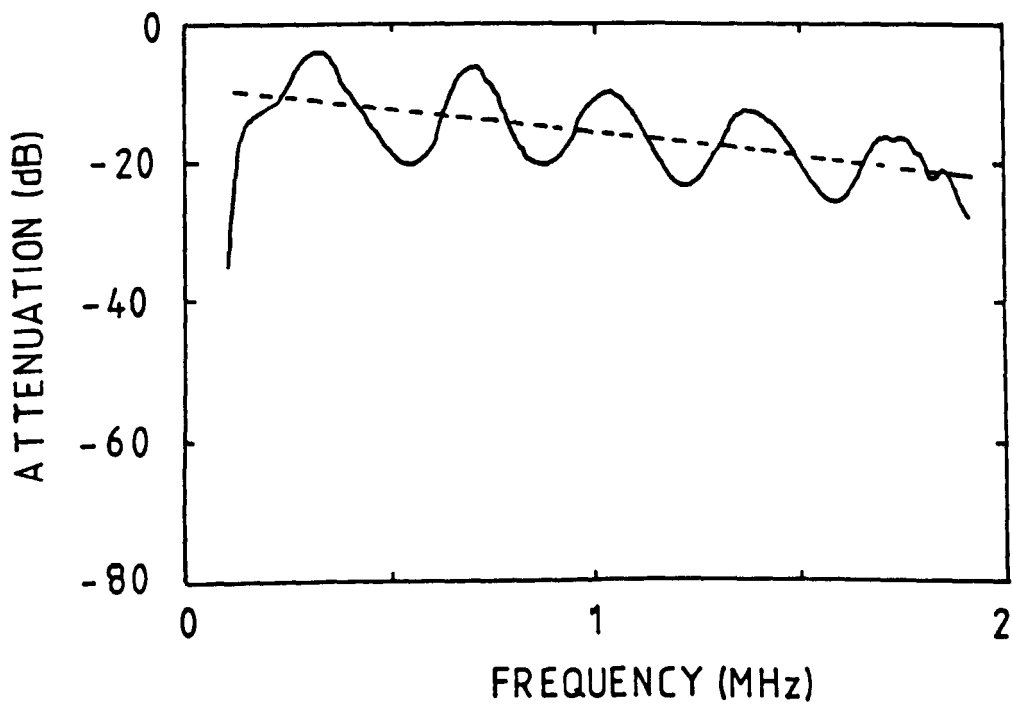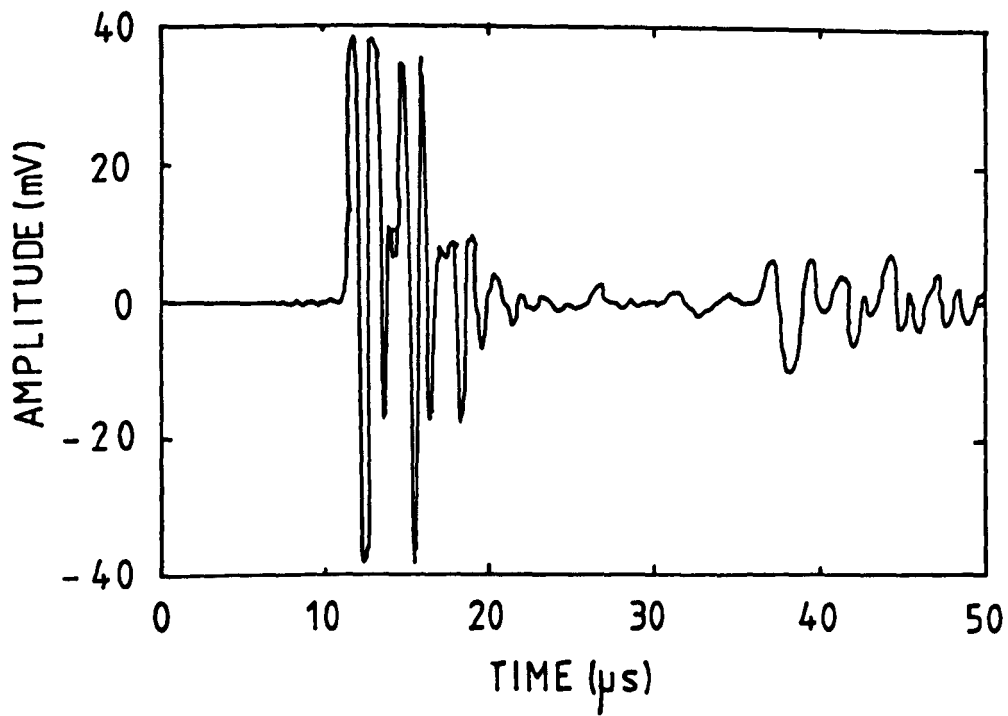
Figure 4.19 Frequency trace including the best fit line for the signal
propagating through a cortical sample.

Table 4.3 Density, ultrasonic slope, velocity and impedance for 10 cortical samples.

No.	density (kg m^3)	ultrasonic slope (dB MHz^{-1}cm^{-1})	longitudinal velocity (m s^{-1})	characteristic impedance (10^6 kg m^{-1}s^{-1})
1	2025	4.9	3378	6.8
2	2028	7.0	3571	7.2
3	1970	7.6	3318	6.5
4	2058	5.5	3440	7.1
5	2043	9.6	3251	6.6
6	2006	7.4	3441	6.9
7	2038	7.2	3387	6.9
8	2023	5.1	3311	6.7
9	2018	10.2	3444	6.9
10	2006	4.5	3254	6.5
mean	2021	6.9	3380	6.8
st. dev.	24	1.9	99	
cancellous bone range	940 - 1170	4 - 35	1650 - 2100	1.7 - 2.3

$$f = \frac{n\ c}{2\ L} \tag{4.3}$$

where   n is an integer

c is the velocity

and   L is the length of the sample.

The slope of the attenuation as a function of frequency was calculated over the range 0.2 to 1 MHz, and it was assumed this averaged out the effect of the interference, figure 4.19.

The results for the ten cortical samples are given in table 4.3. There is little difference between the samples as all the cows can be assumed to be healthy and of similar age. The mean of the results are given at the base of the table together with the range of comparable results obtained from the cancellous samples.

The reflection losses at the bone surface are very important for the cortical samples. The average acoustic impedance of the samples was 6.8×10^6 kg m^{-2} s^{-1} (standard deviation 0.2) resulting in a total loss of 4.5 dB from both surfaces of the sample. This will be constant over the frequency range used as no velocity dispersion should occur in the homogenous cortical bone. Thus it will not affect the value of the attenuation as a function of frequency. It will, however, affect the actual attenuation values obtained. For instance, in figure 4.19, the ultrasonic attenuation at 500 kHz is given by the regression line as 5 dB. The losses due to the impedance mismatch have to be subtracted from this, to give an effective attenuation of only 0.5 dB. This represents a 90% decrease in the actual attenuation.

The measurements carried out on the cortical bone are intended to demonstrate the difference between the ultrasonic properties of cancellous and cortical bone, rather than as an actual analysis of the ultrasonic parameters of the cortex. Many papers have already been published by a variety of researchers on the ultrasonic properties of cortical bone. A summary carried out by Goss et al in 1978 lists all the measurements available to that date, and the results for density and velocity in this work are in good agreement with those listed, as well as with more recent work (Ramachandraiah and Suryanarayana, 1987. Andre et al, 1980 and Meunier et al, 1982).

Garcia et al (1978) carried out attenuation measurements on bovine cortical bone but using a frequency range of 1 to 7 MHz. However, the attenuation was less than 12 dB cm^{-1} at 1 MHz, excluding reflection losses. Hyodynmaa et al (1986) obtained a mean attenuation coefficient of 9.6 dB cm^{-1} for *in vivo* measurements of human cortical bone around a central frequency of 2 MHz.

The higher density and velocity, and more particularly the much lower ultrasonic attenuation show that the ultrasound propagates easily through cortical bone, completely different to the propagation in cancellous bone.

4.8 Comparison to Quantitative Computed Tomography.

Quantitative computed tomography (QCT) measurements have been carried out on the os calces and trabecular samples from one batch of bones, in conjunction with Dr. Clifford and Dr. Fordham of the Middlesbrough Health Authority. The measurements were carried out on a Technicare 2020 CT scanner, and consecutive 4 mm sections obtained at 120 kV and 50 mA. The reconstructed image was made up from a 512 square matrix. The bone density was calculated in the required region in Hounsfield Units (HU). The equipment had been calibrated with a standard phantom prior to the measurements and was operated

by a radiographer at the South Cleveland Hospital. Typical reproducability of the technique has been discussed in section 2.2.4.

4.8.1 Os calces.

33 os calces were scanned both ultrasonically and with QCT. The ultrasonic measurement consisted of the attenuation slope per unit length for each bone. Up to three consecutive slices were imaged for each os calcis during the QCT scanning, and a 5 cm^2 ovoid section used as the area in which the bone density was calculated for each slice. This area coincided with the path along which the ultrasound propagated during the BUA measurements. An average bone density was found from all the readings taken for each os calcis.

Figure 4.20 shows the correlation of 0.92 between the two measurements. The regression line does not pass through the origin as might be expected because the ultrasonic reading includes the cortical surfaces of the os calcis whereas the QCT uses an area taken from slices within the heel bone. Thus the ultrasound registers a reading when there is effectively no trabecular bone present, section 4.4.2. The correlation is very highly significant for the 33 bones measured.

The BUA and QCT measurements correlated equally well with the physical density of the os calces. The graph for the QCT results is shown in figure 4.21 with a highly significant correlation of 0.84. The correlation with density for the same 33 bones measured ultrasonically is also 0.84.

4.8.2 Trabecular Samples.

33 cancellous samples were also measured by both BUA and QCT. These were not necessarily from the same 33 os calces used in the previous section, as one or two of the lowest density samples collapsed during preparation. One 4 mm slice was used from each sample for the QCT measurement, and the cross
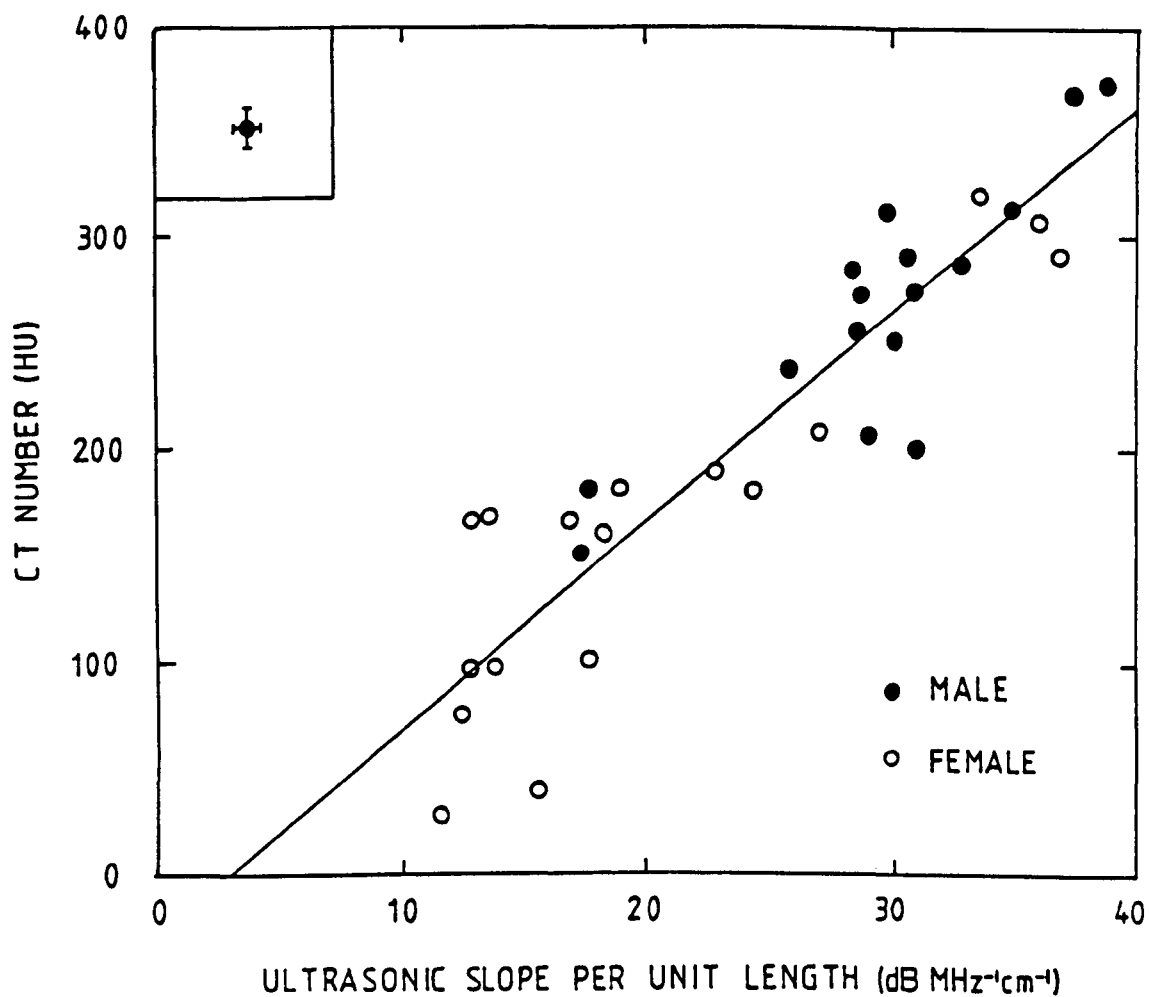
Figure 4.20 Bone density evaluated by QCT plotted against the ultrasonic

slope per unit length for 33 os calces.

gradient = 9.7 +/- 0.8

intercept = -29 +/- 20

correlation coefficient = 0.92
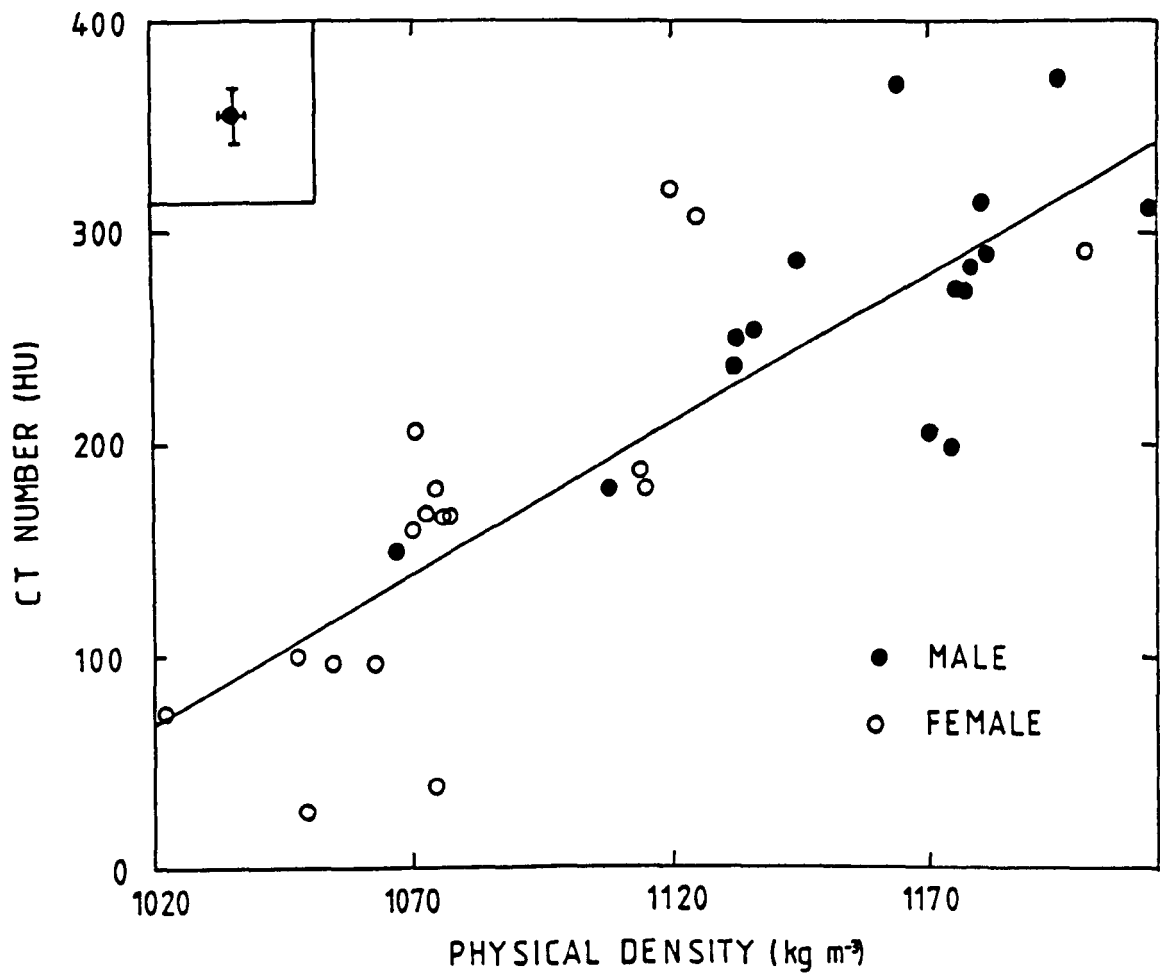
Figure 4.21 Bone density evaluated by QCT plotted against the physical density
of 33 os calces.

gradient = 1.4 +/- 0.2

correlation coefficient = 0.84

section of the core used to define the area in which the bone density is calculated. Five such images produced near zero or negative bone density values. Inspection of the film and the values obtained suggested that the 4 mm slice had extended over the end of the actual sample, thus greatly reducing the effective bone density measured. These five results were neglected.

The results for the 28 samples are shown in figure 4.22. The correlation for the two measurements is 0.86. The regression line in this case would be expected to pass through the origin, but in fact has an intercept on the y axis of 52 +/- 20 HU. However, the two low density samples that were measured suggest that the regression line should in fact be steeper, with a much smaller y axis intercept. It is very unfortunate that so few low density samples were successfully measured by both techniques. The correlation is lower than that for the whole os calces, although it is still highly significant, and may be due to a larger error in the QCT values. Only one slice was imaged during the QCT measurement of the trabecular samples, whereas readings from up to 3 consecutive slices were averaged for the QCT measurement of the whole os calces. This averaging is often used in QCT measurements (see section 2.2.4) and produces a more reliable result.

Both techniques again correlate highly significantly with the physical density of the samples. Figure 4.23 shows the results for the QCT measurements. The ultrasonic slope per unit length correlated with the physical density of the same 28 samples with r = 0.85.

4.9 Discussion and Conclusions.

This chapter has detailed the results of ultrasonic measurements of os calces and of trabecular samples obtained from those os calces.

The attenuation measurements were intended to mimic the clinical BUA system currently available, and were therefore based on the attenuation as a function
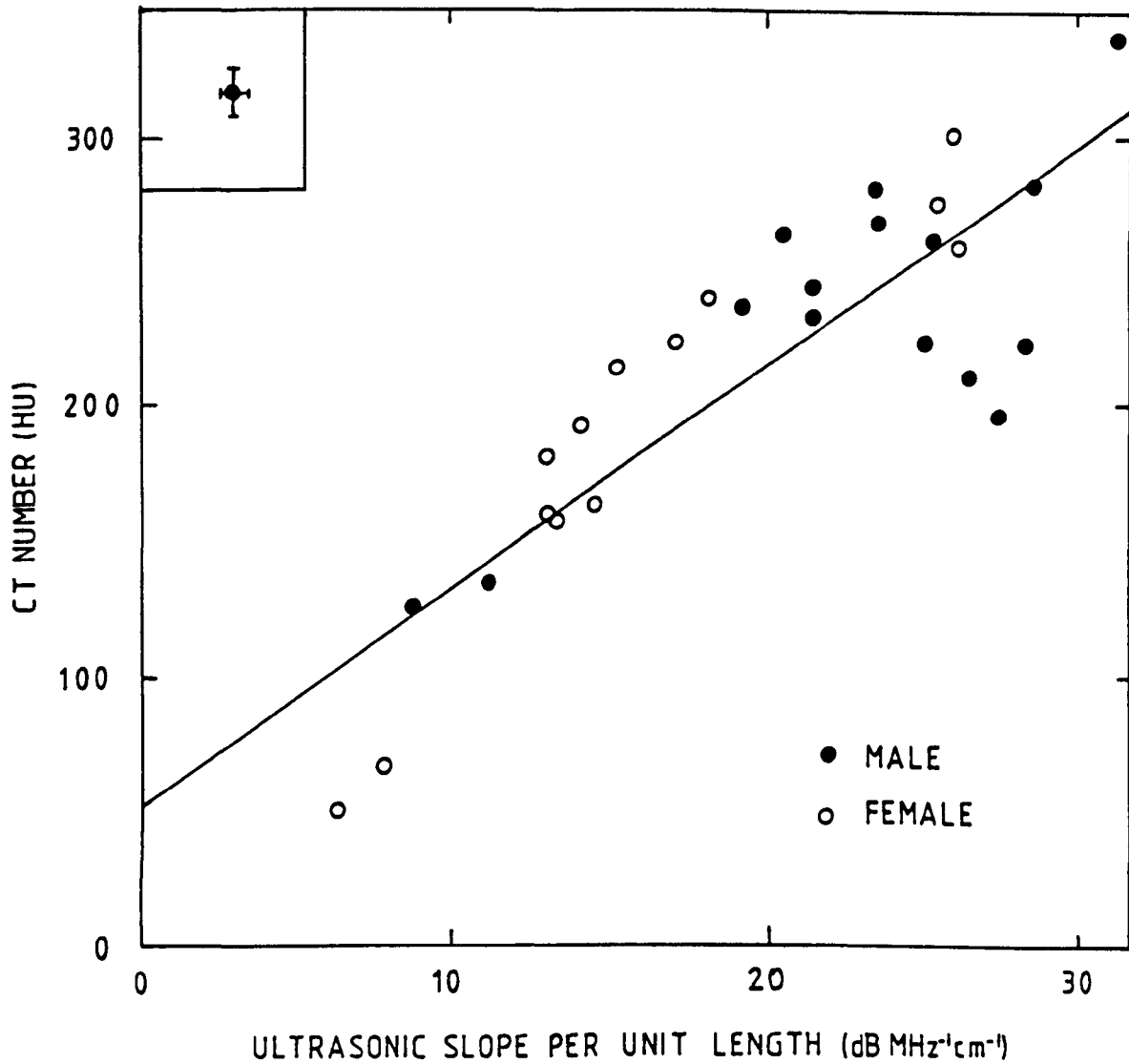
Figure 4.22 Bone density evaluated by QCT plotted against the ultrasonic

slope per unit length for 28 trabecular samples.

gradient = 8.2 +/- 1.0

intercept = 52 +/- 20

correlation coefficient = 0.85
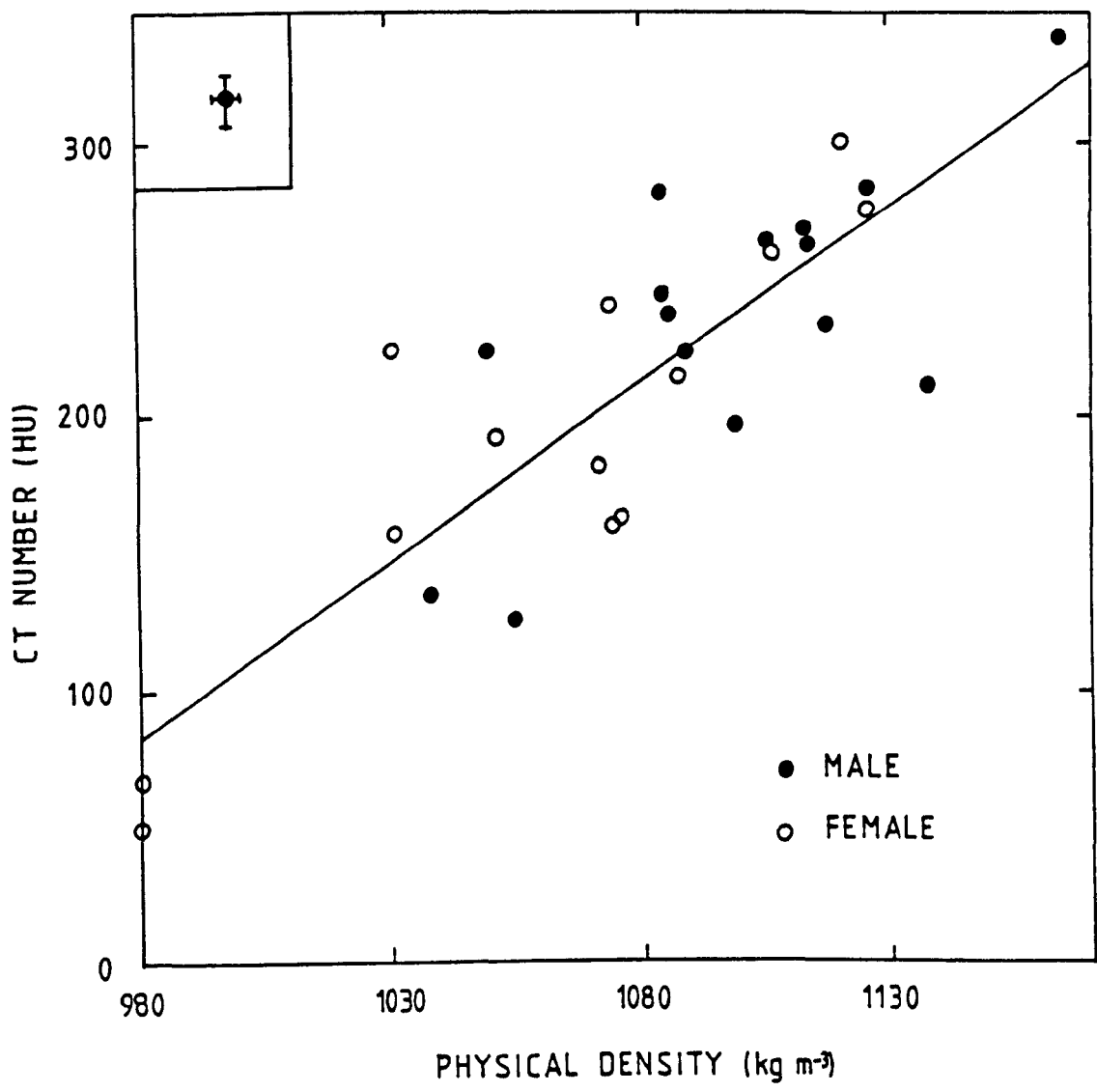
Figure 4.23 Bone density evaluated by QCT plotted against the physical density

of 28 trabecular samples.

gradient = 1.3 +/- 0.2

correlation coefficient = 0.85

of frequency from 200 to 600 kHz for the human os calcis. They showed that the ultrasonic slope per unit length correlated directly with the physical density of the os calcis, and therefore with the bone mineral density. The slope itself gives an excellent correlation with the physical density, showing that the *in vivo* measurements can be relied upon to give a good indication of the bone mineral density. Measurements were also carried out for purely trabecular samples, and the correlation with density was highly significant.

Velocity measurements were conducted on the trabecular samples and these correlated slightly with the density. More importantly, these were used to calculate the characteristic impedance and reflection losses due to the surfaces of the samples. The measurements carried out on the trabecular samples showed that it was indeed the cancellous bone that mainly affects the ultrasonic propagation, and not the shape or the surface of the os calcis. This is a very important conclusion that proves the BUA technique does measure the variation in properties of the trabecular bone itself.

Ultrasonic measurements have been conducted on cancellous bone on only a few occasions previous to the development of the BUA technique. The dependence on physical density shows that the results rely greatly on the skeletal site and mammal from which the samples are taken. However, many such experiments have been conducted on cortical bone. The importance of the lower frequency range is clear for cancellous bone measurements, as the attenuation is extremely high even at the top of the frequency range used in the current work. Medical ultrasonics usually involves frequencies higher than 1 MHz.

Lehmann and Johnson (1958) carried out measurements on cancellous bone taken from a pig. The typical density was 1250 kg m^{-3}, higher than the largest density of 1170 kg m^{-3} for the cancellous samples used in the current work. They measured the velocity to be 2407 +/- 554 m s^{-1} over the range of samples
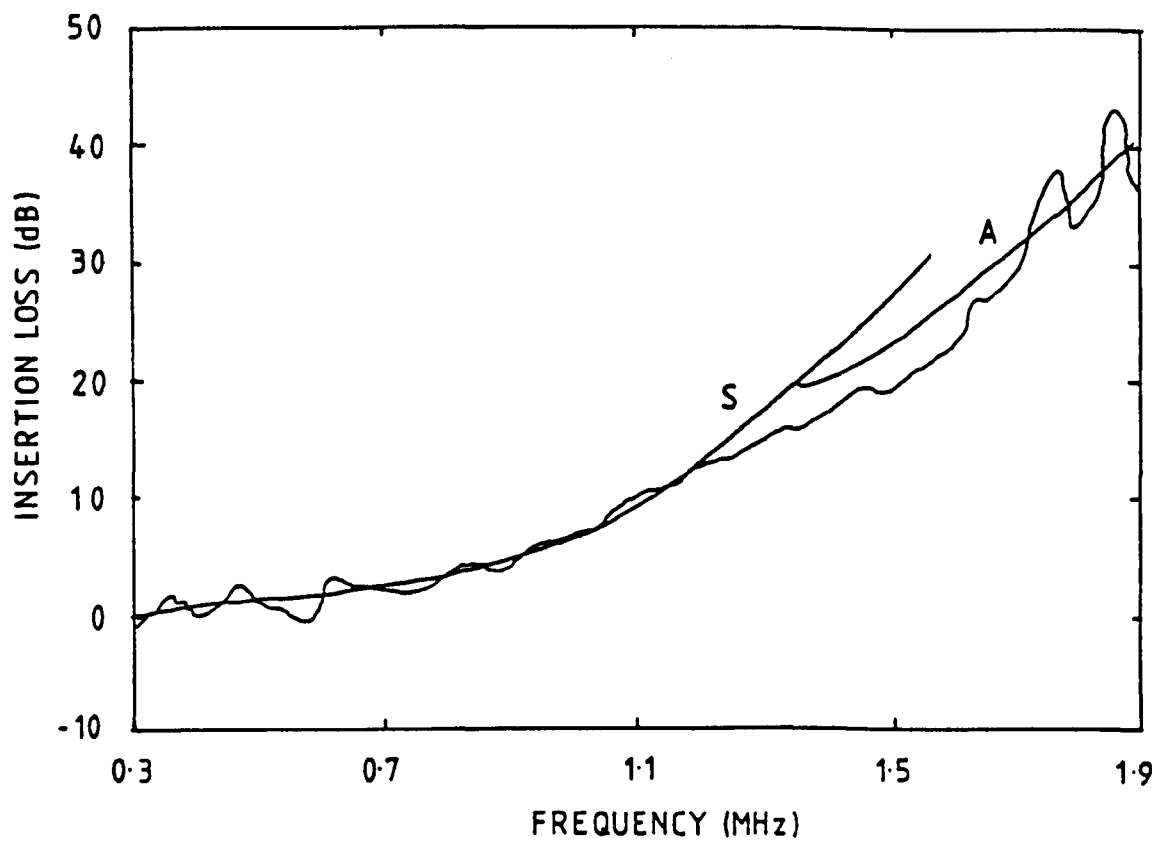
Figure 4.24 Scatter and absorption of ultrasound by the diploe layer of skull

as a function of frequency.

(Fry and Barger, 1978)

tested, again generally higher than the values obtained here although the ranges do overlap. However, with the density higher, the velocity is expected to be greater. The ultrasonic attenuation for a complete pig thigh bone was quoted as 8.4 dB cm^{-1}, but this will be mainly cortical bone. The measurements were conducted at 1 MHz.

Fry and Barger (1978) used samples from the human skull for a range of ultrasonic experiments. The skull is composed of a cancellous diploe layer between the outer and inner ivory tables. The aim of the work was to prove that ultrasound could be used to image objects, such as tumours, within the skull successfully, without being affected by losses and small scale inhomogenieties in the bone itself. The diploe layer was the most important feature when ultrasonic losses were considered. The density of the samples, over 1700 kg m^{-3}, was substantially larger than that of the cancellous samples used in the present work and the samples were extremely thin, usually only a few millimetres, as might be expected from the structure of the skull.
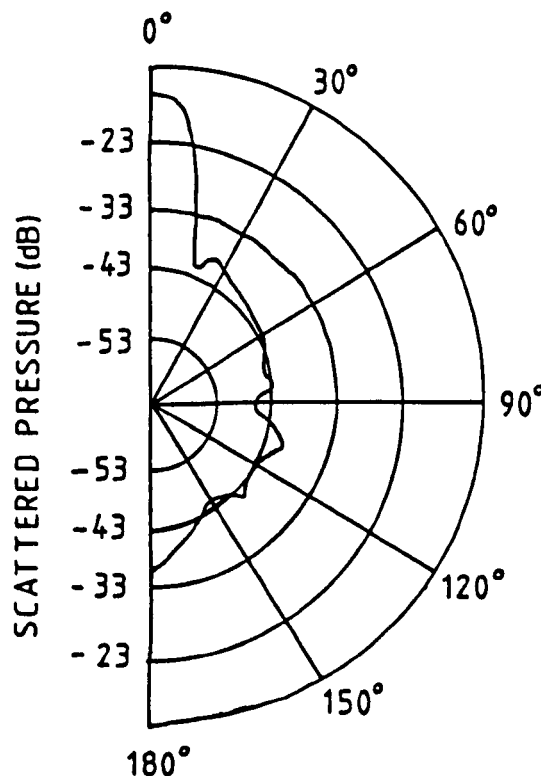
Figure 4.25 The ultrasonic scatter at 1 MHz from the diploe layer of a skull.
(Fry and Barger, 1978)

Fry and Barger suggest that scattering becomes important around 1.3 MHz, with absorption being the main method of attenuation at the lower frequencies, figure 4.24. They found an attenuation of 13 dB cm^{-1} at 1 MHz and a linear dependence on frequency up to about 2 MHz. This attenuation is at the lower end of the range found in the current work, despite the density being much larger. They used the volumetric bulk modulus variation to describe the scatter and attenuation, a theory attributed to Mason and McSkimin (1947). This was also the basis of the theory used by Langton (1984).

Fry and Barger also carried out an experiment looking at the scattered sound. The result of their single test is shown in figure 4.25. The large signal at 0° is sound that has been reflected by the solid ivory table. The smaller peak at 180° is the transmitted signal. The decibel levels are relative to the incident wave, and there is an even distribution of a small signal around the wider angles. This is in agreement with the results of section 4.5. The samples used in the present work were purely cancellous, with no solid cortical layer, hence there was no large reflected peak as found by Fry and Barger.

Section 4.6 is an attempt to assess the effect of the trabecular pattern on the ultrasonic slope. If the cubes were of a size comparable to the width of the 1 MHz broadband beam, it could be assumed that the ultrasound propagates through the entire volume of the sample. However, because of diffraction effects around the smaller samples, focussed transducers had to be used. The actual material through which the beam passes for each orientation of sample is slightly different, figure 4.17, so the average density of the bone for each path may also vary slightly, as discussed in section 4.6. It would seem that the changes in ultrasonic slope between the different sample orientations are too large in many cases to be accounted for by slight variations in the

physical density. Therefore the ultrasonic attenuation as a function of frequency is affected by the architectural pattern of the bone, the orientation of the trabeculae and hence the permeability of the structure.

The comparison between the ultrasonic attenuation and velocity of the cortical samples with the cancellous bone also suggests that the ultrasound is affected by the trabecular structure. If the results for the cortex were extrapolated back to the lower densities, comparable to cancellous bone, the expected ultrasonic parameters would be very different to those obtained experimentally. For a particular bone mineral content, the BUA technique would register a different result depending on whether the sample is trabecular or cortical. This is a difference in attenuation as a function of frequency which is not accounted for by the fat content of the trabecular bone. Jones et al (1987) have demonstrated similar results. The real density of trabecular bone, calculated from the mass and volume of the bone itself without the fat or marrow, is comparable to ordinary cortical bone densities, so even if this was used as a basis for comparing the attenuation slope of trabecular and cortical bone, there would still be a large difference in the results obtained. Therefore, the structure of the trabecular bone does affect the ultrasonic attenuation as a function of frequency.

The final part of this chapter is a comparison of BUA a technique currently used in hospitals for the measurement of bone mineral. By measuring the same samples, a direct comparison can be made between methods.

The BUA results correlated very well with the QCT measurements for both the os calces and the trabecular samples from an elderly population, suggesting the new ultrasonic technique is just as effective as the existing method for evaluating the physical density of cancellous bone in vitro. The correlation between systems measuring the same site has not often been investigated in the past, as individual systems are usually developed for scanning one particular site. There have been comparisons between QCT and dual

photon absorption (DPA) as both techniques measure the spine. Ott et al (1984) found only a correlation of 0.26, but the DPA measured bone density for the whole vertebrae where as the QCT found the bone density of the trabecular bone. This situation is, however, comparable to the tests reported in this thesis for the measurements on the whole os calces as the ultrasound is affected by the cortical surfaces whereas the QCT is not. A more complete study was reported by Genant et al (1984) where the bone mineral content and the density of the whole vertebrae were measured by both techniques in 50 patients, representing a broad range of metabolic bone disorders. The correlations were 0.88 and 0.84 respectively. Mazess and Vetter (1984) investigated ten excised vertebrae with DPA and dual energy QCT and obtained a correlation of 0.87 for total bone mineral density and 0.82 for trabecular mineral density. The correlations reported here between BUA and QCT are comparable to the published results comparing existing techniques.

This chapter has demonstrated that the BUA technique gives an excellent indication of the physical density of cancellous bone. The ultrasonic measurements also correlate well with quantitative computed tomography, a well used clinical method for evaluating bone density. Such detailed ultrasonic measurements on cancellous bone have not been published before, and represent an extension to the well documented measurements on cortical bone.

Chapter Five.

THE COMPRESSIVE STRENGTH OF TRABECULAR BONE.

5.1 Introduction.

The most important property of both cortical and trabecular bone is its strength. For vertebrae in particular, since they collapse by being crushed, the compressive strength will give a good indication of the quality of the bone and the degree of osteoporosis. Generally, the presence of crush fractures in a spine, as seen on a radiograph, is used to diagnose whether a patient has osteoporosis or not.

There have been a variety of studies investigating the compressive strength of bone from many skeletal sites in addition to the spine, with early work relating the strength to physical parameters such as density and strain rate (Carter and Hayes, 1976) and more recent work comparing the compressive strength to results from non-invasive diagnostic techniques (Horsman and Currey, 1983. Hvid et al, 1985).

The work in this chapter is aimed at investigating two areas: first, the relationship between the compressive strength of vertebrae and ultrasonic measurements of the same bones, and second, the correlation between the BUA measurement of the os calcis and the compressive strength of vertebrae from the same cadaver.

5.2 Compressive Strength Testing.

Commercial materials testers, such as those made by Instron, are used to load samples at known rates. A chart recorder produces a record of the load against the deformation as the test takes place. The maximum compressive

strength is taken as the load at which the sample breaks, the maximum point on the load - deformation curve, figure 5.1. With a porous substance such as trabecular bone, this point represents the load at which the trabecular struts break. As the bone is compressed even further, another peak will occur on the trace until the solid bone itself is fractured. The important value is the load at which the trabeculae break, as this will be comparable to vertebrae being crushed in the spine.
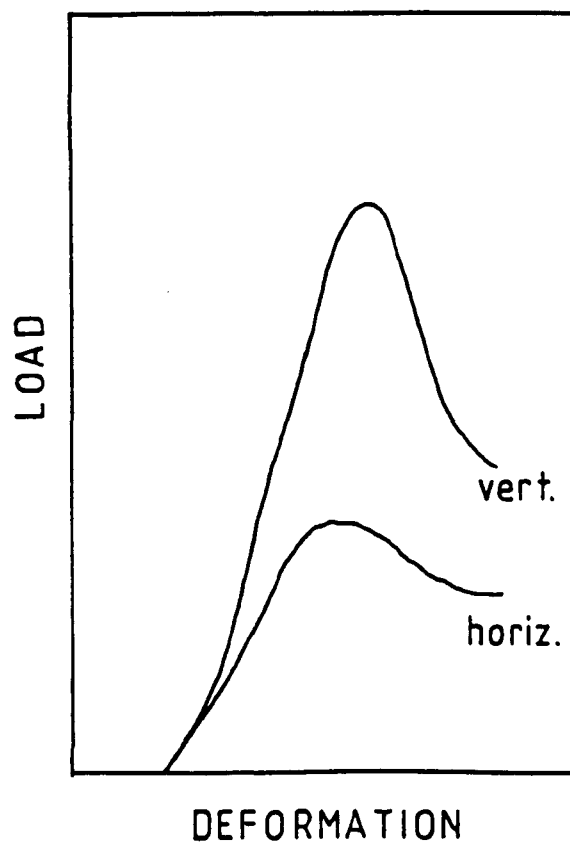
Figure 5.1 A typical load - deformation curve for trabecular bone.
(Mosekilde et al, 1985)

Different sites contain different structural patterns of trabeculae, depending on the everyday stresses acting on that site. This means that the compressive strength of the cancellous bone depends on the site from which it is obtained. Clinically, the vertebrae are the most interesting because of the crush fractures of the spine. Figure 5.2 shows the typical maximum compressive strength for the vertebrae along a normal spine. It is the thoracic region that suffers initially from osteoporotic fractures since the lumbar vertebrae are larger and stronger. Figure 5.3 shows the strength of the vertebrae as they weaken with age. The weakest will spontaneously collapse under the normal forces acting on the spine.

Carter and Hayes (1976) showed an excellent correlation between the compressive strength and the density of bone. They included the previously published results of other researchers and suggested that the maximum compressive strength depended upon the square of the apparent density. The apparent density is defined as the wet weight of the bone without the marrow, divided by the total sample volume, including the pore spaces. Carter and Hayes carried out their compressive strength tests with the marrow *in situ* and used their own results for trabecular bone and previously published results for cortical bone.They showed that the relation holds true for cortical, trabecular, human and bovine samples. No effort was made to separate cortical and trabecular bone in the analysis, and, by not doing this, Carter and Hayes deliberately ignored the structural differences of cancellous and cortical bone.

The apparent density should be slightly but consistently less than the physical density. The physical density, used in this thesis, includes the mass of the marrow as well as the bone, divided by the total sample volume.

Hvid et al (1985) measured the maximum compressive strength of nearly 200 samples obtained from the proximal tibial epiphyses of mature mongrel dogs. An
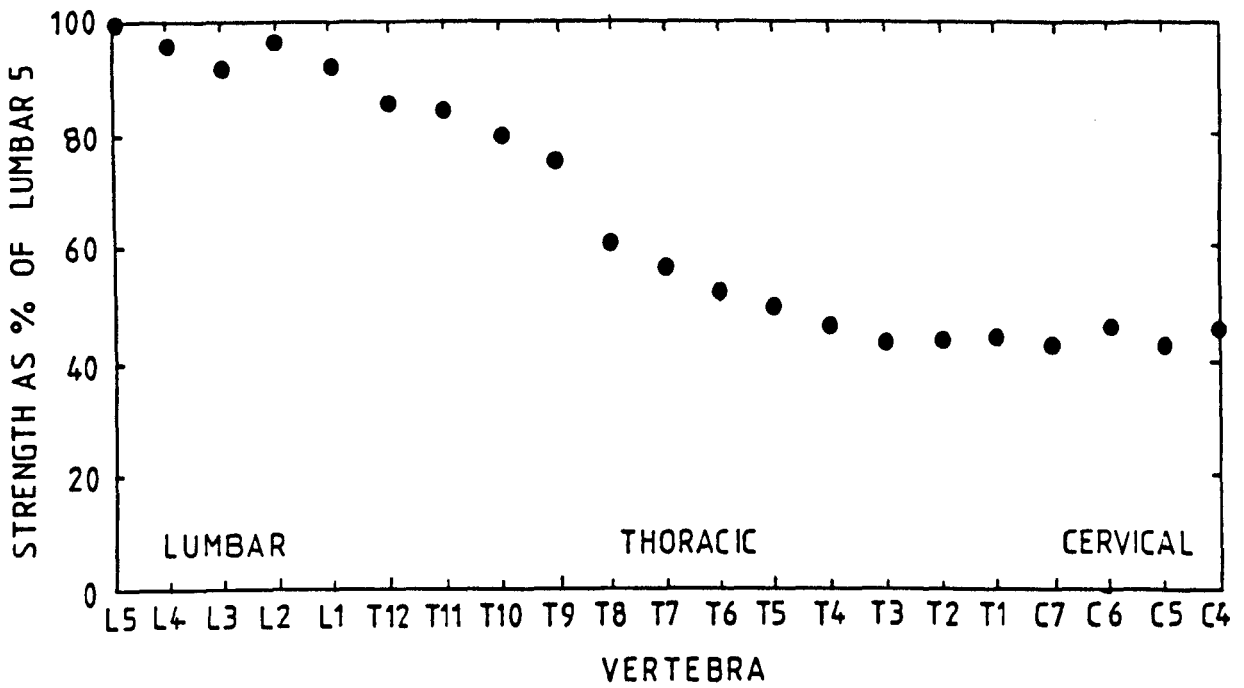
Figure 5.2 Compressive strength of each vertebrae along the spine of a

healthy person.

(Mazess, 1983b)
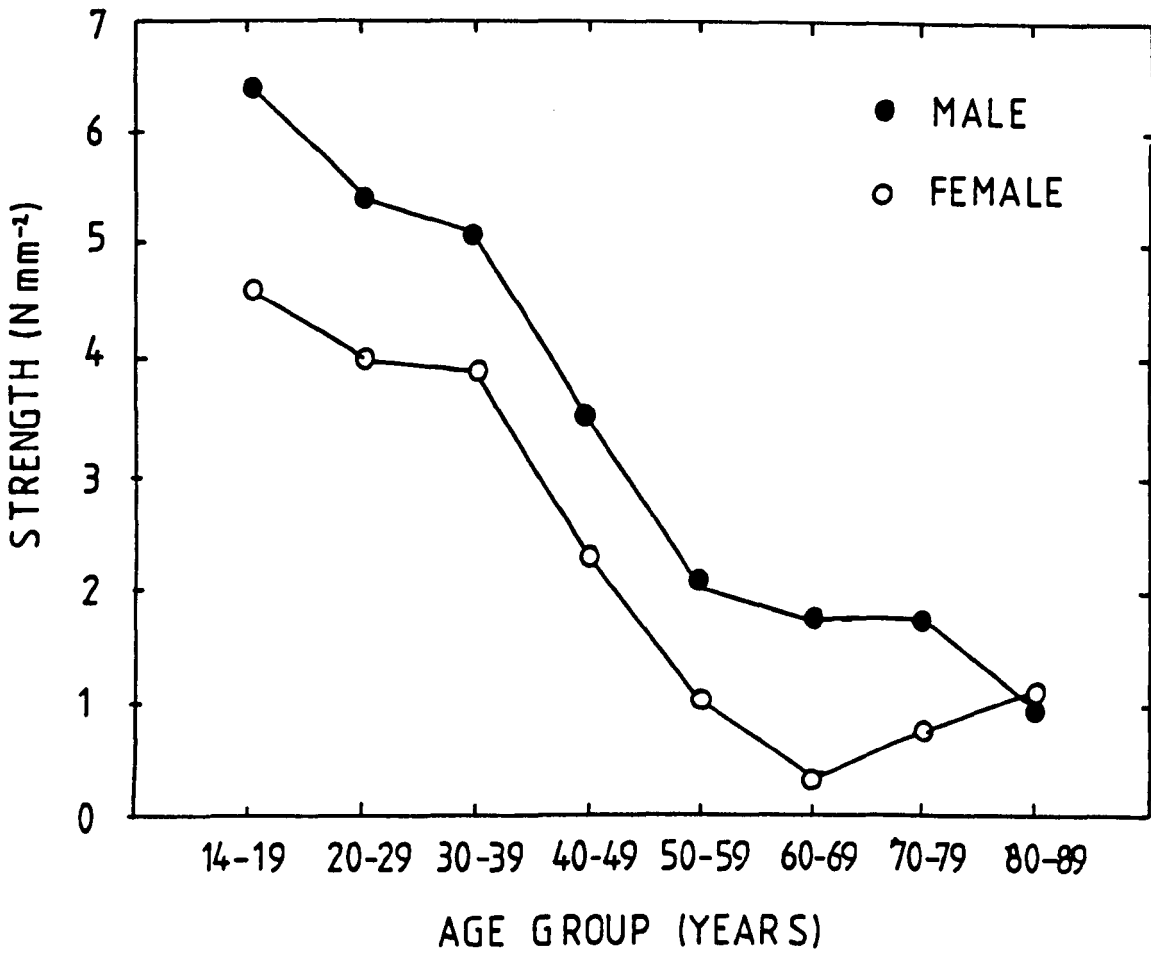
Figure 5.3 Compressive strength of the vertebrae in males and females as a
function of age.

(Mazess, 1983b)

excellent correlation with density was found, suggesting that the compressive strength depends on the density to the power 1.5. These tests did not include cortical samples.

Galante et al (1970) state that the orientation of the trabeculae is important for the strength of the bone, and this has been confirmed by many more recent papers (Kleerekoper et al, 1985. Parfitt, 1987). All these researchers agree that the relation between the maximum compressive strength and the apparent density is more important than a comparison with the real density. The real density is calculated from the mass and volume of the bone alone, and therefore does not include any consideration of the pore spaces. Mosekilde et al (1985) demonstrated the importance of orientation by testing iliac and vertebral bone oriented horizontally and vertically. The iliac bone produced a smaller difference between orientations than the vertebral bone. This might be expected, since the latter is far more isotropic, allowing it to cope with the forces acting both up and down the spine. In further work, Mosekilde et al (1986) corrected results for bone mass by normalising with the ash weight of the samples. A significant decrease in strength and stiffness was still apparent with age, and was therefore entirely due to the structural aspects rather than the changes in bone mass.

The compressive strength is sometimes quoted as the load required to fracture a sample and sometimes as the force per unit area. The latter value is important if samples of different cross section are to be compared. When vertebrae are crushed, the preparation of the samples should also be noted. Whole vertebrae are obviously stronger than a sample of purely cancellous bone, with partially cut vertebrae being different again.

Two studies were set up to compare the broadband ultrasonic attenuation with the maximum compressive strength. The first involved 148 vertebrae from Denmark and the second used 12 vertebrae from Leeds.

5.3 The Danish Vertebral Samples.

5.3.1 The Danish Samples.

148 vertebrae from 28 cadavers were frozen directly after being excised. An age range of 63 to 90 was covered, with the exception of two, aged 16 and 44 (total mean age 71.8, standard deviation 14.7). Both lumbar and thoracic vertebrae were used, with anything from three to seven vertebrae from each cadaver.

The vertebral arch was removed and the remaining body was sliced at either end to produce a parallel sided sample of cancellous bone with a cortical layer around the elliptical edge, figure 5.4. The samples remained frozen until they were irradiated to the level required to sterilise tissue (Ley, 1973) and were then refrozen until measurement.

5.3.2 Experimental Procedure.

The vertebral slices were fixed on to brass mounts to allow for repositioning and evacuated overnight under water before measurement. All the samples were oriented so that the ultrasound passed through the bulk cancellous body of the vertebrae and remained unaffected by the outer cortical ring. The reference point on the mount ensured that the samples could be repositioned. The attenuation readings and slope calculations were carried out by the same program used during the os calcis measurements, so the results are completely comparable. The thickness of each sample was noted and the slope values normalised for unit length.

Some of the Danish vertebrae, especially those from the lower thoracic region, presented a surface that was too small for the ultrasonic beam to propagate through the trabecular bone without being affected by the cortical
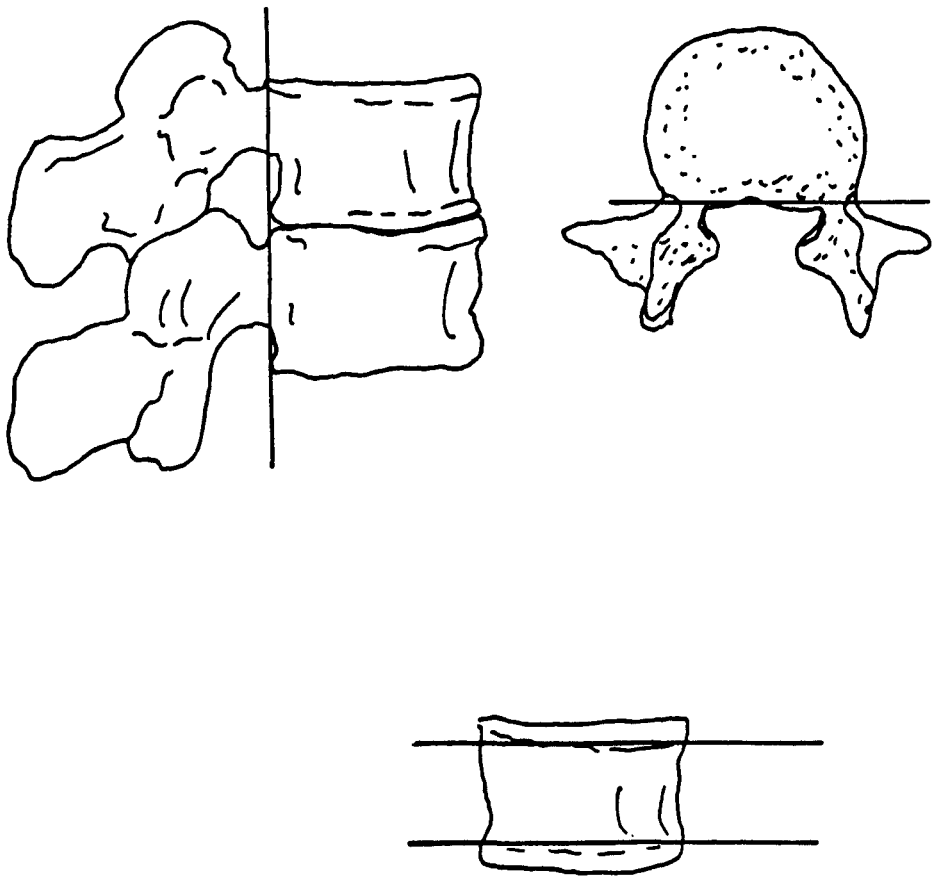
Figure 5.4 The preparation of the vertebral slices.

edges. The values obtained for these bones were neglected, resulting in 128 vertebrae being measured successfully.

The compressive strength testing was carried out in conjunction with the staff of the Institute of Anatomy at the University of Aarhus, in conjunction with Dr. F. Melsen, Ms. H. Brockstadt-Rasmussen and Dr. Li. Mosekilde.

The mean cross sectional area of the samples was calculated from the volume, found by immersion, and the thickness. The compressive strength results were normalised per unit area. All the samples were tested with the outer cortical ring present. The load - deformation curves were recorded for each sample at a constant strain rate and the maximum compressive strength calculated from each trace. The equipment and technique has been described by Mosekilde et al (1985).

The ash weight of each of the samples was determined by Dr. Mosekilde.

5.3.3 Compressive Strength and Ultrasonic Results.

The relation between the ultrasonic attenuation slope per unit length and the compressive strength per unit area is shown in figure 5.5. There is a very large scatter of results, but a regression line is shown on the graph. The correlation between measurements is 0.53 for the 120 vertebrae tested successfully by both methods.

The results from the 16 year old are neglected throughout, as they were so different to those from the older samples. However, both the strength and the slope per unit length were very high for all the vertebrae measured from this cadaver.

A more useful comparison may be obtained with one vertebra from each cadaver. The results for the L1 vertebra are shown in figure 5.6. The male and female samples are distributed fairly evenly around the regression line, but the correlation coefficient is only 0.46.
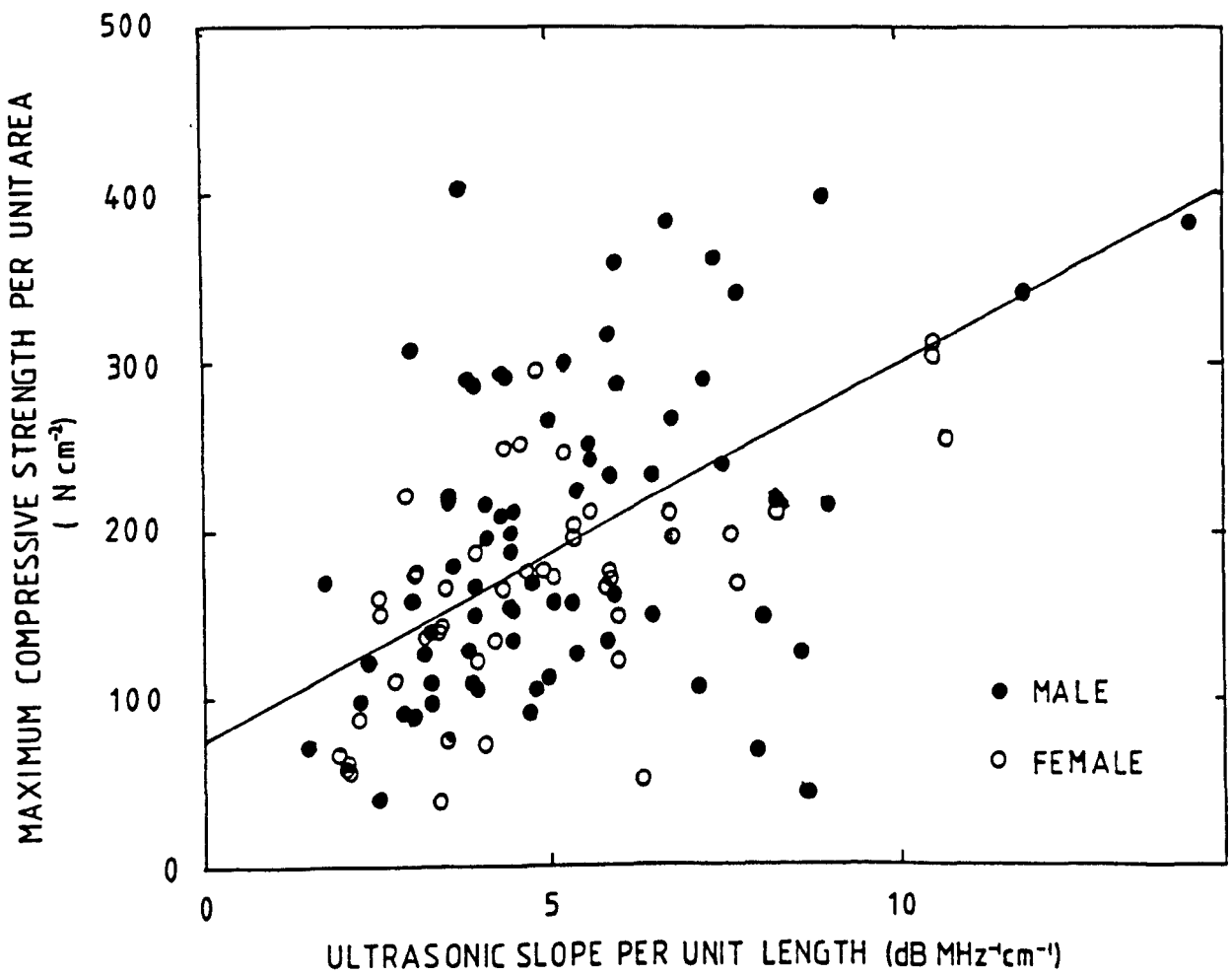
Figure 5.5 The maximum compressive strength per unit area plotted against the ultrasonic slope per unit length for 120 vertebral slices.

gradient = 22 +/- 3

correlation coefficient = 0.53
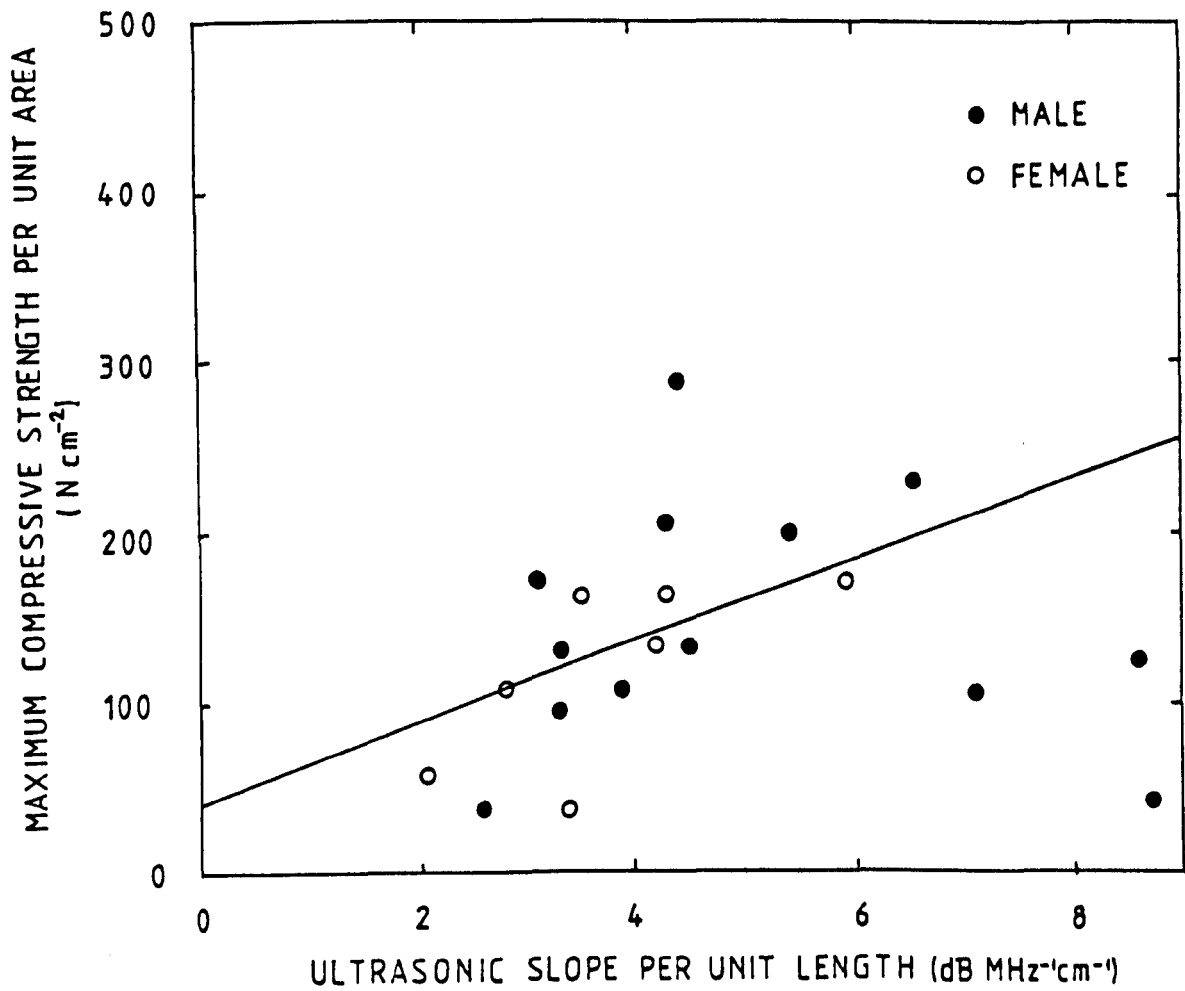
Figure 5.6 The maximum compressive strength per unit area plotted against the ultrasonic slope per unit length for 27 L1 vertebral slices.

gradient = 24 +/- 11

correlation coefficient = 0.46

The mean results from the 27 cadavers are plotted in figure 5.7. The mean compressive strength and the mean ultrasonic slope were calculated from all the vertebrae measured from each cadaver. Again the males and females are evenly distributed around the regression line, but the correlation of 0.82 is highly significant. The increase in correlation is not due to a decrease in population from the individual samples, as the previous graph for the L1 vertebrae shows.

It would seem that using a representative mean value for the ultrasonic slope from several vertebrae gives an excellent indication of the mean maximum comressive strength. This method of averaging over several vertebrae is common in bone mineral measurements that scan the spine, and produces a more reliable result (Rosenthal et al, 1985).

Figure 5.8 shows the age dependency of the mean ultrasonic slope for each cadaver, with the two regression lines representing the male and female populations. Although the dashed line, showing the female loss with age, is slightly steeper, there is little difference. The total population consisted of 16 male and 11 females, again excluding the 16 year old. For comparison, the strength as a function of age produced similar results. The 16 year old female had a mean ultrasonic slope of 30.1 dB MHz^{-1} cm^{-1} and a maximum compressive strength mean value of 371.6 N cm^{-2}, both substantially higher than the ranges shown in the graphs.

5.3.4 Ash Weight and Ultrasonic Results.

The ash weight results were treated in a similar way to the compressive strength. A representative value for each cadaver was obtained by finding the mean result of all the samples used. The ash weights of the total 128 vertebrae correlated with the unnormalised slope with r = 0.49, but figure 5.9 shows the correlation of 0.84 between the representative values. The

Figure 5.7 Mean value of maximum compressive strength per unit area plotted against the mean ultrasonic slope per unit length for the vertebral slices from 27 cadavers.

gradient = 38 +/- 5

correlation coefficient = 0.82
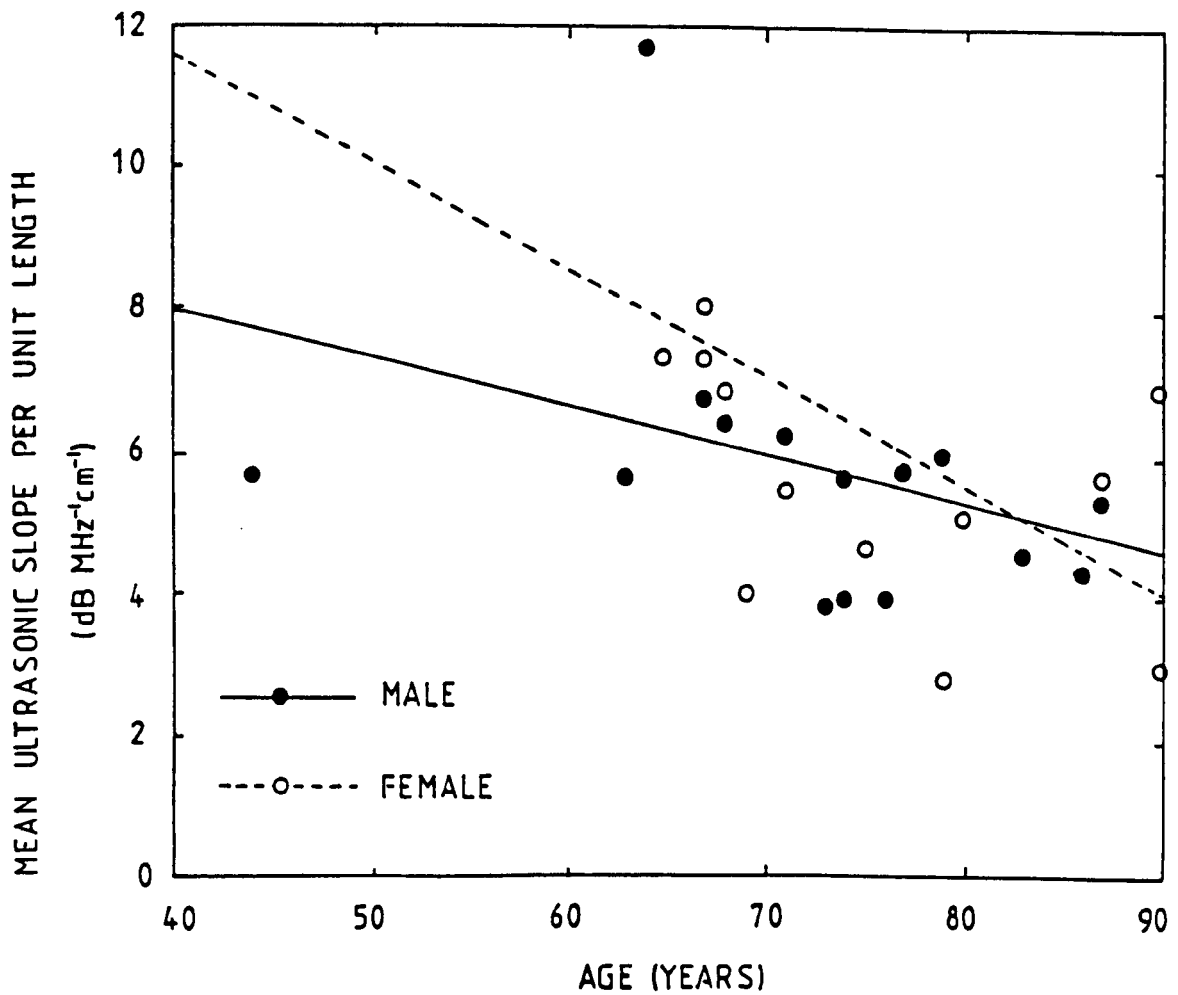
Figure 5.8 Mean ultrasonic slope per unit length of the vertebral slices as a function of age for 27 cadavers.

	female	male
	n = 11	n = 16
	gradient = -0.08 +/- 0.06	gradient = -0.07 +/- 0.04
	r = -0.43	r = -0.38
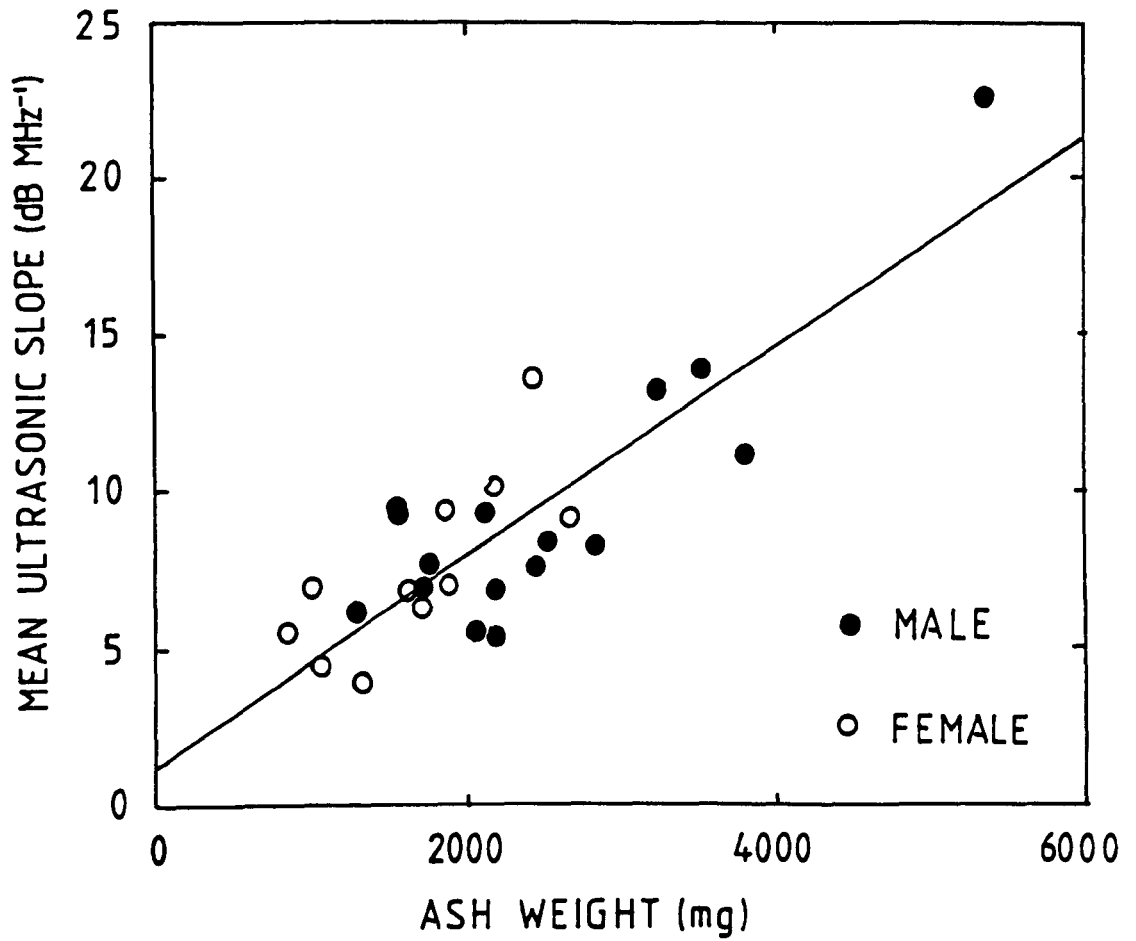
Figure 5.9 Mean values of the ultrasonic slope plotted against the ash weight

for the vertebral slices of 27 cadavers.

gradient = 0.0033 +/- 0.0002

correlation coefficient = 0.84

unnormalised slope has been used as the ash weight is taken from each whole sample.

Figure 5.10 shows the representative values of the ash weights and the compressive strength per unit area. Strictly, the total compressive strength should be used for this comparison, but this data is now not available. The area normalisation of the strength probably accounts for the poorer correlation coefficient of 0.65. If the normalised slope is used, a comparable coefficient with the ash weight of 0.67 is obtained.

5.4 The Leeds Vertebral Samples.

5.4.1 The Leeds Samples.

A pair of lumbar vertebrae were removed together with one os calcis from six cadavers. An age range of 18 to 73 was covered (mean 42.5, standard deviation 23.8) and five of the six cadavers were male. All the samples were stored in formal saline solution (Smeathers, 1986).

The vertebral arch and discs were removed from the body of the vertebrae. Once all the vertebrae had been measured ultrasonically, one sample from each pair was mounted in paraffin wax and cored at the site of measurement by the same technique used for the os calces (section 3.4.1). The cortical layer on the ends of the cores was sliced off to leave a regular cylinder of purely cancellous bone. Hence twelve vertebrae and six cores were measured ultrasonically but only six vertebrae and six cores were subject to compressive strength testing.

It should be noted that due to the very small number of samples for these tests, the results are not considered to be significant. In fact, most of the correlations produced were not significant statistically, as discussed in the following sections.
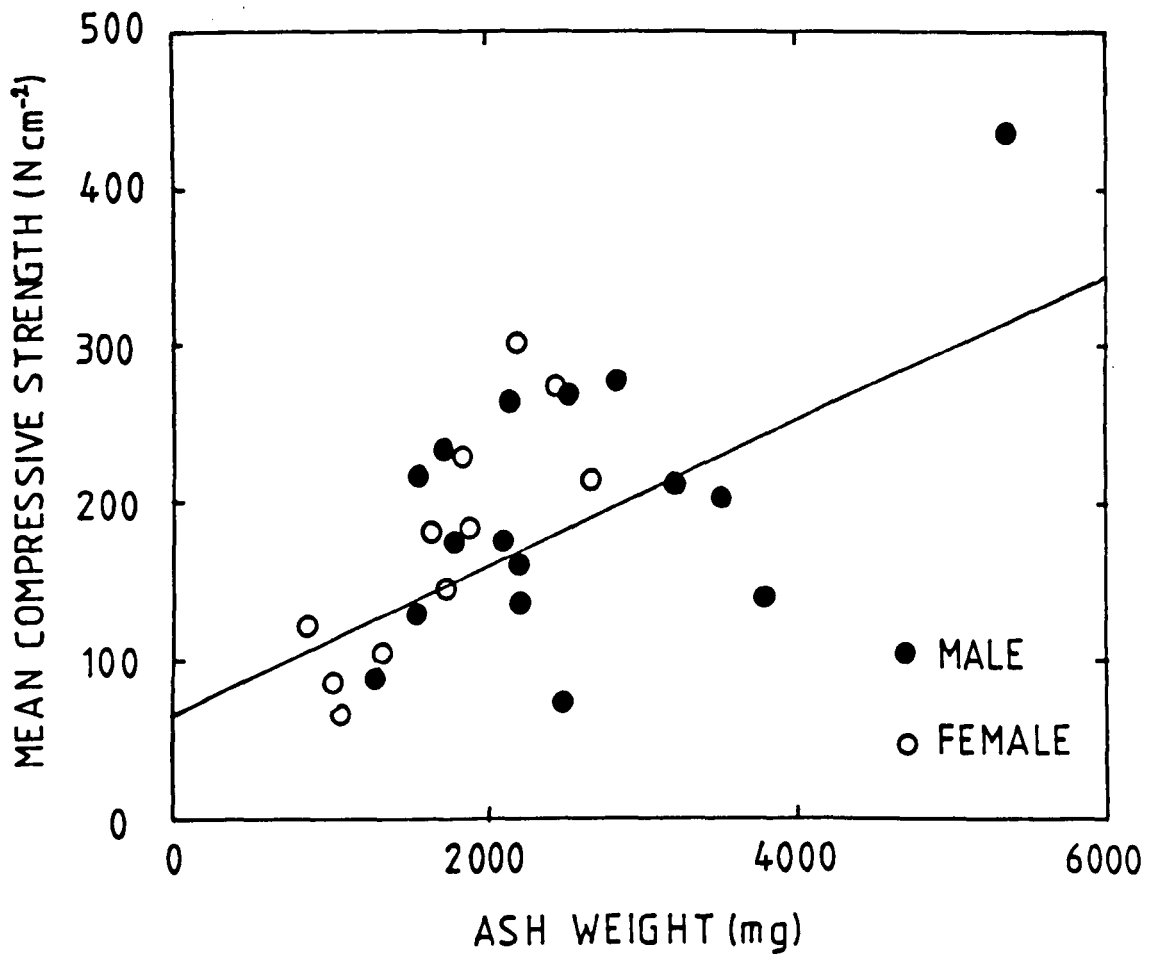
Figure 5.10 Mean values of maximum compressive strength plotted against the ash weight for the vertebral slices of 27 cadavers.

gradient = 0.06 +/- 0.01

correlation coefficient = 0.65

5.4.2 Experimental Procedure.

The slope per unit length was found for all the Leeds vertebrae by mounting the bones on to the brass mounts and positioning so that the ultrasonic beam passed through the body of the vertebrae. The six cancellous cores were measured in the same way as the cores obtained from the os calces.

The standard error of measurement for the whole vertebrae was 4.2%, with differences in positioning producing a change in attenuation slope because of the irregular surfaces.

The compressive strength tests were carried out in conjunction with Dr. J. Smeathers of the Rheumatology and Rehabilitation Unit of the University of Leeds on an Instron 8105 materials tester. The samples and the whole bones were tested in the same way.

The sample was positioned between the metal plates and fixed with bone cement polymethylmethacrylate (PMMA) which sets under a 20 N preload in about 15 minutes. A strain rate of 0.1 mm s^{-1} for the cancellous samples, or 0.02 mm s^{-1} for the whole vertebrae, was applied until the sample fractured and the load - deformation curve recorded.

The cores of cancellous bone were all of the same diameter, so the unnormalised load is representative of the maximum compressive strength. The cores were also of comparable length. The results for the whole vertebrae were normalised per unit area to account for their different sizes using the volume and width of each bone to calculate the mean cross sectional area. The error in such measurements is mainly due to the limitations in reading the peak of the load - deformation curve, which results in at most a 0.5% error.

The ash weight of the cancellous samples was found by Prof. J. Currey of the Biology Department at the University of York. The crushed cores were kept separated in formal saline until the tests. The apparent density was calculated from the bone weight and the total core volume.

5.4.3 Compressive Strength and Ultrasonic Results.

Twelve whole vertebrae were measured ultrasonically, but only six of these were crushed. There was a wide range of results for the whole vertebrae, 6 to 60 dB MHz^{-1} cm^{-1}. The top end of the range is much higher than the results obtained from the os calces. The densities of these bones were from 1170 to 1230 kg m^{-3}, again generally higher than for the heel bones because of the larger quantity of cortex. These ultrasonic slopes were all very much higher than those obtained from the Danish samples, partly because of the more general age distribution and of course, because the cortex and rough surface was included.

Due to an error in labelling at the time of coring, both vertebrae from one cadaver were cored and none of the vertebrae from another. Six cores were produced, however, and six vertebrae remained whole.

The comparison between the maximum compressive strength per unit area and the ultrasonic slope per unit length for the 6 vertebrae is shown in figure 5.11. There is no apparent relation between the two measurements, with the correlation of 0.43 comparable to that for the individual vertebrae results from the Danish samples. The maximum compressive strength correlated very significantly with the overall density of the vertebral samples, r = 0.9, figure 5.12, whereas there was no significant relation between the density and the ultrasonic slope per unit length.

5.4.4 The Cancellous Cores.

The six cancellous cores covered a density range of 1075 to 1140 kg m^{-3}, at the upper end of the range of cancellous cores obtained from the os calces. The ultrasonic results covered a range of 2 to 42 dB MHz^{-1} cm^{-1} and correlated with the density for the six samples with r = 0.8, but with a regression line
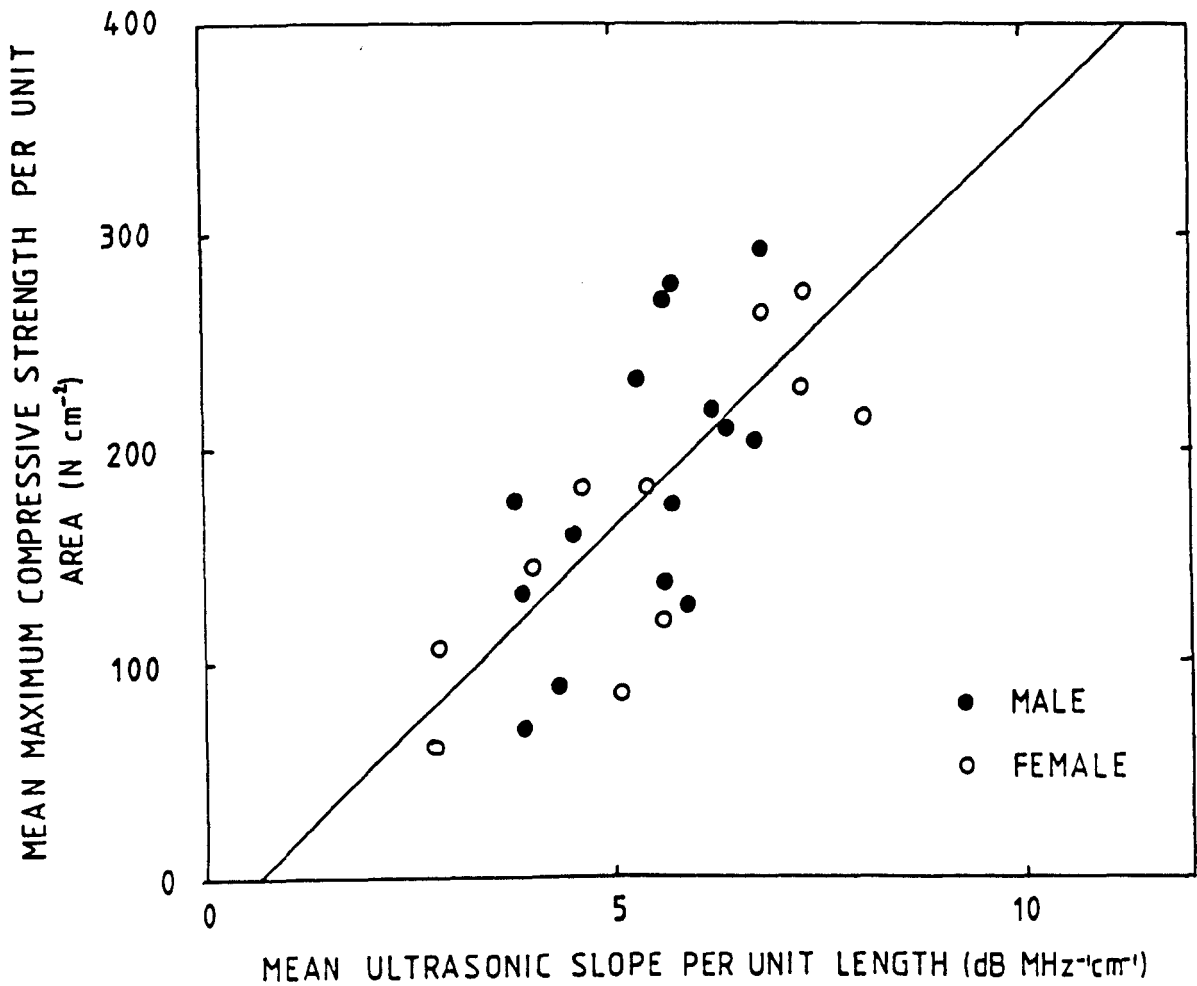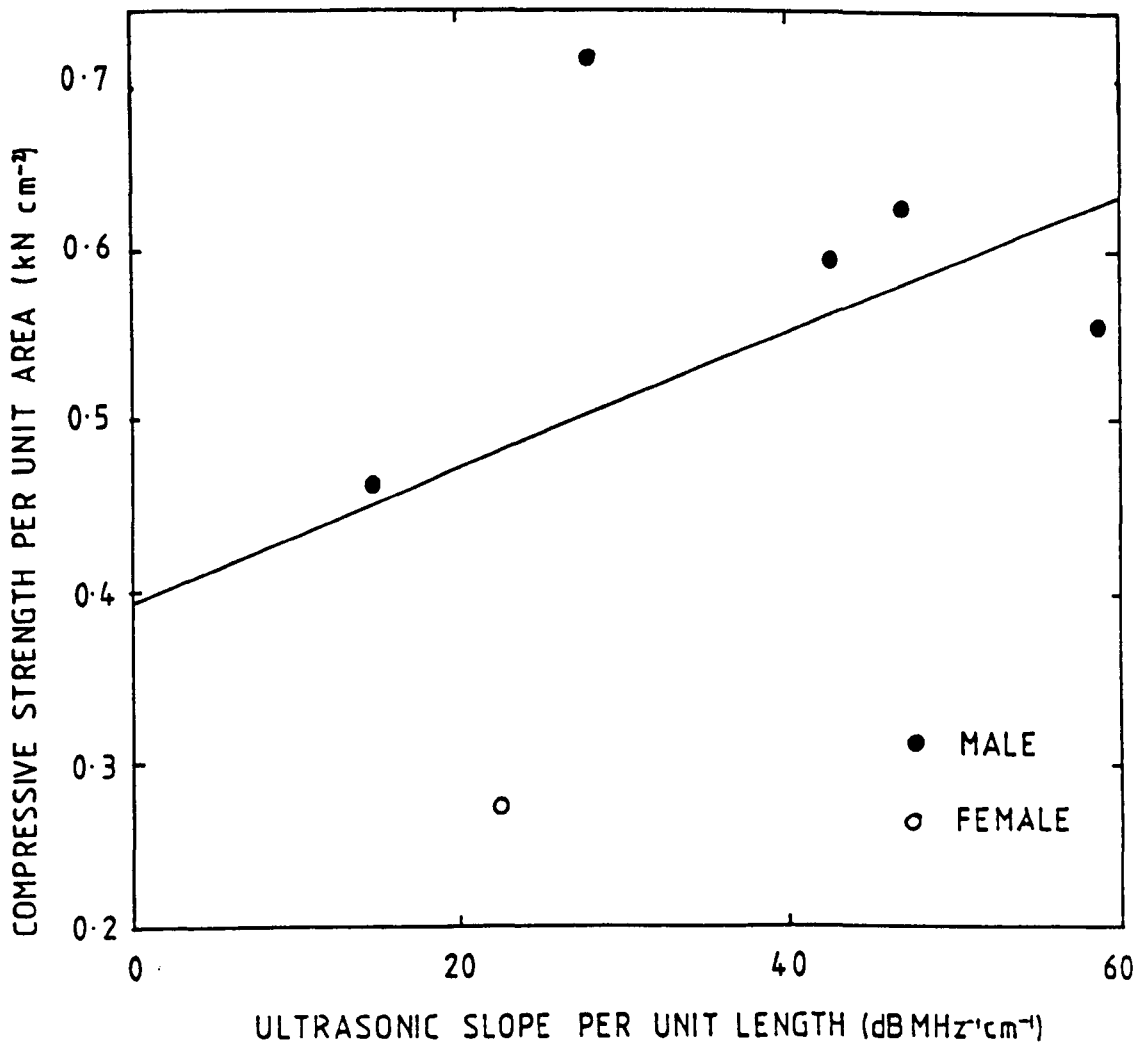
Figure 5.11 Maximum compressive strength per unit area plotted against the

ultrasonic slope per unit length for 6 whole vertebrae.

gradient = 0.004 +/- 0.004

correlation coefficient = 0.43
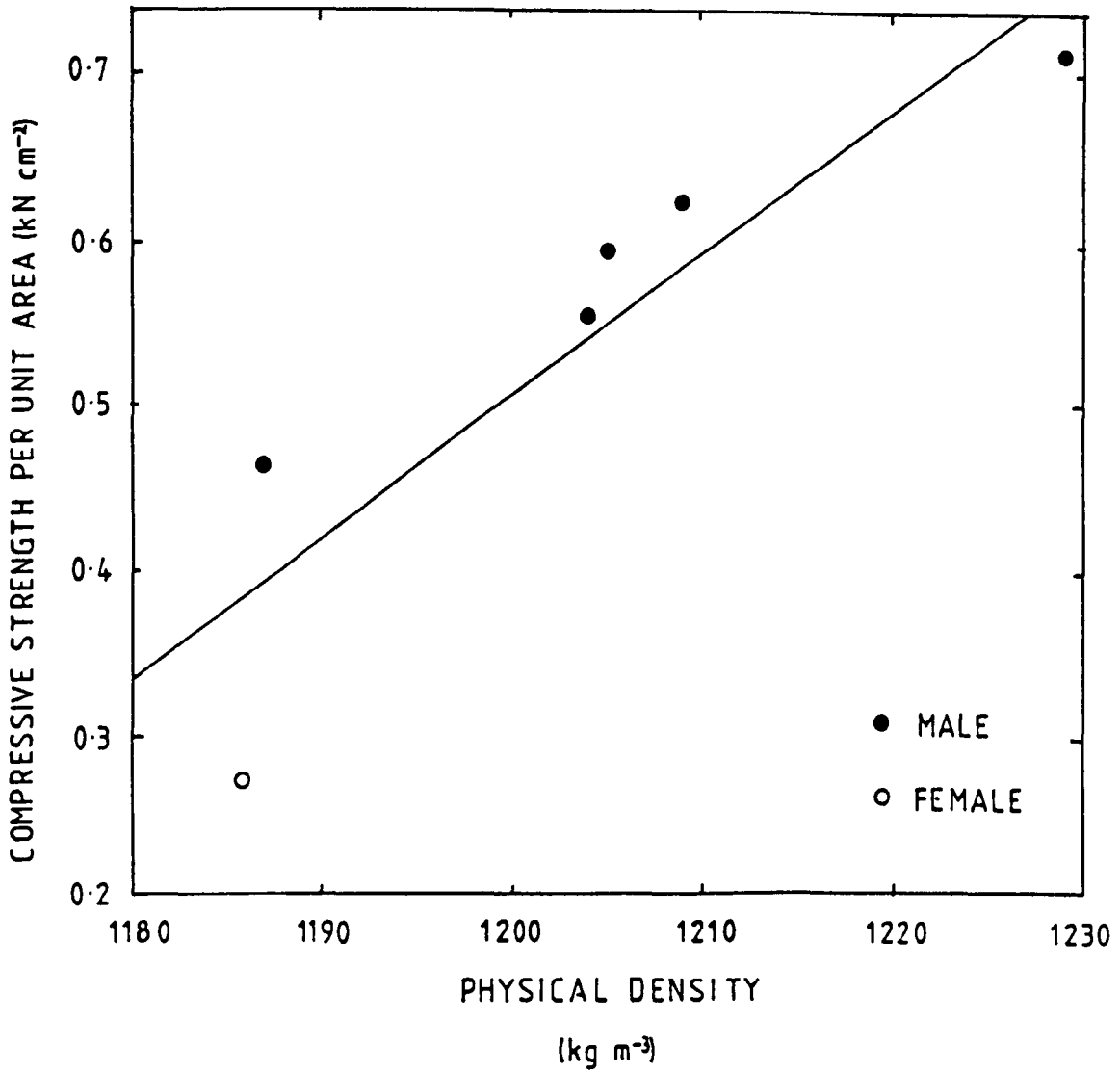
Figure 5.12 Maximum compressive strength per unit area plotted against the
physical density for 6 whole vertebrae

gradient = 0.009 +/- 0.002

correlation coefficient = 0.90

of gradient 0.55 +/- 0.2, much steeper than the equivalent graph for the

calcaneal samples. The range of ultrasonic slopes was very large considering

the small density range. The maximum compressive strength correlated with the

density with a coefficient of 0.73.

The ultrasonic slopes obtained for the trabecular samples varied

consistently with those for the whole vertebrae. In comparison with section

4.4.2, figure 5.13 shows the ultrasonic slope per unit length plotted for the

whole vertebrae and the corresponding cancellous samples. The gradient of 1.0

+/- 0.1 shows the same effect as the cores from the os calces. It is the

trabecular bone that is responsible for the variation in ultrasonic parameters

from bone to bone, with the offset for the vertebrae, 3 +/- 2 dB MHz^{-1} cm^{-1},

representing the average attenuation due to the cortex and irregular shape of

the surfaces.

Figure 5.14 shows little relation between the maximum compressive strength

and the ultrasonic slope per unit length for the trabecular samples cored from

the vertebrae. Again, the correlation of 0.59 is comparable to that obtained

for the individual Danish vertebrae. The cores were all of the same cross

sectional area, so the results were not normalised per unit area. Four samples

were from a pair in which the corresponding whole vertebra was also crushed,

and the maximum compressive strength of the cancellous sample was about 80%

that of the corresponding whole bone.

5.4.5 Ash weight and Ultrasonic Results.

The results of the ash weight determinations are shown in table 5.1. It is

immediately obvious that the apparent density, calculated from the mass of the

bone itself and the core volume, varies substantially over the six samples

whereas the physical density and the calcium content vary only by a few per

cent.
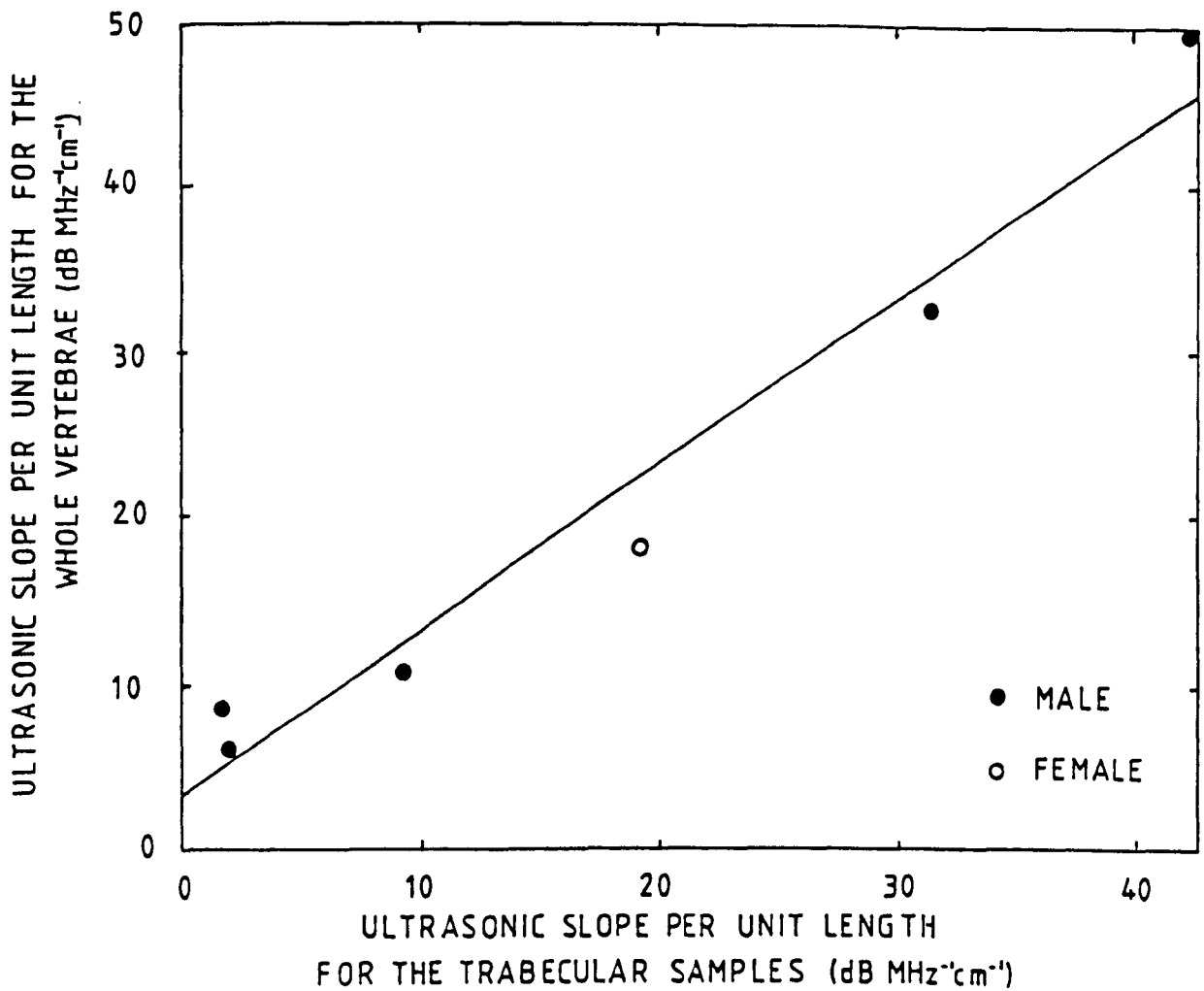
Figure 5.13 Ultrasonic slope per unit length of 6 whole vertebrae plotted against the slope per unit length for the corresponding trabecular samples.

gradient = 1.0 +/- 0.1

intercept = 3   +/- 2

correlation coefficient = 0.98
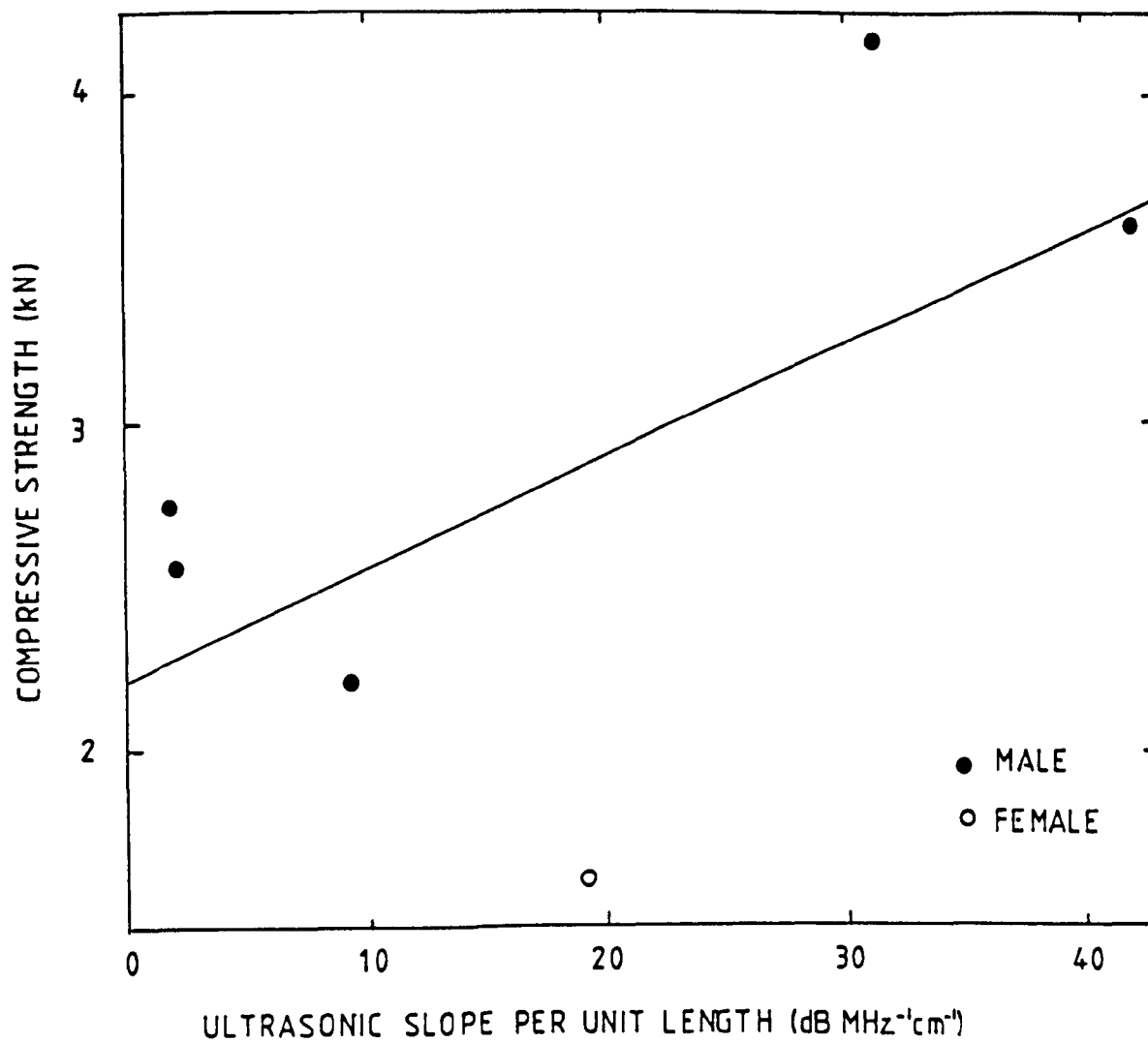
Figure 5.14 Maximum compressive strength plotted against the ultrasonic slope
per unit length for 6 trabecular samples.

gradient = 0.03 +/- 0.02

correlation coefficient = 0.59

Table 5.1 Slope, strength, calcium content and apparent density for 6 vertebral cancellous samples.

No.	Calcium content $(mg\ gm^{-3})$	Apparent density $(g\ cm^{-3})$	Ultrasonic slope $(dB\ MHz^{-1} cm^{-1})$	Compressive strength (kN)
1	237.8	0.24	31.4	4.1
2	229.4	0.17	19.2	1.6
3	239.6	0.16	9.2	2.2
4	241.9	0.19	2.0	2.6
5	235.2	0.25	42.0	3.6
6	240.5	0.22	1.7	2.7

There was no significant correlation between either the maximum compressive strength with the calcium content or the ultrasonic measurement with the apparent density. Figure 5.15a shows the significant correlation of 0.89 between the maximum compressive strength and the apparent density. There was also no significant correlation between the ultrasonic slope and the calcium content of the cancellous cores. The unnormalised slope was used for this comparison as it represents a total content reading rather than a density value.

To compare the compressive strength results to others published, the maximum compressive strength is plotted logarithmically against the apparent density in figure 5.15b. The gradient, showing the power dependence of the strength on the apparent density, is 1.6 +/- 0.4. A similar plot for the ultrasonic results produced insignificant results due to the large error on the calculated gradient.

5.4.6 Vertebral Calcaneal Comparison.

An os calcis was measured from each of the six cadavers. The range of slope per unit length obtained was much smaller than the range of results from the vertebrae. The ultrasonic slope per unit length of the os calcis is plotted against the mean slope per unit length of the two corresponding vertebrae in figure 5.16. The correlation of 0.47 is not significant for the six samples used.

5.5 Discussion and Conclusions.

It must be noted that the technique used for the ultrasonic measurements of the vertebrae can not be used *in vivo*, unlike the method used for the os calces. The ultrasound is transmitted through the body of the vertebrae which would be impossible for the *in situ* spine. However, the natural forces acting

Figure 5.15 a) Maximum compressive strength plotted against the apparent

density for 6 trabecular samples.

gradient = 22 +/- 6

correlation coefficient = 0.89
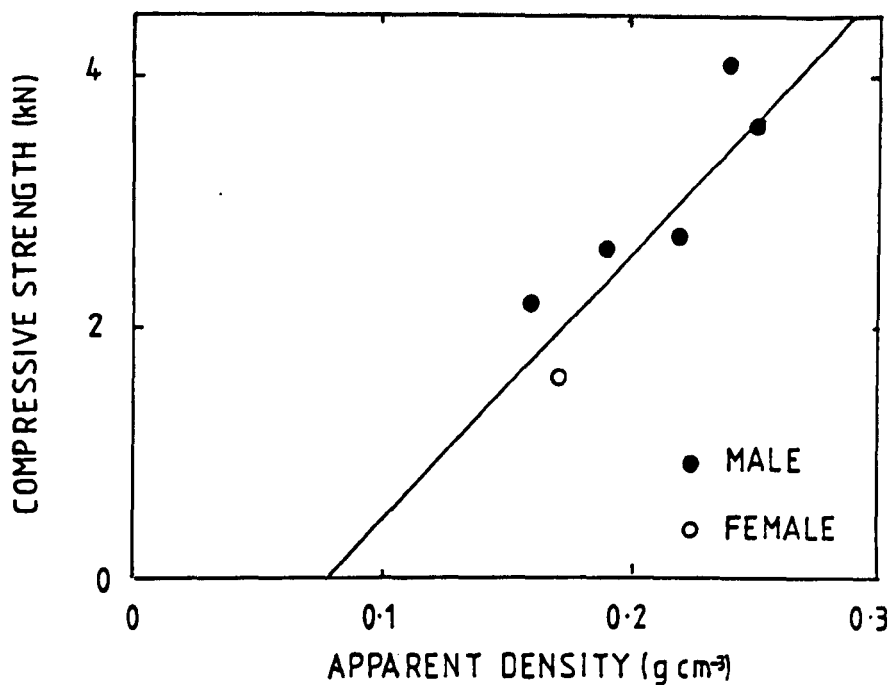
(a)
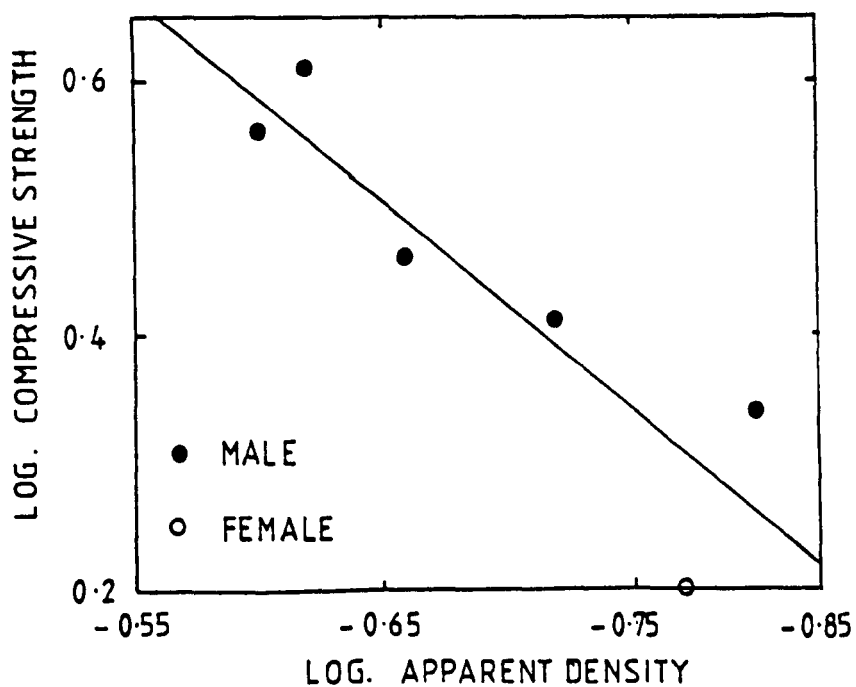
(b)

b) Logarithmic plot of the maximum compressive strength against

the apparent density.

gradient = 1.6 +/- 0.4
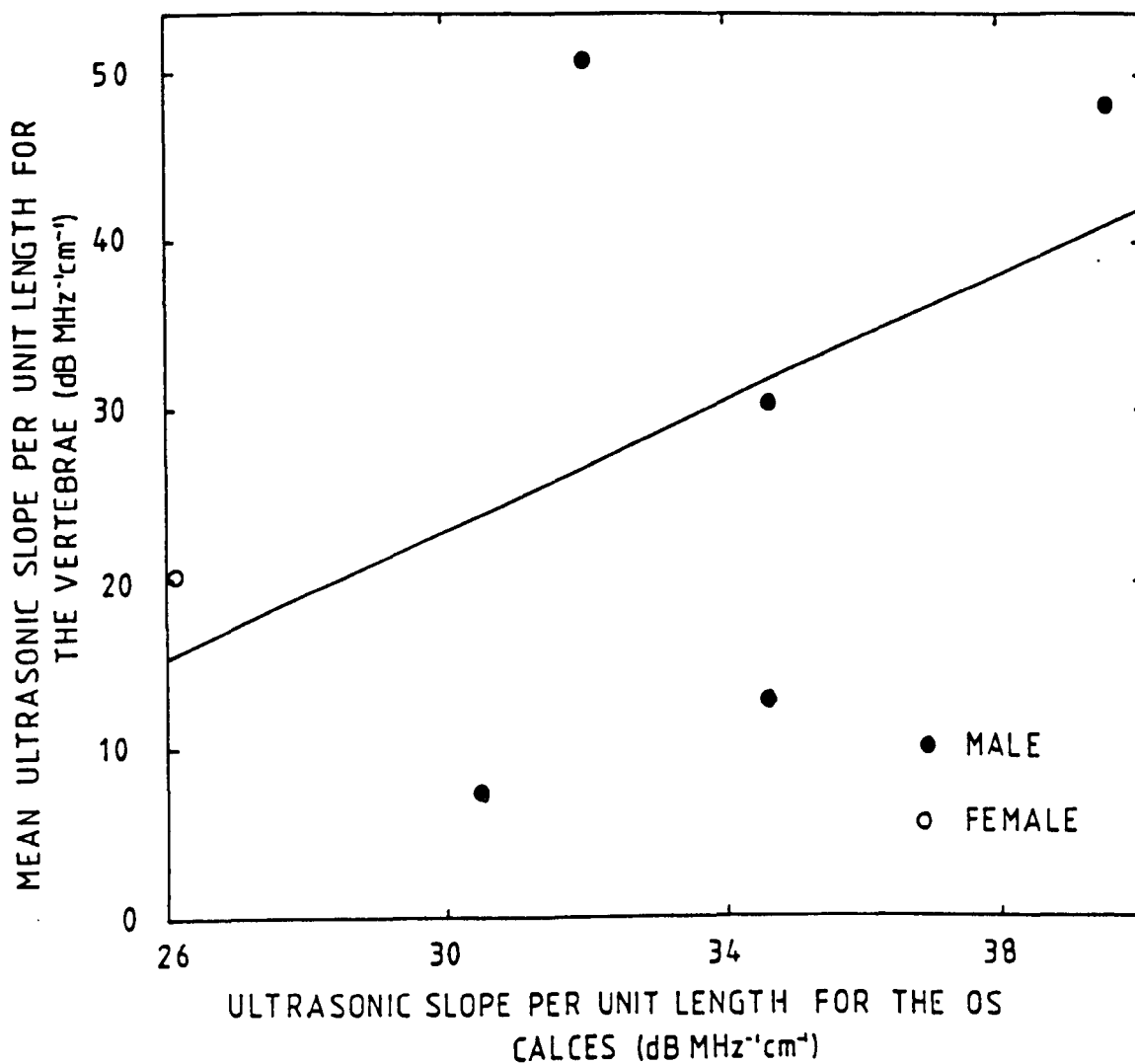
Figure 5.16 Mean ultrasonic slope per unit length for 6 pairs of whole
vertebrae plotted against that for the corresponding os calcis.

gradient = 1.9 +/- 1.8

intercept = -33 +/- 59

correlation coefficient = 0.47

on the spine act in this direction, so the *in vitro* compressive strength testing was designed to mimic these forces. The ultrasonic readings were therefore made in a comparable way. An *in vivo* ultrasonic technique would have to rely on a reflected signal from the spine rather than the transmission method used in the current work.

The individual vertebral measurements on the Danish samples suggested little connection between the maximum compressive strength and the ultrasonic slope per unit length, even when a single representative vertebra was considered from each cadaver. However, by using the mean results from each cadaver, a significant correlation was obtained between the two measurements. The averaging of readings over several vertebrae is standard practice for *in vivo* measurements on the spine, for instance with dual photon absorption and quantitative computed tomography. The mean ash weight values produced similar results, suggesting a definite consistency in the ultrasonic results obtained.

The range of samples used in the current work is small, shown by the much higher values for ultrasonic slope and strength obtained for the samples from the 16 year old. Both readings were very much higher, suggesting that a correlation does exist over the wider range. It was noticeable, however, that the values obtained from the samples of the 16 year old did not fit well with the regression lines obtained for the older samples.

The range of samples as well as the number can affect the correlation between measurements. For instance, the data of Hvid et al (1985) is spread over a range of 0.2 to 2.6 kN cm^{-2}, but the scatter around the regression line is still widespread, comparable to the results here. However, the much smaller range used in the current work produces a far less significant correlation coefficient than a similar number of samples over a much larger range.

Hvid et al (1985) obtained a highly significant correlation of 0.92 between the maximum compressive strength and the bone mineral content obtained by

single photon absorption for 192 individual samples. This is a far better correlation than any acheived in the current work, especially when the results for the individual vertebrae are considered. Horsman and Currey (1983) found a correlation of 0.83 between the bone mineral content and the maximum compressive strength of the distal forearm, also much more significant than the results for individual samples obtained here. However, as with Hvid et al, a large age range of samples was used. Ortoft et al (1987) used an elderly population, and obtained a correlation of 0.70 between the bone mineral content per unit length established by dual photon absorption and the compressive strength of 46 vertebrae.

The relation between the maximum compressive strength and the ultrasonic slope per unit length for the Leeds vertebrae and the cancellous cores were comparable to the individual results for the Danish vertebral slices, despite the different types of sample. Three types were tested, whole vertebrae, vertebral sections including the cortical ring and samples of purely cancellous bone. For all these types, the ultrasonic measurement reflects the trabecular part and not the cortical surfaces which may play an important role in the compressive strength. However, even for the cancellous samples, there was no better correlation between the BUA measurement and the maximum compressive strength.

There was a large variation in the correlation of each of the measurements with the overall physical density. The cortical surface of the whole bones is responsible for a large proportion of the bone mineral present and therefore a large proportion of the overall density. The cortex will also have a supportive effect on the bone during the compressive strength testing, so a better correlation with density is expected for the strength rather than the ultrasonic reading, which is not greatly affected by the cortex. This was in fact what was found. The density correlated with the measurements on the

cancellous samples with r = 0.80 and r = 0.73 for the ultrasonic and strength testing respectively. This slightly better but still not significant result would be expected, as in this situation only the cancellous bone is being tested. It was noticeable that the one particular sample produced a much lower slope per unit length and maximum compressive strength than the density suggested, indicating a possible error in the density measurement. This was confirmed by the relatively low apparent density found during the ash weight testing for that sample.

The logarithmic plot of the compressive strength against the apparent density produced a gradient of 1.6 +/- 0.4, in good agreement with the results found by Hvid et al (1985), but no significant correlation was found for the ultrasonic readings. Equally, there was no correlation between the ultrasonic slope and the calcium content of the six cancellous samples.

It is worth noting that the two sets of samples were stored in different ways, and this appeared to make little difference to either the ultrasonic results or the strength testing, as long as the frozen samples did not remain defrosted for more than a couple of days. It was impossible to treat os calces in the same way if they had to be cored and remeasured, as it takes several days for the preparation and measurements. The length of time of storage in formal saline did not seem to affect the results of the Leeds bones.

It is important that a significant correlation does occur for the mean results from each cadaver. Further work using larger numbers of samples over a more complete age range might show if the ultrasonic reading correlates better to the maximum compressive strength of purely cancellous samples as opposed to samples supported by a cortical surface.

The last section of this chapter is a comparison between the mean ultrasonic slope per unit length for the two vertebrae and the slope per unit length of the corresponding os calces for only six samples. The correlation of

0.47, although not significant, is comparable to that obtained by Dalen and Jacobson (1974) between the third lumbar vertebra and the os calcis using X-ray spectrophotometry. Such comparisons depend very much on the ratio of cortical to cancellous bone and the trabecular structure at each site, section 1.5. Dalen and Jacobson compared many sites using the same measuring technique, but rarely found correlation coefficients greater than 0.5. Further studies comparing skeletal sites *in vitro* could prove useful because of the different structural patterns formed by the various forces acting on the bone. The BUA technique provides a simple method applicable to different bones, as long as the propagation path of the ultrasound can be clearly defined.

Chapter Six.

BONE HISTOMORPHOMETRY.

6.1 Introduction.

The structural aspect of the trabecular bone is just as important as the bone content when the strength of the bone is considered. To obtain numerical details of the structure of the cancellous bone, histomorphometery is required. The dimensions of both the pores and the trabeculae are pertinent to the ultrasonic propagation as well as the actual porosity of the samples. The method of Whitehouse and colleagues provided a means of preparing samples for study under a scanning electron microscope (SEM) without having to produce the thin sections normally required for two dimensional histomorphometry.

A commercial image capturing system for an IBM-PC compatible was used and software written to calculate the areas and dimensions required.

6.2 Histomorphometry.

Histomorphometry is a method frequently used to analyse the structural aspects of trabecular bone as well as to obtain details of formation and resorption surfaces. The computing power available in desk-top machines has meant that new techniques for the analysis of the images are becoming available all the time. Original methods involved point counting on a grid superimposed on the image, to obtain areas and dimensions (Parfitt, 1983). New techniques try to obtain more information by looking at the branching characteristics (Garrahan et al, 1986). Many researchers are transferring to computer techniques and include comparisons between traditional point and intersection counting, standard eye-piece graticules and digitising tablets in the reports

of their work. Parfitt et al (1983) found correlations of 0.96 and 0.94 for the same measurements made by point counting and on a digitiser tablet.

Both dynamic and static parameters can be investigated using different staining techniques. The former include formation and resorption rates that can be calculated from active surface areas, and the latter comprise trabecular size and spacing and osteoid volume (Recker, 1983). Such analysis has led to a more detailed understanding of bone turnover, and the way trabecular bone in particular is affected by osteoporosis (Parfitt, 1987).

6.3 Experimental Technique.

The technique for sample preparation was originally described by Whitehouse and colleagues (Whitehouse et al, 1971. Whitehouse 1974) who used it to study the trabecular pattern of human vertebrae.

Thick samples of a few millimetres are used rather than the fine sections of several microns required by light microscopy. This means that only the trabecular dimensions may be analysed and requires a low magnification. The full three dimensional structure of the bone is clearly visible under a SEM, and can be used to ensure that the surface is representative of the general structure, something that is not possible with thin sections. However, only a few samples can be taken from a particular os calcis, so the results will not necessarily be valid for all depths of trabecular structure within that bone.

6.3.1 Sample Preparation.

A slice of approximately 5 mm was taken from each cancellous sample using the bone cutter. Three discs of 12 mm diameter were then cored from each slice. This means that the samples for analysis represented different areas within the path of the ultrasound but were all at the same depth into the os calcis itself.

The discs were mounted on to SEM stubs with cyanoacrylate glue and attached to a specially constructed wooden handle. To obtain a flat surface without damaging the structure, the samples were frozen and hand ground on coarse emery paper under liquid nitrogen (Whitehouse et al, 1971).

Whitehouse and colleagues used a jet of water to remove the marrow from the ground samples but vertebral marrow is much more loosely held in the pores than the fat of the os calcis. The samples, frozen under liquid nitrogen were removed from the stubs and wire wrapped round them as a holder. There was no damage as the samples were still frozen hard. 2.5 gm sodium hydroxide was dissolved in 200 cc distilled water and gradually brought to boiling point. Once the bone samples had warmed to room temperature they were placed in the sodium hydroxide solution and maintained at just boiling. The wire holder prevented damage from bumping.

As soon as the fatty marrow was removed, after ten to fifteen minutes, the samples were rinsed, dried and remounted on to SEM stubs. They were stored in an evacuated dessicator before being studied under the SEM. A total of 82 discs were prepared, representing 28 os calces. Two samples were discarded due to surface damage that occurred after polishing.

6.3.2 Scanning Electron Microscopy.

The samples remained uncoated and were studied under low magnification on a Cambridge Stereoscan 600 at 1.5 kV. Conductive coating is usually required for samples of non-conducting material, but problems occurred when gold sputter coating was attempted due to the very large surface area presented by the samples. However, working at the lowest filament voltage and low magnification, it was found that excellent images were produced without coating.

Only small adjustments of focus were required for different thicknesses of sample due to the large depth of focus of a SEM. Photomicrographs were obtained directly from the phosphor screen and showed the surface of the cross section necessary for quantitative analysis together with the complete three dimensional structure below. Scratch marks from the grinding were often visible and aided the definition of the top surface.

Two photomicrographs were taken from each disc at well separated sites. This produced six images for each os calcis, covering a total area of

29.2 mm^2. This area is slightly greater than that used by other researchers for comparable tests (Weinstein and Hutson, 1987). Any damaged areas, particularly at the edges of the samples, were clearly identifiable under the SEM and were avoided.

6.3.3 Image Analysis.

The Microsight 1 image capture system was used with an IBM-PC compatible computer and Hitachi CCTV Vidicon black and white video camera to digitise the images. The Microsight 1 digitises a 512 by 512 matrix to 256 grey levels, and stores this information directly in the memory of the PC. One image takes about 20 seconds. An enhanced graphics system (EGA) was used to ensure the resolution of the digitiser was fully utilised, figure 6.1

It was originally intended that the images be digitised directly from the 35 mm film negatives, but it proved impossible to define the surface area well enough with this equipment. 8 by 10 inch prints were made of each of the images and the required areas traced. Large prints were used to ensure the accuracy of the tracing. These tracings were then digitised and displayed by the computer using artificial colour, figure 6.2.

The software included quick and more detailed display, image editing, re-assigning the artificial colour, area and length sizing and was written to
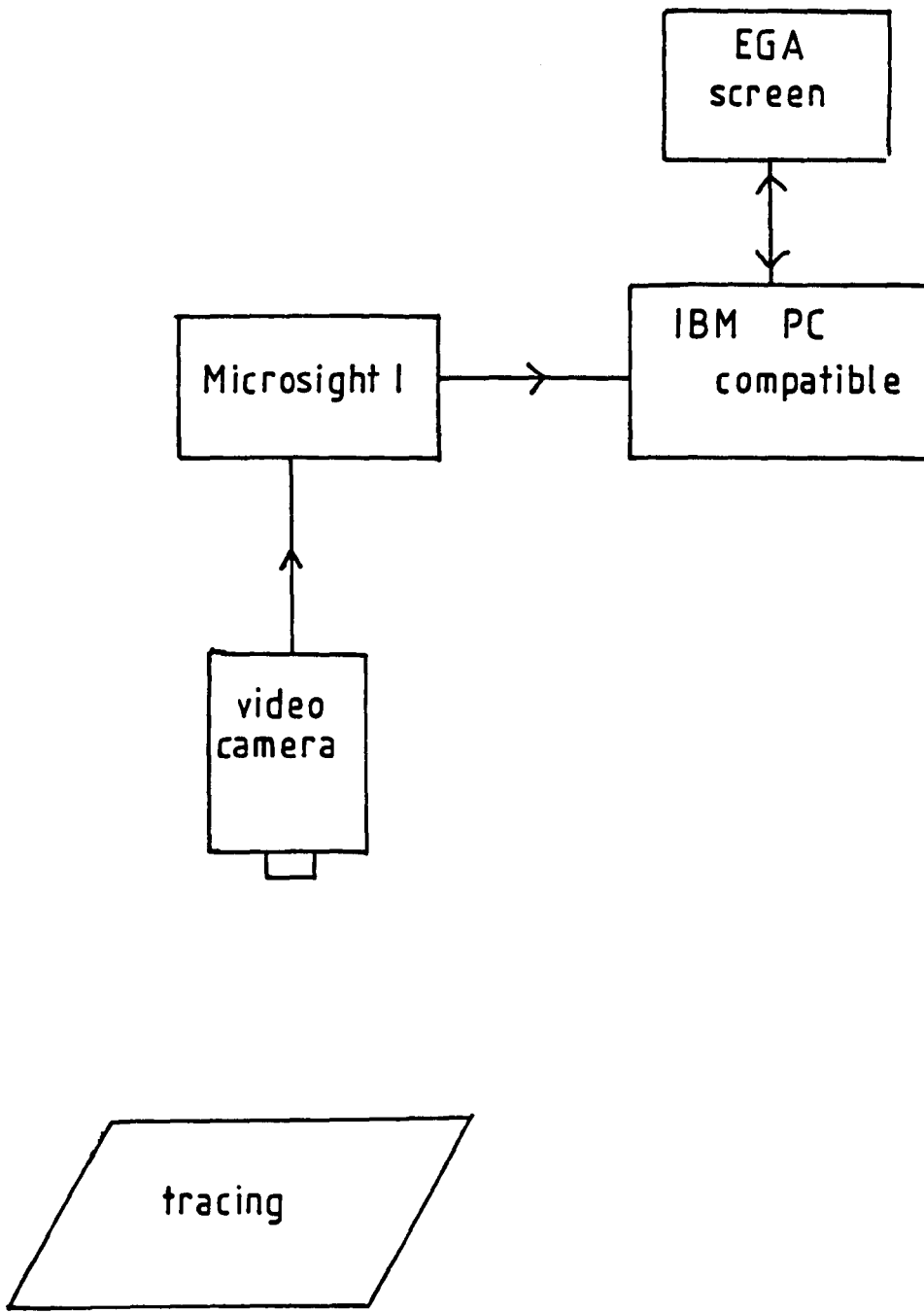
Figure 6.1 Block diagram of the imaging system.

Figure 6.2 An example of the photographic image and
associated tracing.
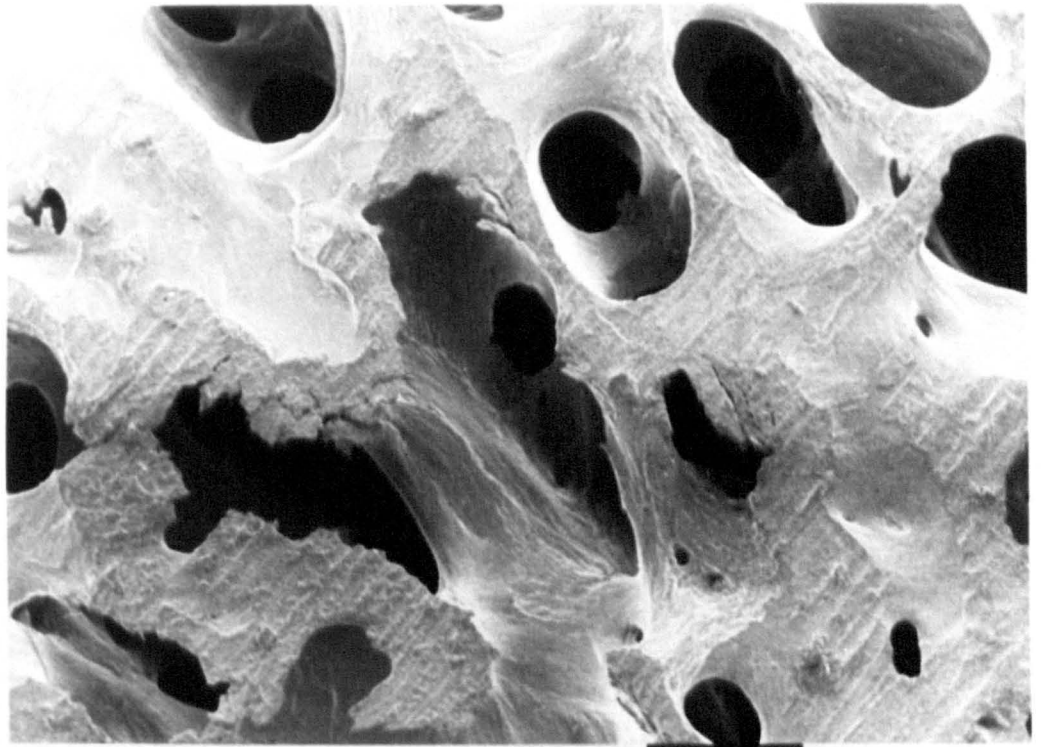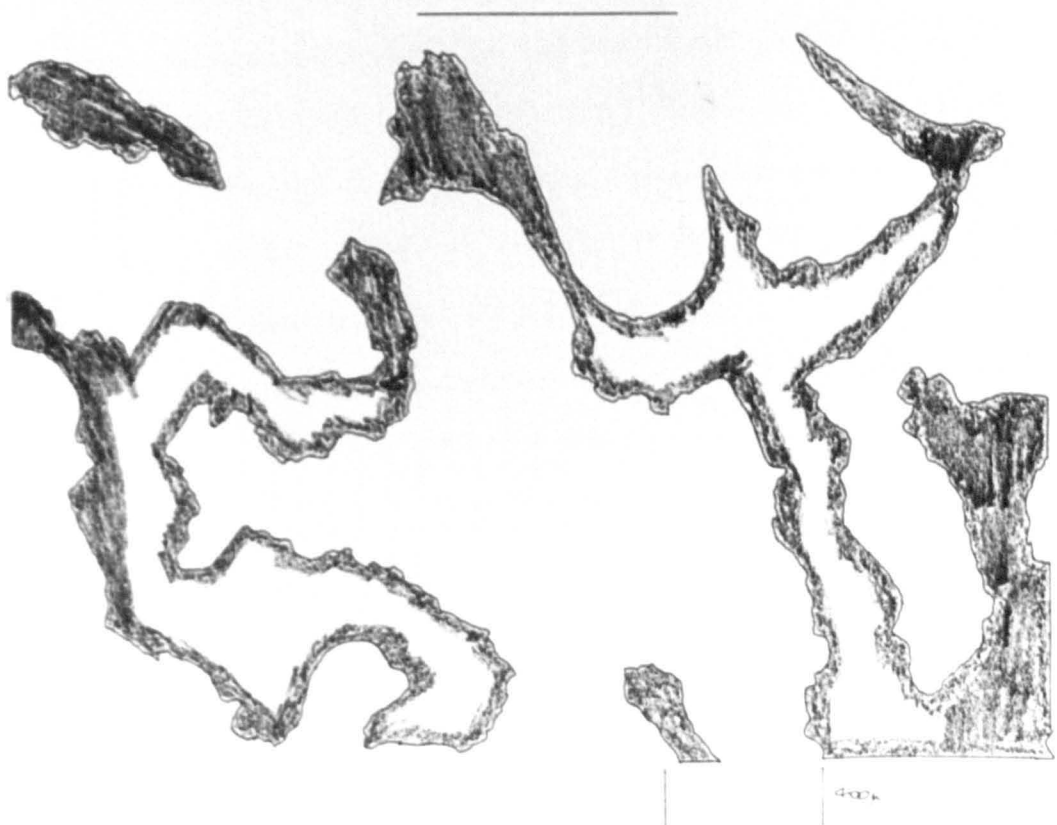
allow scaling in both the horizontal and vertical directions using the scale bar of 400 μm present on every photomicrograph. This resulted in a pixel width of 6.8 μm and a height of 5.6 μm, different because although imaged on a square 512 by 512 matrix, the screen is rectangular. This represents the ultimate possible resolution of the system.

The total area of the bone for each image, A_b in mm^2, was measured by counting pixels and converted to an area measurement using the scaling factors. The total area of the image was calculated from its length and breadth, 2617.0 μm by 1861.1 μm, an area A_t of 4.87 mm^2. Thus the ratio of the trabecular bone area to the total image area could be found, and is equivalent to the percentage trabecular bone volume, TBV, regardless of structural orientation (Parfitt, 1983).

Trabecular widths were measured directly using the cursor to mark points and the distance between them calculated and scaled to give the width in μm. Measurements were taken on each image on all the trabeculae which could be analysed without including trabecular junctions, figure 6.3, and the mean width, or the mean trabecular plate thickness MTPT, established for each bone. The number of trabeculae per image was counted by defining a trabecular plate to be a piece of bone extending between junctions, or in the two dimensional view, sometimes from one junction (Aaron et al, 1987). To ensure consistency, protruberences less than half the width of the trabecula on which they occur were excluded, figure 6.3. Thus the mean number of trabeculae per image for each bone could be calculated.

The full three dimensional structure visible in each photomicrograph was used to define whether the typical structure was composed of plates or rods and a ratio of length to width used as an estimate for the cross sectional shape, so that a rating of 5 : 1 suggests fairly short thick structures, and

40 : 1 represents much longer thinner trabeculae. Example images showing the stick like structures and the plate formations are given in figure 6.4.

These are all the parameters evaluated directly from the photomicrographs. Further information can be established ... and calculations (Parfitt et al, 1983).

A value that is ... for finding the turnover rate, is the surface area of the bone itself per ... volume of ... tissue, S_v. This is established from the total ... of the ... on an image, divided by the total image area, ... , and ... by the factor 1.199. This factor is an experimentally derived ... (Schwartz and ..., 1981).

$$S_v = \frac{1.199\ P_b}{A_t} \tag{6.1}$$

Figure 6.3 Simplified diagram showing trabeculae and junctions.

For a structure which is oriented perpendicular to the plane of section, this factor would be equal to unity. For a perfectly isotropic structure, where there is an equal probability of the structure being oriented at any angle to the plane of section, the factor is 4/π (1.273). In general, trabeculae can be considered to follow the curvature of a spheroid, and this results in a slightly smaller value, in agreement with that obtained experimentally from cancellous bone of the pulse ...

The bone surface to volume ratio can be calculated from the surface area to total tissue volume ratio by using the volume to bone surface ...

40 : 1 represents much longer thinner trabeculae. Example images showing the stick like structures and the plate formations are given in figure 6.4.

These are all the parameters evaluated directly from the photomicrographs. Further information can be established using standard calculations (Parfitt et al, 1983).

A value that is useful for finding the turnover rates is the surface area of the bone itself per unit volume of total tissue, S_v. This is established from the total perimeter, P_b in mm, of the trabeculae on an image, divided by the total image area, A_t in mm^2, multiplied by the factor 1.199. This factor is an experimentally derived number (Schwartz and Recker, 1981).

$$S_v = \frac{1.199 \ P_b}{A_t}$$

(6.1)

For a structure which is oriented perpendicular to the plane of section, this factor would be equal to unity. For a perfectly isotropic structure, where there is an equal probability of the structure being oriented at any angle to the plane of section, the factor is $4/\pi$ (1.273). In general, trabeculae can be considered to follow the curvature of a spheroid, and this results in a slightly smaller value, in agreement with that obtained experimentally from cancellous bone of the iliac crest.

The bone surface to volume ratio can be calculated from the surface area to total tissue volume ratio by using the trabecular bone volume

$$\frac{S}{V} = \frac{P_b}{A_t} \frac{1.199 \ 100}{TBV}$$

(6.2)

400μ
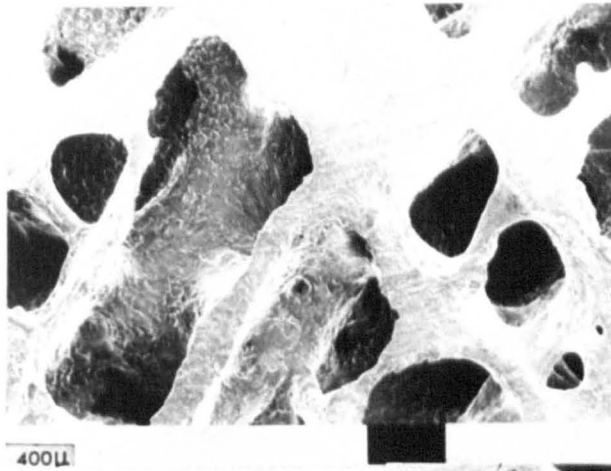
Figure 6.4 Examples of photomicro-
graphs showing the extreme
cases of trabecular
structure
a) full plates

400μ

400μ

b) stick like

400μ
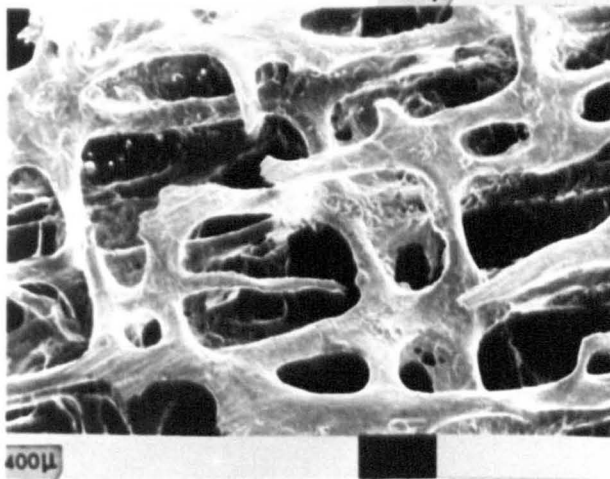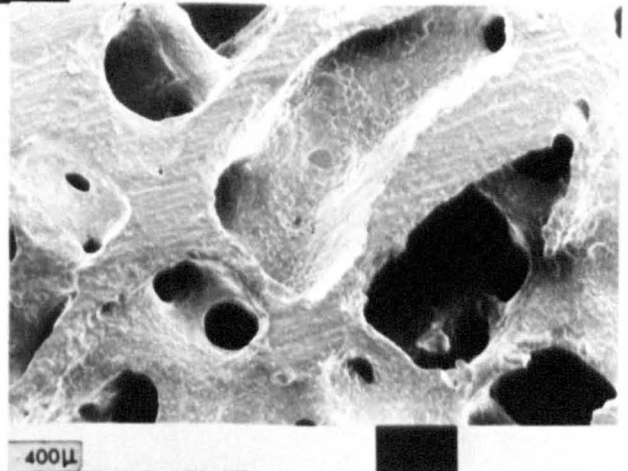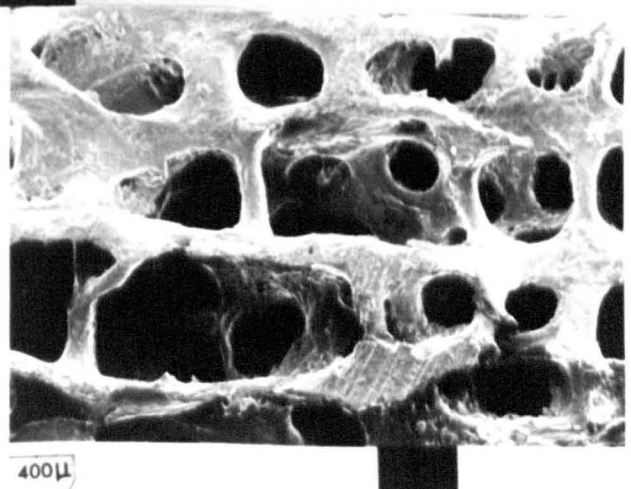
but
$$TBV = \frac{100 \, A_b}{A_t}$$

so

$$\frac{S}{V} = \frac{1.199 \, P_b}{A_b} \qquad (6.3)$$

An indirect value for the mean trabecular plate thickness in μm is given by

$$MTPT = \frac{2000}{S/V}$$

$$= \frac{2000 \quad A_b}{P_b \; 1.1999} \qquad (6.4)$$

and this was used to find the mean trabecular bone perimeter, P_b in mm, from the measured MTPT.

A value similar to, but more standardised than the number of trabeculae per image is the mean trabecular plate density, MTPD in mm^{-1}, the number of plates per millimetre. This is given by the trabecular bone volume and mean thickness:

$$MTPD = \frac{10 \quad TBV}{MTPT} \qquad (6.5)$$

and the mean separation of the plates, MTPS in μm, is given by

$$MTPS = \frac{1000}{MTPD} - MTPT \qquad (6.6)$$

This gives the shortest distance between plates assuming that they are parallel. Multiplying by $\pi/2$ gives an estimate of the mean pore size assuming the trabeculae follow the surface shape of spheroids (Parfitt, 1983).

Thus the following independent mean parameters were established for each os calcis sample:

trabecular bone volume, TBV, per cent

mean trabecular plate thickness, MTPT, in µm

mean trabecular plate density, MTPD, im mm^{-1}

mean trabecular plate separation, MTPS, in µm

The standard deviation of the MTPT over all the trabeculae imaged for each bone was recorded, and gives an excellent indication of the variation within the overall trabecular pattern.

6.3.4 Limitations.

The trabeculae are built up along the lines of stress within the bone and so their structure and size will vary with skeletal position and situation at a particular site. The ultrasonic measurement of the os calcis is carried out on a central position in the bone, but there will still be some variation in trabecular pattern, both over the cross section of the site measured and along the path propagated through the bone itself.

The samples for histomorphometry were taken from a comparable site from each heel bone and covered the full cross sectional area. Two photomicrographs at well separated positions were taken for each sample, resulting in six images for each os calcis. The samples were sliced from the edge of each cancellous core, as the remainder of the bone was required for further testing in Sheffield, but the surface imaged was on the inner side of the slice, so it was towards the centre of the heel bone.

The standard deviation of the measurements gives an indication of the variation in the trabecular structure considered, but can not be assumed to account for the trabecular pattern throughout the whole heel bone. The use of thick samples showing the structure behind the surface analysed ensures that the areas used are representative of the surrounding structure, but also means that a relatively small number of samples can be taken.

No account can be made for the direction of the trabeculae with this technique, which has been shown to have an effect on the ultrasonic attenuation, section 4.6. A much more general three dimensional picture would be needed for this, and would involve many problems. Current histomorphometric analysis can not account for such detail.

The errors inherent in the overall technique are discussed by Whitehouse (1976) and standard texts on histomorphometry (Recker, 1983). The main source of error in the microscopy itself is that the surface could be at an angle across the image, effectively changing the distances on the final two dimensional image. This was minimised in the Cambridge Stereoscan by tipping the samples as required.

The measurements are taken on the very top surface of the image only, and scratch marks left by the grinding procedure help define this surface with the background structure ensuring that the surface is consistent with the surroundings. Misplacing the boundary of such surfaces could introduce fairly substantial errors in the final results, but the overall reproducibility covers this effect. Letting the software size objects rather than pointing out boundaries with the screen cursor ensures more consistency.

6.3.5 Accuracy.

The accuracy of the technqiue was assessed by comparing the mean trabecular plate thickness obtained for each image to that found by using a completely separate imaging system, courtesy of Dr. Bryanston-Cross of the Engineering Department at the University of Warwick.

An Olivetti M28 with an image grabbing extension board was used with the commercially available SEMPER software. This system works on a displayed 'grabbed' or frozen digitised video image rather than on a stored artificial colour image and produced excellent views directly from the 35 mm negatives of the photomicrographs. A 512 by 512 matrix is used and this resulted in a pixel resolution of 7.2 μm, slightly larger than that obtained using the Microsight system. Again the screen is rectangular, but the resolution in the vertical direction was forced to be the same as that in the horizontal by multiplying measurements by the aspect ratio, 2 : 2.88. This was checked by imaging and measuring a circle.

The trabecular widths were measured on 100 images using this system, and the mean width calculated for each frame was compared to that found by the Microsight system. The mean difference was 4.68 μm, with the Microsight producing significantly higher results. This difference is in fact comparable to the overall reproducability.

6.3.6 Reproducibility.

20 tracings were imaged twice and measurements carried out on both sets of frames, table 6.1. The mean difference in trabecular thickness was 4.4 μm and the mean difference in bone area was 0.032 mm^2. For the mean values obtained, this represents a standard error of 5% for both the MTPT and the TBV.

6 pictures were retraced and the image analysis repeated on the new tracings. The results are listed in table 6.2. The mean difference in

Table 6.1 Reproducibility of the imaging technique, using 20 random images.

image no.	first reading bone area (mm^2)	first reading mean trabecular thickness (μm)	second reading bone area (mm^2)	second reading mean trabecular thickness (μm)	difference bone area (mm^2)	difference mean trabecular thickness (μm)
2/10a	0.856	93.76	0.845	96.39	0.011	-2.63
4/3	0.476	104.10	0.519	95.86	-0.043	8.24
4/29	0.478	91.23	0.535	81.90	-0.057	9.33
6/5	0.406	63.05	0.401	68.84	0.005	-5.79
8/34	0.425	79.60	0.457	78.36	-0.032	1.24
13/34	1.273	118.78	1.326	111.78	-0.053	7.00
13/17	0.479	85.46	0.493	85.06	-0.014	0.40
14/15	0.642	105.34	0.633	100.70	0.009	4.64
15/16a	0.966	99.46	1.063	98.57	-0.097	0.89
18/25	1.679	128.70	1.715	138.87	-0.036	-10.17
20/3a	0.421	82.50	0.405	80.77	0.016	1.73
21/28a	0.224	65.60	0.231	64.85	-0.007	0.75
23/6	0.864	106.44	0.822	98.30	0.042	8.14
24/27	1.069	109.71	1.071	105.70	0.002	4.01
25/31	0.729	83.37	0.746	83.79	-0.017	-0.42
26/13a	0.718	99.33	0.753	104.10	-0.035	-4.77
26/17a	0.845	95.63	0.778	90.88	0.067	4.75
28/37a	0.678	90.81	0.670	93.68	0.008	-2.87
30/b1	0.573	85.73	0.586	86.42	-0.013	-0.69
35/40a	1.034	78.95	1.110	87.70	-0.076	-8.75
mean	0.742	93.80	0.758	92.63	0.032	4.36
st. dev.					0.027	3.31
st. error					5%	5%

Table 6.2 Reproducibility of re-drawing the bone outlines, for 6 images.

image no.	first drawing		second drawing		difference	
	bone area	mean trabecular thickness	bone area	mean trabecular thickness	bone area	mean trabecular thickness
	(mm^2)	(μm)	(mm^2)	(μm)	(mm^2)	(μm)
14/10	0.616	121.5	0.611	118.5	0.005	3.0
31/36a	1.805	151.7	1.747	153.2	0.058	-1.5
32/23a	2.467	119.2	2.398	123.0	0.069	-3.8
29/45	0.709	114.3	0.657	110.7	0.052	3.6
16/41	0.206	67.0	0.219	58.7	-0.013	8.3
3/7a	0.376	89.7	0.358	89.1	0.018	0.6
mean					0.032	1.7
st. dev.					0.033	4.3
st. error					6%	6%

trabecular thickness is 1.7 μm, but the standard deviation is 4.3 μm. The mean difference in bone area is 0.032 mm^2. The standard error from these results for both the MTPT and TBV is 6%, and this represents the overall reproducibility of the imaging technique.

6.4 Results.

These are considered in two groups. The histomorphometric parameters alone, and their relation to each other, and then the correlation between the ultrasonic readings and the structural parameters.

6.4.1 Histomorphometric Results.

The four independent parameters listed at the end of section 6.3.3 for each os calcis are given in table 6.3, together with the ultrasonic slope per unit length.

The trabecular bone volume varies from 4.8% up to 28.9%, which represents a substantial range. The mean trabecular plate thickness varies from 71 to 122 μm with the standard deviation in plate thickness for each heel bone anything up to 36 μm, approximately 30%, showing a large variation in structure across the area considered. The mean trabecular spacing, calculated from the TBV and MTPT, varied from 300 μm to nearly 1400μm and the mean trabecular plate density from 0.7 mm^{-1} to 2.4 mm^{-1}.

The correlations between the histomorphometric parameters are shown in figures 6.5 to 6.7. The correlation between the TBV and the MTPT, figure 6.5 is 0.67, showing that a high bone content does not necessarily imply a high trabecular width. The relation between TBV and MTPS is shown in figure 6.6. The correlation here is -0.89, with the low TBV samples having a particularly large mean trabecular spacing and the high value TBV bones appearing to tend

Table 6.3 Histomorphometry Results.

No.	Ultrasonic slope $(dB\ MHz^{-1}cm^{-1})$	TBV (%)	MTPT (μm)	St.dev. TPT (μm)	MTPS (μm)	MTPD (mm^{-1})
2	15.4	16.0	99.4	22.6	519.3	1.6
3	13.1	10.2	92.9	20.3	820.9	1.1
4	18.3	10.9	91.1	30.3	747.3	1.2
6	13.2	6.3	71.4	21.4	1064.8	0.9
8	30.4	18.3	106.6	30.0	476.9	1.7
9	19.3	13.1	99.2	24.5	655.8	1.3
10	26.3	14.9	82.4	19.4	470.2	1.8
11	8.9	7.2	96.7	22.7	1245.9	0.7
12	11.3	9.2	103.3	26.5	1014.1	0.9
13	21.6	16.9	103.1	34.6	505.4	1.6
14	23.5	13.1	106.0	27.0	704.0	1.2
15	14.3	13.9	84.7	21.4	526.5	1.6
16	14.7	12.3	93.6	25.8	667.7	1.3
17	8.0	11.1	86.7	26.1	692.2	1.3
18	20.6	21.7	108.2	36.5	391.1	2.0
20	26.0	16.9	83.0	19.5	407.8	2.0
21	6.4	4.8	69.7	14.0	1391.4	0.7
23	10.4	12.9	87.5	31.1	590.0	1.5
24	25.1	18.7	98.5	30.7	428.7	1.9
25	28.4	19.1	84.7	17.1	358.0	2.3
26	23.7	16.6	92.3	26.4	461.8	1.8
27	28.7	21.6	103.7	29.2	375.3	2.1
28	13.5	11.8	87.1	22.4	649.4	1.4
29	21.6	14.4	91.2	19.2	543.4	1.6
30	27.6	20.9	107.4	30.4	406.7	1.9
31	31.5	28.9	121.9	30.6	299.4	2.4
32	25.5	24.2	104.4	19.2	327.2	2.3
35	25.5	21.7	95.3	27.4	344.3	2.3

TBV - trabecular bone volume
MTPT - mean trabecular plate thickness
with standard deviation of trabecular plate thickness
MTPS - mean trabecular plate separation
MTPD - mean trabecular plate density
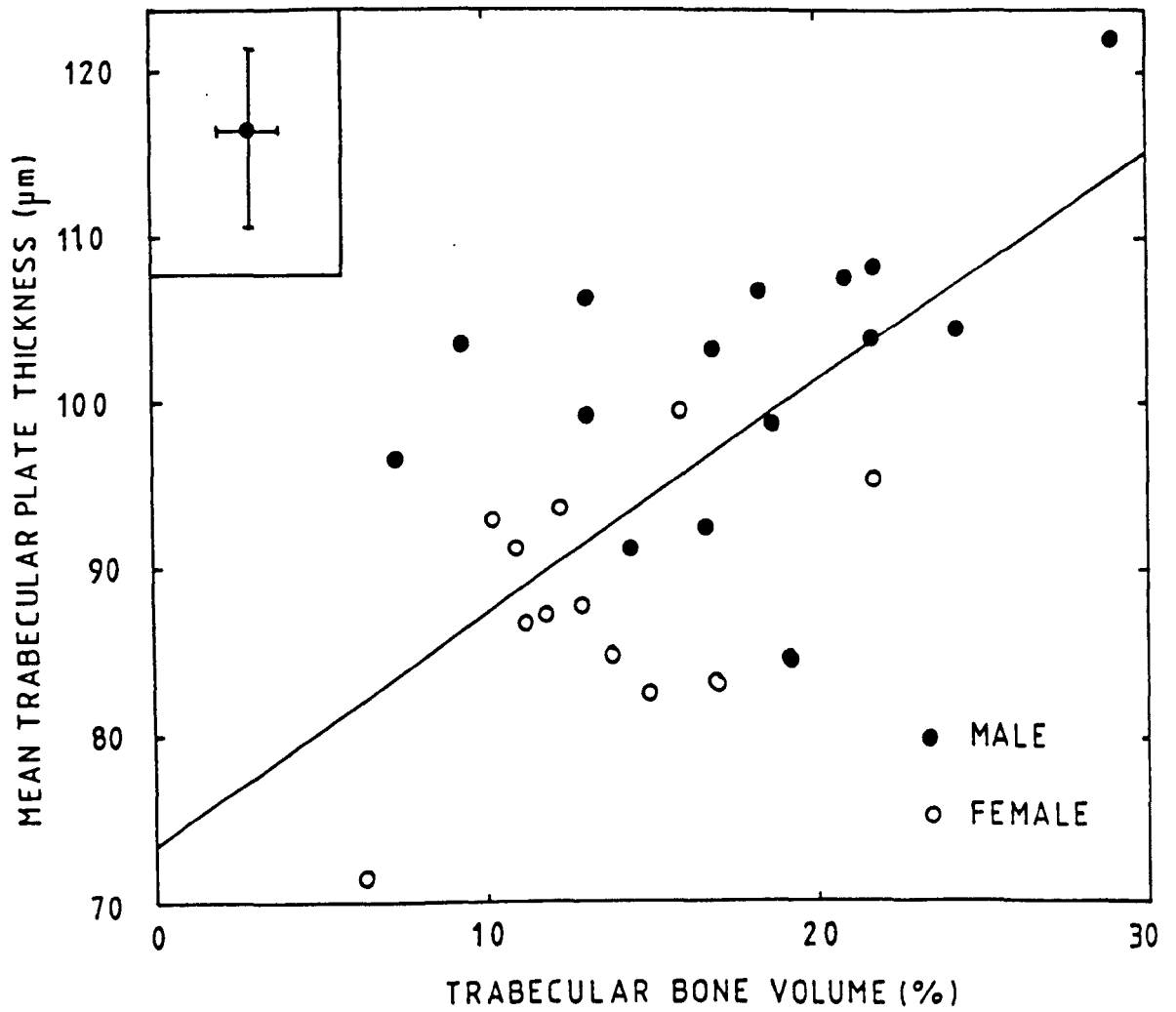
Figure 6.5 The mean trabecular plate thickness (MTPT) plotted against trabecular bone volume (TBV) for samples from 28 os calces.

gradient = 1.4 +/- 0.3

correlation coefficient = 0.67
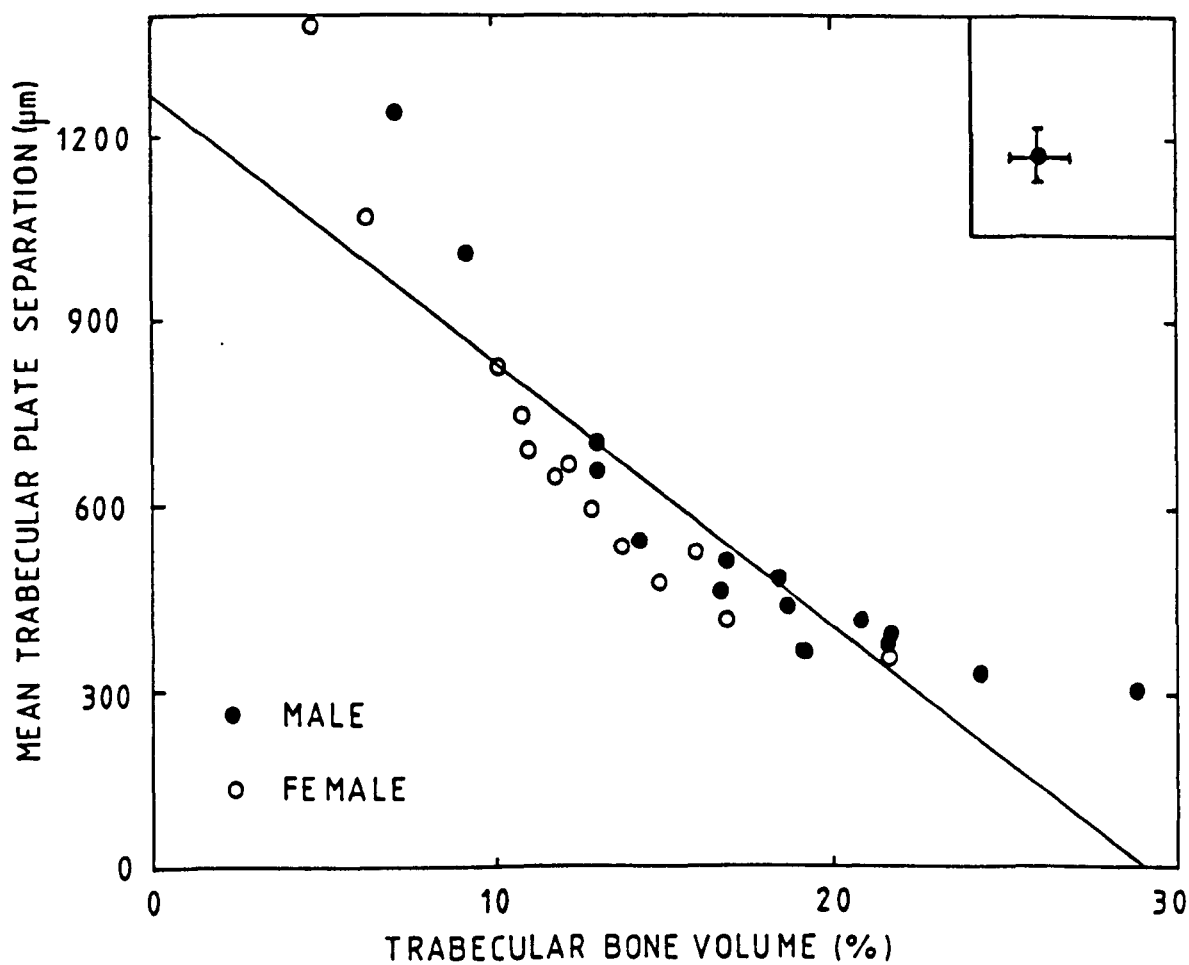
Figure 6.6 The mean trabecular plate separation (MTPS) plotted against

trabecular bone volume (TBV) for samples from 28 os calces.

gradient = -44 +/- 5

correlation coefficient = -0.89
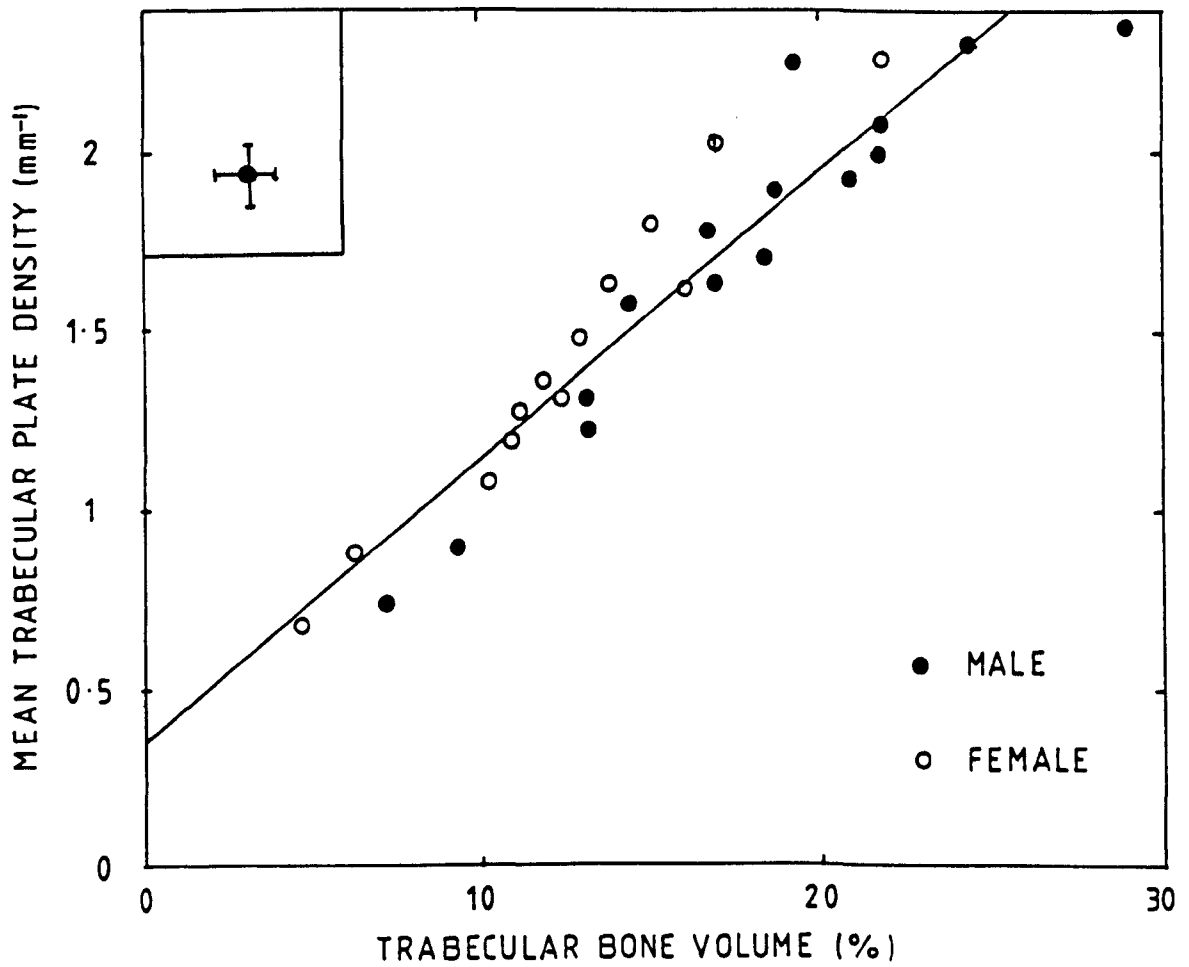
Figure 6.7 The mean trabecular plate density (MTPD) plotted against
trabecular bone volume (TBV) for samples from 28 os calces.

gradient = 0.082 +/- 0.005

correlation coefficient = 0.95

towards a minimum trabecular spacing of about 300 μm. A high correlation would be expected between TBV and the trabecular density, figure 6.7, and r = 0.95.

Although nearly all the samples were 60 years or older, see section 3.3, the males were generally higher in TBV, MTPT and MTPD and lower in MTPS. The effect of age has been investigated in many publications both for normal and osteoporotic individuals (Aaron et al, 1987. Parfitt et al, 1983. Weinstein and Hutson, 1987).

6.4.2 Ultrasonic Results.

The correlation between the ultrasonic slope per unit length and the TBV is r = 0.83, figure 6.8, similar to that obtained between the slope per unit length and the physical density, as would be expected. There is a very even distribution around the regression line of both male and female samples.

Figure 6.9 shows the relation between the MTPT and the ultrasonic slope per unit length. The correlation of 0.51 is not significant and suggests there is no direct link between the ultrasonic attenuation as a function of frequency and the trabecular thickness. The correlation between the MTPS and the slope per unit length is -0.79, figure 6.10, with the lowest slope bone tending to have very large pore sizes, similar to the effect seen in figure 6.6. The MTPS used here is the estimated minimum separation value, see section 6.3.3.

The MTPD is highly correlated to the TBV, hence the correlation between the slope per unit length and the MTPD is 0.83, figure 6.11, similar to that for the TBV and slope.

6.5 Discussion and Conclusions.

The results from the histomorphometric analyses are intended for use in investigating the propagation of ultrasound through the cancellous bone, but also prove interesting in their own right. The site usually used for such
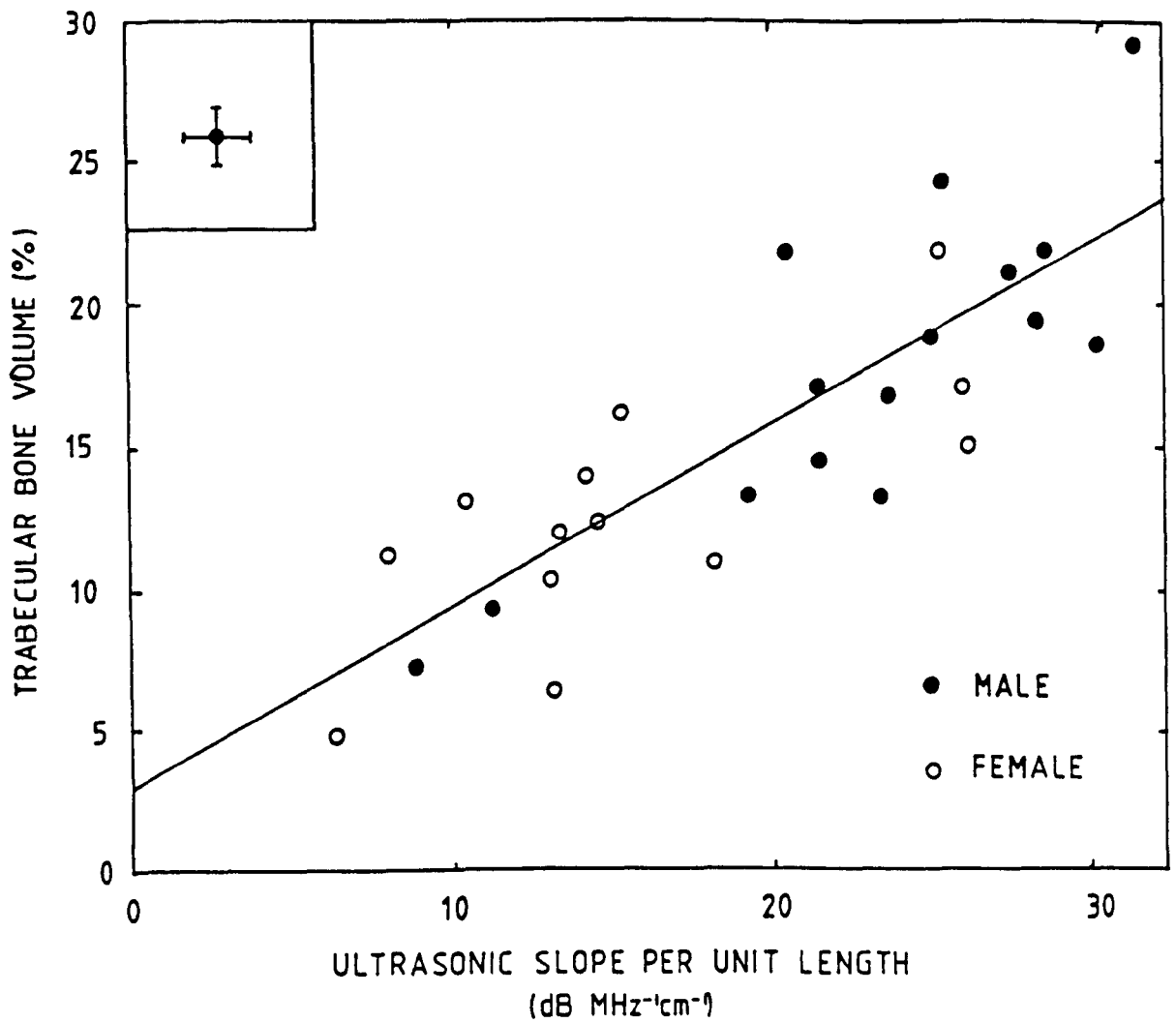
Figure 6.8 Trabecular bone volume (TBV) plotted against the ultrasonic slope per unit length for samples from 28 os calces.

gradient = 0.63 +/- 0.08

correlation coefficient = 0.83
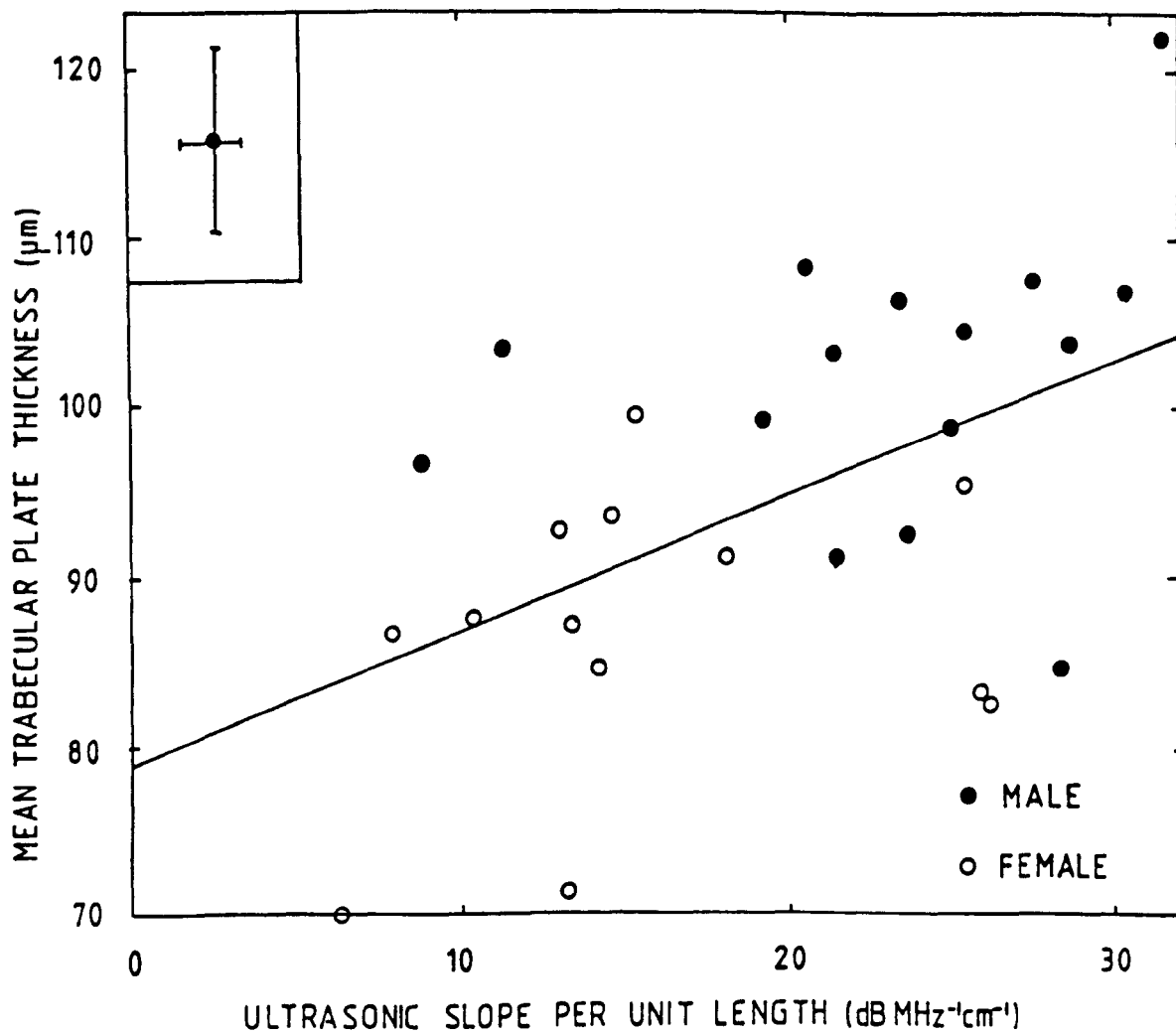
Figure 6.9 Mean trabecular plate thickness (MTPT) plotted against the ultrasonic slope per unit length for samples from 28 os calces.

gradient = 0.8 +/- 0.3

correlation coefficient = 0.51
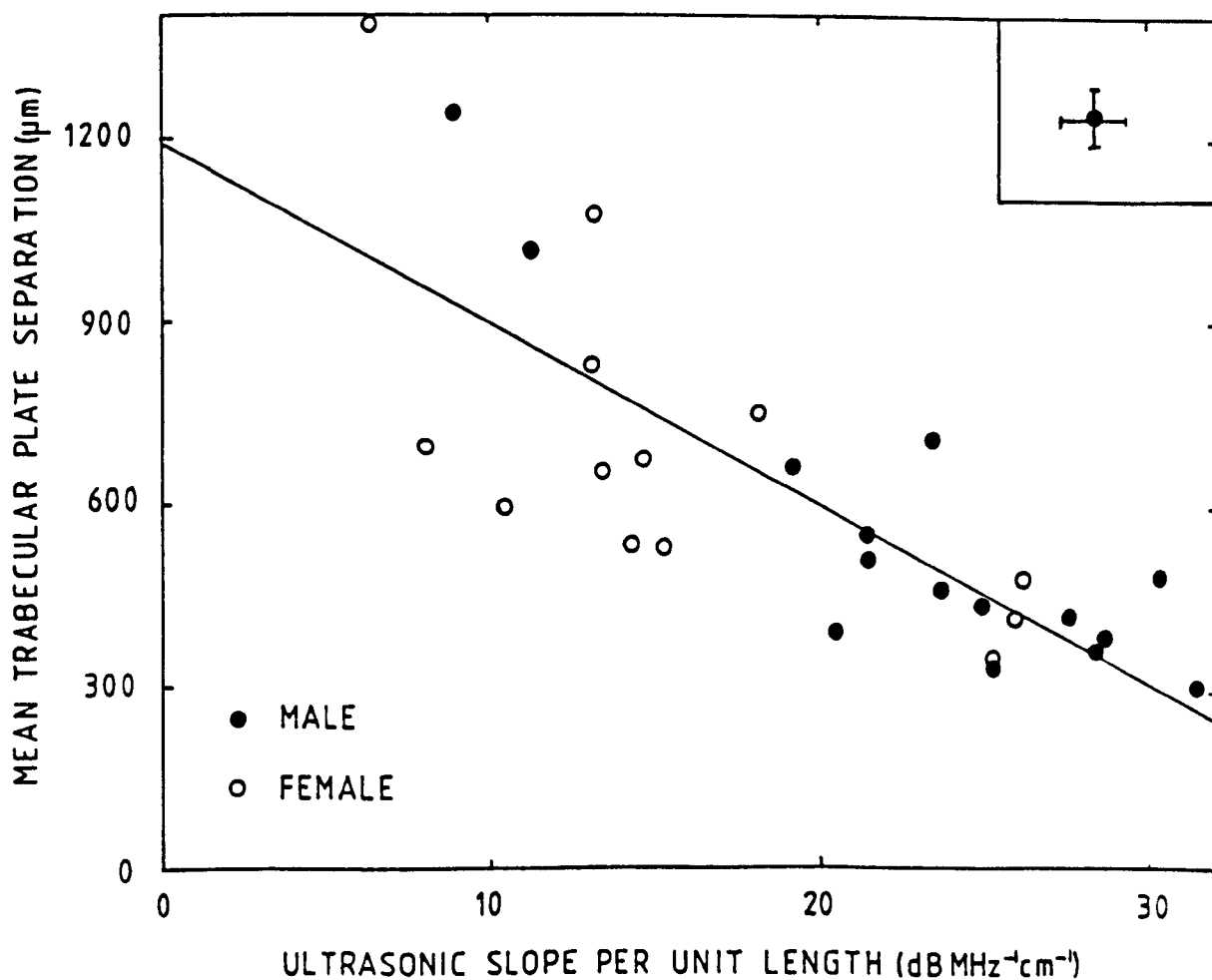
Figure 6.10 Mean trabecular plate separation (MTPS) plotted against the
ultrasonic slope per unit length for samples from 28 os calces.

gradient = -30 +/- 5

correlation coefficient = -0.79
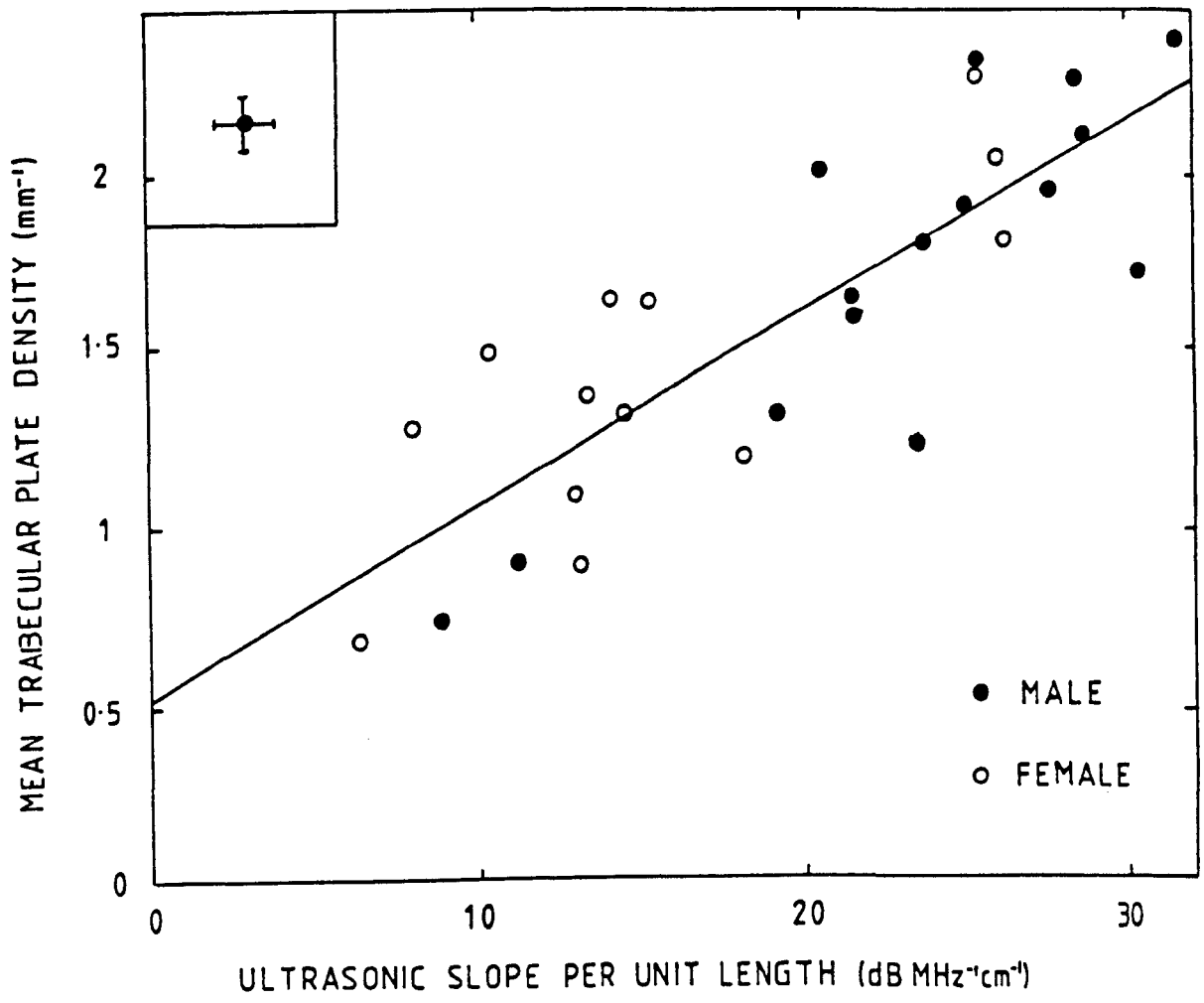
Figure 6.11 Mean trabecular plate density (MTPD) plotted against the
ultrasonic slope per unit length for samples from 28 os calces.

gradient = 0.054 +/- 0.007

correlation coefficient = 0.83

studies is the iliac crest, as biopsies are taken from here *in vivo*, perhaps before a hip replacement. Trabecular structure varies from skeletal site to site as well as from individual to individual, so the results can only be qualitatively compared to those published previously.

The correlations between the histomorphometric parameters are similar to those obtained by others for the iliac crest. The correlation between the TBV and the MTPT was 0.67, compared to 0.76 and 0.60 (Weinstein and Hutson, 1987 and Parfitt et al, 1983 respectively). The relation between the TBV and the MTPS was found to be $r = -0.89$ in the current work, compared with -0.82 (Weinstein and Hutson, 1987). The correlation of 0.95 obtained between the TBV and the MTPD was much higher than that obtained by Parfitt et al (1983) from iliac crest samples, $r = 0.83$.

There are few publications comparing diagnostic techniques to histomorphometric parameters, and those papers that do usually compare different sites, such as the vertebral BMC to the TBV at the iliac crest. Thus only qualitative comparisons can be made between the current work and previous publications in this area too. Jensen et al (1979) found a correlation of 0.75 between the bone mass of the forearm established by QCT and the TBV of the iliac crest. A similar study by Foldes et al (1987) found correlations of 0.76 or less between Compton scattering and SPA of the trabecular or cortical bone density of the forearm and iliac biopsy TBV. Podenphant et al (1987) carried out a detailed study including SPA of the wrist, DPA of the spine and histomorphometry of iliac crest samples on patients with wedge and crush vertebral fractures and a group of normals. Crushed vertebrae represent a more severe form of osteoporosis than wedged vertebrae. The researchers found that there was a large trabecular loss and a substantial deterioration of microstructure in those with crush fractures, but could not relate any individual measurement to the severity of the disease.

Ideally it would be aesthetically pleasing to relate the ultrasonic slope, perhaps with another ultrasonic parameter, directly to the structural detail of the cancellous bone, as mentioned in section 2.3.3, where other work relating to the BUA system is reviewed. The slope and the attenuation at 200 kHz are used to define the ultrasonic characterisation of each bone. The slope per unit length correlates well with the TBV and MTPD and gives some indication of the trabecular thickness and separation, but there is still a significant spread of results around each regression line. In general, those os calces above the regression line between the slope per unit length and the TBV are also above the regression line between MTPD and slope and are below the line between MTPS and the ultrasonic slope. This suggests, for example, that a bone of particular TBV, MTPT and MTPS will have a certain ultrasonic slope, but a bone with a higher MTPS and lower MTPT (but similar TBV) will have a lower ultrasonic slope. However, vary all three parameters and there is no unique slope value predicted. The slope alone can not give sufficient information about all the parameters. It has been suggested that the attenuation at 200 kHz could be used together with the slope to uniquely define the quality of the bone structure (Langton, 1987). Do those bones with a higher than expected attenuation at 200 kHz lie off the regression lines between the slope and the structural parameters?

The correlation between the attenuation at 200 kHz per unit length and the slope per unit length, figure 6.12, is 0.89 and there is some scatter around the regression line. However, the scatter is not comparable to that around any of the regression lines between the slope and the structural parameters, so the 200 kHz attenuation is not directly providing any further information. Correlations calculated between the 200 kHz attenuation per unit length and any of the structural parameters are slightly lower than the corresponding correlation between the slope per unit length and the histomorphometric data.
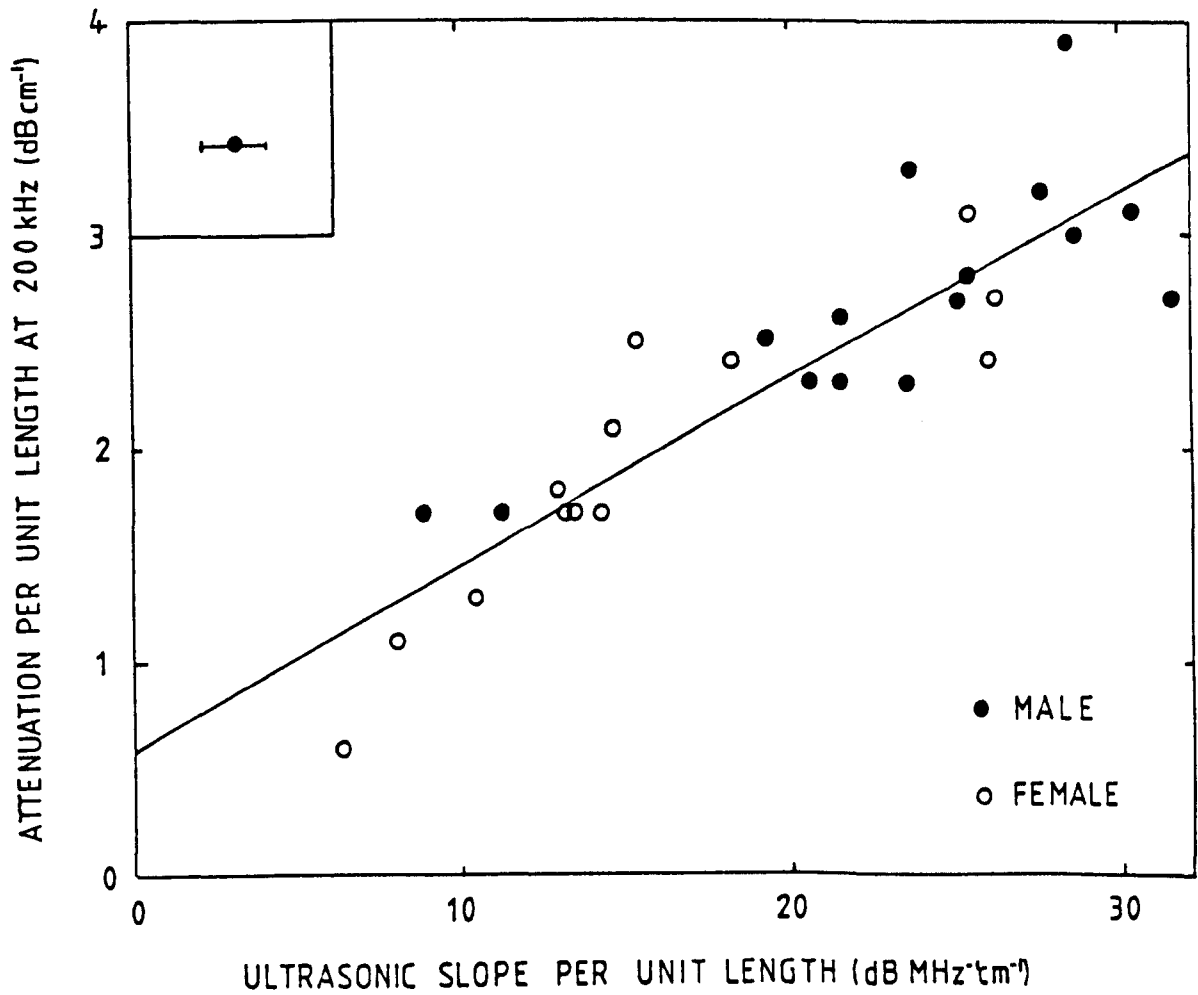
Figure 6.12 The ultrasonic slope per unit length plotted against 200 kHz

attenuation per unit length for 28 os calces.

gradient = 0.088 +/- 0.009

correlation coefficient = 0.89

This suggests that the attenuation at 200 kHz is registering similar details to the overall ultrasonic slope, but perhaps less accurately, due to the larger errors involved with the very small reading.

In conclusion, there is a large variation in structural parameters between the os calces studied. There is also a substantial variation in structure within each heel bone. The ultrasonic slope per unit length correlates with the trabecular bone volume of the samples wih $r = 0.83$, comparable to the correlation with the physical density, as might be expected. The slope also gives some indication about other structural parameters, but can not be used directly to uniquely define the trabecular pattern. It appears that the attenuation at 200 kHz does not provide any further information to that obtained from the slope value where the structural parameters are concerned.

Chapter Seven.

REVIEW OF ULTRASONIC PROPAGATION IN COMPOSITE MATERIALS.

7.1 Introduction.

Ultrasonic attenuation is the loss of energy from an ultrasonic signal passing through a medium. It is due to several effects. Some energy will be reflected at the boundary of the material both on entering and leaving the sample; these are the reflection losses and can be calculated from the impedance mismatch between the sample and its surroundings. Mode conversion may also occur at the boundary of the material. Absorption is the loss of energy due to frictional or viscous losses, thermal losses and molecular exchanges, and represents the energy that is lost, usually in the form of heat, as the wave actually passes through the material. The term attenuation is often used to describe absorption, and the attenuation coefficient usually quoted for materials represents the losses due to absorption. If the medium is inhomogeneous, the ultrasound will be affected by the changes in impedance and the size of the inhomogeneities. This leads to a scattering effect, where the direction of the energy propagation is altered by the inclusion or obstacle.

This chapter reviews the theories that have been developed, usually for a particular application, to explain the propagation (velocity and attenuation) of ultrasound in inhomogeneous material and the possibility of their application to cancellous bone. Firstly, though, the mechanisms of ultrasonic attenuation are discussed in more detail.

7.2 Attenuation Mechanisms.

The main causes of ultrasonic attenuation in any material can be split in to reflection losses and absorption. Once inhomogeneities are introduced, the

scattering effect becomes important and possibly multiple scattering if the scattering objects are not well separated within the medium.

7.2.1 Reflection Losses.

Reflection losses occur at any boundary which the ultrasonic wave meets, and the reflection and transmission coefficients are defined as the ratio of the reflected or transmitted intensity to the incident intensity. An acoustic boundary is a discontinuity of characteristic impedance, and it is assumed that the size of the boundary is large compared to the incident wavelength. If this is not the case, the ultrasound will be scattered rather than geometrically reflected and transmitted.

If the propagation through a finite sample is being considered, the losses at each boundary must be included, and if these boundaries are parallel, the situation can be described as transmission through a layer of material. The form of the coefficients for normal incidence will depend on the distance between the two boundaries and the duration of the incident signal. If the time taken to propagate through the sample and back is long compared to the duration of the incident signal, the coefficients can be calculated by repeating the reflection losses at a single interface for each boundary (Kinsler et al, 1982).

The reflection losses in the cancellous samples have been evaluated in section 4.4.1 using the equation representing repeated boundaries for the transmission coefficient at normal incidence on a smooth surface, as the cancellous bone is assumed to be a homogeneous material with the average density and ultrasonic velocity values. The impedance mismatch is small, resulting in only a little energy loss, but this will be increased by the cortical surface and the irregular shape of the os calcis. The differences are accounted for experimentally by comparing the total bone cores to the

corresponding purely cancellous samples, section 4.4.2. The shape of the heel bone means that the ultrasonic beam is not always at normal incidence to the surface, and this will produce reflected waves in directions away from the receiver. It may also introduce mode conversion, where some longitudinal wave energy is converted to other wave modes, such as shear or surface waves. Mode conversion becomes more important as the angle of incidence increases.

7.2.2 Absorption.

Absorption is the dissipation of acoustic energy, ultimately in to thermal energy, as the wave propagates through a material. The classical explanation for absorption in fluids is the viscous losses, where the frictional forces oppose the movement of the fluid in the regions of rarefaction and compression of the longitudinal wave. The extent of the energy absorbed depends upon the density and viscosity of the fluid as well as the frequency of the ultrasonic wave. Slight temperature differences between the regions of rarefaction and compression will result in energy loss due to thermal conduction.

Molecular exchanges or relaxation losses involve interactions with the material at a molecular level. Energy in any material, such as molecular vibration or rotation, lattice vibration and weak molecular bonds, is affected by the passing ultrasonic wave, and results in a reduction of the ultrasonic intensity and an increase in the potential energy of the system.

Absorption coefficients for biological materials are available in the literature (Wells, 1977) although there is a wide range of values for each material owing to the variability of the tissues. In calcaneal cancellous bone, it is assumed in the current work that the bone itself is comparable to cortical bone and the pores are filled with a fat and tissue fluid mixture. The former assumption is based on the real density values for the bone from cancellous samples which are similar to the density of cortical bone (Galante

et al, 1970). The second assumption is based on visual inspection of the os

calces.

Absorption is usually included in theories of ultrasonic propagation by

using a complex propagation constant or wave number, k, such that

$$k = \frac{w}{c(1 + i\alpha)}$$ (7.1)

where w is the angular frequency, c is the velocity and α is the attenuation

coefficient in Np m^{-1}. This method is extended to produce complex bulk and

shear moduli to account for the absorption of the individual constituents of

the medium. A complex modulus is written as

$$K = K_r (1 + \delta i)$$ (7.2)

where the real part, K_r, is multiplied by the decrement, δ, where

$$\delta = \frac{\alpha c}{\nu}$$ (7.3)

(Truell et al, 1969).

7.2.3 Scattering.

Sudden spatial changes in the elastic properties of the material will

affect the propagation of the wave, and an inhomogeneous material will

introduce a scattering effect, depending on the size of the obstacles compared

to the wavelength of the incident signal.

The scattering effect can be split in to three regimes:

i) the Raleigh region, where $\lambda \gg a$ and the scatter coefficient

$$s \propto a^6 / \lambda^4.$$

ii) the random or stochastic region, where $\lambda \approx a$ and the scatter coefficient

$$s \propto a^2 / \lambda^2.$$

iii) the diffusion region, where $\lambda \ll a$ and the scatter coefficient

$$s \propto 1 / a^2.$$

The diffusion region is comparable to geometric optics, where half the scattered energy is spread fairly evenly in all directions, but the other half interferes destructively with the transmitted wave behind the obstacle to produce a shadow zone. If the obstacle is small compared to the wavelength, the Raleigh region, the scattered wave is generally propagated in all directions. There is no definite shadow area as only a small amount of scattered energy propagates in the direction of the transmitted wave, making destructive interference negligible. There is also no shadow formed when stochastic scattering takes place, although interference effects do occur.

The Raleigh and stochastic mechanisms are the most common scattering situations in ultrasonics, and indeed it is these types of scattering that would be expected in cancellous bone. The scattering caused by a cylinder of radius larger then the incident wavelength has been calculated in section 4.5

Lord Raleigh (1926) was the first to show that the scattered energy from small particles increases as the fourth power of frequency compared to the incident energy. Mason and McSkimin (1947) demonstrated the three regimes by comparing the scattering losses in an aluminium rod to those in a glass rod. The glass rod produced a loss directly proportional to frequency, but the aluminium, composed of grains, produced an attenuation that could be modelled
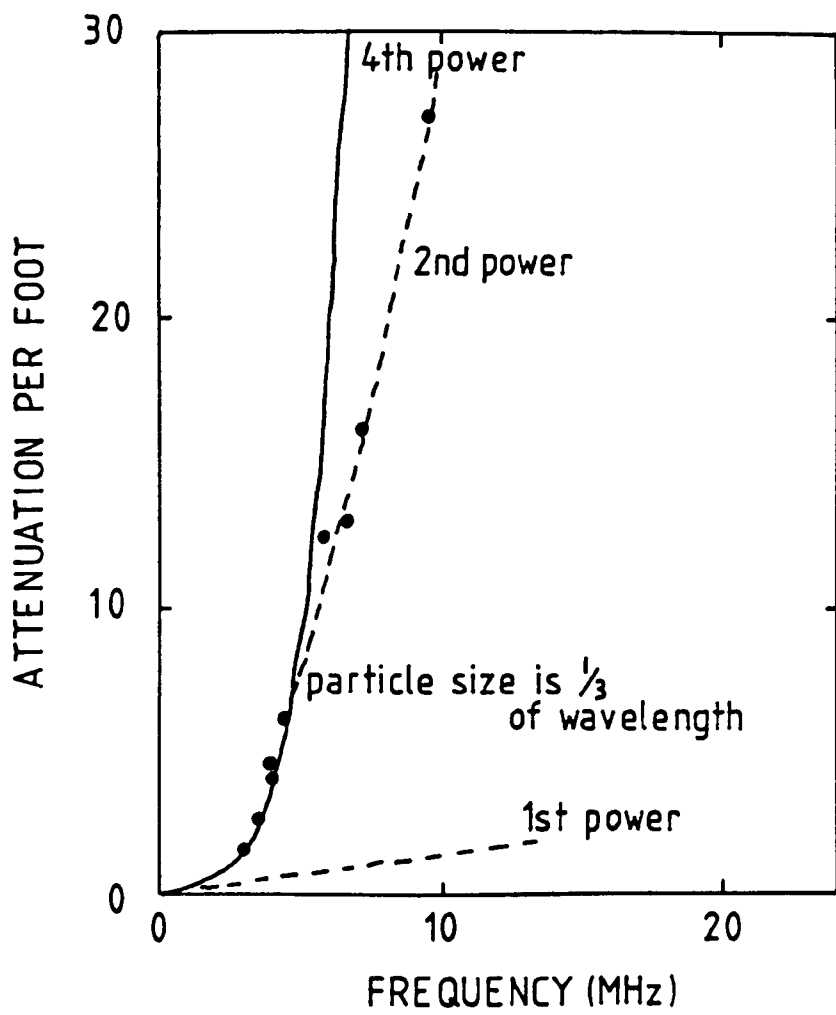
Figure 7.1 Scattering losses for an aluminium rod.
(Mason and McSkimin, 1947)

by a fourth power law at low frequencies and a square law at higher frequencies, figure 7.1. The change over point was when the grain size was one third of the wavelength.

Scattering theory is usually developed by expressing the incident wave, or the wave if the obstacle was not present, as an infinite series of Bessel functions, spherical or cylindrical depending on the shape of the scatterer. The out-going wave, defined so that the combination of radial velocities at the surface of the scatterer is zero, is also an infinite series. Coefficients are then found with the combined velocity set to zero at the surface of the obstacle (Morse and Ingard, 1968). There is a close connection between the scattered wave and the wave that the obstacle would produce if it were radiating sound energy itself. The intensity of the scattered wave at some distance from the obstacle can then be found explicitly, or with specific assumptions for the Raleigh or diffusion regions.

The theory assumes that the scattered wave remains unaffected as it propagates away from the obstacle producing it and hence is referred to as single scattering. If there are many obstacles present, the incident wave will be scattered by all of them. If the scattered energy is very small compared to the incident energy, the scattering is said to be weak, and the Born approximation can be made. This is based on finding the scattered wave by estimating it as the incident wave plus a series of approximations which will eventually converge to a result. If, in fact, the first term of the series is small compared to the incident wave, that single term produces a satisfactory answer. This will be true if the scattering cross section of the individual obstacles is small, and is called the Born approximation (Morse and Ingard, 1968).

However, as the number of obstacles increase they become separated by smaller distances, and the scattered wave from one obstacle will be affected

Figure 7.2 Ultrasonic scattering modes:

      a) single

      b) double

      c) triple through different particles

(a)

incident

(b)

incident

(c)

incident

(d)

incident

(e)

incident
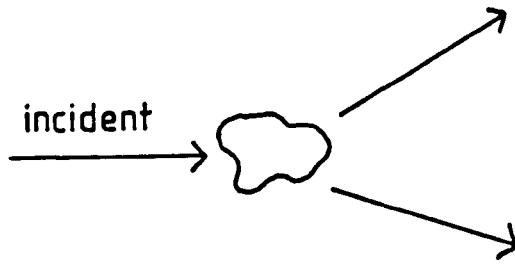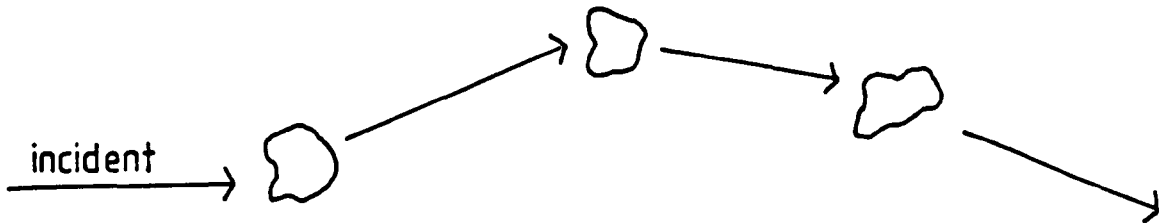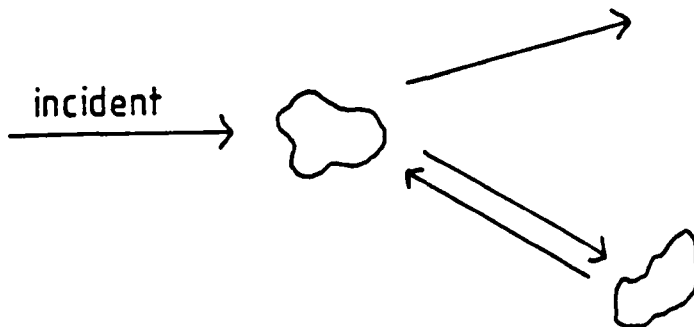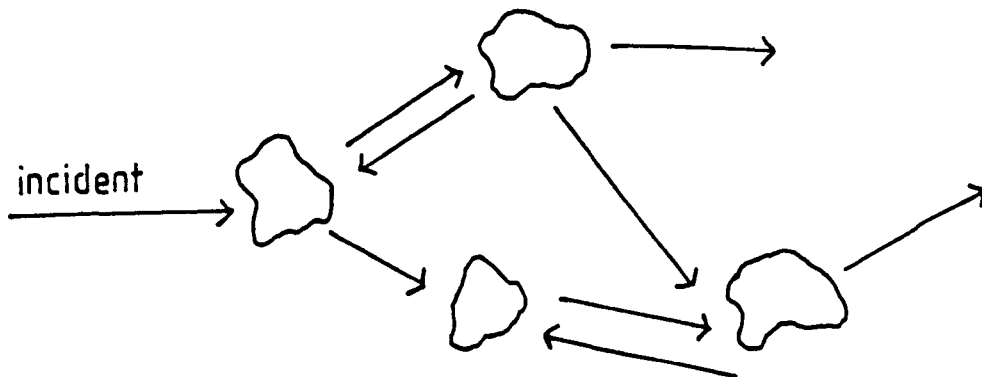
      d) triple with a repetitive propagation path

      e) multiple

    (Ishimaru, 1978)

by a second obstacle, and possibly by a third or fourth. This situation is usually termed multiple scattering, and figure 7.2 represents the difference between single and multiple scattering diagrammatically.

Many present day approaches to the evaluation of multiple scattering are based on the work of Foldy (1945) who mathematically averaged over a probability distribution for a particular configuration of scatterers over all possible configurations. The incident wave and the scattered wave from all other scatterers are used to define an exciting wave which impinges on a particular obstacle (Waterman and Truell, 1961). The total field is the sum of the incident and all scattered waves and is found from the configurational average of the exciting field. This leads to a propagation constant (or complex wave number) for the scattering medium, k, being found in terms of the volume density of scatterers, n_0, and the far field amplitude for the individual obstacles, f(0).

$$\left(\frac{k}{k_1}\right)^2 = \left(1 + \frac{2\pi n_0 f(0)}{k_1^2}\right)^2 - \left(\frac{2\pi n_0 f(\theta)}{k_1^2}\right)^2 \qquad (7.4)$$

where k_1 = w / c is the real wave number for the incident wave. The scattering cross section of the individual obstacles, δ, can be determined, and if

$$\frac{n_0 \delta}{k_1} \quad \ll 1 \qquad (7.5)$$

weak scattering can be assumed, so the square terms can be neglected (Truell et al, 1969).

There are many publications based on this theory, usually under a specific assumption such as Raleigh scattering or negligible density changes between

the obstacles and the surrounding material. These are discussed in section 7.7.

Thus the ultrasonic attenuation in an inhomogeneous material is due to several factors: reflection losses, energy absorption by various mechanisms, and the scattering of the sound from the direction of propagation. All of these are important in the evaluation of the ultrasonic velocity as well as the attenuation. Many theories have been developed to explain the ultrasonic propagation in inhomogeneous material, usually for a specific application, and some of these are reviewed in more detail in the following sections.

7.3 Simple Mixture Theories.

The most obvious way to approach a composite material is to take the volume average of the parameters that affect the ultrasonic propagation. For instance, to find the velocity in a two component medium where one constituent represents β fraction of the whole, the following equation would be used:

$$c = (\ (\beta\rho_1 + (1 - \beta)\rho_2)\ (\beta\ K_1 + (1 - \beta)\ K_2\ )\ )^{0.5} \tag{7.6}$$

where ρ and K are the density and bulk modulus respectively. This method is generally attributed to Wood (1930) but, as it stands, applies only to fluid mixtures. Duykers (1970) volume averaged the complex shear moduli as well as the complex bulk moduli to model the attenuation and velocity in a kaolin and water mixture. His results corresponded with experimental data for mixtures of up to around 30% kaolin, although he stresses the importance of the mixtures being dispersed. It is suggested that particle flocculation in undispersed systems increases the effective particle size, which affects the relaxation

time associated with the losses due to viscosity, accounted for by the imaginary part of the complex moduli.

This simple approach appears to be valid for many applications, especially for particles in suspension, but for high density mixtures, where the inclusions are packed closely together, the effect of the particles touching must be taken in to account. This means that shear waves, which would not normally propagate because of the fluid, will be able to pass through the material via the framework of touching particles. In the case of cancellous bone, the marrow fat and the bone separately form continuous frameworks throughout the sample, suggesting that the simple mixture approach is insufficient to explain the ultrasonic propagation in this case.

In practice, the use of the simple mixture theory is comparable to considering the attenuation as a function of the trabecular bone volume, as discussed in section 6.4.2. It is not strictly the actual attenuation of the cancellous bone used in that discussion, but the attenuation as a function of frequency. If the attenuation at a particular frequency is considered, however, the results are similar, as discussed in section 6.5 for the attenuation at 200 kHz. There is a correlation between the trabecular bone volume and the attenuation but there is also a large scatter of results around the regression line. Thus it would seem that the mixture theory does explain the trend of the ultrasonic attenuation with trabecular bone content, but does not explain the full variation of the results. It would not account for the differences found in section 4.6 either, where the attenuation depended on the direction of propagation through the same sample of cancellous bone.

7.4 The Biot Theory.

The idea of a framework of touching particles in a suspension can be reversed to a porous medium with connecting pores. Any theory to be applied to such a medium must account for both the framework and the interconnecting holes, which could be filled with another material. A theory which has been developed to explain the ultrasonic propagation in a porous medium is that due to Biot (1956, 1962a and 1962b) and has been used by many researchers for a variety of applications. Other theories have been published, but Biot's has been used over a very wide variety of applications. A full review of ultrasonic propagation in porous materials has been published by Attenborough (1982).

The theory is based on the frictional interaction of the fluid as it flows through the pores influenced by the ultrasonic wave. The matrix, or the material in which the pores are situated, is not rigid but has its own elasticity. Under isothermal conditions, the constitutive relations equating the stress components and the static equilibrium pressure in the pores and the Lagrangian formulation for the wave equations are found, including the coupling factors between the fluid in the pores and the matrix material. These can be rewritten by including a parameter representing the volume of fluid entering or leaving unit volume of the porous material. All the constants used by Biot can then be related to known or measurable moduli and structural parameters. The theory is developed in detail in section 8.5 where it is specifically applied to cancellous bone.

The assumptions underlying the derivation are that the porous material is isotropic and of constant porosity and that the pore walls are impervious to the fluid. The pore size is represented by an average value around which the actual values must be concentrated, and, most important ultrasonically, the pore size must be less than the wavelength. This last assumption means that

scattering is neglected in the development of the theory and represents the main limitation in its application to cancellous bone.

The theory predicts two longitudinal waves as well as a shear wave, the faster one associated with movement in phase with the motion of the frame and the slower one out of phase. It was only in 1980 that the second wave was demonstrated experimentally (Plona, 1980) and quantitatively matched to the predictions of Biot's theory (Berryman, 1980a). Plona observed the slower wave only when glass spheres in water were fused together, thus differentiating between touching and separated particles. Lakes et al (1983) observed a slow wave in wet bovine cortical bone that was not travelling at the velocity of a shear wave which could have been produced by mode conversion. They suggest that this wave is Biot's second longitudinal wave but made no attempt to model the wave velocity using the theory.

Biot developed the theory to explain the ultrasonic propagation in geo-physical situations, and it has been applied successfully to fluid saturated porous rocks (Ogushwitz, 1985) and marine sediments (Stoll, 1974). It has also been extended, among other applications, for use with high porosity elastic foams (Lambert, 1983).

Chapter six has shown that the pore size in cancellous bone is smaller than or comparable to the wavelength of the ultrasound over the frequencies used and is therefore, at best, at the very limit of the application of the Biot theory. However, it does represent the only fully developed theory for general porous materials and gives a comparison to scattering theories which require far more idealised situations. The Biot theory is developed in detail and applied to cancellous bone in section 8.5.

7.5 Theories Developed From the Single Scattering Approach.

Single scattering theories, based on the assumption that the total effect of a collection of scatterers is the sum of the effects from the individual scatterers, have been successful in predicting the ultrasonic velocity and attenuation in composites, especially particles suspended in a fluid, for concentrations up to around 30%.

Urick (1948) suggested a formulation that showed the attenuation could be expressed as the sum of a scattering component and a viscous effect from the movement of the fluid with respect to the particles. Duykers (1967) showed agreement with this theory and the experimental propagation in sediments, and suggested the viscous effects have the same frequency dependence at high and low frequencies as the theory developed by Biot, despite the difference in approach and the fact that the particles in suspension do not form a framework in the same way as the matrix material in a porous substance. Many single scattering applications are included in the review of ultrasonic propagation in inhomogeneous material published by Anson and Chivers (1984).

The frequency effect, leading to velocity dispersion, can be included by using the Kramers-Kronig relationship. These equations were originally developed to model the dispersion of electromagnetic waves in dielectrics and have been re-evaluated for ultrasonic applications (Weaver and Pao, 1981). The relationship between the wave number and frequency is developed by considering the condensation, $s(t)$, as an integral over infinite time of the compressibility, K, and the pressure. This is Fourier transformed to give the frequency dependence and then the assumption that the compressibility at a particular time is real, so $K(-w) = K^*(w)$, and that the present condensation should not depend on the future pressure, so $s(t) = 0$ if $t < 0$ (O'Donnell et al, 1981). In evaluating the results, it is necessary to know the phase velocity at an infinite frequency, and this is often used as an adjustable

parameter. This approach essentially finds the velocity dispersion from a knowledge of the attenuation and the static velocity, and is therefore not applicable to the current work.

7.6 Comparative Media Methods.

A completely different approach that utilises the single scattering assumption is the comparative media method. It is assumed that the wave propagates in a composite material as if it were in an isotropic material with effective parameters obtained by comparing the effect to the wave of introducing a small volume of the composite.

The parameters of the effective material can be varied until the inclusion of the composite has no effect on the propagating wave. The elastic parameters can then be considered to represent the actual composite as well as the theoretical effective material. This self consistent approach has been developed by Berryman (1980b) who obtained specific equations for spheroidal inclusions using a single scattering effect for the inclusion of the composite in the theoretical effective medium. The solution is symmetrical for the constituents of the composite, so either part can be considered as the inclusion or the surrounding matrix. The so called self consistent theory (SCT) is developed in detail in section 8.4 and applied to cancellous bone.

Devany and Levine (1980) suggest that the symmetry of Berryman's theory is unphysical due to the assumption of discrete particles in it which can not apply to a continuous matrix. Devany (1980) used the explicit assumption of inclusions in a continuous homogeneous matrix, and also included multiple scattering effects. He stresses the importance of the multiple scattering by showing how different his results are at higher concentrations to those who have used a similar method but with the assumption of single scattering. Devany also obtains specific equations for the ultrasonic velocities under the

assumption of Raleigh scattering, where the wavelength is larger than the scatterer. His theory includes the prediction of a second slower moving longitudinal wave, the only theory apart from that of Biot to do so. This second wave has been observed (Plona, 1980) but Devany points out that the assumption of Raleigh scattering is not valid for the experiment concerned so there is no possibility of quantitatively comparing the data to the theory. It is interesting to note that Biot also assumes the wavelength is larger then the pores, but his theory has been used to model successfully the Plona data.

Kuster and Toksoz (1974) obtained equations for spheroidal inclusions using the comparative media method and single scattering equations which have been the basis of further work by Gaunard and Uberall (1982), who include frequency dependence. Gaunard refers to his theory as a resonance theory, but the explicit assumption of Raleigh scattering is still used.

7.7 Multiple Scattering.

Multiple scattering effects are important when the composite is comprised many structures spatially close together. Devany has shown a second longitudinal wave, otherwise only predicted by Biot, by taking multiple scattering in to account. Many of the single scattering theorems do not model ultrasonic propagation so successfully for higher concentrations of mixtures, as the particles become closer together.

The work of Foldy (1945) extended by Waterman and Truell (1961) for more general use with finite particle size as opposed to point scatterers, is the basis of calculations published by many researchers to model multiple scattering in controlled man-made samples such as copper spheres in polymethylmethacrylate (PMMA) (Latiff and Fiore, 1975) or glass balls in a polymer (Datta and Pethrick, 1980). Lefebvre et al (1980) compared the experimental attenuation of concrete to that predicted by the Waterman and

Truell equations, and showed little agreement. They point out that the wavelength of the sound at the frequencies used is comparable to the grain size of the concrete, and also that the condition (7.5) required by Waterman and Truell is not valid. To check their technique, they produced samples of marbles in Araldite which conformed to the requirement of equation (7.5) and showed good agreement between theory and experiment. However, (7.5) is an assumption of weak scattering and only represents the case where the squared terms in the theory are neglected. Lefebvre et al appeared to use the full equations, so this was not strictly a limitation.

Sayers (1980) has used the Waterman and Truell equations with a self consistency approach to try and generalise the relations to all concentrations. Under the Raleigh regime, using the first three terms in the series for the far field amplitude of individual obstacles, $f(\theta)$, he suggests that the frequency dependence of the bulk modulus for the composite should disappear when the fraction concentration is either 0 or 1, that is, when the composite is actually made up of either one material only or the other. He calculates a correction factor and shows better results at higher concentrations, still under the Raleigh assumption for scattering (Sayers and Smith, 1982).

Twersky (1964) has done much analysis evaluating the Foldy approach to multiple scattering. From a practical viewpoint, Twersky's theory neglects the terms representing a scattered wave that is affected by a particular obstacle more then once. This reduces the number of terms in the series summation substantially (Ishimaru, 1978), but in this form is not useful for producing practical values. He has reworked the theory to produce a set of integral equations and introduced correction factors based on self consistency. He sets up the self consistency problem slightly differently to that used by Berryman, as he assumes the scatterers are embedded in a material which actually has the

parameters of the composite although the sound is scattered only in to the matrix material.

Twersky (1977) has also considered the importance of the assumption of randomness in the composite, and has included the effects of pair correlated scatterers. As the concentration of obstacles increases, some correlation between positions is bound to occur. Lax (1952) used a similar approximation to solve his series of related equations by assuming that the field with the position of one particle known is the same as that with two particles known. This assumption is exact if the particles are positioned in a regular lattice, so Lax called the approach the quasi-crystalline approximation. It has been used with self consistency methods to improve single scattering results at higher concentrations (Varadan et al, 1985).

7.8 Summary.

There have been many attempts to explain the ultrasonic propagation in composite materials, from the simplistic but effective to the extremely involved. Overall, they can be split in to three categories, depending on whether scattering is taken in to account or not, and, if it is, whether single or multiple scattering is assumed. Any theory that includes scattering requires the particles to be separated, although some produce similar results to the Biot theory which explicitly assumes that both constituents of the composite form a continuous framework. Nearly all the scattering theories, as they become more developed, use the Raleigh condition to allow simplifications which result in the calculation of practical parameters such as the complex moduli of the inhomogeneous material.

There are many researchers who have published work on the ultrasonic propagation in composites which have not been covered by this chapter. Many represent extensions to the main theories mentioned and so have not been

considered. A full review of ultrasonic propagation in inhomogeneous material has been published by Anson and Chivers (1984), while Attenborough (1982) covered propagation in porous substances. Chivers (1977) has also reviewed scattering processes in human tissue, although not bones, including both single and multiple scattering mechanisms.

The application of the simple mixture theory to cancellous bone has already been discussed, section 7.3. The Biot theory (no scatter), Berryman's self consistent theory (single scatter) and the multiple scattering theory based on Waterman and Truell are analysed in more detail in the next chapter in an attempt to apply them to cancellous bone. It is obvious that some assumptions implicit in the theories are not valid for the trabecular structure of the bone, but as the survey of theories has shown, no method is ideally suited for this application.

Chapter Eight.

APPLICATION OF ULTRASONIC PROPAGATION THEORIES TO CANCELLOUS BONE.

8.1 Introduction.

There have been many theories published to explain the ultrasonic propagation in inhomogeneous material as summarised in the previous chapter. None of them are immediately obvious for their possible application to cancellous bone, as assumptions regarding the wavelength of the ultrasound compared to the inhomogenieties or the fact that the scatterers have to be separated are often implicit in the development.

In this chapter, the theory used by Langton in his thesis (1984) is reviewed and compared to the ultrasonic results obtained in the current work. The parameters pertinent to the ultrasonic propagation are evaluated for cancellous bone, and three particular theories are considered in detail and used in an attempt to fully explain the propagation of ultrasound in cancellous bone.

It must be stressed that no attempt has been made to adapt these theories to improve their applicability. This work is purely an exercise to establish whether existing theories can be applied successfully to the specialised material cancellous bone.

8.2 Review of Langton's Theory.

The ninth chapter of Langton's thesis (1984) was an attempt to explain the variation in attenuation of the os calces he had measured *in vivo*, by considering reflection losses, absorption and scattering.

Langton initially considered the reflection losses due to the boundaries of the bone and included the cortical layer on each side of the os calces, giving

a total of four interfaces. He assumed 50% bone volume for the cancellous bone, which has been shown in chapter 6 to be very high, and calculated reflection losses of 4.3 dB. Most of these losses were due to the water cortex interface, so reducing the proportion of bone in the trabecular section would have little effect. He assumed the boundaries were parallel and normal to the incident wave, so, in fact, the reflection losses would be expected to be higher due to the irregular shape of the surfaces, section 7.2.1.

It has been shown in the current work that the attenuation due to the losses from the cortex and irregular surface are much smaller than those calculated by Langton for the os calces surfaces. On average, they represent 2.7 dB, section 4.4.2. It would appear that the ultrasound is efficiently transmitted by the cortical layer, which is smaller than the wavelength of the incident ultrasound (Kinsler et al, 1982).

Langton also considered the absorption of the separate components of the os calcis, using the coefficients for cortical bone and fat, which for his 50% model of cancellous bone produced an attenuation of 0.88 dB at 200 kHz. This would only be reduced slightly if the ratio of the constituents was changed to the typical values found in chapter 6.

The reflection losses are frequency independent and the frequency dependence of the absorption does not explain the wide variation in results obtained for cancellous bone, so Langton went on to consider the scattering effect. He used the Raleigh scattering equations used by Mason and McSkimin (1947) to model losses from the grains in aluminium. These depend on the differences between the bulk moduli and the densities of the two components. Langton showed that the difference in density was small compared to the difference in bulk modulus for fat and bone, and hence neglected the density effect. He found the scattering cross section of an ideal trabecula of particular volume and summed over all the trabeculae in the material to give

the scattered power, which can be related directly to the attenuation coefficient. The Raleigh assumption, of course, produced a dependence on the fourth power of frequency, which does not compare well with the experimental results. The linear fit used to produce the attenuation slope as a function of frequency is a good fit, as seen by the errors due to the fitting procedure. The scattering coefficient was calculated from the volume of the individual scatterer (taken as the cube of the trabecular thickness multiplied by $\pi/3$), the frequency dependence, the velocity of ultrasound in the material (estimated at 2500 m s^{-1}), the difference in bulk moduli and the number of scatterers.

It is important to note that Langton's approach uses the trabeculae rather than the pores as the scatterers, which is not the case for theories considering propagation in a porous material. The use of the bulk modulus alone does not account for the possibility of shear waves which may be produced by mode conversion in the bone matrix even though they will not propagate through the fluid marrow.

Single scattering was assumed and the Raleigh regime used in the initial calculations for the scattering cross section. Langton assumed that the stochastic regime limit is when the wavelength of the ultrasound is one eighth of the scatterer size, which he calculated to be 390 kHz, and hence he split the frequency dependence of the attenuation in to two sections around this value. This he suggested may produce the change in slope observed with fairly high density os calces. This change was not observed for the purely trabecular samples in the current work and is therefore possibly a function of the cortical layer and shape of the os calcis. As with any theory based on scattering from particular sized objects, it would not predict the results of section 4.6, where the ultrasonic attenuation depended on the direction of propagation through the cancellous bone.

Figure 7.1 shows the three scattering regimes that are commonly defined, as in section 7.2.3. For cancellous bone at the ultrasonic frequencies used, ka is of the order of unity and   is therefore   in the stochastic or random regime, where there is no fixed dependence even in the ideal case of spherical scatterers. Langton noted this point and suggested that all three regions were covered by the frequency range under consideration.

Langton's approach produced a reasonable estimate of the attenuation as a function of frequency, although the parameters for bone content, trabecular thickness and velocity have been shown in the current work to be poor estimates of the actual values. As with any purely scattering theory, the dependence of the attenuation on the direction of propagation can not be accounted for.

8.3 Parameters for Cancellous Bone.

This section comprises a list of the parameters required by the three ultrasonic theories that are to be investigated. The parameter values are presented together with an explanation of the source of each value.

The main parameters required in any attempt to explain ultrasonic propagation in a composite are the density and ultrasonic velocities of the individual constituents of the material. For bone and marrow, the components of cancellous bone, there is a wide range of published data available. Each component is variable in itself (see chapter 1), so the data is well spread. The density values used in the current work are:

$$\text{marrow density, } \rho_m = 950 \text{ kg m}^{-3}$$

$$\text{bone density, } \rho_b = 1800 \text{ kg m}^{-3}$$

The marrow of the os calcis is mainly fat with some watery fluids permeating through it, rather than the red marrow of the vertebrae, where blood flows

freely through the bone structure. The density value quoted above is that of fat (Wells, 1977), slightly increased to account for the fluid content. Red marrow density has been quoted at 1100 kg m^{-3} (Spiegl and Jurist, 1975) but this contains a greater quantity of higher density blood than the fatty marrow of the os calcis. The bone density value is in the middle of the range quoted by Wells (1977) for cortical bone and is also representative of the values listed by Goss et al (1978) and Greenfield et al (1981). The values for cortical bone must be used for the bone component of cancellous bone as no measurements can be done on the bone component alone due to the size of individual trabeculae. The bone is actually physiologically the same as cortical bone (see section 1.2), so the use of the cortical values is reasonable. If anything, one might expect the bone of the cancellous samples to be slightly less dense than cortex. The density value used here is slightly lower than the density found experimentally for the bovine cortical samples measured in section 4.7.

The ultrasonic velocity values for each component of the cancellous bone were assigned as follows:

longitudinal velocity in marrow, $\quad c_m = 1470 \text{ m s}^{-1}$

transverse velocity in marrow, $\quad t_m = 0$

longitudinal velocity in bone, $\quad c_b = 3300 \text{ m s}^{-1}$

transverse velocity in bone, $\quad t_b = 1800 \text{ m s}^{-1}$

Again the marrow value is typical of those quoted for fat (Wells, 1977. Goss et al, 1978). A transverse wave would not be expected to propagate in the marrow because of its fluid content. The longitudinal velocity for bone is typical of the results described in section 4.7 and agrees well with published

results discussed in that section. The transverse velocity is taken from Goss et al (1978) and is in agreement with the results of Meunier et al (1982).

The absorption coefficients are frequency dependent, and this must be accounted for in the calculations. Absolute attenuation is difficult to measure, and because of this there is a wide range of published data for both fat and cortical bone as well as due to the natural variation of the materials themselves. Typical values were used in this work, taken from Wells (1977) and Goss et al (1978), and are in good agreement with data extrapolated from the results of Garcia et al (1978).

longitudinal attenuation in marrow, α_m = 5 dB MHz^{-1} m^{-1}

transverse attenuation in marrow, α_m = 0

longitudinal attenuation in bone, α_b = 45 dB MHz^{-1} m^{-1}

transverse attenuation in bone, α_b = 50 dB MHz^{-1} m^{-1}

The value used for the longitudinal attenuation in cortical bone is slightly lower than the values obtained in section 4.7 for the bovine samples.

The complex bulk and shear moduli for each component are calculated from the product of the density and velocity for the real part, with the attenuation giving the imaginary part (see section 7.2.2).

The porosity of the samples is obtained from the results of chapter 6, and covers the range from 0.70 to 0.95. This also represents the ratio of marrow and bone in the cancellous samples. The range of sizes of the structures and pores are also taken from this chapter. The trabecular width varies from 70 to 110 μm and the pore size from 470 to 2200 μm, given by π/2 multiplied by the values listed in table 6.3, as discussed in section 6.3.3. These values represent the total size of the structures, whereas theories often require a half size, or radius. The shape factors required by the Biot and self

consistent theories are discussed in the relevant sections, but were chosen because of the detailed structure seen in the work of chapter 6, and were either prolate spheroid or spherical.

The permeability of the cancellous bone architecture is an important parameter. It is only considered by the Biot theory as this explicitly allows the marrow to flow through the bone structure. The permeability of the trabecular structure was estimated at a maximum of 10 darcy ($9.8E-8$ cm^2). This is large compared to values used for more frequent applications, such as porous rocks, and is difficult to assess because of this. It proved virtually impossible to remove the marrow completely from a cancellous core if the bone structure was to remain intact and therefore impossible to measure the permeability. It was possible to do this for the SEM samples (chapter 6) because of their much smaller size. A range of permeability from 0.5 to 10 darcy was used.

A list of the symbols used in the following developments is given in table 8.1.

8.4 The Self Consistent Theory.

This section develops Berryman's self consistent theory (SCT) and applies it to cancellous bone. The theory does not take specific account of frequency, and in fact is more accurate for the theoretical limit of zero frequency (Berryman, 1979), so the data required to mimic the frequency dependence of ultrasonic attenuation is not available from this theory. However, the Biot theory, developed and discussed in the next section, uses the SCT to evaluate the complex moduli of the composite before the frequency dependent effects of the fluid movement are considered. Therefore it was considered necessary to include the full development of the SCT with a brief description of its application to cancellous bone.

Table 8.1 Symbols used for the development of theories.

ρ	density	ω	angular frequency
α	attenuation coefficient	c	longitudinal velocity
K	bulk modulus	t	transverse velocity
μ	shear modulus	λ	wavelength
β	porosity	k	longitudinal wave number
θ	angle (radians)	s	transverse wave number
γ	strain tensor	t	time
u,v	displacement	λ μ	Lame coefficients
c	elastic tensor	ζ	position
x	3D space	r	relative position
δ	delta function	g()	Green's Function
V	volume	W	strain energy
p	pressure	a	pore radius
η	viscosity	τ	stress
Pn	Legendre polynomials	U	fluid displacement
ξ	elemental fluid volume	K	permeability
f(θ)	scattering coefficient at angle θ		

F(χ)	friction effect	U,T Wu's tensor
P,Q	shape factors	
m,H,C,M	Biot's coefficients	
A,B,C,D	Scattering coefficients	

8.4.1 Development of the SCT.

The usual approach to finding the bulk moduli for inhomogeneous media involves the stress and strain tensors. Berryman's approach (Berryman, 1979, 1980a and 1980b) started with the displacement vector u, which is related to the strain tensor ε_{ij} by

$$\varepsilon_{ij} = \frac{d\,u_i}{d\,x_j} + \frac{d\,u_j}{d\,x_i} \tag{8.4.1}$$

and used the equations developed by Mal and Knopoff (1967) which were further evolved by Kuster and Toksoz (1974).

The incident field is $u_0(x)$ exp $(-i\omega t)$, the total field outside a region V containing an inhomogeniety is $u(x)$ exp$(-i\omega t)$ and the field inside the region is $v(x)$ exp$(-i\omega t)$ such that

$$u(x) = u_0(x) + u_s(x) \qquad x \text{ not in } V$$

$$v(x) = v_0(x) + v_s(x) \qquad x \text{ in } V \tag{8.4.2}$$

The subscript s indicates the scattered field. The incident field and the total field outside the region both satisfy

$$c^m_{lnpq} \frac{d^2 u_p}{dx_n dx_q} + \rho_m \omega^2 u_l = 0 \tag{8.4.3}$$

where the superscripts m and i represent the matrix and inclusion respectively. The field inside the region satisfies

$$c^m_{lnpq} \frac{d^2 v_p}{dx_n dx_q} + \rho_m \omega^2 v_l = 0 \qquad (8.4.4)$$

where l, n, p and q take the values 1, 2 or 3 and the summation convention applies for all the subscripts. The elastic tensor is given by

$$c^m_{lnpq} = \lambda_m \delta_{ln} \delta_{pq} + \lambda_m (\delta_{lp} \delta_{nq} + \delta_{np} \delta_{lq})$$

$$(8.4.5)$$

$$c^i_{lnpq} = \lambda_i \delta_{ln} \delta_{pq} + \lambda_i (\delta_{lp} \delta_{nq} + \delta_{np} \delta_{lq})$$

If the position of the region containing the inclusion is ζ then with

$$r = | x - \zeta |$$

$$k = \omega \left[\frac{\rho_m}{\lambda_m 2\mu_m} \right]^{0.5} \qquad (8.4.6)$$

$$s = \omega \left[\frac{\rho_m}{\mu_m} \right]^{0.5}$$

where k and s are the magnitude of the longitudinal and transverse wave vectors respectively, Mal and Knopoff (1967) derived the following integral equation governing the field

$$u_l(x) = u^0_l(x) + \int d\zeta \ (\Delta \rho^i \omega^2 v_n(\zeta) - \Delta c^i_{njpq} \frac{dv_p}{d\zeta_q} \frac{d}{d\zeta_j}) \ g_{ln}(x_i \zeta) \qquad (8.4.7)$$

where $g(x_i \zeta)$ is Green's function.

Part of the second term within the brackets can be rewritten due to the p q invariance as

$$\Delta \, c^i_{njpq} \frac{dv_p}{d\zeta_q} = 0.5 \, \Delta \, c^i_{njpq} \left(\frac{dv_p}{d\zeta_q} + \frac{dv_q}{d\zeta_p} \right) = \Delta \, c^i_{njpq} \, \varepsilon_{pq} \qquad (8.4.8)$$

from equation 8.4.1.

To evaluate equation 8.4.7, the strain and the displacement within the inclusion are needed. The Born approximation suggests that they may be estimated by the incident strain and displacement at that point if the inclusion were not there. For small scatterers, this approximation for the displacement is valid, as the displacement must be continuous across the inclusion boundary. However, the strain will not be continuous in this way, so this does not represent a good approximation for the strain values.

Wu (1966) developed the relationship between the strain for spheroidal inclusions and the overall strain at infinity ε^o_{pq} and this can be used to evaluate the strain required in 8.4.7.

$$\varepsilon_{pq} = T_{pqrs} \, \varepsilon^o_{rs} \qquad (8.4.9)$$

If the wavelength is large compared to the inclusion radius, the field both inside and outside the region containing the inclusion will be static and uniform (Eshelby, 1957) so the strain $\varepsilon_{pq}(\zeta)$ and the field $v(\zeta)$ can be approximated by that at the centre of the ellipsoid

$$v \, (\zeta) = u^o(\zeta) \qquad (8.4.10)$$

$$\Delta\, c^i_{njpq}\, \frac{dv_p}{d\varepsilon_q} \simeq c^i_{njpq}\, T_{pqrs}\, \varepsilon^o_{rs}\, (\zeta_i) \qquad (8.4.11)$$

and substitution in to 8.4.7 gives

$$u_1(x) = u^o_1(x) + \int_{V_i} d\zeta\, (\Delta\, \rho^i \omega^2 u^o_n(\zeta_i) - \Delta\, c^i_{njpq} T_{pqrs} \varepsilon^o_{rs}(\zeta_i) \frac{d}{d\varepsilon_j}) g_{1n}(x\zeta) \quad (8.4.12)$$

Wu's tensor is symmetrical, and the δ function allows simplification to

$$u_1(x) = V_i \Big[\Delta\, \rho^i \omega^2 u^o_n(\zeta_i) g_{1n}(x\zeta) - (\Delta\lambda^i T_{pqrs} \delta_{nj} + 2\Delta\mu^i T_{njrs}) \times \qquad (8.4.13)$$

$$\varepsilon^o_{rs}\, \frac{d\, g_{1n}(x\,\zeta)}{d\zeta_j} \Big]$$

The use of Wu's tensor in this way assumes that the principle axes of the inclusion are aligned with the co-ordinate axes. If this ideal situation is not so in practise, the tensor must be replaced by U_{pqrs} such that U is T multiplied by the appropriate direction cosines. This can result in an extremely involved equation because of the summations for each subscript.

For the general application of isotropic composites, the average of U_{pqrs} over all possible angles must be found. This has been evaluated by Wu as

$$\overline{U}_{pqrs} = \frac{1}{3}\, (P-Q)\delta_{pq}\delta_{rs} + \frac{1}{2}Q\, (\delta_{pr}\delta_{qs} + \delta_{ps}\delta_{qr}) \qquad (8.4.14)$$

which is of the same form as equations 8.4.5. Equations for P and Q were evaluated by Wu (1966) and Berryman (1980b).

The above equations have applied to a single inclusion positioned at ζ_i. If N inclusions are all contained within a small volume V_i of radius a, centred at ζ_0 and multiple scattering is neglected, then for long wavelengths with respect to a, equation 8.4.13 is written as

$$<u_1^s(x)>^m \simeq \sum_{i=1}^{N} V_i[\Delta \rho^i \omega^2 u_n^0(\zeta)g_{1n}(x \zeta_0)] -$$

$$(\Delta\lambda^{i}U_{pqrs}^{mi}\delta_{nj} + 2\mu^{i} U_{pqrs}^{mi}) \varepsilon_{rs}^0 \frac{d}{d\zeta_i} g_{1n}(x \zeta_0) \qquad (8.4.15)$$

Kuster and Toksoz (1974) considered a model composite as illustrated in figure 8.1. Type 1 spheres are introduced in to a type 2 material. For single scattering and ka << 1, the total scattering depends only on the relative concentration of the type 1 material. This scattering must be equal to that from a homogeneous sphere with effective moduli K^*, μ^* and ρ^* of the size shown in the diagram.

Thus the scattering from the mixed sphere imbedded in the type 2 matrix is

$$u_1^s(x) = V (\rho_1 - \rho^*)\omega^2 u_n^0(\zeta_0) g_{1n}(x\zeta_0) - \qquad (8.4.16)$$

$$[(\lambda_1 - \lambda^*)U_{pprs}^{1*}\delta_{nj} + 2 (\mu_1 - \mu^*) U_{njrs}^{1*}] \varepsilon_{rs}^0(\zeta_0)\frac{d}{d\zeta_j} g_{1n}(x \zeta_0)$$

and this must be equivalent to 8.4.15 if m is type 2. Overall
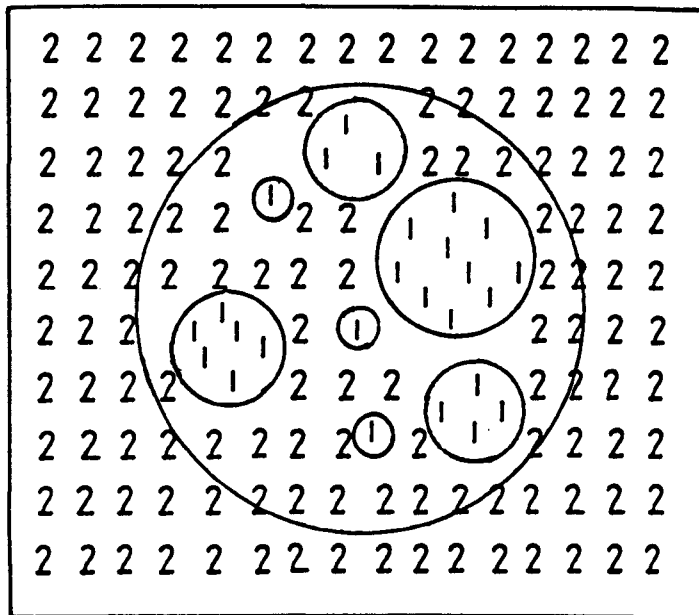
Figure 8.1 The conceptual model of a composite used by Kuster and Toksoz (1974).
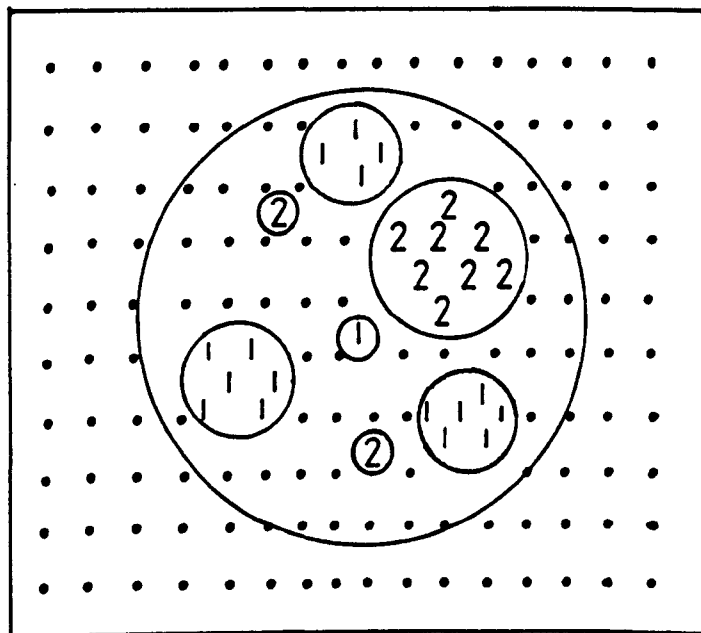
Figure 8.2 The conceptual model of a composite used by Berryman (1980a).

$$u_1^S(x) \simeq \; < u_1^S(x) >^i \tag{8.4.17}$$

If the inclusion volume is chosen such that $c_1 = \sum \dfrac{a_i^3}{a^3}$ then by equating the parts of equations 8.4.15 and 8.4.16 we get

$$\rho_1 - \rho^* = \sum_i c_i (\rho_1 - \rho_i)$$

$$(K_1 - K^*) \frac{3K_i + 4\mu_1}{3K^* + 4\mu_2} = \sum_i c_i (K_1 - K_i) P^{*2}$$

$$\tag{8.4.18}$$

$$(\mu_1 - \mu^*) \frac{\mu_1 + F_1}{\mu^* + F_1} = \sum_i c_i (\mu_1 - \mu_i) Q^{*2}$$

$$F_1 = \frac{\mu_2}{6} \; \frac{9K_1 + 8\mu_1}{K_1 + 2\mu_1}$$

It is evident from the subscript distribution that these equations are not symmetrical - the type 1 and 2 materials can not be considered as the matrix and inclusions rather than the other way round. The equations may be expanded simply to account for several types of constituents.

Berryman (1980a) used a slightly different conceptual model for describing the inclusions and effective material, figure 8.2. In this set up, the overall model is represented by spheres of both type 1 and 2 material in the correct relative proportions within a sphere of the effective material. This imbedding material, the effective medium representing the actual composite, can have

arbitrary parameters, but when the type 1 and 2 spheres are introduced, the net scattering must disappear, as it should be the same as introducing some of the actual composite. Only single scattering is considered, but Berryman suggested this approach should be superior to the Kuster Toksoz method for larger concentrations.

Due to the different definitions of the model composite, equation 8.4.17 is rewritten as

$$< u_1^s(x) >^* = 0 \qquad\qquad (8.4.19)$$

which leads to

$$\sum_{i=1}^{2} c_i \, (\rho_i - \rho^*) = 0$$

$$\sum_{i=1}^{2} c_i \, (K_i - K^*) \, P^{*i} = 0 \qquad\qquad (8.4.20)$$

$$\sum_{i=1}^{2} c_i \, (\mu_i - \mu^*) \, Q^{*i} = 0$$

These expressions are symmetrical and in fact involve an iterative process rather than a direct calculation to find the effective moduli.

$$(K^*)_{n+1} = \sum_{i=1}^{2} c_i K_i (P^{*i})_n \Big/ \sum_{i=1}^{2} c_i (P^{*i})_n$$

$$(8.4.21)$$

$$(\mu^*)_{n+1} = \sum_{i=1}^{2} c_i \mu_i (Q^{*i})_n \Big/ \sum_{i=1}^{2} c_i (Q^{*i})_n$$

Berryman carried out extensive comparisons of these results with previously published parameters, and suggested greater consistency within the physical limits.

Calculations to find the effective bulk and shear moduli of cancellous bone were performed in the present work on an IBM PC compatible, using FORTRAN. Complex moduli representing the ultrasonic velocity and attenuation were used as discussed in section 7.2.2. P and Q were evaluated as the inclusion shape required and iterations carried out until both moduli converged to a difference of 0.00001. The velocity and attenuation in the overall effective medium can then be calculated from the complex effective moduli.

The program was also used to reproduce the published results of Berryman (1980b) as a check. The same pattern of attenuation and fast compressional wave velocity as a function of concentration was produced but with different numerical values, figure 8.3. The differences were not considered great enough to be a problem, as the SCT was used in excellent agreement with published data in conjunction with the Biot theory, see the next section. The transverse wave is not explicitly considered in the results discussed in this chapter, but is of course included within the calculations.
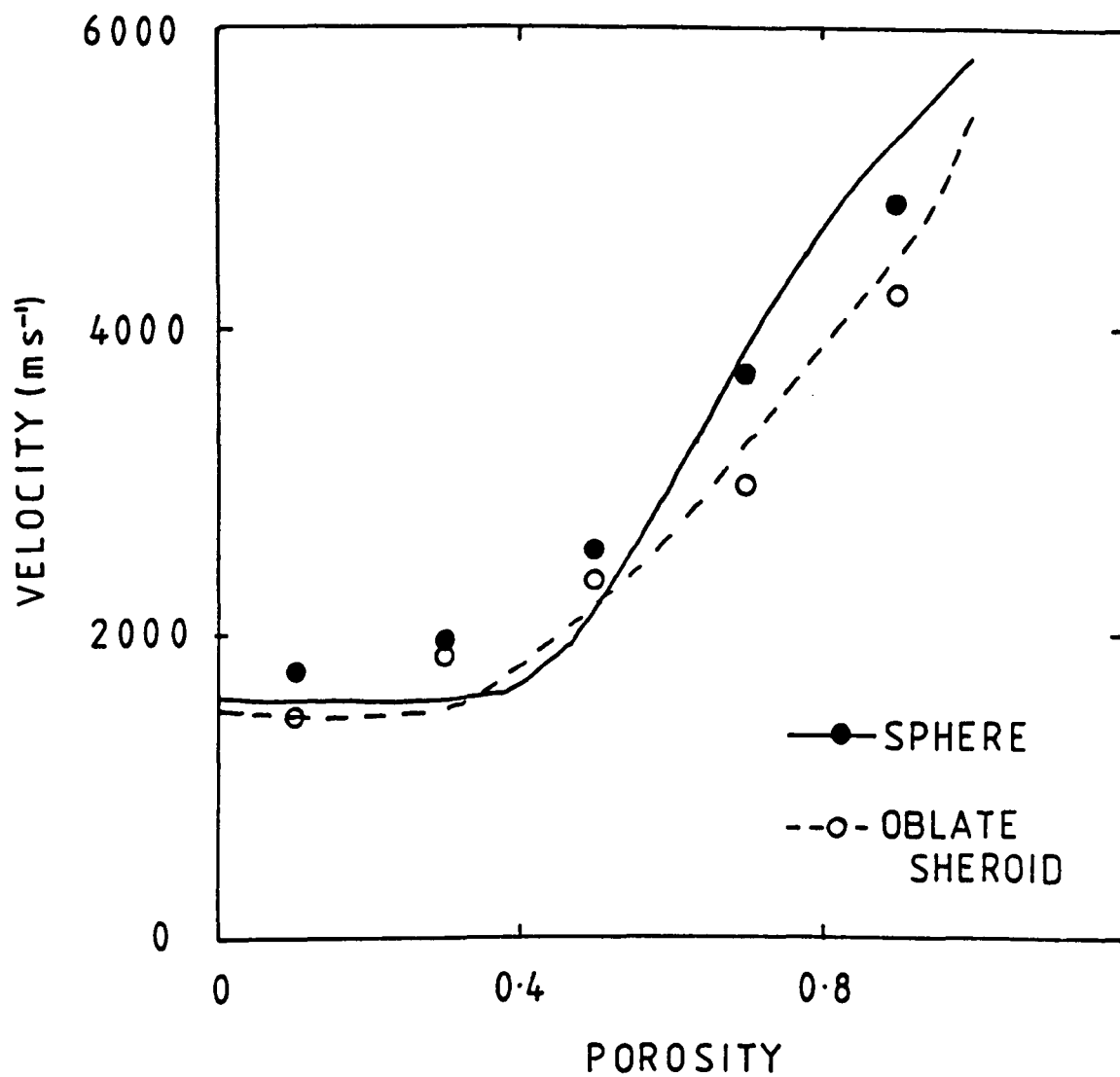
Figure 8.3 Comparison between calculated results using the SCT and those of Berryman (1981a)

8.4.2 Application to Cancellous Bone.

The self consistent theory was applied to cancellous bone using the parameters discussed in section 8.3. Two sets of parameters were used, representing osteoporotic and normal bone, the differences being introduced by the proportion of bone to marrow and the shape of the trabeculae as the inclusions in a matrix of marrow.

As the frequency dependence of the ultrasonic propagation is not explicitly included in the development of the theory, virtually no variation in the ultrasonic velocity or attenuation as a function of frequency was produced. This is obviously not what is found in practise. The SCT is not intended for application to frequency dependent effects. However, the Biot theory, developed and evaluated in the following section, uses the SCT to calculate the effective moduli for the composite which is then used in the calculation of the frequency dependence effects.

8.5 The Biot Theory.

Biot developed a theory over several years which was intended for application to porous rocks to analyse ultrasonic propagation for geophysical testing (Biot, 1956, 1962a, 1962b). It is the only well developed existing theory to take account of the intricacy of the structural patterns of the components in the overall composite.

Biot's theory utilises two possible loss mechanisms, the inelasticity of the skeletal frame and the viscosity of the fluid moving with respect to the frame. The theory predicts three ultrasonic waves, two longitudinal and one transverse, and suggests that inelastic losses predominate at wavelengths long compared to the pore size while viscosity losses occur mainly at the higher frequencies. The following development is based on Stoll's review of the Biot

theory (Stoll, 1974) and utilises Berryman's discussion of the frame moduli (Berryman, 1981a, 1981b).

8.5.1 Development of the Biot theory.

Let the vector u represent the displacement of all regions in the frame of the composite and U the displacement of the fluid. If β is the porosity of the overall medium, then the volume of fluid flowing in or out of an element of volume of the framework is

$$\xi = \beta \, \text{div} \, (u - U) \qquad (8.5.1)$$

For small strains, the displacement of the frame may be written as

$$e = e_x + e_y + e_z = \text{div} \, u \qquad (8.5.2)$$

For an isotropic linear material, the strain energy is a quadratic function

$$W = C_1 I_1^2 + C_2 I_2 + C_3 I_1 \xi + C_4 \xi^2$$

$$I_1 = e_x + e_y + e_z = e \qquad (8.5.3)$$

$$I_2 = e_x e_y + e_y e_z + e_x e_z - \tfrac{1}{4}(\gamma_x^2 + \gamma_y^2 + \gamma_z^2)$$

where γ are the components of shear strain.

The strain energy can be related directly to the constants used by Biot (H,C,M)

$$W = \frac{H}{2} e^2 - 2\mu^* I_2 - Ce\xi + \frac{M}{2} \xi^2 \qquad (8.5.4)$$

The stresses are then given by the respective differentiations of equation 8.5.4

$$\tau_{xx} = He - 2\mu^*(e_y + e_z) - C\xi$$

$$\tau_{yy} = He - 2\mu^*(e_z + e_x) - C\xi$$

$$\tau_{zz} = He - 2\mu^*(e_x + e_y) - C\xi \qquad (8.5.5)$$

$$\tau_{xy} = \delta_z \, \mu^*$$

$$\tau_{yz} = \delta_x \, \mu^*$$

$$\tau_{xz} = \delta_y \, \mu^*$$

$$p_f = M\xi - Ce$$

To relate the convenient constants to practical parameters, two tests can be considered.

Stoll (1974) used these two theoretical tests and referred to them as the jacketted and unjacketted tests. The former involves the saturated material being placed in an impervious bag loaded with an external isotropic pressure p, where p is applied such that

$$-p = \tau_{xx} = \tau_{yy} = \tau_{zz} \qquad (8.5.6)$$

$$\tau_{xy} = \tau_{yz} = \tau_{xz} = 0$$

and using equations 8.5.5, this gives

$$-p = (H - \frac{4\mu}{3})e - C\xi \qquad (8.5.7)$$

and the bulk modulus of the frame is given by

$$K_b = \frac{-p}{e} = H - \frac{4\mu}{3} - \frac{C^2}{M} \qquad (8.5.8)$$

The second test, the unjacketted test, submerges the material in a bath of fluid so that the fluid can not flow freely when the external pressure is applied. Thus the pressure of the fluid is equal to the external pressure. Hence

$$\delta = \frac{-e}{p} = \frac{1 - C/M}{H - 4\mu/3 - C^2/M} \qquad (8.5.9)$$

and also

$$\gamma = \frac{-\xi}{p} = \frac{H - 4\mu/3 - C}{(H - 4\mu/3 - C^2/M)M} \qquad (8.5.10)$$

using equations 8.5.5 and 8.5.7. Under constant volume ratio, ie constant porosity, δ is equivalent to the compressibility of the frame and γ may be rewritten in terms of β and the compressibility of the pore fluid. The bulk modulus is the inverse of the compressibility, so γ and δ may be written as

$$\gamma = \beta \left(\frac{1}{K_f} - \frac{1}{K_g} \right) \qquad (8.5.11)$$

$$\delta = \frac{1}{K_g} \qquad (8.5.12)$$

The previous six equations provide enough information for the three constants used by Biot to be found in terms of the bulk and shear moduli

$$H = \frac{(K_g - K^*)}{D - K^*} + K^* + \frac{4\mu^*}{3}$$

$$C = K_g \frac{(K_g - K^*)}{D - K^*}$$

$$M = K_g^2 \big/ (D - K^*)$$

(8.5.13)

where $\quad D = K_g(1 + \beta (K_g/ K_f - 1))$

Throughout this development the subscripts g and f represent the grains and fluid forming the composite, and superscript * represents the frame itself. Berryman (1981a, 1981b) developed the theory equivalent to the two conceptual tests described above, and in the general case produced the same equations, given in 8.5.13, stressing the use of the frame moduli. The frame moduli can be estimated by using the self consistent theory (SCT) with the grain and fluid moduli being the two phases of the material. The development and use of this theory has been discussed in the previous section.

The actual movement of the fluid and frame must now be considered. The stress equation of motion is

$$\frac{d\tau_{xx}}{dx} = \frac{d^2}{dt^2} [\beta \, \rho_f u_x + (1-\beta)\rho_g u_x - \beta \, \rho_f(u_x - U_x)]$$

(8.5.14)

and using τ_{xx} from 8.5.4 gives

$$\nabla^2 \ (He - C\xi) = \frac{d^2}{dt^2} \ (\rho e - \rho_f \xi) \qquad (8.5.15)$$

The motion of the fluid relative to the frame is given by

$$\beta \frac{d\rho_f}{dx} = \frac{d^2}{dt^2} \ [\beta \rho_f U_x] + \frac{\beta \eta}{K} \ \frac{d}{dt} \ [\ \beta (\ U_x - u_x)] \qquad (8.5.16)$$

and substituting for ρ_f from 8.5.4 gives

$$\nabla^2 (Ce - M\xi) = \frac{d^2}{dt^2} \ (\rho_f e - m\xi) - \frac{\eta}{K} \ \frac{d\xi}{dt} \qquad (8.5.17)$$

The parameter m is introduced here to account for the tortuosity of the structure, as all the fluid can not move in a particular direction if the matrix structure is multi-directional. The parameter can be considered to be a corrective term for α such that

$$m = \alpha \ \rho_f \ / \ \beta \qquad (8.5.18)$$

where $\alpha \ >= 1$. For uniform pores, parallel to the direction of the pressure gradient, $\alpha = 1$. α represents the inertia of the frame in the fluid environment. Biot considered three densities in his original development (Biot, 1956) such that

$$\rho_{11} + \rho_{12} = (1-\beta) \ \rho_g$$

$$\rho_{22} + \rho_{12} = \beta \rho_f \qquad (8.5.18)$$

Biot interpreted ρ_{11} as the total effective density of the frame, with $-\rho_{12}$ being the apparent density. A third equation follows from this interpretation of using the induced mass of oscillation of solid particles in a fluid (Lamb, 1924)

$$\rho_{11} = (1-\beta) \left(\rho_g + r\rho_f \right) \qquad (8.5.19)$$

r = 0.5 for a sphere and remains between 0 and 1 for all ellipsoids.

Using

$$\rho_{22} = \alpha \, \beta \, \rho_f \qquad (8.5.20)$$

allows the definition of α

$$\alpha = 1 - r(1 - 1/\beta) \qquad (8.5.21)$$

The two equations, 8.5.17 and 8.5.15 represent Pouiselle flow, an idealised situation where there is a constant ratio of fluid flow to pressure gradient. The frequency dependence of the viscous resistance to the fluid flow must be introduced. Biot used a factor $F(\frac{a\omega\rho_f}{\eta})$ such that $\frac{\beta^2 F\eta}{K}$ gives the ratio of the friction exerted by the fluid on the frame to the average velocity for the oscillatory motion. Thus $\frac{\eta}{K}$ in equation 8.5.17 is replaced by

$$F(X) = \frac{1}{4} \frac{XT(X)}{1 - 2T(X)/iX}$$

$$T(X) = \frac{ber'(X) + i\ bei'(X)}{ber(X) + i\ bei(X)} \qquad\qquad (8.5.22)$$

$$X = a\ (\omega\ \rho_f/\eta\ )^{0.5}$$

For low frequencies, F approaches unity, mimicking Pouiselle flow. This factor has the limitation of applying only when the wavelengths are larger than the pore size.

Equations 8.5.15 and 8.5.17 gives the wave equation governing the propagation of longitudinal waves.

$$\nabla^2(\ -M\xi + Ce) = \frac{d^2}{dt^2}\ (\rho_f e - M\xi) - \frac{\eta F}{K} \frac{d\xi}{dt} \qquad\qquad (8.5.23)$$

$$(H - \mu^*)\ \nabla^2 e + \mu\nabla^2 e - C\nabla^2\xi = \frac{d^2}{dt^2}\ (\rho_e - \rho_f\xi)$$

$$\qquad\qquad (8.5.24)$$

$$= H\ \nabla^2 e - C\ \nabla^2\xi$$

If it is assumed that the results for e and ξ will be of the form

$$e = A_1\ exp\ (i(\omega t - lx)) \qquad\qquad (8.5.25)$$

$$\xi = A_2\ exp\ (i(\omega t - lx))$$

then it is straight forward to find

$$- Ml^2 + Cl^2 = \rho_f \omega^2 - M\omega^2 - \frac{\eta F}{K} i\omega \qquad (8.5.26)$$

$$Hl^2 - Cl^2 = \rho\omega^2 - \rho_f\omega^2$$

Rewritten as

$$- \rho_f\omega^2 + Cl^2 = - Ml^2 + M\omega^2 - i\omega\eta \, F \, / \, K \qquad (8.5.27)$$

$$-Cl^2 + \rho_f\omega^2 = Hl^2 - \rho\omega^2$$

multiplying and solving for l^2, and therefore l, is equivalent of finding the determinant, equal to zero, of

$$\begin{vmatrix} Hl^2 - \rho\omega^2 & \rho_f\omega^2 - Cl^2 \\ \\ Cl^2 - \rho_f\omega^2 & m\omega^2 - Ml^2 - \dfrac{i\,\omega F\eta}{K} \end{vmatrix} = 0 \qquad (8.5.28)$$

There will be two possible physical roots, each representing a wave travelling at ω/l_r with attenuation l_{im} (Np m^{-1}). These are the fast and slower compressional waves of the first and second kind respectively (see section 7.4).

Berryman has used this theory to compare the results obtained by Plona (1980) with those predicted by the Biot theory. Plona was the first to observe Biot's predicted slow compressional wave. Ogushwitz (1985) has also utilised Berryman's development of the theory to analyse ultrasonic propagation in porous sandstones and ocean sediments.

The computer program written in FORTRAN on a IBM PC compatible for the current work was also used to reproduce the published results of Berryman's analysis of Plona's experiments and the results of Ogushwitz (1985). Good agreement was obtained in both cases, and acts as a check for the correctness of the program. Excellent agreement with the results published by Ogushwitz for Navajo sandstone was obtained for the fast longitudinal wave velocity. The slow wave velocity and the attenuation is not discussed by Ogushwitz and the transverse wave velocity was not calculated explicitly in the current work. Ogushwitz also reviewed the work of Berryman by evaluating Plona's results using the Biot theory. Using the parameters listed by Ogushwitz, excellent agreement was obtained with both longitudinal wave velocities as a function of porosity, figure 8.4.

8.5.2 Application to Cancellous Bone.

A program, listed in appendix A , was run with data as discussed in section 8.3 to represent cancellous bone. The results for normal bone are given in table 8.2. The frequency slope, as used in the BUA measurements is given with the actual velocity and attenuation evaluated by the program at the frequencies listed. The ultrasonic slope (dB $MHz^{-1}cm^{-1}$) acheived here is typical of the results obtained for the cancellous samples (section 4.2.3), but at 9.3 dB $MHz^{-1}cm^{-1}$ is rather low for healthy bone.

To explain the ultrasonic propagation successfully, the theory must also model the differences in ultrasonic slope obtained for different samples. Parameters intended to represent a more osteoporotic bone, increased trabecular spacing, thinner trabeculae and a more porous structure, produced the results listed in table 8.3. The ultrasonic slope has decreased substantially to less than 1 dB $MHz^{-1}cm^{-1}$ and the actual calculated values
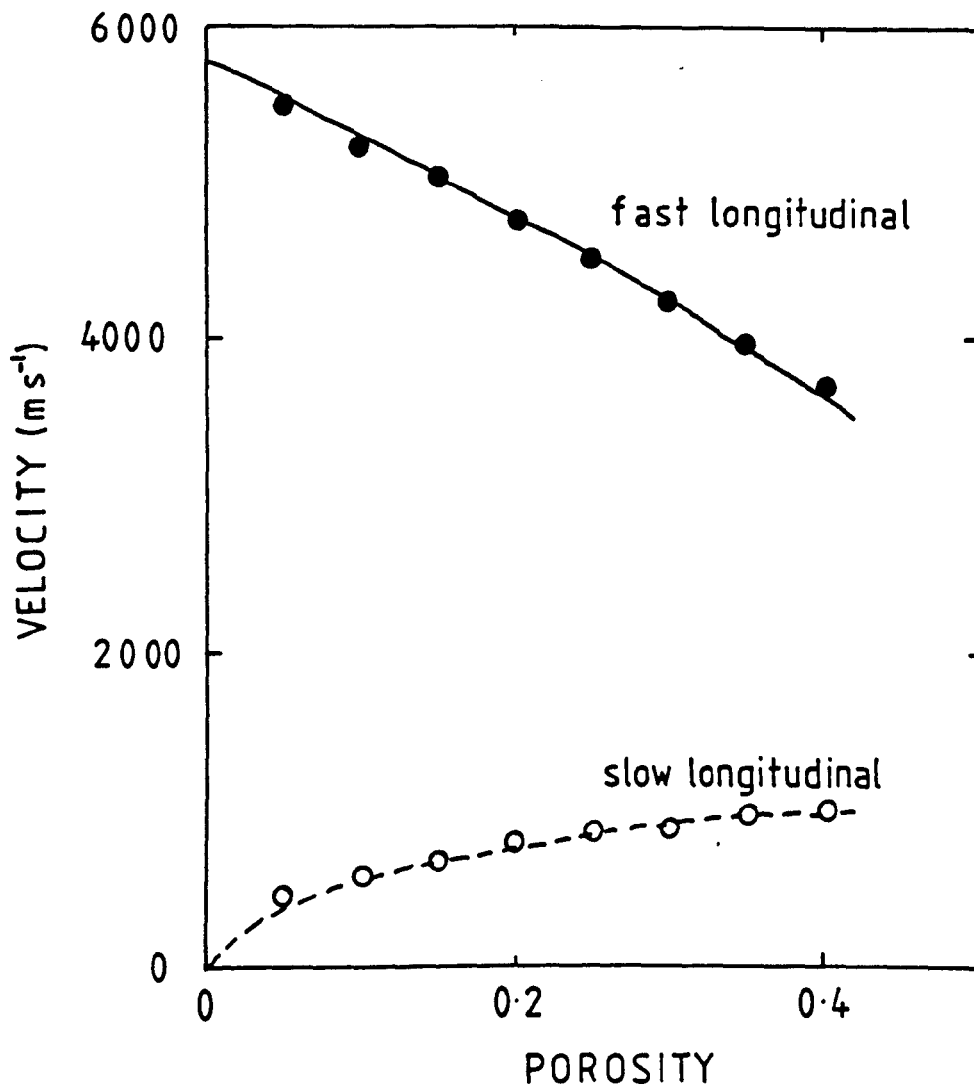
Figure 8.4 Comparison bewteen calculated results using Biot's theory and those
of Ogushwitz for the Plona (1980) data. (Ogushwitz, 1985).

Table 8.2 Results of Biot theory for normal model.

frequency (kHz)	longitudinal velocity $(m\ s^{-1})$	attenuation $(dB\ m^{-1})$
200	2061	155.2
300	2077	250.2
400	2090	345.9
500	2100	440.7
600	2109	533.9
700	2116	625.2
800	2123	714.4
900	2129	801.7
1000	2134	887.1

ultrasonic slope = 9.3 dB $MHz^{-1}cm^{-1}$

Table 8.3 Results of Biot theory for osteoporotic model

frequency (kHz)	longitudinal velocity $(m\ s^{-1})$	attenuation $(dB\ m^{-1})$
200	4321	48.0
300	4337	59.1
400	4346	68.5
500	4352	76.8
600	4357	84.3
700	4360	91.2
800	4363	97.7
900	4366	103.8
1000	4368	109.5

ultrasonic slope = 0.4 dB $MHz^{-1}cm^{-1}$

have also decreased, as found experimentally for more porous samples (section 4.2.3). The actual permeability of the samples has not been established, but will vary from sample to sample as well as directionally within a sample. An increased permeability will be associated with a more porous bone, and an increased value for permeability was also used to model the osteoporotic bone.

The tables also show that the velocity is not predicted correctly by the Biot theory. The velocity of the ordinary longitudinal wave for normal bone is fairly representative of the results obtained in section 4.3 but the velocity calculated for the parameters representing osteoporotic bone is far too high. This could be because the velocities used for the marrow component are too large compared to the actual values, but it must be noted that the Biot theory predicts an increase in velocity with decreasing bone content. This was not observed in practise, as the measured velocity values decreased for the more osteoporotic bone.

The Biot theory, intended for application to porous rocks and sediments, appears to partly explain the ultrasonic propagation in porous bone. It successfully predicts the changes in attenuation that have been found in practise, and, more importantly, also predicts the behaviour of the attenuation as a function of frequency. However, it does not predict the velocity changes and does not cover the full range of attenuation values that have been measured. As the only theory which includes the effects of the structure directionality in the tortuosity and permeability factors, it also predicts differences in the ultrasonic propagation depending on the direction of propagation through the sample, as seen in section 4.6. Theories based purely on scattering can not account for these differences. The Biot theory is limited to applications where the wavelength of the ultrasound is longer than the pore size of the structure. This limit is rather too close for cancellous bone, with pore sizes of 400 to 2200 μm (chapter 6) and frequencies of 200 kHz

to 1 MHz. In water, this frequency range represents a wavelength range of 1.5

to 7.4 mm, but using a typical velocity for cancellous bone of 1800 m s^{-1}

produces a wavelength range of 1.8 to 9 mm.

8.6 Multiple Scattering.

The theory of multiple scattering to be used in the current work is based

on the development of Truell et al (1969). The single scattering results are

averaged over an assembly of scatterers and the total field found from the sum

of the incident wave and all the scattered waves.

Many applications of this theory have been made under specific assumptions,

such as negligible density difference between the scatterers and the matrix

(Sayers, 1980) or low scatterer concentration. These assumptions allow

simplification of the equations.

The full theory has been used by Latiff and Fiore (1975) and Lefebvre et al

(1980) with differing results. The former used the theory as developed by

Truell et al while the latter suggested and corrected an error in the

development. Programs were written during the evaluation of multiple

scattering for its application to cancellous bone, but poor agreement was

obtained with the published results of both Latiff and Fiore, and Lefebvre et

al.

As the single scattering results are used, a program was written to

calculate the scattering cross section for a single sphere in a matrix, and

run for the example parameters discussed in the appendix of Truell et al.

Excellent agreement was obtained with the published graphs. Unfortunately, no

examples for multiple scattering are given by Truell et al. Latiff and Fiore

published analyses of copper spheres in polymethylmethacrylate (PMMA) at a

variety of frequencies over a range of low concentrations. Some agreement was

obtained with the published attenuation data, particularly at the lower frequencies, figure 8.5.

Lefebvre et al chose slightly different forms for the solutions of the wave equations and therefore a different form for the forward and backward scattering coefficients f(0) and f(π). Using their equations, the results produced were very poor and bore no relation to the published data. In the vast majority of cases, the equations did not converge . An attempt was made to mimic Lefebvre et al's results using the Latiff and Fiore method, but with little success.

The development used here is that of Waterman and Truell (1961) used by Truell et al (1969) and Latiff and Fiore (1975). A fairly general derivation is given here, as the results of the application to cancellous bone do not warrant a more detailed analysis. It might be considered that the whole area of this particular multiple scattering approach needs to be redeveloped to prevent further confusion and contradiction, referred to by Lefebvre et al (1980).

8.6.1 Development of the Multiple Scattering Theory.

The equation for the displacement of an isotropically elastic medium is

$$(\lambda + \mu) \nabla \nabla u + \mu \nabla^2 u = \rho \frac{d^2 u}{dt^2} \qquad (8.6.1)$$

where, for an harmonically periodic wave $u = u_0 e^{i\omega t}$

If s_0 is a function of spatial coordinates only, then it may be written using potentials Ψ and Π as
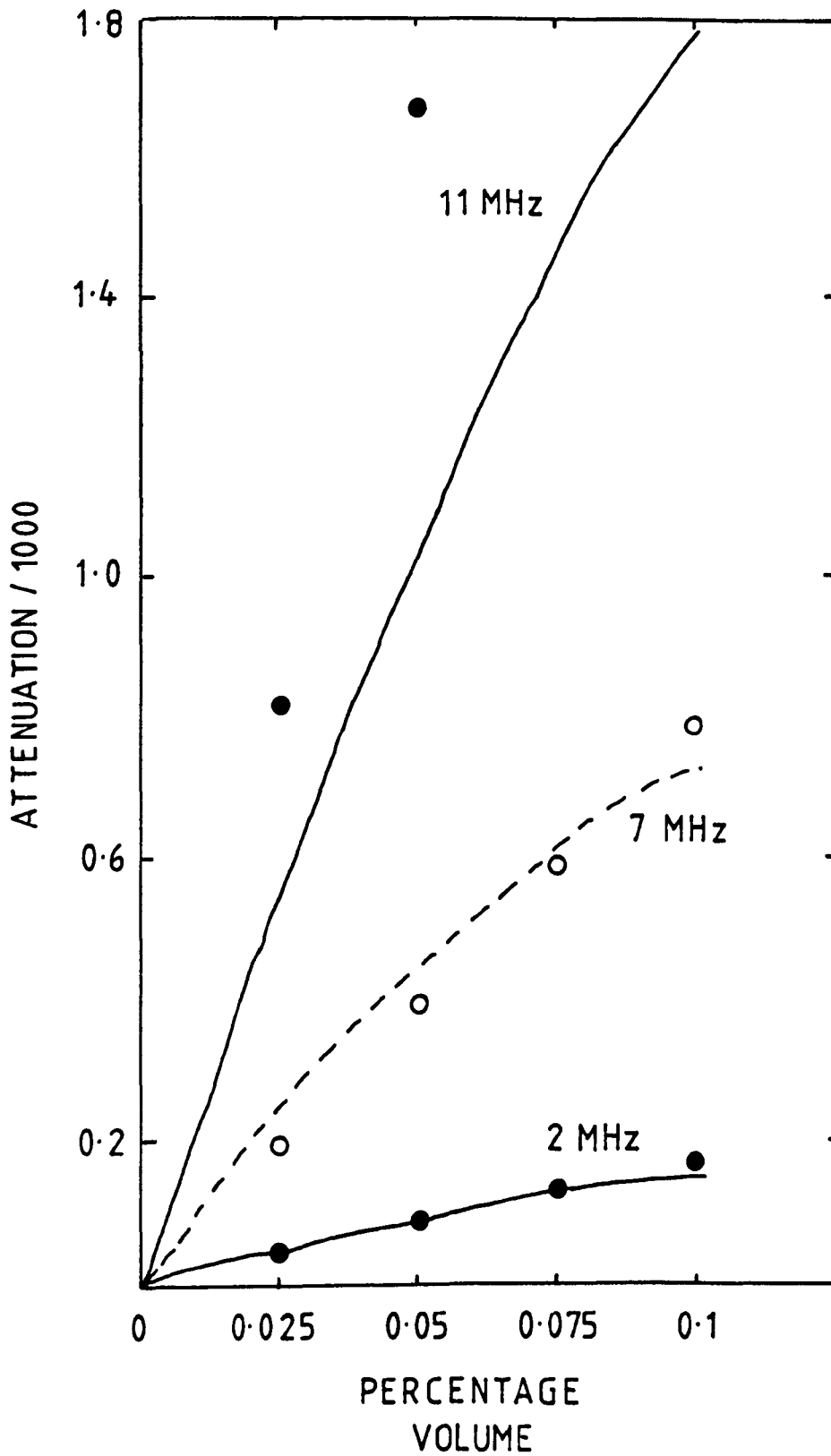
Figure 8.5 Comparison between the calculated results of multiple scattering and those of Latiff and Fiore (1980).

$$U = -\nabla \Psi + \nabla \wedge [\nabla \wedge (r\Pi)] \tag{8.6.2}$$

where the potentials fulfil

$$(\nabla^2 + k^2)\Psi = 0 \tag{8.6.3}$$

$$(\nabla^2 + s^2)\Pi = 0$$

and represent the longitudinal and transverse parts of the wave respectively. The potentials may be summed in the same way as the incident and scattered waves themselves, so the total potentials are given by

$$\Psi_1 = \Psi_i + \Psi_s$$

$$\Pi_1 = \Pi_i + \Pi_s = \Pi_s$$

$$(\nabla^2 + k_1^2)\Psi_i = 0 \tag{8.6.4}$$

$$(\nabla^2 + k_1^2)\Psi_s = 0$$

$$(\nabla^2 + s^2)\Pi_s = 0$$

where the incident and scattered waves all fulfil equations 8.6.3 and subscript 1 refers to the matrix.

Inside the obstacle

$$\Psi_2 = \Psi_q \qquad \Pi_2 = \Pi_q$$

$$(\nabla^2 + k_2^2)\Psi_q = 0 \tag{8.6.5}$$

$$(\nabla^2 + s_2^2)\Pi_q = 0$$

where subcript 2 refers to the material of the obstacle and q to the wave in the obstacle. The general solution in spherical coordinates is of the form

$$\sum_{m=0}^{\infty} c_m z_m(1r) P_m(\cos\theta) \tag{8.6.6}$$

and the chosen form is

$$\Psi_s = \sum_{m=0}^{\infty} (-i)^{m+1} a \ (2m+1) A_m h_m(k_1 r) P_m(\cos\theta)$$

$$\Pi_s = \sum_{m=0}^{\infty} (-i)^{m+1} a \ (2m+1) B_m h_m(s_1 r) P_m(\cos\theta) \tag{8.6.7}$$

$$\Psi_q = \sum_{m=0}^{\infty} (-i)^{m+1} a \ (2m+1) C_m j_m(k_2 r) P_m(\cos\theta)$$

$$\Pi_q = \sum_{m=0}^{\infty} (-i)^{m+1} a \ (2m+1) D_m j_m(s_2 r) P_m(\cos\theta)$$

Ying and Truell (1956) and Lefebvre et al (1980) chose slightly different factors as the multipliers of the coefficients A_m, B_m, C_m and D_m. In the form given here, these coefficients are dimensionless. The wave outside the sphere is

$$\Psi = \Psi_i + \Psi_s \qquad \Pi = \Pi_s$$

$$\Psi_i = \sum_{m=0}^{\infty} (-i)^{m+1} k_1^{-1} (2m+1) j_m(k r) P_m(\cos\theta) \qquad (8.6.8)$$

$$\Psi_s = \sum_{m=0}^{\infty} (-i)^{m+1} a (2m+1) A_m h_m(k_1 r) P_m(\cos\theta)$$

$$\Pi_s = \sum_{m=0}^{\infty} (-i)^{m+1} a (2m+1) B_m h_m(s_1 r) P_m(\cos\theta)$$

and on the inside of the sphere

$$\Psi = \Psi_q \qquad \Pi = \Pi_q$$

$$\Psi_q = \sum_{m=0}^{\infty} (-i)^{m+1} a (2m+1) C_m j_m(k_2 r) P_m(\cos\theta) \qquad (8.6.9)$$

$$\Pi_q = \sum_{m=0}^{\infty} (-i)^{m+1} a (2m+1) D_m j_m(s_2 r) P_m(\cos\theta)$$

For a general elastic sphere, the stresses and displacements vary continuously across the boundary of the sphere, hence

$$s_{ri} + s_{rs} = s_{rq}$$

$$s_{\theta i} + s_{\theta s} = s_{\theta q} \qquad (8.6.10)$$

$$\sigma_{ri} + \sigma_{rs} = \sigma_{rq}$$

$$\sigma_{\theta i} + \sigma_{\theta s} = \sigma_{\theta q}$$

where σ is the stress, and substitution of these conditions in to equations 8.6.8 and 8.6.9 produces explicit linear equations in A_{em}, B_{em}, C_{em} and D_{em}. These equations are generally complex. They can be solved explicitly for m=0, but for higher orders must be considered as

$$A_{em} = x_1^m + ix_2^m$$

$$B_{em} = x_3^m + ix_4^m$$

$$C_{em} = x_5^m + ix_6^m$$

$$D_{em} = x_7^m + ix_8^m$$

(8.6.11)

where the x^m are real and can be written as

$$\sum_{j=1}^{8} \varepsilon_{ij}^m x_j^m = \delta_i^m \qquad i = 1,..,8$$

(8.6.12)

The individual matrix elements are listed in Truell et al (1969). The scattering cross section for a single scatterer is given by

$$\gamma_N = 4 \sum_{m=0}^{\infty} (2m+1)[\ |A_m|^2 + m(m+1)(\frac{k_\perp}{s_\perp}) \ |B_m|^2]$$

(8.6.13)

but of more interest in the current work is the use of the coefficients evaluated here for multiple scattering applications.

Waterman and Truell (1961) used the configurational averaging technique of Foldy (1945) to obtain an excited field which is incident on a particular

scatterer and is comprised the incident field and all scattered waves from

other scatterers. A complex propagation constant k^* is produced

$$\frac{k^*}{k_1}^2 = \left[1 + \frac{2\pi n_0 f(0)}{k_1^2} \right]^2 - \left[\frac{2\pi n_0 f(\pi)}{k_1^2} \right]^2 \qquad (8.6.14)$$

where the forward and backward scattering of the obstacles are given by

$$f(0) = - \sum_{m=0}^{\infty} (-i)^m A^*_{em} \qquad (8.6.15)$$

$$f(\pi) = - \sum_{m=0}^{\infty} (-i)^m (-i)^m A^*_{em}$$

The coefficient A_{em} is evaluated for an elastic sphere in the same way as

described above. The complex propagation constant contains the velocity and

attenuation details.

8.6.2 Application to Cancellous Bone.

The application of this theory to cancellous bone assumes the trabeculae

are the spherical scatterers. The theory requires these scatterers to be

independent of each other, ie not touching, which is obviously not valid in

this case. Neither pores or trabeculae are independent of each other or

spherical, but the aim of this section of work was to see if multiple

scattering produced trends in the attenuation and velocity observed

experimentally, without considering the actual numbers produced, ie increased

attenuation with frequency and lower attenuation for samples with fewer,

smaller trabeculae.

The development of the theory assumes a transverse wave can propagate in the matrix of the composite as well as in the scatterers, which is not valid for a fluid matrix. In the following discussion, a non-zero transverse wave number was assumed for the fatty marrow. The value was established by using a fraction of the longitudinal velocity, although in fact it is still an arbitrary value. The transverse velocity was assumed to be 1200 m s^{-1} in the marrow, with the other values being set to the values discussed in section 8.3.

The program to evaluate multiple scattering involves the inversion of an 8x8 matrix. A general matrix inversion routine was used for this, and the product of the original matrix and its inversion printed out to act as a check for a successful inversion. Some matrices produced were singular, but in general the equations converged to 0.00001 within a few iterations. Bessel and Neumann functions also had to be generated, and this was done in a separate subroutine which had been checked for accuracy against published tables. As such a wide variety of values were required, published tables could not be used directly.

The parameters required by this theory are the ultrasonic velocities. The attenuation of the individual components themselves are not included. The size and volume concentration of the scatterers may be varied. Both parameters have larger values for modelling normal bone than for osteoporotic bone. A FORTRAN program, run on a PC compatible, was used to evaluate the multiple scattering, and is given in appendix B . The attenuation and velocity results obtained as a function of frequency for both normal and osteoporotic bone are given in table 8.4.

The immediately obvious result is that the attenuation calculated is always negative. If this is ignored, there is an increase in attenuation with frequency for both sets of results, and the model with fewer, smaller

Table 8.4 Multiple Scattering results for normal and osteoporotic models

frequency (kHz)	NORMAL velocity (m s^{-1})	attenuation (dB cm^{-1})	OSTEOPOROTIC velocity (m s^{-1})	attenuation (dB cm^{-1})
200	1470	-4.05	1470	-0.50
300	1470	-6.02	1470	-0.27
400	1470	-7.96	1470	-0.36
500	1470	-9.83	1470	-0.45
600	1470	-11.63	1470	-0.54
700	1470	-13.34	1470	-0.62
800	1470	-14.97	1470	-0.71
900	1470	-16.51	1470	-0.79
1000	1470	-17.95	1470	-0.88

scatterers(%)	0.5	27.0
scatterer size (μm)	60	120

density fat	950 kg m^{-3}
density bone	1800 kg m^{-3}
transverse velocity fat	1200 m s^{-1}
transverse velocity bone	1800 m s^{-1}
longitudinal velocity fat	1470 m s^{-1}
longitudinal velocity bone	3300 m s^{-1}

scatterers appeared to attenuate less than that with more, larger scatterers, which is in good agreement with the experimental results. The velocity, however, is not affected by either the frequency or the size and number of the scatterers, which is not what is observed experimentally. It is difficult to assess the value of these calculations as the results should not be negative and because of the fundamental assumptions of separated scatterers and a transverse wave propagating in the fatty marrow, but with a more detailed examination of the theory, including the effects of the attenuation of the individual components, may provide some interesting results.

8.7 Discussion.

It is clear from the models discussed above that the single scattering based self consistent theory does not explain the dependence of the ultrasonic attenuation and velocity observed experimentally. Howvever, the Biot theory appears to model some of the observed results. The attenuation values, of the correct order of magnitude, increase with frequency and also more generally are higher for a sample with increased trabecular number and thickness, and decreased spacing, although they do not cover the full range of results measured. The behaviour of velocity with changing bone content is also not correctly predicted by the Biot theory.

Figure 8.6 shows the attenuation calculated by the Biot theory plotted as a function of frequency for parameters modelling normal and osteoporotic bone. There is some similarity to the attenuation plots obtained experimentally, for example figure 4.6. For high density, whole os calces, a change in slope appeared at around 700 kHz (Langton, 1984) but this was not observed generally for the purely trabecular samples, suggesting it may be a function of the shape or cortical surface of the os calcis. This effect is not mimicked by the Biot theory in agreement with the supposition.
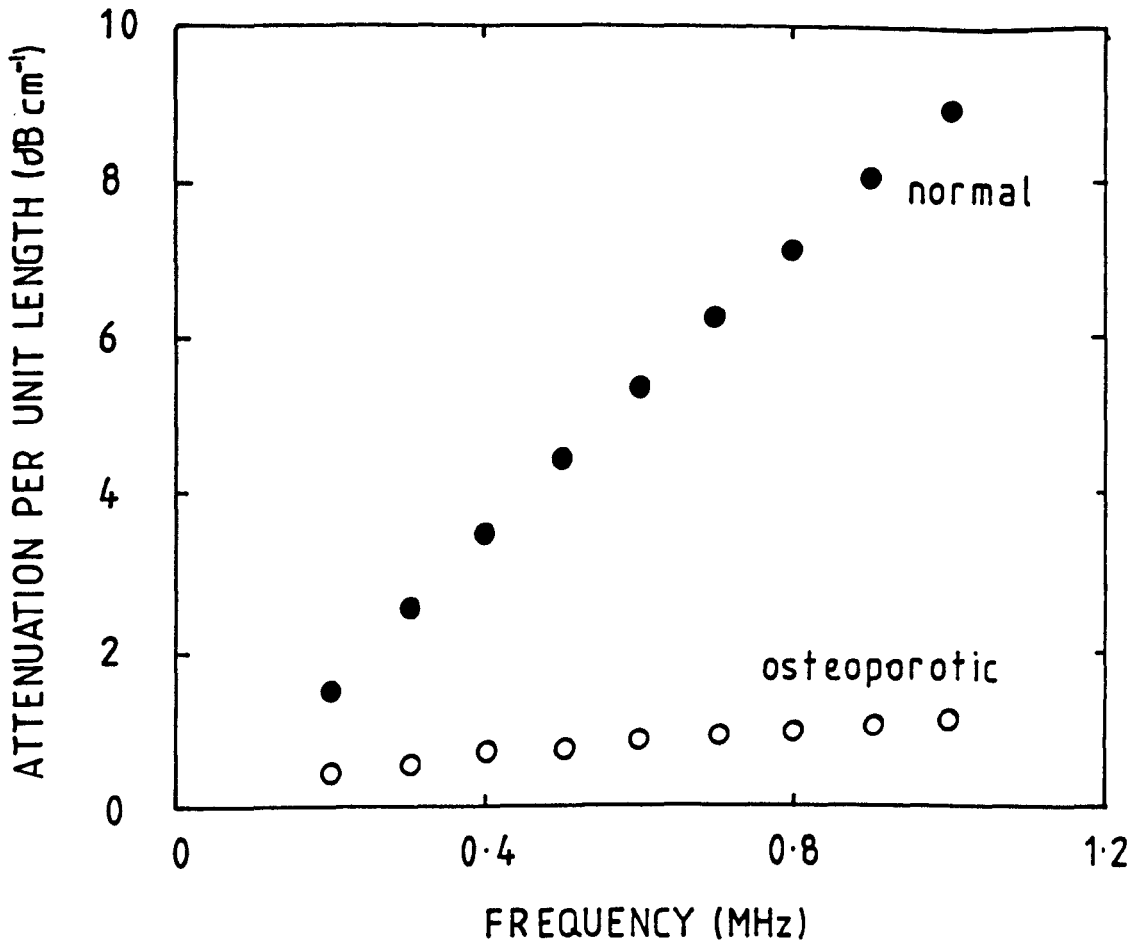
Figure 8.6 Calculated attenuation as a function of frequency modelled by the Biot theory for normal and osteoporotic bone.

As a further extension to test the Biot theory, it was applied for a range of parameters, figure 8.7, representing severely osteoporotic to healthy normal. The calculated slope is plotted as a function of bone content (porosity as a percentage) in the same way as figure 6.7. The parameters used are given in table 8.5, and include variations of permeability, width and spacing to mimic the properties discussed in chapter 6. Although there is an increase in slope with decreased porosity, the Biot theory predicts a maximum of 15 dB MHz^{-1}cm^{-1} for the range of values used. This limit is not observed, and also represents a fairly low attenuation slope compared to the experimental values obtained. Varying the parameters used for the theory can produce substantial changes in the calculated results, and some of the values used here are only estimates. A great deal more work could be carried out in this area, obtaining accurate values for the moduli rather than estimates from cortical bone and measuring the range of permeability of the samples. The parameters could be tuned endlessly, and this may be necessary to mimic such a complicated structure as cancellous bone.

The Biot theory accounts for the tortuosity of the structure and the ease of fluid flow with the permeability, which is the only way to explain the differences in attenuation observed in section 4.6, depending on the direction of propagation through the sample. An increased permeability resulting from a more open structure produces a decrease in attenuation as might be expected. However, it must be remembered that the cancellous bone is not isotropic, so the permeability will vary with direction even though the volume averaged size parameters (eg. trabecular width and number) do not.

Multiple scattering theory provided some interesting results that are likely to be unreliable because of the fundamental assumptions involved. None of the theories discussed are ideal for their application to cancellous bone, but the underlying assumptions in the development of the multiple scattering

Table 8.5

Parameters used for calculated values in figure 8.7

	Parameters		
	Pore size	porososity	permeability
Osteoporotic	2200	0.95	5.0×10^{-7}
1	1855	0.90	8.0×10^{-8}
2	1509	0.85	5.0×10^{-8}
3	1163	0.80	1.0×10^{-8}
4	877	0.75	8.0×10^{-9}
Normal	471	0.72	5.0×10^{-9}

ρ bone 1800 Kgm^{-3}

ρ fat 950 Kgm^{-3}

fat 1.495 Nsm^{-2}

shape factor bone	prolate spheriod
shape factor fat	spherical

bone:	longtitudinal velocity	$3300 ms^{-1}$
	longtitudinal attenuation	45 dB MHz^{-1} m^{-1}
	transverse velocity	1800 ms^{-1}
	transverse attenuation	50 dB MHz^{-1} m^{-1}
fat	longtitudinal velocity	1470 ms^{-1}
	longtitudinal attenuation	5 dB MHz^{-1} m^{-1}
	transverse velocity	0
	transverse attenuation	0
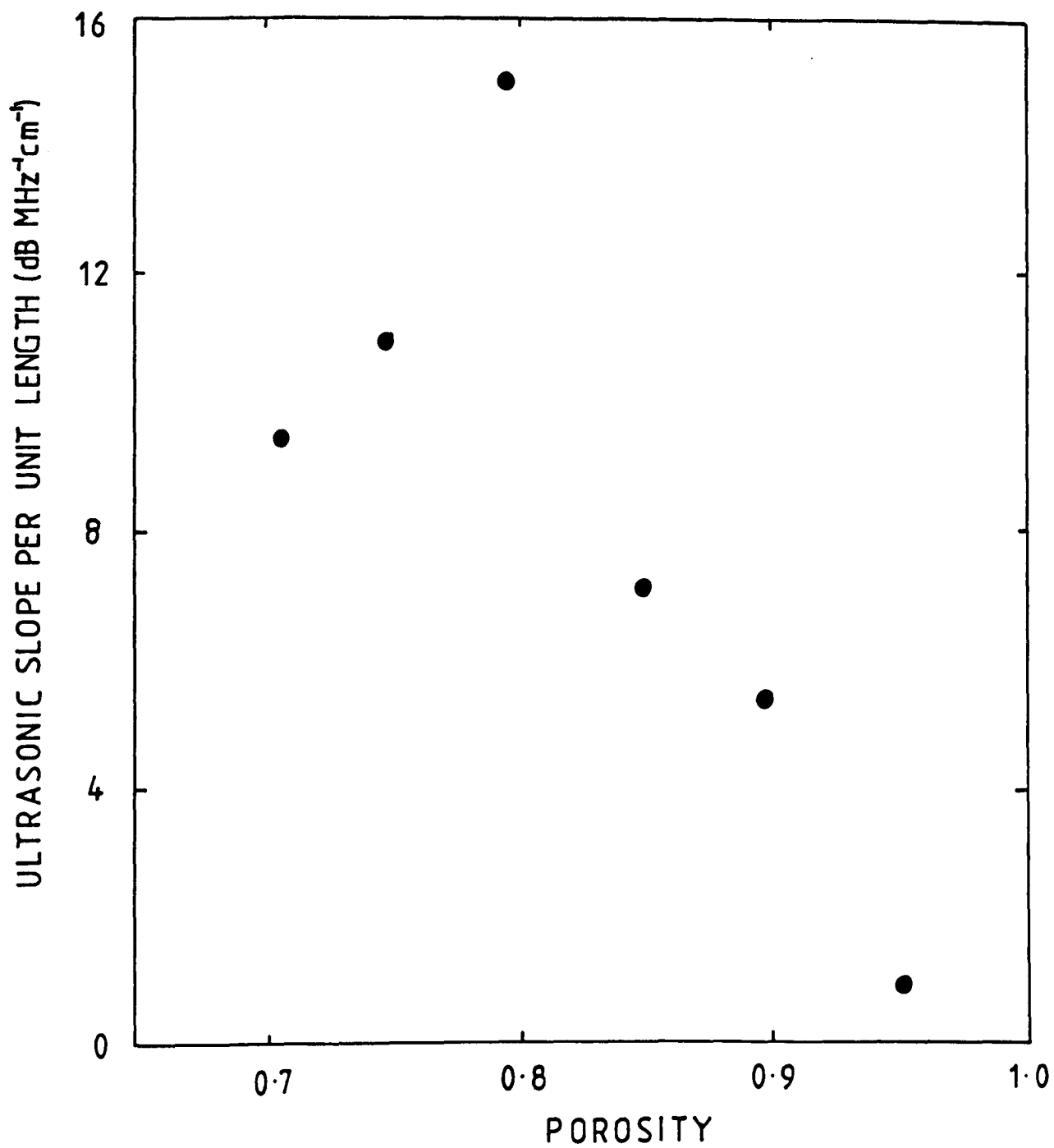
Figure 8.7 Calculated ultrasonic slope as a function of bone porosity, evaluated by the Biot theory.

equations are not strictly relevant to the trabecular structure of cancellous bone.

The Biot theory is the most successful of the theories evaluated that could be used to predict the ultrasonic propagation in cancellous bone, although there are still severe limitations. However, the parameters could be obtained more accurately for the individual components of cancellous bone, and this may result in an improved prediction of the ultrasonic propagation.

Ideally, in practise, the ultrasonic attenuation would be used to predict the physical dimensions of the bone structure from an *in vivo* measurement, so that an estimate of the pore size, trabecular thickness and number can be made directly from the ultrasonic slope. This is, in fact the inverse problem of the work discussed in this chapter. However, if the ultrasonic propagation can be predicted from a detailed knowledge of the bone architecture, then we are a long way towards solving the reverse process.

It appears from the work presented in this thesis that the answer is not as clear cut as might at first be thought. The ultrasonic attenuation as a function of frequency depends on so many factors that it is unlikely that one unique combination of parameters will produce a unique slope value. The theories for ultrasonic propagation studied in this chapter are certainly not enough to explain the attenuation or velocity patterns observed in cancellous bone, although it must be stressed that they were not adapted in any way for this particular application. Should some assumptions be altered and accounted for in the development of an adapted theory, then some more accurate predictions may be acheived.

A more detailed knowledge of the bone structure may lead to a better evaluation of the ultrasonic attenuation, allowing the reverse process to at least produce a range of possible values for the architectural parameters of the cancellous bone.

CONCLUSIONS AND FURTHER WORK.

The aim of the current work is to investigate the ultrasonic propagation in cancellous bone, with particular emphasis on the frequency dependence of the attenuation. This emphasis is important because the work is related to the ultrasonic diagnosis of the bone disease osteoporosis. Ideally, details of the bone quality, ie porosity and structure, need to be known to assess the strength of the bone and therefore the likelihood of fracture. Ultrasonic diagnosis offers the potential to investigate these factors in both *in vitro* and safely *in vivo*.

The reproducability of the *in vitro* method is comparable to other diagnostic techniques, but the problems associated with measuring absolute ultrasonic attenuation, such as diffraction, are even more apparent with such a variable material as cancellous bone. Thus the attenuation is always quoted as a change in attenuation in decibels with increasing frequency in MHz. There are very few previously published results available, and none of these look at the range of cancellous bone from osteoporotic to healthy. Some results were taken in the current work specifically because of the relevence of ultrasonic attenuation to the diagnosis of osteoporosis eg frequency dependence of attneuation rather than absolute.

Chapter 4 detailed the ultrasonic results obtained during the current work. The measurements on cortical bone are mainly for comparison and are similar to published work but detailed measurements on cancellous bone have not been carried out before. There is a close correlation between the ultrasonic attenuation as a function of frequency (ultrasonic slope) with the physical density of the cancellous bone, suggesting that the ultrasound can be used successfully to measure bone mineral content, the parameter assessed by all other diagnostic techniques. The differences between the propagation in cortical

and cancellous bone suggest that the structure of the trabeculae is an important factor. The attenuation slope was also found to vary with the direction of propagation within the bone, implying that the propagation depends on detailed structural parameters such as permeability and the orientation of the trabeculae.

The relation between the attenuation slope for whole os calces and the purely cancellous samples taken from them provided important results showing that the BUA technique does actually measure the properties of the cancellous bone and not the shape of the heel bone itself. Typical losses due to the cortical surface and the shape of the os calcis were much lower than originally suggested by Langton (1984) and reflection losses from the regular cancellous samples were demonstrated to be negligible with respect to the other attenuation losses.

The *in vitro* measurements discussed in chapter 4 are the first to study the variation in cancellous bone using ultrasound, and could be used as a basis for studying typical age effects and other factors. They also represent an extension to the well documented measurements on cortical bone.

The comparison between the ultrasonic results and measurements made using quantitative computed tomography (QCT) on the same samples provide further evidence for the effectiveness of the BUA technique as a diagnostic tool, and represents the type of comparison requested by some medical staff.

The compressive strength measurements proved interesting when compared to the ultrasonic attenuation results. Ideally, if the ultrasound is giving a direct indication of the quality of the cancellous bone then it would be expected to correlate well with the maximum compressive strength of the bone. The two experiments carried out were completely different, one using many samples from a mainly elderly population, and the other using only a few samples covering a wide age range. Both sets of samples were hardly ideal, but still produced relevant results. On an individual basis, there was little

connection between the compressive strength and the attenuation slope of each vertebra, but once a mean value for each cadaver was established, a high correlation was produced that was not a function of the effectively reduced population. This averaging technique is common when measuring bone mineral in the vertebral column and has been used to increase the reliability of the results of standard diagnostic methods. All the samples used in this experiment were vertebral slices, and were tested with the outer cortical ring intact. This will have a great influence on the strength of the sample as well as the density and ash weight, but will not affect the ultrasound at all. On average, the BUA technique does appear to give an indication of the strength of cancellous bone.

The second set of compressive strength measurements were intended to provide a more detailed comparison between the strength and the ultrasonic attenuation, by using purely cancellous samples as well as whole vertebrae. Unfortunately, mainly due to the small number of samples available, this proved inconclusive. There was no significant correlation between the strength and the ultrasonic slope for either the whole vertebrae or the cancellous samples. More detailed analysis of the samples, using the ash weight and the apparent density also proved inconclusive when related to the ultrasonic measurements.

One important result to arise from these testsis the comparison between the ultrasonic slope of the whole vertebrae and the corresponding cancellous samples. This confirmed that the variation in attenuation depends on the cancellous bone and not the cortex or overall shape of the sample. It also proved the validity of the BUA technique for assessing cancellous bone from any skeletal site, not just the os calcis, as long as the propagation path can be defined.

This work provided the opportunity to compare BUA measurements on different bones from the same cadaver, as lumbar vertebrae and an os calcis were available. The correlation produced, 0.47, although not significant and for very few samples, is comparable to similar tests using other diagnostic techniques. This shows that BUA is consistent with the methods currently in use.

Chapter 6 described a thick section histomorphometry technique for obtaining typical structural parameters for the cancellous bone of the os calcis. Such information is not available as it is nearly always the iliac crest that is analysed because of its application to hip replacements. The histomorphometry method used here was developed for use on vertebral cancellous bone, and was refined in the current work with the use of computerised image analysis. The results obtained represented average values for each os calcis, although ideally more sites should be analysed per heel bone. A limit had to be drawn because of the shear bulk of the analyses required. These results are valuable in themselves, as well as providing vital parameters for the theoretical evaluation of the ultrasonic propagation.

Comparisons between the structural values produced correlations entirely consistent with published work for cancellous bone from other skeletal sites, even though the published work involved thin section histomorphometry. This shows that the experimental work carried out is valid and self consistent. The values themselves show the wide range of structural detail in cancellous bone from only one site of the skeleton. The ultrasonic attenuation could not be considered to give direct information about these structural parameters in addition to that of the physical density, even though the correlation of -0.79 between the BUA and the mean trabecular spacing is highly significant. This work also showed that the attenuation at 200 kHz, an independent ultrasonic

reading from the actual slope, does not appear to give any further information about the trabecular structure than the slope alone.

The final section of this thesis is an analysis of theories commonly used to explain the ultrasonic propagation in composite materials and an attempt to use three of these to explain the propagation in cancellous bone. None of the theories were ideally suited for its application to the complex trabecular structure, but represented completely different ways of looking at the problem.

The most successful theory was the Biot theory, which predicted increasing attenuation with frequency and also increasing attenuation slope for parameters representing more healthy bone. However, it did not predict the observed changes in velocity. It is open to question whether any of the theories discussed can be strictly applied to cancellous bone, but it was intended that they may go some way to explaining the propagation of ultrasound in the trabecular structure. For many of the parameters, the values used were estimates, and in some cases a range of values more accurately represents the structure of a single sample. For instance, the trabecular and pore sizes vary considerably over a small volume of sample, yet only an average value could be used in the theoretical model. Despite these limitations, the Biot theory does explain some details of the ultrasonic propagation, especially when the permeability is taken in to account. This is an important parameter, as yet unmeasured, which varies with direction within the trabecular structure. Linton Johnson et al (1982) have showed the importance of this kind of architectural information when considering ultrasonic propagation in fairly regular samples of fused glass beads. It is reasonable to assume that it is even more important in a structure as irregular as cancellous bone. Scattering theories, single or multiple, have no method by which they can explain the

different ultrasonic attenuation observed when considering propagation in different directions through the cancellous structure.

This represents an important area for further work. More details about the trabecular structure are required to produce more reliable theoretical models. The variation between samples is so great that many must be analysed and typical ranges established. Ideally, the permeability and the tortuosity should be measured. It would also be useful to conduct a further investigation in to the changes in ultrasonic slope with respect to the direction of propagation. This will probably reveal more information about the importance of the trabecular orientation and associated parameters such as the tortuosity and the permeability.

The ultimate aim, of course, is to be able to predict the bone density and structural parameters from the ultrasonic attenuation as a function of frequency. To do this, a full understanding of the theoretical aspects of the propagation must be achieved. The work in this thesis suggests that there is too much variation in the architecture of the bone to be able to say definitely that a particular ultrasonic slope corresponds to a unique cancellous structure. However, with a more detailed knowledge of the architectural parameters, it may be that a typical structure can be attributed to a particular value of ultrasonic slope.

The other main area for further work is the comparison of BUA to existing diagnostic techniques, including destructive ones such as compressive strength testing. The measurement of the same purely cancellous samples by several techniques will provide direct comparisons between the methods. A full analysis of a comparison between BUA and QCT is given in this thesis, and a comparison with single photon absorption (SPA) is nearing completion, but this leaves neutron activation analysis, dual photon absorption (DPA) and Compton scattering. More importantly, one of the experiments described here, the BUA

and compressive strength of purely cancellous samples, should be repeated for a larger and more representative sample size.

It has been shown in the current work that the ultrasonic slope varies with direction of propagation through the cancellous bone. The maximum compressive strength also varies with the orientation of the trabecular structure, as discussed in section 5.2, so one particular area of interest would be to compare the dependence of each measurement on the orientation of cancellous samples.

The use of the frequency dependence of ultrasonic attenuation in assessing cancellous bone suggested by Langton et al (1984) has opened up a wide area of research aimed at diagnosing osteoporosis safely and accurately, with the eventual goal of reducing the risk of severe disease in many elderly people. It is hoped that this work has provided at least a small insight in to how ultrasonic attenuation may be used to indicate the quality of the bone structure, and hence allow an assessment of the likelihood or severity of osteoporosis in individual patients.

REFERENCES.

AARON J.E., MAKINS N.B., SAGREIYA K. (1987) The Microanatomy of Trabecular Bone Loss in Normal Aging Women. Clin.Orth.Rel.Res. 215 p260-271.

ALBRIGHT F., SMITH P.H., RICHARDSON A.M. (1941) Postmenopausal Osteoporosis: its Clinical Features. J.Amer.Med.Assoc. 116 p2465-2474.

ALWENS W. (1926) Spatrachitis, Osteomalazie, Senile Osteoporose, Hungerosteopathie. In Handbuch der Inneren Medizin, G. Bergmann and R. Staehelin (Eds.), Springer, Berlin. p584-676.

ANDERSON J., OSBORN S.B., TOMLINSON R.W.S., NEWTON D., RUNDO J., SMITH J.W. SALMON L. (1964) Neutron Activation Analysis in Man in vivo. The Lancet 2. p1201-1205.

ANDRE M.P., CRAVEN J.D., GREENFIELD M.A., STERN R. (1980) Measurement of Velocity of Ultrasound in Human Femur in vivo. Med.Phys. 7 p324-330.

ANSON L.W., CHIVERS R.C. (1984) Ultrasonic Wave Propagation in Inhomogeneous Media. Interim Report No.5, Physics Dept., Univ. Surrey.

ATTENBOROUGH K. (1982) Acoustical Characteristics of Porous Materials. Phys.Rep. 82 p181-227.

AVIOLI L.V. (1983a) Osteoporosis. In Bone and Mineral Research Annual 1, W.A. Peck (Ed.), Excerpta Medica, Amsterdam. p280-318.

AVIOLI L.V. (1983b) Management of Geriatric Osteoporotic Women. In The Osteoporotic Syndrome, 1st Ed., L.V. Avioli (Ed.), Grune and Stratton, New York. p145-153.

BARGER J.E. (1979) Attenuation and Dispersion of Ultrasound in Cancellous Bone. In Ultrasonic Tissue Characterisation 2, M. Linzer (Ed.), Nat.Bur.Stand.Spec.Publ. 525 p197-201.

BERRYMAN J.G. (1979) Theory of Elastic Properties of Composite Materials. Appl.Phys.Lett. 35 p856-858.

BERRYMAN J.G. (1980a) Confirmation of Biot's Theory. App.Phys.Lett. 37 p382-384.

BERRYMAN J.G. (1980b) Long Wavelength Propagation in Composite Elastic Media. J.Ac.Soc.Am. 68 p1809-1831.

BERRYMAN J.G. (1981a) Elastic Wave Propagation in Fluid-Staurated Porous Media J.Ac.Soc.Am. 69 p416-424.

BERRYMAN J.G. (1981b) Elastic Wave Propagation in Fluid-Saturated Porous Media. J.Ac.Soc.Am. 70 p1754-1756.

BIOT M.A. (1956) Theory of Propagation of Elastic Waves in a Fluid-Saturated Porous Solid. J.Ac.Soc.Am. 28 p168-191.

BIOT M.A. (1962a) Generalised Theory of Acoustic Propagation in Porous Dissipative Media. J.Ac.Soc.Am. 34 p1254-1264.

BIOT M.A. (1962b) Mechanics of Deformation and Acoustic Propagation in Porous Media. J.App.Phys. 33 p1482-1498.

BIRO L., DAS P., MEUNIER A., KATZ J.L. (1983) Digital Ultrasonic Imaging and its Application to Skeletal Tissues, Ultrasonics International Proceedings, IEEE. p79-84.

BLOOM R.A., LAWS J.W. (1970) Humeral Cortical Thickness as an Index of Osteoporosis in Women. Brit.J.Radiol. 43 p522-527.

BOURNE G.H. (1956) The Biochemistry and Physiology of Bone. Academic Press, New York.

BROWN C.E., ALLAWAY J.R., BROWN K.L., BATTOCLETTI J.H. (1987) Non-invasive Evaluation of Mineral Content of Bone Without Use of Ionizing Radiation. Clin.Chem. 33 p227-236.

CAMERON J.R., SORENSON J. (1963) Measurement of Bone Mineral in vivo: an Improved Method. Science. 142 p230-232.

CANN C.E., GENANT H.K. (1980) Precise Measurement of Vertebral Mineral Content using Computed Tomography. J.Comput.Assis.Tomogr. 4 p493-500.

CARTER D.R., HAYES W.C. (1976) Bone Compressive Strength: The Influence of Density and Strain Rate. Science. 194 p1174-1176.

CHESNUT C.H., NELP W.B., LEWELLEN T.K. (1981) Neutron Activation Analysis for Whole Body Calcium Measurement. In Osteoporosis: Recent Advances in Pathogenesis and Treatment, H.F. Deluca et al (Eds.), University Park Press, Baltimore. p19-23.

CHIVERS R.C. (1977) The Scattering of Ultrasound by Human Tissues - Some Theoretical Models. Ultr.Med.Biol. 3 p1-13.

CHRISTIANSEN C. (1984) Prophylactic Treatment for Age-related Bone Loss in Women In Osteoporosis, Proceedings of International Symposium on Osteoporosis, C. Christiansen et al (Eds.), Aalborg Stiftsbogtrykkeri. p587-593.

CHRISTIANSEN C., RODBRO P., JENSEN H. (1975) Bone Mineral Content in Forearm Measured by Photon Absorptiometry. Scand.J.Clin.Lab.Invest. 35 p323-330.

COHN S.H. (1982) Intercomparison of Techniques for the Non-invasive Measurement of Bone Mass. In Non-Invasive Bone Measurements: Methodological Problems, J. Dequeker and C.C. Johnson (Eds.), IRL Press, Oxford. p18-26.

COMPSTON J.E., CHADHA S., MERRETT A.L. (1980) Osteomalacia Developing During Treatment of Osteoporosis with Sodium Flouride and Vitamin D. Brit.Med.J. 281 p910-911.

CUMMINGS S.R. (1987) The Epidemiology of Hip Fractures. In Osteoporosis 1987, Proceedings of International Symposium on Osteoporosis, C.Christiansen et al (Eds.), Osteopress, Copenhagen. p40-44.

CUMMINGS S.R., BLACK D. (1986) Should Perimenopausal Women be Screened for Osteoporosis? Annals Int.Med. 104 p817-823.

CURREY J.D. (1987) private communication.

DALEN N., JACOBSON B. (1974) Bone Mineral Assay: Choice of Measuring Sites.

Invest.Radiol. 9 p174-185.

DATTA P.K., PETHRICK R.A. (1980) Ultrasonic Studies of Glass-filled Polymer Solids. J.Phys.D:Appl.Phys. 13 p153-161.

DAVIES R., SAHA S. (1985) Osteoporosis. AFP 32, p107-114.

DEVANY A.J. (1980) Multiple Scattering Theory for Discrete Elastic Random Media. J.Math.Phys. 21 p2603-2611.

DEVANY A.J., LEVINE H (1980) Effective Elastic Parameters of Random Composites. Appl.Phys.Lett. 37 p377-379.

DOHERTY W.P., BOVILL E.G., WILSON E.L. (1974) Evaluation of the Use of Resonant Frequencies to Characterize Physical Properties of Human Long Bones. J. Biomechanics. 7 p559-561.

DUYKERS L.R.B. (1967) Sound Attenuation in Liquid Solid Mixtures. J.Ac.Soc.Am. 41 p1330-1335.

DUYKERS L.R.B. (1970) Relaxation in Kaolin-Water Mixtures. J.Ac.Soc.Am. 47 p396-398.

ESHELBY J.D. (1957) The Determination of the Elastic Field of an Ellipsoid Inclusion and Related Problems. Proc.Roy.Soc.London Ser.A. 241 p376-396.

ETTINGER B., GENANT H.K., CANN C.E. (1987) Postmenopausal Bone Loss is Prevented by Treatment with Low Dosage Estrogen with Calcium. Annals Int.Med. 106 p40-45.

FENTON-LEWIS A. (1981) Fracture Neck of Femur: Changing Incidence. Brit.Med.J. 283 p1217-1220.

FOLDES J., LEICHTER I., GAZIT D., LIDOR J., STEINBERG R., MENCZEL J., BAB I. (1987) In vivo Measurement of Bone Density by Compton Spectroscopy and Histomorphmetry in Postmenopausal Osteoporosis. In Proceedings of International Symposium on Osteoporosis, C.Christiansen et al (Eds.), Aalborg.

FOLDY L.L. (1945) The Multiple Scattering of Waves. Phys.Rev. 67 p107-119.

FRY F.J., BARGER J.E. (1978) Acoustical Properties of the Human Skull.
J.Ac.Soc.Am. 63 p1576-1590.

GALANTE J., ROSTOKER W., RAY R.D. (1970) Physical Properties of Trabecular
Bone. Calcif. Tissue Res. 5 p236-246.

GARCIA B.J., COBBOLD R., FOSTER F.S., McNEILL K.G. (1978) Ultrasonic
Attenuation in Bone, Ultrasonics Symposium Proceedings, IEEE p327-330.

GARN S.M. (1981) The Phenomenon of Bone Formation and Bone Loss. In Osteo-
porosis: Recent Advances in Pathogenesis and Treatment, H.F. Deluca et al
(Eds.), University Park Press, Baltimore. p3-16.

GARRAHAN N.J., MELLISH R.W.E., COMPSTON J.E. (1986) A New Method for Two
Dimensional Analysis of Bone Structure in Human Iliac Crest Biopsies.
J. Microscopy 142 p341-349.

GAUNARD G.C., UBERALL H. (1982) Resonance Theory of Effective Properties of
Perforated Solids. J.Ac.Soc.Am. 71 p282-295.

GENANT H.K., CANN C.E. (1981) Vertebral Mineral Determination using
Quantitative Computed Tomography. In Osteoporosis: Recent Advances in
Pathogenesis and Treatment, H.F. Deluca et al (Eds.), University Park
Press, Baltimore. p37-47.

GENANT H.K., CANN C.E., FAUL D.D. (1982) Quantitative Computed Tomography for
Assessing Vertebral Bone Mineral. In Non-Invasive Bone Measurements:
Methodological Problems, J. Dequeker and C.C. Johnson (Eds.), IRL Press,
Oxford. p216-249.

GENANT H.K., POWELL M.R., CANN C.E., STEBLER B., RUTT B.K., RICHARDSON M.L.,
KOLB F.O. (1984) Comparison of Methods for in vivo Spinal Bone Mineral
Measurement. In Osteoporosis: Proceedings of International Symposium on
Osteoporosis. C.Christiansen et al (Eds.), Aalborg Stiftsbogtrykkeri. p97-
102.

GOLDSTONE L.A. (1983) Understanding Medical Statistics, Heinemann Medical
Books Ltd., London. p177.

GOSS S.A., JOHNSTON R.L., DUNN F. (1978) Comprehensive Compilation of
Empirical Ultrasonic Properties of Mammalian Tissues. J.Ac.Soc.Am. 64
p423-457.

GOTFREDSEN A., NILAS L., RIIS B.J., THOMSEN K., CHRISTIANSEN C. (1986) Bone
Changes Occurring Spontaneously and Caused by Estrogen in Early Menopausal
Women: a Local or Generalised Phenomenon? Brit.Med.J. 292 p1098-1100.

GRECH P., MARTIN T.J., BARRINGTON N.A., ELL P.J. (1985) Diagnosis of Metabolic
Bone Disease. Chapman and Hall, London.

GREENFIELD M.A., CRAVEN J.D., HUDDLESTON A., KEHRER M.L., WISHKO D., STERN R.
(1981) Measurement of Velocity of Ultrasound in Human Cortical Bone in
vivo. Radiology 138 p701-710.

GUSTAFSSON L., JACOBSON B., KUSOFFSKY L. (1974) X-ray Spectrophotometry for
Bone Mineral Determinations. Med.Biol.Eng. 12 p113-119.

HALL F.M., DAVIS M.A., BARAN D.T. (1987) Bone Mineral Screening for
Osteoporosis New Eng.J.Med. 316 p212-214.

HEANEY R.P. (1983) Prevention of Age Related Osteoporosis in Women. In
The Osteoporotic Syndrome, 1st Ed., L.V. Avioli (Ed.), Grune and Stratton,
New York. p123-144.

HEANEY R.P. (1984) Risk Factors in Age-related Bone Loss and Osteoporotic
Fracture. In Osteoporosis, Proceedings International Symposium on
Osteoporosis, C. Christiansen et al (Eds.), Aalborg Stiftsbogtrykkeri.
p245-253.

HEANEY R.P. (1987) Qualitative Factors in Osteoporotic Fracture: The State of
the Question. In Osteoporosis 1987, Proceedings of International Symposium
on Osteoporosis, C.Christiansen et al (Eds.), Osteopress, Copenhagen.
p281-287.

HEANEY R.P., RECKER R.R. (1981) Osteoporosis Related Nutritional Influences on Bone: Calcium. In Osteoporosis: Recent Advances in Pathogenesis and Treatment, H.F. Deluca et al (Eds.), Univerity Park Press, Baltimore. p253-256

HORSMAN A., NORDIN B.E.C., AARON J., MARSHALL D.H. (1981) Cortical and Trabecular Osteoporosis and Their Relation to Fractures in the Elderly. In Osteoporosis: Recent Advances in Pathogenesis and Treatment, H.F. Deluca et al (Eds.) University Park Press, Baltimore. p175-184.

HORSMAN A., CURREY J.D. (1983) Estimation of Mechanical Properties of the Distal Radius from Bone Mineral Content and Cortical Width. Clin.Orth.Rel.Res. 176 p298-304.

HOSIE C.J., SMITH D.A., DEACON A.D., LANGTON C.M. (1987) Comparison of Broadband Ultrasonic Attenuation of the os calcis and Quantitative Computed Tomography of the Distal Radius. Clin.Phys.Physiol.Meas. 8 p303-308

HVID I, JENSEN N.C., BUNGER C., SOLUND K., DJURHUUS J.C. (1985) Bone Mineral Assay: its Relation to the Mechanical Strength of Cancellous Bone. Engin. in Med. 14 p79-83.

HYODYNMAA S.J., KARELLAS A., WHITING J.S., CRAVEN J.D, GREENFIELD M.A., (1986) In vivo Measurement of Ultrasonic Attenuation Coefficient in Cortical Bone private communication

ISHIMARU A. (1978) Wave Propagation and Scattering in Random Media, Vol.2. Academic Press, New York. p253-294.

JACKSON T.K., ULLRICH I.H. (1984) Understanding Osteoporosis. Postgrad.Med. 75 p118-125.

JENSEN P.S., ORPHANOUDAKIS S.C., BARON R., LANG R., RAUSCHKOLB E.N., RASMUSSEN H. (1979) Determination of Bone Mass by CT and Correlation with Quantitative Histomorphometic Analysis. J.Comput.Assis.Tomog. 3 p847.

JHAMARIA N.L., LAL K.B., UDAWAT M., BANERJI P., KABRA S.G. (1983) Trabecular Pattern of the Calcaneum as an Index of Osteoporosis. J.Bone Joint Surg. 65-B p195-198.

JOHNSTON C.C. (1982) Clinical Relevance of Single Energy Photon Absorptiometry. In Non-Invasive Bone Measurements: Methodological Problems, J.Dequeker and C.C. Johnston (Eds.), IRL Press, Oxford. p182-184.

JOHNSTON C.C. (1983) Non-invasive Methods for Quantitating Appendicular Bone Mass. In The Osteoporotic Syndrome, 1st Ed., L.V. Avioli (Ed.), Grune and Stratton, New York. p73-84.

JONES P.R.M., LANGTON C.M., CARR H. (1987) Broadband Ultrasonic Attenuation Studies in Sedentary and Active Young Male Adults and in Bovine Cancellous and Cortical Bone. In Ultrasonic Studies of Bone, S.B. Palmer and C.M. Langton (Eds.), IOP Publishing Ltd., Bristol. p27-35.

JONSON R, ROOS B., HANSSON T. (1986) Bone Mineral Measurement with a Continuous Roentgen Ray Spectrum and a Germanium Detector. Acta Radiol.Diag. 27 p105-109.

JURIST J.M. (1970) In vivo Determination of the Elastic Response of Bone. Phys.Med.Biol. 15 p417-434.

KATZ J.L., YOON H.S. (1984) The Structure and Anisotropic Mechanical Properties of Bone, IEEE Transacs.Biomed.Eng. BME-31 p878-884.

KIMMEL D.B. (1981) Cellular Basis of Bone Accumulation during Growth: Implications for Metabolic Bone Disease. In Osteoporosis: Recent Advances in Pathogenesis and Treatment, H.F. Deluca et al (Eds.), University Park Press, Baltimore. p87-95.

KINSLER L.E., FREY A.R., COPPENS A.B., SANDERS J.V. (1982) Fundamentals of Acoustics, 3rd Ed. Wiley and Sons, New York. p127-129.

KLEEREKOPER M., VILLANUEVA A.R., STANCIU J., SUDHAKER RAO D., PARFITT A.M., (1985) Role of Three Dimensional Trabecular Microstructure in the Pathogenesis of Vertebral Compression Fractures. Calcif.Tissue Int. 37 p594-597.

KLEEREKOPER M., FELDKAMP L.A., GOLDSTEIN S.A., FLYNN M.J., PARFITT A.M. (1987) Cancellous BoneArchitecture andBoneStrength. In Osteoporosis 1987, Proceedings of International Symposium on Osteoporosis, C.Christiansen et al (Eds.), Osteopress, Copenhagen. p294-300.

KROLNER B., PORS NIELSEN S (1980) Measurement of Bone Mineral Content of the Lumber Spine: Theory and Application of a New Two Dimensional Dual Photon Attenuation Method. Scand.J.Clin.Lab.Invest. 40 p653-663.

KROLNER B., PORS NIELSEN S. (1982) Clinical Application of Dual Photon Absorptiometry of the Lumbar Vertebrae. In Non-Invasive Bone Measurements: Methodological Problems, J. Dequeker and C.C. Johnston (Eds.), IRL Press, Oxford. p 202-205.

KUSTER G.T., TOKSOZ M.N. (1974) Velocity and Attenuation of Seismic Waves in Two-Phase Media. Geophysics. 39 p587-618.

LAKES R., YOON H.S., KATZ J.L. (1983) Slow Compressional Wave Propagation in Wet Human and Bovine Cortical Bone. Science. 220 p513-515.

LAMB H. (1924) Hydrodynamics. 5th Ed. Cambridge University Press, Cambridge. p143-147

LAMBERT R.F. (1983) Propagation of Sound in Highly Porous Open-cell Elastic Foams. J.Ac.Soc.Am. 73 p1131-1138.

LANGTON C.M. (1984) The Measurement of Broadband Ultrasonic Attenuation in Cancellous Bone. Ph.D. thesis, Hull.

LANGTON C.M. (1987) Critical Analysis of the Ultrasonic Interrogation of Bone and Future Developments. In Ultrasonic Studies of Bone, S.B. Palmer and C.M. Langton (Eds.), IOP Publishing Ltd., Bristol. p73-89.

LANGTON C.M., PALMER S.B., PORTER R.W. (1984) The Measurement of Broadband
Ultrasonic Attenuation in Cancellous Bone. Engin. in Med. 13 p89-91.

LANYON L.E. (1981) Bone Remodelling, Mechanical Stress and Osteoporosis. In
Osteoporosis: Recent Advances in Pathogenesis and Treatment, H.F. Deluca
et al (Eds.), University Park Press, Baltimore. p129-138.

LATIFF R.H., FIORE N.F. (1975) Ultrasonic Attenuation and Velocity in Two
Phase Microstructures. J.Ac.Soc.Am. 57 p1441-1447.

LAX M. (1952) Multiple Scattering II: Effective Field of Dense Systems.
Phys.Rev. 85 p621-629.

LEFEBVRE J., FROHLY J., TORGUET R., BRUNEEL C., ROUVAEN J.M. (1980)
Experimental and Theoretical Study of the Multiple Scattering of
Acoustical Waves in Inhomogeneous Material. Ultrasonics. 18 p170-174.

LEHMANN J.F., JOHNSON E.W. (1958) Some Factors Influencing the Temperature
Distribution in Thighs Exposed to Ultrasound. Arch.Phys.Med.Rehab. 39
p347-356.

LEICHTER I., BIVAS A., GIVEON A., MARGULIES J.Y., WEINREB A. (1987) The
Relative Significance of Trabecular and Cortical Bone Density as a
Diagnostic Index for Osteoporosis. Phys.Med.Biol. 32 p1167-1174.

LEY F.J. (1973) The Effect of Ionizing Radiation on Bacteria. In Manual on
Radiation Sterilization of Medical and Biological Materials, International
Atomic Energy Agency, Vienna. p37-63.

LING S.S., RUSTGI S., KARELLAS A., CRAVEN J.D., WHITING J.S., STERN R.,
GREENFIELD M.A. (1982) Measurement of Trabecular Bone Mineral Density
using Coherant and Compton Scattered Photons in vitro. Med.Phys. 9
p208-215.

LINTON-JOHNSON D., PLONA T.J., SCALA C., PASIERB F., KOJIMA H. (1982)
Tortuosity and Acoustic Slow Waves. Phys.Rev.Lett. 49 p1840-1844

MAL A.K., KNOPOFF L. (1967) Elastic Wave Velocities in Two-Component Systems

J.Inst.Math.Applics. 3 p376-387

MASON W.P., McSKIMIN H.J. (1947) Attenuation and Scattering of High Frequency Sound Waves in Metals and Glasses. J.Ac.Soc.Am. 19 p464-473.

MAZESS R.B. (1983a) The Non-invasive Measurement of Skeletal Mass. In Bone and Mineral Research Annual 1, W.A. Peck (Ed.), Excerpta Medica, Amsterdam. p223-279.

MAZESS R.B. (1983b) Non-invasive Methods for Quantitating Trabecular Bone. In The Osteoporotic Syndrome, 1st Ed., L.V. Avioli (Ed.), Grune and Stratton, New York, p85-114.

MAZESS R.B. (1987) Bone Density in Diagnosis of Osteoporosis: Thresholds and Breakpoints. Calcif.Tiss.Int. 41 p117-118.

MAZESS R.B., VETTER J. (1984) Comparison of Dual Photon Absorption and Dual Energy Quantitative Computed Tomography for Vertebral Mineral. In 4th International Workshop on Bone and Tissue Densitometry, France.

MAZESS R.B., HARPER A.E., DELUCA H., (1985) Calcium Intake and Bone. Amer.J.Clin.Nut. 42 p568-571.

MELTON L.J., RIGGS B.L. (1983) Epidemiology of Age Related Fractures. In The Osteoporotic Syndrome, 1st Ed., L.V. Avioli (Ed.), Grune and Stratton, New York, p45-72.

MERZ W.A., SCHENK R.K. (1970) Quantitative Structural Analysis of Human Cancellous Bone. Acta Anat. 75 p54-66.

MEUNIER P.J. (1983) Histomorphometry of the Skeleton. In Bone and Mineral Research Annual 1, W.A. Peck (Ed.), Excerpta Medica, Amsterdam. p191-222.

MEUNIER A., YOON H.S., KATZ J.L. (1982) Ultrasonic Characterization of some Pathological Human Femora. Ultrasonics Symposium Proceedings, IEEE. p713-717.

MILLER C.G. (1987) private communication.

MILLER C.G., PORTER R.W. (1987) The Prediction of Fracture of the Proximal Femur by Broadband Ultrasonic Attenuation. In Osteoporosis 1987, Proceedings of International Symposium on Osteoporosis, C.Christiansen et al (Eds.), Osteopress, Copenhagen. p414.

MORSE P.M., INGARD K.U. (1968) Theoretical Acoustics. McGraw-Hill, New York. p400-466.

MOSEKILDE Li., VIIDIK A., MOSEKILDE Le. (1985) Correlation Between Compressive Strength of Iliac and Vertebral Trabecular Bone in Normal Individuals. Bone 6 p291-295.

MOSEKILDE Le., MOSEKILDE Li., DANIELSEN C.C. (1986) Age Related Changes in Vertebral Trabecular Bone Mechanical Competence in Normal Individuals. Calcif.Tiss.Int.Suppl. 39 pA61.

MURRAY S.A. (1986) private communication.

MURRAY S.A., MILLER C.G., KANIS J.A. (1987) Specificity and Sensitivity of Ultrasound Attenuation in Bone. In Ultrasonic Studies of Bone, S.B. Palmer and C.M. Langton (Eds.), IOP Publishing Ltd, Bristol. p67-72.

NICHOLAS D, HILL C.R. (1975) Tissue Characterization by an Acoustic Bragg Scattering Process. Ultrasonics Int. Conf. Proc. p269-272.

NORDIN B.E.C. (1983) Osteoporosis with Particular Reference to Menopause. In The Osteoporotic Syndrome, 1st Ed., L.V. Avioli (Ed.), Grune and Stratton, New York, p13-44.

NORDIN B.E.C. (1987) The Definition and Diagnosis of Osteoporosis. Calcif. Tissue Int. 40 p57-58.

NORDIN B.E.C., PEACOCK M., CRILLY R.G., FRANCIS R.M., SPEED R., BARKWORTH S. (1981a) Summation of Risk Factors in Osteoporosis. In Osteoporosis: Recent Advances in Pathogenesis and Treatment, H.F. Deluca et al (Eds.), University Press, Baltimore. p359-367.

NORDIN B.E.C., AARON J., SPEED R., CRILLY R.G. (1981b) Bone Formation and

Resorption as the Determinants of Trabecular Bone Volume in Postmenopausal Osteoporosis. The Lancet 2 p277-279.

O'DONNELL M., JAYNES E.T., MILLER J.G. (1981) Kramers-Kronig Relationship Between Ultrasonic Attenuation and Phase Velocity. J.Ac.Soc.Am. 69 p696-701.

OGUSHWITZ P.R. (1985) Applicability of the Biot Theory. J.Ac.Soc.Am 77 p429-464.

ORTOFTE G., MOSEKILDE Li., HASLING C., MOSEKILDE Le. (1987) The Predictive Value of D.P.A. for Lumbar Body Compressive Strength and Ash Weight in Elderly Individuals. In Osteoporosis 1987, Proceedings International Symposium on Osteoporosis, C.Christiansen et al (Eds.), Osteopress, Copenhagen. p358-360.

OTT S.M. (1986) Should Women get Screening Bone Mass Measurements? Annals Int. Med. 104 p874-876.

OTT S.M., CHESNUT C.H., HANSON J.A., KILCOYNE R.F., MURANO R., LEWELLEN T.K (1984) Comparison of Bone Mass Measurements Using Different Diagnostic Techniques in Patients with Postmenopausal Osteoporosis. In Osteoporosis Proceedings of International Symposium on Osteoporosis, C.Christensen et al (Eds.), Aalborg Stiftsbogtrykkeri. p94-96.

OTT S.M., KILCOYNE R.F., CHESNUT C.H. (1986) Longitudinal Changes in Bone Mass After One Year as Measured by Different Techniques in Patients with Osteoporosis. Calcif.Tissue Int. 39 p133-138.

OVERTON T.R., HANGARTNER T.N., HEATH R., RIDLEY J.D. (1981) Effect of Physical Activity on Bone: Gamma Ray Computed Tomography. In Osteoporosis: Recent Advances in Pathogenesis and Treatment, H.F. Deluca et al (Eds.), University Park Press, Baltimore. p147-158.

PACIFICI R., SUSMAN N., CARR P.L., BIRGE S.J., AVIOLI L.V. (1987) Single and Dual Energy Tomographic Analysis of Spinal Trabecular Bone: a Comparative

Study in Normal and Osteoporotic Women. J.Clin.Endocrin.Metab. 64 p209-214.

PALMER H.E., NELP W.B., MURANO R., RICH C. (1968) The Feasibility of in vivo Neutron Activation Analysis of Total Body Calcium and Other Elements of Body Composition. Phys.Med.Biol. 13 p269-279.

PARFITT A.M., MATHEWS C.H.E., VILLANUEVA A.R., KLEEREKOPER M., FRAME B., RAO D.S. (1983) Relationships Between Surface, Volume and Thickness of Iliac Trabecular Bone and Aging and Osteoporosis. J.Clin.Invest. 72 p1396-1409.

PARFITT A.M. (1983) Stereological Basis of Bone Histomorphometry: Theory of Quantitative Microscopy and Reconstruction of the Third Dimension. In Bone Histomorphometry: Techniques and Interpretation, R.R. Recker (Ed.), CRC Press, Florida. p54-87.

PARFITT A.M. (1984) Closing Remarks on Relevance of Measurements to Pathogenesis Diagnosis and Evaluation of Treatment in Osteoporosis. In Osteoporosis, Proceedings of International Symposium on Osteoporosis, C. Christiansen et al (Eds.), Aalborg Stiftsbogtrykkeri. p233-239.

PARFITT A.M. (1987) Trabecular Bone Architecture in the Pathogenesis and Prevention of Fracture. Am.J.Med. 82(1B) p68-72.

PETLEY G.W., HAMES T.K., COOPER C., LANGTON C.M., CAWLEY M. (1987) Comparison Between B.U.A. and S.P.A. of the Os Calcis. In Osteoporosis 1987, Proceedings of International Symposium on Osteoporosis, C.Christiansen et al (Eds.), Osteopress, Copenhagen. p410-411.

PLONA T.J. (1980) Observation of a Second Bulk Compressional Wave in a Porous Medium at Ultrasonic Frequencies. App.Phys.Lett. 36 p259-261.

PODENPHANT J., HERSS NELSEN V.A., RIIS B.J., GOTFREDSEN A., CHRISTANSEN C. (1987) Bone Mass, Bone Structure and Vertebral Fractures in Osteoporotic Patients. Bone 8 p127-130.

POLL V., COOPER C., CAWLEY M.I.D (1986) Broadband Ultrasonic Attenuation in the os calcis and Single Photon Absorption in the Distal Forearm, a Comparative Study. Clin.Phys.Physiol.Meas. 7 p375-379.

PUGH J.W., ROSE R.M., RADIN E.L. (1973) Elastic and Viscoelastic Properties of Trabecular Bone: Dependance on Structure. J.Biomechanics 6 p475-485.

PUUMALAINEN P., UIMARIHUHTA A., ALHAVA E., OLKKONEN H. (1976) A New Photon Scattering Method for Bone Mineral Density Measurements. Radiology 120 p723-726.

RAISZ L.G. (1984) Regulation of Bone Metabolism. In Osteoporosis, Proceedings of International Symposium on Osteoporosis, C. Christiansen et al (Eds.), Aalborg Stiftsbogtrykkeri. p409-414.

RALEIGH (1926) Theory of Sound Vol.2. McMillan, London. p149-154.

RAMACHANDRAIAH P, SURYANARAYANA M (1987) An Ultrasonic Sing-around System for Thin Solid Samples. J.Phys E:Sci.Instrum. 20 p85-87.

RECKER R.R. (1982) Non-invasive Measurements of Bone Loss. In Non-Invasive Bone Measurements: Methodological Problems, J. Dequeker and C.C. Johnston (Eds.), IRL Press, Oxford. p2-13.

RECKER R.R. (1983) Bone Histomorphomtery: Techniques and Interpretation. CRC Press, Florida.

RICHELSON L.S., WAHNER H.W., MELTON L.J., RIGGS B.L. (1984) Relative Contributions of Aging and Estrogen Deficiency to Postmenopausal Bone Loss. New Eng.J.Med. 311 p1273-1275.

RIGGS B.L., SEEMAN E., HODGSON S.F., TAVES D.R., O'FALLON W.M. (1982) Effect of Flouride/Calcium Regimen on Vertebral Fracture Occurrence in Postmenopausal Osteoporosis. New Eng.J.Med. 306 p446-450.

RIGGS B.L., WAHNER H.W., MELTON L.J., RICHELSON L.S., JUDD H.L., OFFORD K.P. (1986) Rates of Bone Loss in Appendicular and Axial Skeletons of Women J.Clin.Invest. 77 p1487-1491.

RIIS B., THOMSEN K., CHRISTIANSEN C. (1987) Does Calcium Supplementation Prevent Postmenopausal Bone Loss? New Eng.J.Med. 316 p173-177.

ROBERTS J.G., LIEN J.W.K., WOOLEVER C.A., WEBBER C.E. (1984) Photon Scattering Measurements of Calcaneal Bone Density: Results of in vivo Longitudinal Studies. Clin.Phys.Physiol.Meas. 5 p193-200.

ROSENTHAL D.I., GANOTT M.A., WYSHAK G., SLOVIK D.M., DOPPELT S.H., NEER R.M. (1985) Quantitative Computed Tomography for Spinal Density Measurement, Factors Affecting Precision. Invest.Radiol. 20 p306-310.

ROSS R.K., PAGANINI-HILL A., MACK T.M. (1984) Reduction of Fracture and Other Effects of Estrogen Replacement in Human Populations. In Osteoporosis, Proceedings of International Symposium on Osteoporosis, C. Christiansen et al (Eds.), Aalborg Stiftsbogtrykkeri. p289-297.

RUEGSEGGER P., ANLIKER M., DAMBACHER M. (1981) Quantification of Trabecular Bone with Low Dose Computed Tomography. J.Comput.Assis.Tomogr. 5 p384-390.

RUEGSEGGER P., DAMBACHER M.A., RUEGSEGGER E., FISCHER J.A., ANLIKER M. (1984) Bone Loss in Premenopausal and Postmenopausal Women. J.Bone Joint Surg. 66-A p1015-1023.

RUNDGREN A., EKLUND S., JONSON R. (1984) Bone Mineral Content in 70 and 75 Year Old Men and Women: an Analysis of Some Anthropometric Background Factors. Age and Ageing 13 p6-13.

SAHA S., LAKES R.S. (1977) The Effect of Soft Tissue on Wave Propagation and Vibration Tests for Determining the in vivo Properties of Bone. J.Biomechanics 10 p393-401.

SAHA S., SINGH S., GIYANANI V.L., THOMPSON H.E., ALBRIGHT J.A. (1984). Ultrasonic and CT Measurement of Skeletal Mass. Frontiers of Engin. and Computing in Health Care, IEEE. p112-114.

SAYERS C.M. (1980) On the Propagation of Ultrasound in Highly Concentrated Mixtures and Suspensions. J.Phys.D:Appl.Phys. 13 p179-184.

SAYERS C.M., SMITH R.L. (1982) The Propagation of Ultrasound in Porous Media. Ultrasonics 20 p201-205.

SCHAADT O., BOHR H. (1982) Loss of Bone Mineral in Axial and Peripheral Skeleton in Aging, Prednisone Treatment and Osteoporosis. In Non-Invasive Bone Measurements: Methodological Problems, J. Dequeker and C.C. Johnston (Eds.), IRL Press, Oxford. p208-214.

SCHWARTZ M.P., RECKER R.R. (1981) Comparison of Surface Density and Volume of Human Iliac Trabecular Bone Measured Directly and by Applied Stereology. Calcif.Tiss.Int. 33 p561-565.

SELLE W.A., JURIST J.M. (1966) The Onset of Postmenopausal Osteoporosis as Studied by a New Technique. J.Am.Geriatrics Soc. 14 p930-934.

SHUKLA S.S, KARELLAS A., LEICHTER I., CRAVEN J.D., GREENFIELD M.A. (1985) Quantitative Assessment of Bone Mineral by Photon Scattering: Accuracy and Precision Considerations. Med.Phys. 12 p447-448.

SINGH M., NAGRATH A.R., MAINI P.S., (1970) Changes in Trabecular Pattern of the Upper End of the Femur as an Index of Osteoporosis. J.Bone Joint Surg. 52-A p457-467.

SLOVIK D.M., ROSENTHAL D.I., DOPPELT S.H., POTTS J.T., DALY M.A., CAMPBELL J.A., NEER R.M. (1986) Restoration of Spinal Bone in Osteoporotic Men by Treatment with Human Parathyroid Hormone and 1,25 Dihydroxyvitamin D. J.Bone Min.Res. 1 p377-381.

SMEATHERS J. (1986) private communication.

SPIEGL P.V., JURIST J.M. (1975) Prediction of Ulnar Resonant Frequency. J.Biomechanics. 8 p213-217.

STEIGER P., GLUEER C.C., GENANT H.K. (1987) Simultaneous Calibration of QCT: A Comparison of Commercial Calibration Phantoms. 6th International Workshop on Bone and Soft Tissue Densitometry, Buxton. p36.

STOLL R.D. (1974) Acoustic Waves in Saturated Sediments. In Physics of Sound

in Marine Sediments, L.Hampton (Ed.), Plenum Press, New York. p19-39.

TEITELBAUM S.L. (1983) Osteoporosis and Bone Biopsy. In The Osteoporotic Syndrome, 1st Ed., L.V. Avioli (Ed.), Grune and Stratton, New York. p115-122.

TRUELL R., ELBAUM C., CHICK B.B. (1969) Ultrasonic Methods in Solid State Physics. Academic Press, London. p58 and p161-179.

TWERSKY V. (1964) On Propagation in Random Media of Discrete Scatterers. Proc. Am.Math.Soc.Symp.Stochas.Proc.Math.Phys.Eng. 16 p84-116.

TWERSKY V. (1977) Coherant Scalar Field in Pair Correlated Random Distribution of Aligned Scatterers. J.Math.Phys. 18 p2468-2486.

URICK R.J. (1948) The Absorption of Sound in Suspensions of Irregular Particles. J.Ac.Soc.Am. 20 p283-289.

VARADAN V.K., MA Y., VARADAN V.V. (1985) A Multiple Scattering Theory for Elastic Wave Propagation in Discrete Random Media. J.Ac.Soc.Am. 77 p375-385.

WAHNER H.W. (1982) Clinical Aspects of Dual Photon Absorptiometry. In Non-invasive Bone Measurements: Methodological Problems, J. Dequeker and C.C. Johnston (Eds.), IRL Press, Oxford. p192-196.

WASNICH R.D., ROSS P.D., HEOLBRUN L.K., VOGEL J.M. (1987) Selection of the Optimal Skeletal Site for Fracture Risk Prediction. Clin.Orth.Rel.Res. 216 p262-268.

WATERMAN P.C., TRUELL R. (1961) Multiple Scattering of Waves. J.Math.Phys. 2 p512-537.

WEAVER R.L., PAO Y.H. (1981) Dispersion Relations for Linear Wave Propagation in Homogeneous and Inhomogeneous Media. J.Math.Phys. 22 p1909-1918.

WEBBER C.E. (1987) The Effect of Fat on Bone Mineral Measurements in Normal Subjects with Recommended Values of Bone, Muscle and Fat Attenuation Coefficients. Clin.Phys.Physiol.Meas. 8 p143-158.

WEINSTEIN R.S., HUTSON M.S. (1987) Decreased Trabecular Width and Increased
Trabecular Spacing Contribute to Bone Loss with Aging. Bone 8 p137-142.

WELLS P.N.T. (1977) Biomedical Ultrasonics. Academic Press, New York. p121.

WHITEHOUSE W.J., DYSON E.D., JACKSON C.K. (1971) The Scanning Electron Micro-
scope in Studies of Trabecular Bone from a Human Vertebral Body. J.Anat.
108 p481-496.

WHITEHOUSE W.J. (1974) The Quantitative Morphology of Anistropic Trabecular
Bone. J.Microscopy 101 p153-168.

WHITEHOUSE W.J. (1976) Errors in Area Measurement in Thick Sections with
Special Reference to Trabecular Bone. J.Microscopy 107 p183-187.

WOOD A.B. (1930) A Textbook of Sound. Bell and Sons, London. p326-329.

WU T.T. (1966) The Effect of Inclusion Shape on the Elastic Moduli of a Two
Phase Material. Int.J.Solids Structures 2 p1-8.

YANO K., WASNICH R.D., VOGEL J.M., HEILBURN L.K. (1984) Bone Mineral Measure-
ments Among the Middle-aged and Elderly Japanese Residents in Hawaii.
Amer.J.Epidemiol. 119 p751-764.

YEATER R.A., MARTIN R.B. (1984) Senile Osteoporosis: the Effects of Exercise.
Postgrad.Med. 75 p147-163.

YING C.F., TRUELL R. (1956) Scattering of a PLane Longitudinal Wave by a
Spherical Obstacle in an Isotropically Elastic Solid. J.App.Phys. 27
p1086-1097

YOON H.S., KATZ J.L. (1976) Ultrasonic Wave Propagation in Human Cortical Bone
I,II and III. J.Biomechanics 9 p407-412,459-464,537-540.

ZEMANEK J. (1971) Beam Behaviour Within the Nearfield of a Vibrating Piston.
J.Ac.Soc.Am. 49 p181-191.

APPENDIX A.

FORTRAN listing of the program to evaluate Biot's theory for cancellous bone.

```
      PROGRAM BIOT
      IMPLICIT COMPLEX*16 (Z)
      COMPLEX SZBG,SZSHG,SZBF,SZSHF
      COMMON/SHAPE/THETA,F,AA,CC
      REAL KAPPA,M,LVELG,LVELF,LATTG,LATTF,IBF,IBG,ISHF,ISHG
      OPEN(13,FILE='BIOTDAT',STATUS='OLD')
      READ(13,*) RHOG,RHOF,ETA,PERMD,BETAD
      READ(13,*) PORED,ZBE,ZSHE,R,ISH1,ISH2,AA,CC,BETA
      READ(13,*) LVELG,TVELG,LVELF,TVELF,LATTG,TATTG,LATTF,TATTF
      CLOSE(13)
      PCONS=PERMD*((1.0-BETAD)**2)/(BETAD**3)
      POCONS=(PORED**2)/PERMD
      TPI=6.28318
      ZI=(0.0,1.0)
      RSHF=RHOF*TVELF*TVELF
      RBF=RHOF*LVELF*LVELF-4.0/3.0*RSHF
      RSHG=RHOG*TVELG*TVELG
      RBG=RHOG*LVELG*LVELG-4.0/3.0*RSHG
      WRITE(6,320) LVELG,TVELG,LATTG,TATTG
      WRITE(6,320) LVELF,TVELF,LATTF,TATTF
      WRITE(6,322) BETA,ISH1,ISH2,AA
      WRITE(6,323) PERMD,ETA,PORED
      WRITE(6,*)
      WRITE(6,*)
  322 FORMAT (4X,F5.3,3X,2I3,4X,F5.1)
  323 FORMAT (3E12.2)
  320 FORMAT (4(3X,F8.1))
      DO 100 FR=200.0,1000.0,100.0
      FREQ=FR*1000.0
      W=TPI*FREQ
      W2=W*W
      IF (TATTF .EQ. 0.0) THEN
        ISHF=ETA*W/RHOF
      END IF
      IF (TATTF .NE. 0.0) THEN
        ISHF=RSHF*TATTF*TVELF*FR/(1000.0*8.686*FREQ)
      END IF
      IBF=RBF*LATTF*LVELF*FR/(1000.0*FREQ*8.686)
      IBG=RBG*LATTG*LVELG*FR/(1000.0*8.686*FREQ)
      ISHG=RSHG*TATTG*TVELG*FR/(1000.0*8.686*FREQ)
      ZBG=RBG+ZI*IBG
      ZBF=RBF+ZI*IBF
      ZSHG=RSHG+ZI*ISHG
      ZSHF=RSHF+ZI*ISHF
      RHOE=BETA*RHOF+(1.0-BETA)*RHOG
      ALPHA=1.0-R*(1.0-1.0/BETA)
      PERM=PCONS*(BETA**3)/((1.0-BETA)**2)
      A=SQRT(POCONS*PERM)
      M=ALPHA*RHOF/BETA
      CALL SCT(ZBG,ZSHG,ZBF,ZSHF,BETA,ZBE,ZSHE,ISH1,ISH2)
      ZD=ZBG*(1.0+BETA*(ZBG/ZBF-1.0))
      ZD=ZD-ZBE
```

```
      ZH=((ZBG-ZBE)**2)/ZD+ZBE+4.0/3.0*ZSHE
      ZC=ZBG*(ZBG-ZBE)/ZD
      ZM=ZBG*ZBG/ZD
      KAPPA=A*SQRT(W*RHOF/ETA)
      ZT3=ZF(KAPPA)
      ZT1=ZH*(M*W2-ZI*W*ZT3*ETA/PERM)
      ZT2=RHOE*W2*ZM-2.0*RHOF*W2*ZC
      ZCC=(RHOF**2)*(W2**2)-RHOE*M*(W2**2)
      ZCC=ZCC+ZI*(W**3)*RHOE*ZT3*ETA/PERM
      ZBB=ZT1+ZT2
      ZAA=ZC*ZC-ZH*ZM
      ZAA=ZAA/1.0E20
      ZBB=ZBB/1.0E20
      ZCC=ZCC/1.0E20
      ZFAC=CDSQRT(ZBB*ZBB-4.0*ZAA*ZCC)
      ZL1=CDSQRT((-ZBB+ZFAC)/(2.0*ZAA))
      ZL2=CDSQRT((-ZBB-ZFAC)/(2.0*ZAA))
      VC1=ABS(W/REAL(ZL1))
      VC2=ABS(W/REAL(ZL2))
      ATTEN1=8.686*ABS(IMAG(ZL1))
      ATTEN2=8.686*ABS(IMAG(ZL2))
      WRITE(6,300) FR,VC1,VC2,ATTEN1,ATTEN2
  100 CONTINUE
  300 FORMAT (F5.0,3(4X,F8.2),e15.2)
      STOP
      END
C
C
      COMPLEX*16 FUNCTION ZF(X)
      IMPLICIT COMPLEX*16 (Z)
      DOUBLE PRECISION XI,XI2,BER,BEI,BERD,BEID,PI
      ZI=(0.0,1.0)
      PI=3.141592
      IF (X .LE. 8.0) THEN
      XI=X/8.0
      XI2=XI*XI
      BER=1.0-64.0*XI2**2+113.77777774*XI2**4
      BER=BER-32.36345652*XI2**6+2.4191397*XI2**8
      BER=BER-8.349609E-2*XI2**10+1.22552E-3*XI2**12
      BER=BER-9.01E-6*XI2**14
      BEI=16.0*XI2-113.77777774*XI2**3
      BEI=BEI+72.817777742*XI2**5-10.56765779*XI2**7
      BEI=BEI+0.52185615*XI2**9-1.103667E-2*XI2**11
      BEI=BEI+1.1346E-4*XI2**13
      BERD=-4.0*XI2+14.22222222*XI2**3
      BERD=BERD-6.06814810*XI2**5+0.66047849*XI2**7
      BERD=BERD-2.609253E-2*XI2**9+4.5957E-4*XI2**11
      BERD=(BERD-3.94E-6*XI2**13)*X
      BEID=0.5-10.66666666*XI2**2
      BEID=BEID+11.37777772*XI2**4-2.31167514*XI2**6
      BEID=BEID+0.14677204*XI2**8-3.79386E-3*XI2**10
      BEID=(BEID+4.609E-5*XI2**12)*X
      ZT=(BERD+ZI*BEID)/(BER+ZI*BEI)
      ELSE
      XI=8.0/X
      XI2=XI*XI
      ZFAC=SQRT(PI/(2.0*X))
```

```
      ZFAC1=CDEXP(-(1.0+ZI)*X/SQRT(2.0)+ZTH(-XI))
      ZFAC=ZFAC*ZFAC1
      ZFAC1=CDEXP((1.0+ZI)*X/SQRT(2.0)+ZTH(XI))
      ZFAC1=ZFAC1/SQRT(2.0*PI*X)
      ZB=ZFAC1+ZI/PI*ZFAC
      ZTT=-ZFAC*ZPHI(-XI)*ZI/PI
      ZTT=ZFAC1*ZPHI(XI)+ZTT
      IF (ABS(ZTT) .GT. 1.0E30 .OR. ABS(ZB) .GT. 1.0E30) THEN
      ZTT=ZTT/(1.0E25)
      ZB=ZB/(1.0E25)
      END IF
      ZT=ZTT/ZB
      END IF
      ZF=X*ZT/(4.0*(1.0+2.0*ZI*ZT/X))
      RETURN
      END
C
C

      COMPLEX*16 FUNCTION ZTH(X)
      IMPLICIT COMPLEX*16 (Z)
      DOUBLE PRECISION X
      Z1=(0.0,-0.3926991)+(1.110486E-2,1.10485E-2)*X
      Z1=Z1+(0.0,-9.765E-4)*X**2
      Z1=Z1+(-9.06E-5,-9.01E-5)*X**3
      Z1=Z1+(-2.25E-5,0.0)*X**4
      Z1=Z1+(-3.4E-6,5.1E-6)*X**5
      Z1=Z1+(6.0E-7,1.9E-6)*X**6
      ZTH=Z1
      RETURN
      END
C
C

      COMPLEX*16 FUNCTION ZPHI(X)
      IMPLICIT COMPLEX*16 (Z)
      DOUBLE PRECISION X
      Z1=(0.7071068,0.7071068)+(-6.25001E-2,-1.0E-7)*X
      Z1=Z1+(-1.3813E-3,1.3811E-3)*X**2
      Z1=Z1+(5.0E-7,2.45E-4)*X**3
      Z1=Z1+(3.46E-5,3.38E-5)*X**4
      Z1=Z1+(1.17E-5,-2.4E-6)*X**5
      Z1=Z1+(1.6E-6,-3.2E-6)*X**6
      ZPHI=Z1
      RETURN
      END
C
C

      SUBROUTINE SCT(ZBG,ZSHG,ZBF,ZSHF,BETA,ZBE,ZSHE,ISH1,ISH2)
      IMPLICIT COMPLEX*16 (Z)
      COMMON/SHAPE/THETA,F,AA,CC
      TOL=1.0E-6
      IF (ISH1 .EQ. 2 .OR. ISH2 .EQ. 2) THEN
       ASP=AA/CC
       THETA=AA*CC**2/((AA**2-CC**2)**1.5)
       D=LOG((SQRT(4.0*ASP**2-4.0)+2.0*ASP)/2.0)
       D=ASP*SQRT(ASP**2-1.0)-D
       THETA=THETA*D
       F=AA**2*(2.0-3.0*THETA)/(AA**2-CC**2)
```

```
      END IF
      IF (ISH1 .EQ. 3 .OR. ISH2 .EQ. 3) THEN
       ASP=CC/AA
       D=ASP*SQRT(1.0-ASP**2)
       THETA=AA**2*CC/((AA**2-CC**2)**1.5)
       THETA=THETA*(ACOS(ASP)-D)
       F=CC**2*(3.0*THETA-2.0)/(AA**2-CC**2)
      END IF
   10 ZPG=ZP(ZBE,ZSHE,ZBG,ZSHG,ISH1)
      ZPF=ZP(ZBE,ZSHE,ZBF,ZSHF,ISH2)
      ZQG=ZQ(ZBE,ZSHE,ZBG,ZSHG,ISH1)
      ZQF=ZQ(ZBE,ZSHE,ZBF,ZSHF,ISH2)
      ZBE1=(1.0-BETA)*ZBG*ZPG+BETA*ZBF*ZPF
      ZBE1=ZBE1/((1.0-BETA)*ZPG+BETA*ZPF)
      ZSHE1=(1.0-BETA)*ZSHG*ZQG+BETA*ZSHF*ZQF
      ZSHE1=ZSHE1/((1.0-BETA)*ZQG+BETA*ZQF)
      DIFF1=ABS(ZBE1-ZBE)
      DIFF2=ABS(ZSHE1-ZSHE)
      ZBE=ZBE1
      ZSHE=ZSHE1
      IF (DIFF1 .GT. TOL*ABS(ZBE)) GO TO 10
      IF (DIFF2 .GT. TOL*ABS(ZSHE)) GO TO 10
      RETURN
      END
C
C
      COMPLEX*16 FUNCTION ZP(Z1,Z2,Z3,Z4,ISH)
      IMPLICIT COMPLEX*16 (Z)
      COMMON/SHAPE/THETA,F,AA,CC
      IF (ISH .EQ. 0) THEN
       ZP=(Z1+Z2+Z4/3.0)/(Z3+Z2+Z4/3.0)
      END IF
      IF (ISH .EQ. 1) THEN
       ZP=(Z1+4.0/3.0*Z4)/(Z3+4.0/3.0*Z4)
      END IF
      IF (ISH .GE. 2) THEN
       ZA=Z4/Z2-1.0
       ZB=(Z3/Z1-Z4/Z2)/3.0
       ZR=Z2/(Z1+4.0/3.0*Z2)
       ZT1=F+THETA
       ZT2=3.0-4.0*ZR
       ZF1=1.5*ZT1-ZR*(1.5*F+2.5*THETA-4.0/3.0)
       ZF1=1.0+ZA*ZF1
       ZF3=ZT1-ZR*(F-THETA+2.0*THETA**2)
       ZF3=ZA/2.0*(ZA+3.0*ZB)*ZT2*ZF3
       ZF2=1.0+1.5*ZT1-ZR/2.0*(3.0*F+5.0*THETA)
       ZF2=1.0+ZA*ZF2+ZB*ZT2+ZF3
       ZP=ZF1/ZF2
      END IF
      RETURN
      END
C
C
      COMPLEX*16 FUNCTION ZQ(Z1,Z2,Z3,Z4,ISH)
      IMPLICIT COMPLEX*16(Z)
      COMMON/SHAPE/THETA,F,AA,CC
      IF (ISH .EQ. 0) THEN
```

```
      ZGAMMA=(Z2*(3.0*Z1+Z2))/(3.0*Z1+7.0*Z2)
      ZT1=(4.0*Z2)/(Z2+Z4)
      ZT2=2.0*(Z2+ZGAMMA)/(Z4+ZGAMMA)
      ZT3=(Z3+4.0/3.0*Z2)/(Z3+Z2+Z4/3.0)
      ZQ=(ZT1+ZT2+ZT3)/5.0
      END IF
      IF (ISH .EQ. 1) THEN
      ZFI=Z2/6.0*((9.0*Z1+8.0*Z2)/(Z1+2.0*Z2))
      ZQ=(Z2+ZFI)/(Z4+ZFI)
      END IF
      IF (ISH .GE. 2) THEN
      ZA=Z4/Z2-1.0
      ZB=(Z3/Z1-Z4/Z2)/3.0
      ZR=Z2/(Z1+4.0/3.0*Z2)
      ZT1=F+THETA
      ZT2=3.0-4.0*ZR
      ZT3=F-THETA
      ZT4=ZR-1.0
      ZF2=1.0+1.5*ZT1-ZR/2.0*(3.0*F+5.0*THETA)
      ZF2=1.0+ZA*ZF2+ZB*ZT2
      ZFF=F+THETA-ZR*(ZT3+2.0*THETA**2)
      ZFF=ZA/2.0*(ZA+3.0*ZB)*ZT2*ZFF
      ZF2=ZF2+ZFF
      ZF3=1.0+ZA*(1.0-(F+1.5*THETA)+ZR*ZT1)
      ZF4=1.0+ZA/4.0*(F+3.0*THETA-ZR*ZT3)
      ZF5=ZA*(-F+ZR*(ZT1-4.0/3.0))+ZB*THETA*ZT2
      ZF6=1.0*ZA*(1.0+F-ZR*ZT1)+ZB*(1.0-THETA)*ZT2
      ZF7=2.0*ZA/4.0*(3.0*F+9.0*THETA-ZR*(3.0*F+5.0*THETA))
      ZF7=ZF7+ZB*THETA*ZT2
      ZF8=ZA*(1.0-2.0*ZR+(F/2.0*ZT4)+THETA/2.0*(5.0*ZR-3.0))
      ZF8=ZF8+ZB*(1.0-THETA)*ZT2
      ZF9=ZA*(ZT4*F-ZR*THETA)+ZB*THETA*ZT2
      ZF1=ZF4*ZF5+ZF6*ZF7-ZF8*ZF9
      ZF1=ZF1/(ZF2*ZF4)
      ZQ=(2.0/ZF3+1.0/ZF4+ZF1)/5.0
      END IF
      RETURN
      END
```

APPENDIX B.

FORTRAN program to evaluate the multiple scattering theory for cancellous bone.

```fortran
      program multiplescatter
      real kaa(20),no
      double precision k1a,k2a,t1a,t2a,mu12,gamma,gamma1,g
      double precision sbesk1(21),sneuk1(21),sbesk2(21),sneuk2(21),
     c sbest1(21),sneut1(21),sbest2(21),sneut2(21)
      double precision t1,t2,k1,k2,diff1,diff2
      double precision eps(8,8),del(8),x(8),e,t,tt
      complex*16 fz,fz1,fp,fp1,gam
      dimension mm(20),vel(20),atten(20)
      complex*16 aem,bem
      complex j
      j=(0.0,1.0)
      tol=1.0e-3
      pi=3.141592
      aaa=120e-6
      write(6,8)
      write(6,8)
      write(6,8)
      write(6,8)
    8 format (10x)
      write(6,9)
    9 format('Only for non-zero shear velocities.')
      write(6,8)
      write(6,8)
      write(6,11)
   11 format ('Enter densities 1 and 2')
      read(5,*) rho1,rho2
      write(6,12)
   12 format ('Enter longitundinal velocities 1 and 2')
      read(5,*) vl1,vl2
      write(6,13)
   13 format ('Enter transverse velocities 1 and 2')
      read(5,*) vt1,vt2
      write(6,14)
   14 format('Enter no. particles per volume')
      read(5,*) no
      num=0
      do 150 fr=700,1000,100
      freq=fr*1000.0
      k1a=2.0*pi*freq*aaa/vl1
      num=num+1
      k2a=vl1/vl2*k1a
      t1a=vl1/vt1*k1a
      t2a=vl1/vt2*k1a
      mu12=rho2*(t1a**2)/(rho1*(t2a**2))
      write(6,8)
      write(6,19) k1a,k2a
   19 format('k1a and k2a = ',e15.7,5x,e15.7)
      write(6,21) t1a,t2a
   21 format('t1a and t2a = ',e15.7,5x,e15.7)
      write(6,22) mu12
   22 format('mu12 = ',e15.7)
```

```
      write(6,8)
      fp=(0.0,0.0)
      fp1=(0.0,0.0)
      fz=(0.0,0.0)
      fz1=(0.0,0.0)
      m=-1
1  continue
      m=m+1
      if (m .eq. 0) then
         bem=(0.0,0.0)
         e=(t1a**2)/(1.0-k2a/tan(k2a))
         e=rho2/rho1*(e-4.0*(t1a/t2a)**2)
         t=(4.0+e)*k1a*cos(k1a)
         t=((t1a**2)-(4.0+e))*sin(k1a)+t
         tt=(t1a**2-(4.0+e))**2
         tt=sqrt(tt+(4.0+e)**2*k1a**2)
         t=t/(k1a*tt)
         tt=(t1a**2-(4.0+e))/((4.0+e)*k1a)
         aem=t*cdexp(j*(k1a-datan(tt)))
      else
         if (m .eq. 1) then
         call gener(sbesk1,sneuk1,k1a)
         call gener(sbesk2,sneuk2,k2a)
         call gener(sbest1,sneut1,t1a)
         call gener(sbest2,sneut2,t2a)
         end if
         eps(1,1)=k1a*sbesk1(m+2)
         eps(1,2)=k1a*sneuk1(m+2)
         eps(1,3)=m*t1a*sbest1(m+2)
         eps(1,4)=m*t1a*sneut1(m+2)
         eps(1,5)=-1.0*k2a*sbesk2(m+2)
         eps(1,6)=0.0
         eps(1,7)=-1.0*m*t2a*sbest2(m+2)
         eps(1,8)=0.0
         eps(3,1)=sbesk1(m+1)
         eps(3,2)=sneuk1(m+1)
         eps(3,3)=-1.0*((m+1)*sbest1(m+1)-t1a*sbest1(m+2))
         eps(3,4)=-1.0*((m+1)*sneut1(m+1)-t1a*sneut1(m+2))
         eps(3,5)=-1.0*sbesk2(m+1)
         eps(3,6)=0.0
         eps(3,7)=(m+1)*sbest2(m+1)-t2a*sbest2(m+2)
         eps(3,8)=0.0
         eps(5,1)=t1a**2*sbesk1(m+1)-2.0*(m+2)*k1a*sbesk1(m+2)
         eps(5,2)=t1a**2*sneuk1(m+1)-2.0*(m+2)*k1a*sneuk1(m+2)
         eps(5,3)=m*(t1a**2*sbest1(m+1)-2.0*(m+2)*t1a*sbest1(m+2))
         eps(5,4)=m*(t1a**2*sneut1(m+1)-2.0*(m+2)*t1a*sneut1(m+2))
         eps(5,5)=-1.0*mu12*(t2a**2*sbesk2(m+1)-2.0*(m+2)*t2a
     +      *sbesk2(m+2))
         eps(5,6)=0.0
         eps(5,7)=-1.0*mu12*m*(t2a**2*sbest2(m+1)-2.0*(m+2)*t2a
     +      *sbest2(m+2))
         eps(5,8)=0.0
         eps(7,1)=(m-1)*sbesk1(m+1)-k1a*sbesk1(m+2)
         eps(7,2)=(m-1)*sneuk1(m+1)-k1a*sneuk1(m+2)
         eps(7,3)=-1.0*((m**2-1.0-0.5*t1a**2)
     +      *sbest1(m+1)+t1a*sbest1(m+2))
         eps(7,4)=-1.0*((m**2-1.0-0.5*t1a**2)
```

```
    +    *sneut1(m+1)+t1a*sneut1(m+2))
         eps(7,5)=-1.0*mu12*((m-1)*sbesk2(m+1)-k2a*sbesk2(m+2))
         eps(7,6)=0.0
         eps(7,7)=mu12*((m**2-1.0-0.5*t2a**2)
    +    *sbest2(m+1)+t2a*sbest2(m+2))
         eps(7,8)=0.0
         do 20 i=2,8,2
         do 30 k=1,7,2
         eps(i,k)=-1.0*eps(i-1,k+1)
         eps(i,k+1)=eps(i-1,k)
 30      continue
 20      continue
         do 40 i=1,7,2
         del(i)=(-1.0)**m*eps(i,1)/k1a
         del(i+1)=0.0
 40      continue
         call matrix(eps)
         do 50 i=1,8
         x(i)=0.0
         do 60 k=1,8
         x(i)=x(i)+eps(i,k)*del(k)
 60      continue
 50      continue
         aem=x(1)+j*x(2)
         bem=x(3)+j*x(4)
    end if
    fz1=fz1+(-j)**m*dconjg(aem)
    fp1=fp1+(-j)**m*(-j)**m*dconjg(aem)
    if (m .ge. 19) go to 130
    diff1=abs(fp1-fp)
    diff2=abs(fz1-fz)
    write(6,66) diff2
 66 format('Diff2 is ',e15.7)
    write(6,6) diff1
  6 format('Diff1 is ',e15.7)
    fp=fp1
    fz=fz1
    write(6,*) fp
    write(6,*) fz
    if (diff1 .gt. abs(tol*fp) .or. diff2 .gt. abs(tol*fz))
  c go to 1
130 continue
    write(6,8)
    write(6,18) m
 18 format('m is ',i3)
    mm(num)=m
    kaa(num)=fr
    fz1=2.0*pi*fz*aaa**2*no/(k1a**2)
    fp1=2.0*pi*fp*aaa**2*no/(k1a**2)
    gam=(1.0-fz1)**2-(fp1**2)
    gam=cdsqrt(gam)*k1a/aaa
    vel(num)=2.0*pi*freq/real(gam)
    atten(num)=8.686*imag(gam)
150 continue
    write(6,8)
    write(6,8)
    do 160 i=1,num
```

```
      write(6,31) kaa(i),mm(i)
 31 format('k1a is ',f5.1,' m is ',i3)
      write(6,*) vel(i),atten(i)
      write(6,*)
160 continue
      stop
      end




      subroutine matrix(mati)
      double precision mat(8,8),mati(8,8),res(8,8)
      n=8
      do 10 i=1,n
      do 10 j=1,n
      mat(i,j)=mati(i,j)
 10 continue
      call invt(mati)
      do 30 i=1,n
      do 30 j=1,n
      res(i,j)=0.0
      do 30 k=1,n
      res(i,j)=res(i,j)+mat(i,k)*mati(k,j)
 30 continue
      write(6,*)
      call outp(res)
      write(6,*)
      return
      end




      subroutine outp(mat)
      double precision mat(8,8)
      n=8
      do 10 i=1,n
      write(6,2) mat(i,1),mat(i,2),mat(i,3),mat(i,4),mat(i,5)
    c,mat(i,6),mat(i,7),mat(i,8)
  2 format (8(f8.2,1x))
 10 continue
      return
      end




      subroutine invt(eps)
      double precision eps(8,8),temp(8,16),b
      n=8
      do 10 i=1,n
      do 20 k=1,n
      temp(i,k+n)=0.0
      temp(i,k)=eps(i,k)
 20 continue
      temp(i,i+n)=1.0
 10 continue
      k=0
 25 k=k+1
      if (k .ne. n) then
```

```
      m=k
      do 50 i=k+1,n
      if (dabs(temp(i,k)) .gt. dabs(temp(m,k))) then m=i
50    continue
      if (m .ne. k) then
      do 40 j=k,2*n
      b=temp(k,j)
      temp(k,j)=temp(m,j)
      temp(m,j)=b
40    continue
      end if
      end if
      do 60 j=k+1,2*n
      temp(k,j)=temp(k,j)/temp(k,k)
60    continue
      if (k .eq. 1) go to 70
      do 80 i=1,k-1
      do 80 j=k+1,2*n
      temp(i,j)=temp(i,j)-temp(i,k)*temp(k,j)
80    continue
      if (k .eq. n) go to 30
70    continue
      do 110 i=k+1,n
      do 110 j=k+1,2*n
      temp(i,j)=temp(i,j)-temp(i,k)*temp(k,j)
110   continue
30    if (k .lt. n) go to 25
      do 130 i=1,n
      do 130 j=1,n
      eps(i,j)=temp(i,j+n)
130   continue
      return
      end




      subroutine gener(bes,neu,z)
      double precision bes(21),neu(21),z
      bes(1)=dsin(z)/z
      bes(2)=dsin(z)/(z**2)-dcos(z)/z
      neu(1)=-1.0*dcos(z)/z
      neu(2)=-1.0*dsin(z)/z-dcos(z)/(z**2)
      do 10 i=3,21
      bes(i)=(2.0*(i-2)+1)/z*bes(i-1)-bes(i-2)
      neu(i)=(2.0*(i-2)+1)/z*neu(i-1)-neu(i-2)
10    continue
      write(6,1) z
1     format('z is ',e15.5)
      write(6,2)
2     format(' n             bessel          neumann')
      do 40 i=1,21
      write(6,3) i-1,bes(i),neu(i)
3     format(i3,2x,e15.5,2x,e15.5)
40    continue
      return
      end
```